Ozonation-biofiltration for the production of drinking water from organic-rich groundwaters

Natural organic matter transformation, bromate formation and mitigation

Vom Promotionsausschuss der

Technischen Universität Hamburg

zur Erlangung des akademischen Grades

Doktor-Ingenieur (Dr.-Ing.)

genehmigte Dissertation

von

Jakob Kämmler

aus

Schwerin

2023

Gutachter:

1. Gutachter: Prof. Dr.-Ing. Mathias Ernst

2. Gutachter: Prof. Dr.-Ing. Michael Schlüter

3. Gutachter: Dr. Jannis Wenk

Vorsitzender des Prüfungsausschusses:

Prof. Dr.-Ing. Peter Fröhle

Tag der mündlichen Prüfung:

20. Dezember 2022

DOI:

10.15480/882.5208

Acknowledgements

The idea for this work was developed at DVGW Research Centre TUHH where I had the chance to carry out research from 2018 to 2021. In the *COL_EX* project, various processes for selective removal of humic substances from groundwater in drinking water treatment were studied.

I want to thank Mathias Ernst for his patient and assured support throughout this work. Moreover, I would like to thank all former colleagues at DVGW Research Centre and the Institute of Water Resources and Water Supply. I benefited from your experience and was constantly encouraged by your support.

I would like to thank the Oldenburgisch-Ostfriesischer Wasserverband for their support in carrying out the small-scale pilot experiments. Additionally, I am grateful to the Institute for Wastewater Management and Water Protection at TUHH for providing the pilot plant. I would also like to thank Heino Hagenah and Hans-Wilhelm Mehrkens for setting up the electrical equipment of the plant.

At TUHH, I had the privilege of working with resourceful and creative students. I would like to thank Kawa Arkawazi, Athul Bharadwaj, Julia Bosse, Ole Eberhard, Rieke Freer, Noemi Friedrich, Stephan Griep, Zhao Heng Lee, Anastasia Ogay, Luminita Preda, Jörn Sellmann and Jorrit Specker for their fruitful collaboration while completing their student theses. Luminita and Jörn also contributed significantly to this work as student assistants. Everyone of you invested a lot of time and dedication and I could not have realized this work without your efforts.

I would like to thank my fellow PhD candidates at the Institute of Water Resources and Water Supply – Saskia Dillmann, Muhammad Ismahil, Charlotte Kast, Shambhavi Kaushik, Margarethe Langer, Natalie Lüdemann, Tomi Mantel, Jonas Schuster, Jakob Stumme, Anne Trimbach and Muhammad Usman – for intensive discussions, mutual inspiration and openness to share both enthusiasm and disappointment. I am delighted that we could grow together, and continue to support each other.

I am grateful to Jannis Wenk and Garyfalia Zoumpouli for their enduring and productive collaboration in the preparation of the publication on membrane ozonation.

I thank Michael Schlüter and Jannis Wenk for reviewing this dissertation and Peter Fröhle for acting as chairman of the examination board.

I would like to thank each one that is committed to making scientific publications accessible for everyone. I am convinced that research will benefit from this.

Finally, I would like to thank my friends and family who are constantly supporting and accompanying me in my professional career and personal life. My dear parents Frank and Susanne Kämmler: You encouraged my curiosity and supported me on my journey during both joyful and stressful times. For this I thank you from the bottom of my heart.

Abstract

Groundwater resources present a major reservoir for worldwide drinking water production that is used intensively due to its consistent quality and availability. Organic-rich groundwater resources with high concentration of natural organic matter (NOM) are not used to their full potential due to the negative impact of NOM on treatment processes and on water quality, particularly on water coloration.

This work examines the ozonation-biofiltration process to enhance NOM removal in drinking water production from organic-rich groundwater. Objects of research regarding the ozonation-biofiltration of organic-rich groundwater were (i) the transformation of groundwater NOM, (ii) by-product formation and its minimization and (iii) applicability and integration potential into groundwater treatment. An experimental approach was chosen to address these objects of research. Experiments included batch ozonation, small-scale pilot ozonation-biofiltration and membrane ozonation using different natural, organic-rich groundwaters.

Ozonation of organic-rich groundwater is characterized by rapid ozone (O_3) consumption by NOM, normalized to the dissolved organic carbon (DOC) content of groundwater (approximately 0.5 mg_{O3}/mg_{DOC} in the first 30 s of ozonation). This results in significant reduction of ultraviolet absorbance (UV_{254}) and color (SAC_{436}) but in low disintegration of NOM to smaller molecular size and therefore moderate formation of assimilable organic carbon (AOC). The simultaneous formation of bromate, a presumed human carcinogen, may exceed international drinking water limits under these conditions. This is due to high bromide contents of groundwaters and presumably enhanced by hydroxyl radicals formed by ozonation of phenolic NOM.

Biofiltration of ozonated groundwater by granular activated carbon and phonolithe results in significant reduction of AOC and minor reduction of UV_{254}, SAC_{436} and DOC. Overall SAC_{436} removal potential by small-scale pilot ozonation-biofiltration was 40–50 % at bromate concentrations << 10 µg L^{-1}, for two different groundwaters. For other groundwaters used in batch ozonation experiments, SAC_{436} removal potential may be up to 70 %. Decolorization performance of ozonation-biofiltration may be enhanced by the implementation of bromate minimization strategies. Process-oriented strategies (multi-stage ozonation and membrane ozonation) and pH reduction showed the highest potential to improve the trade-off between decolorization and bromate formation. Addition of ammonia or hydrogen peroxide reduced bromate concentration only at high ozone doses or compromised decolorization. Ozonation-biofiltration was performed with different feed water qualities including raw groundwater, aerated groundwater and finished groundwater, indicating high potential for integration into groundwater treatment.

Overall, it was shown that ozonation-biofiltration is applicable in different groundwater matrices, for different feed water qualities, at low ozone doses of < 0.5 mg_{O3}/mg_{DOC}. Its potential may be increased by the development of bromate minimization strategies particularly eligible for organic-rich groundwater treatment.

Zusammenfassung

Grundwasser ist weltweit eine bedeutende Ressource zur Trinkwassergewinnung, unter anderem wegen seiner beständigen Eigenschaften bezüglich Qualität und Verfügbarkeit. Grundwässer mit hohem Gehalt an gelösten natürlichen organischen Stoffen (*natural organic matter*, NOM), werden nicht vollumfänglich genutzt, unter anderem wegen erhöhter Gelbfärbung (*spektraler Absorptionskoeffizient bei 436 nm*, SAK_{436}) solcher Wässer.

In dieser Arbeit wird die Ozonung-Biofiltration als mögliches Verfahren zur Entfernung von NOM und zur Entfärbung organikreicher Grundwässer untersucht. Forschungsfragen zur Ozonung-Biofiltration umfassen (i) die Transformation grundwasserbürtiger NOM, (ii) Nebenproduktbildung und deren Minimierung und (iii) Integationsmöglichkeiten in Anlagen und Prozesse zur Grundwasseraufbereitung. Mit verschiedenen natürlichen, organikreichen Grundwässern wurden wurden Laborversuche zur Becherglas-Ozonung, Pilotversuche zur Ozonung-Biofiltration sowie Laborversuche zur Membranozonung durchgeführt.

Die Ozonung organikreicher Grundwässer zeichnet sich durch eine schnelle Zehrung von Ozon (O_3) aus, bezogen auf den Gehalt an gelöstem organischem Kohlenstoff (*dissolved organic carbon*, DOC) etwa 0.5 mg_{O3}/mg_{DOC} innerhalb von 30 s nach Ozondosierung. Dadurch werden der SAK_{436} und die Absorption von ultraviolettem Licht (UV_{254}) erheblich reduziert, bei geringer bis moderater Entstehung assimilierbaren organischen Kohlenstoffs (*assimilable organic carbon*, AOC). Die Konzentration von Bromat kann unter diesen Bedingungen nationale und internationale Trinkwasser-Grenzwerte (häufig 10 $\mu g\ L^{-1}$) überschreiten. Als Ursache dafür werden neben hohen Gehalten von Bromid auch hohe Konzentrationen von Hydroxylradikalen vermutet, welche bei der Ozonung phenolischer NOM-Bestandteile entstehen können.

Bei der Biofiltration ozonierter Grundwässer mittels Phonolith und granulierter Aktivkohle wird der AOC-Gehalt erheblich reduziert, des Weiteren ergeben sich leichte Verringerungen von UV_{254}, SAK_{436} und DOC-Gehalt.

Insgesamt wurde gezeigt, dass mittels Ozonung-Biofiltration bei geringen Ozonmengen (< 0.5 mg_{O3}/mg_{DOC}) verschiedene Grundwasserqualitäten aufbereitet werden können. In den beiden pilotierten Grundwässern wurde mittels Ozonung-Biofiltration eine Reduktion des SAK_{436} um 40–50 % bei Bromatkonzentrationen << 10 $\mu g\ L^{-1}$ erreicht. Bei anderen in Becherglas-Versuchen getesteten Grundwässern scheinen teils höhere SAK_{436}-Reduktionsraten von bis zu 70 % möglich. Durch prozessbasierte Strategien (Mehrfachdosierung von Ozon sowie Membranozonung) sowie durch eine Verringerung des pH-Werts konnte die Bromatbildung leicht verringert werden. Durch Dosierung von Ammonium oder Wasserstoffperoxid konnte die Bromatbildung ebenfalls verringert werden, jedoch nur bei Anwendung hoher Ozonmengen und teils bei negativer Auswirkung auf die Entfärbung. Die Ozonung-Biofiltration wurde mit verschiedenen Wasserqualitäten duchgeführt (Rohwasser, belüftetes Rohwasser sowie Reinwasser), was eine hohe Flexibilität des Verfahrens verdeutlicht.

Table of Contents

List of Figures

List of Tables

List of Abbreviations and Symbols

AFF water	Aerated, flocculated and filtered water
alk.	Total alkalinity
AOC	Assimilable organic carbon
AOP	Advanced oxidation process
BB	Building blocks
BDOC	Biodegradable organic carbon
BP	Biopolymers
D_{O3}	Diffusion coefficient of ozone in water
CDOC	Chromatographable organic carbon
c_{O3}	Dissolved ozone concentration
$c_{O3,0}$	Ozone dose
$c_{O3,g}$	Feed gas ozone concentration
ct	Time integral of dissoved ozone concentration
D	Inner diameter
D_{O3}	Diffusion coefficient of ozone in water
DOC	Dissolved organic carbon
DOM	Dissolved organic matter
E2:E3	Ratio of absorbance at 254 nm and 365 nm
E_0	Oxidation potential
EAC	Electron accepting capacity
EBCT	Empty-bed contact time
EC_{25}	Electrical conductivity at 25 °C
EDC	Electron donating capacity
GAC	Granular activated carbon
GW	Groundwater
H_2O_2	Hydrogen peroxide
HCl	Hydrochloric acid
HEEB	High-energy electronic beam
HOC	Hydrophobic organic carbon
HOMO	Highest occupied molecular orbital
HRT	Hydraulic retention time

HS	Humic substances
IEX	Ion exchange
IOD	Immediate ozone demand
k_g	Gas-side ozone mass transfer coefficient
k_L	Liquid-side ozone mass transfer coefficient
K_L	Overall ozone mass transfer coefficient
k_m	Membrane-side ozone mass transfer coefficient
$k_{n,n+1}$	First-order ozone decay rate constant between time steps *n* and *n+1*
$k_{O3,NO2-}$	Reaction rate of ozone and nitrite
k_{sec}	First-order ozone decay rate constant for the secondary phase of ozone decomposition
LC-OCD	Liquid chromatography-organic carbon detection
LMWA	Low molecular-weight acids
LMWN	Low molecular-weight neutrals
LUMO	Lowest unoccupied molecular orbital
n.a.	Not available
n.q.	Not quantified
NOM	Natural organic matter
NPOC	Non-purgeable organic carbon
O_3	Ozone
O_3/UV_{254}	UV_{254}-specific ozone dose
OCD	Organic carbon detection
PDMS	Polydimethylsiloxane
PFA	Perfluoroalkoxy alkane
PGV	Provisional guideline value
pK_a	Logarithmic acid dissociation constant
PLC	Programmable logic controller
POC	Particulate organic carbon
PTFE	Polytetrafluoroethylene
PVC	Polyvinyl chloride
R_c	Ratio of hydroxyl radical and ozone concentrations
R_{ct}	Time integral of R_c
$R_{OH,O3}$	Ratio of hydroxyl radical exposure to consumed ozone
ρ	Density
S	Spectral slope

SAC_{436}	Spectral absorbance coefficient at 436 nm
SAC_{440}	Spectral absorbance coefficient at 440 nm
$SSAC_{436}$	Specific spectral absorbance coefficient at 436 nm (SAC_{436}:DOC)
$SUVA_{254}$	Specific UV absorbance coefficient at 254 nm (UV_{254}:DOC)
ϑ	Temperature in °C
t-BuOH	*tert*-Butanol
t_0	Time step *0*
TCC	Total cell count
t_f	Final time step
t_n	Time step *n*
t_{n+1}	Times step *n+1*
TOC	Total organic carbon
TOC_0	Total organic carbon concentration before ozonation
UV	Ultra-violet
UV_{254}	UV absorbance at 254 nm
UV-vis	Ultraviolet and visible light
UVD	Ultraviolet light detection
vol%	Volume percent
WHO	World Health Organization
w/o	Without

1 Introduction

The availability of fresh, high-quality drinking water remains a global challenge. Water demand increases for various purposes, including irrigation, industrial use, and drinking water production. Moreover, climate change and environmental pollution reduce freshwater availability on a global and, more severely, on a regional level (Boretti and Rosa, 2019; UNESCO, 2019). Thus, the United Nations have considered drinking water supply one of their sustainable development goals (UN, 2015).

Groundwater is one of the major resources for global drinking water production (Gleeson et al., 2020; UN Water, 2022). In Germany, groundwater excluding spring water, riverbank filtrate and recharged groundwater, accounted for 61 % of raw water for drinking water production in 2016 (Statistisches Bundesamt, 2019). Drinking water resources in Germany are increasingly stressed by dry periods (Niehues and Merkel, 2021). Regionally, groundwater depletion prompts the efficient utilization of available groundwater resources (Fliß et al., 2021; Möhler et al., 2021). Groundwater resources may contain elevated concentration of natural organic matter (NOM) such as humic substances which may hamper treatment processes and organoleptical water properties, e.g. water color. As color is typically not reduced in conventional groundwater treatment, groundwater resources with high color are often not used for drinking water production to their full potential (Schulz, 2020). Thus, treatment processes that reduce water color and NOM content are eligible to increase the scope of available groundwater resources. The need for NOM removal strategies from groundwater is further stressed by regionally predicted increases in groundwater NOM concentration, as a consequence of climate change and urbanization (McDonough et al., 2020b; Riedel, 2019).

This research work is supposed to contribute to the portfolio of treatment options for groundwater rich in NOM, particularly for colored groundwater. Ozonation-biofiltration was identified as a promising technology for decolorization (Loeb et al., 2012), but is lacking coverage in research regarding effectiveness in different groundwater matrices, specific reaction mechanisms, by-product formation and integration into groundwater treatment.

The aim of this work is to shed light on three major objects of research regarding the use of ozonation-biofiltration for the treatment of colored, organic-rich groundwaters:

i. Transformation of groundwater natural organic matter (NOM) by ozonation and biofiltration at typical decolorization conditions,
ii. by-product formation and minimization in groundwater ozonation,
iii. applicability and integration potential of ozonation-biofiltration into groundwater treatment.

2 Theoretical Background

2.1 Natural Organic Matter in Groundwater Resources and Treatment Processes

2.1.1 Natural Organic Matter Characterization, Classification and Features

The term natural organic matter (NOM) describes the entity of degradation and metabolic products of plants, algae and bacteria in the environment. As part of natural biotic and chemical processes, NOM is ubiquitous in aquatic systems. NOM character depends on origin, transformation conditions and pathways which results in a vast variety in NOM chemical structure and properties (Sillanpää, 2015). NOM transformation processes in water and soil are biological processing (Kaiser and Kalbitz, 2012), photodegradation (Osburn et al., 2001) and mineral sorption (Jardine et al., 1989). These processes vary according to local climate and environmental conditions and may produce a broad scope of NOM compounds (Kellerman et al., 2014). Due to mixing of waterbodies with different NOM fingerprints, a variety of NOM may be found in natural environments, e.g. in groundwaters (McDonough et al., 2020a). Thus, different strategies have been used to cluster NOM with respect to their physical and chemical properties. A summary of established methods is shown in Table I-1 while a more detailed review is given in literature (Leenheer and Croué, 2003; Matilainen et al., 2011; Sillanpää et al., 2015). A well-established technique is the preparative dissolved organic carbon fractionation that classifies NOM depending on their chemical properties, i.e. hydrophobicity and acidity (Aiken et al., 1992; Leenheer, 1981; Thurman, 1985). This classification scheme is depicted in Figure 2-1.

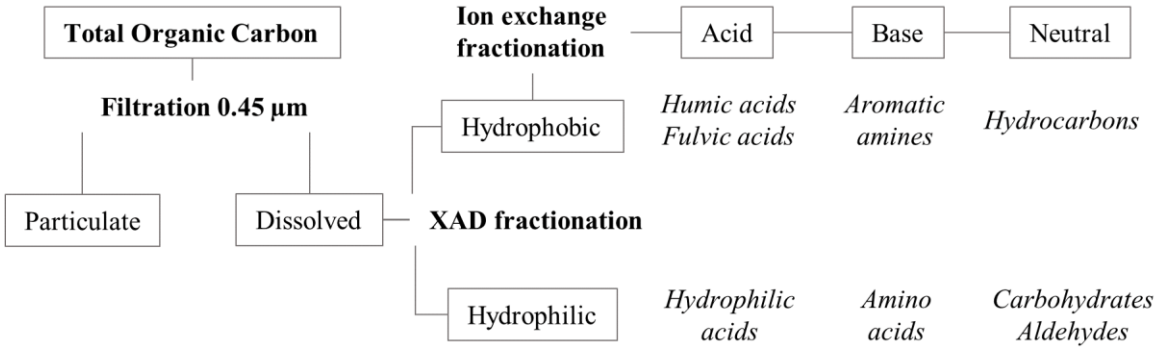

Figure 2-1. Dissolved organic carbon fractionation using XAD and ion exchange resins and examples for classification of different organic compounds (Leenheer, 1981; Leenheer and Croué, 2003; Swietlik et al., 2004)

Another frequent NOM classification method is the liquid chromatography-organic carbon detection (LC-OCD) method (Huber et al., 2011). The main fractionation parameter in this method is molecular size. LC-OCD analysis creates characteristic peaks which are used to quantitatively distinguish between different NOM fractions: biopolymers, humic substances e.g. fulvic and humic acids, building blocks, low molecular-weight acids and low molecular-weight neutrals (Table 2-1).

Table 2-1. LC-OCD fractions and their characteristics according to Huber et al. (2011). *Molecular weight of humic substances according to Thurman et al. (1982).

Fraction	Retention time	Description	Examples
Biopolymers	< 40 min	Hydrophilic, no ultraviolet light (UV) absorbance, molecular weight > 10 kg mol $^{-1}$	Proteins, polysaccharides
Humic substances	≈ 45 min	Hydrophobic, significant UV absorbance, molecular weight* 0.5–10 kg mol $^{-1}$	Humic acids, fulvic acids
Building Blocks	≈ 50–55 min	Breakdown products of humic substances with lower molecular weight	
Low molecular-weight acids	≈ 55 min	Coelution with small humic substances	Oxalic acid, malonic acid, acetic acid
Low molecular-weight neutrals	> 60 min	Hydrophilic or amphiphilic	Amino acids, alcohols, sugars, aldehydes, ketones
Hydrophobic organic carbon	> 120 min	Fraction that remains on the separation column within analysis time due to hydrophobic interaction	–

Features of NOM

Humic substances (HS), which comprise humic and fulvic acids, are the major NOM fraction that entail approximately 50–60 % of NOM found in natural waters (Frimmel, 1998; Thurman, 1985). Moreover, HS are the major driver for NOM visible light absorbance (Thurman, 1985) and may therefore require particular attention in groundwater decolorization. HS exhibit elemental composition roughly in the order C > O >> H > N > S (Sillanpää, 2015; Thurman, 1985). Molar weight of fulvic acids was reported in the range of 0.5–2 kg mol^{-1}. Humic acids are mainly in the range of 1–10 kg mol^{-1} (Thurman et al., 1982), but may also exhibit higher molecular weight (Peuravuori and Pihlaja, 1997). Thus, humic acids are more hydrophobic and aromatic than fulvic acids (Huber et al., 2011). HS contain various functional groups, such as phenolic, amino, carboxylic, methoxy, alcohol or carbonyl groups (Chen et al., 2002; Sillanpää, 2015). Phenolic and carboxylic groups may either be protonated (neutrally charged) or deprotonated (negatively charged) at typical drinking water pH values of 6–8 (Ritchie and Perdue, 2003). The charge of NOM affects their physical properties, e.g. light absorbance (Dryer et al., 2008; Yan et al., 2014), hydrodynamic diameter (Pace et al., 2012), and reactivity to oxidants (Mvula and von Sonntag, 2003).

HS exhibit unsaturated bonds which may extend to conjugated, electron-rich systems (“chromophores”). Irradiation of ultraviolet (UV) and, for highly conjugated material, also lower-energy visible light may induce electron transitions in chromophores. This results in a characteristic light absorbance spectrum of NOM in the UV-visible range (Mostofa et al., 2013). The absorbance spectrum of NOM is continuous and may be modeled by an exponential decay function with varying slope depending on the source of NOM (Twardowski et al., 2004). Chemical

NOM features may also be indicated by single-wavelengths measurements or absorbance ratios (Helms et al., 2008). It was shown that specific UV absorbance at 254 nm ($SUVA_{254}$) strongly correlates with the content of aromatic or unsaturated sp^2 hybridized carbon-carbon bonds in NOM (Weishaar et al., 2003). Moreover, the absorbance ratio at 254 and 365 nm (E2:E3) correlates negatively with aromaticity and molecular weight (Peuravuori and Pihlaja, 1997). This indicates that chromophores absorbing higher-wavelength light are both more unsaturated and larger. In larger chromophores, the scope of transition energies for intramolecular charge-transfer interactions is higher, resulting in increasing absorbance at higher wavelengths (Del Vecchio and Blough, 2004).

Redox properties of HS are quantified as electron donating capacity (EDC) or electron accepting capacity (EAC) (Aeschbacher et al., 2010). Major contributors to EDC are phenolic moieties while EAC was mainly related to quinonic moieties (Aeschbacher et al., 2012; Houska et al., 2021). HS contain EDC and EAC exhibiting moeities simultaneously. This renders HS prone to serve as electron donator or acceptor in various environmental redox processes. E.g., as antioxidant (Aeschbacher et al., 2012) or as electron acceptor in microbial processes (Walpen et al., 2018).

2.1.2 NOM in Groundwater Treatment

Prevalence of NOM in Groundwater

Groundwater dissolved organic carbon (DOC) concentrations were reported to exhibit a global median of 1.2 $mg_{DOC}\ L^{-1}$ (McDonough et al., 2020b). However, aquifers recharged by NOM-rich surface waters and those containing coal deposits can exhibit much higher concentrations of DOC (Thurman, 1985). Groundwater NOM of higher age and such that has been released from peat soil was described as more aromatic and biostable, while NOM formed in surface water has been described as more aliphatic and biolabile due to the impact of photodegradation (McDonough et al., 2020a). Despite broad variety in NOM composition between different groundwater bodies, humic substances often dominate the scope of NOM in groundwater (Rutlidge et al., 2021).

In Northern Germany, groundwater for drinking water production is often taken from aquifers with peat deposits. These waters are typically anaerobic which may result in the release of lignin-derived HS from peat deposits (Kölle, 2010). Dissolved organic carbon (DOC) concentrations of up to 10.5 $mg_{DOC}\ L^{-1}$, specific ultraviolet light (UV) absorption at 254 nm ($SUVA_{254}$) values of 2.6–4.1 $L\ mg_{DOC}^{-1}\ m^{-1}$ and significant color (spectral absorbance coefficient at 436 nm, SAC_{436} of 0.39–1.30 m^{-1}) were reported for drinking waters produced from organic-rich groundwaters in Northern Germany (Schulz, 2020). This is indicating a high content of condensed aromatic and chromophoric structures (Weishaar et al., 2003).

Conventional Groundwater Treatment

Common features of groundwater resources preferably used for drinking water production include low concentrations of particles and trace organic contaminants and low seasonal quality variance (Crittenden et al., 2012) as well as low pathogen concentrations (Payment and Locas, 2011). Due to anaerobic conditions in many groundwaters, reduced species such as ammonia (NH_4^+), manganese (Mn(II)), iron (Fe(II)), hydrogen sulfide (H_2S) and methane (CH_4) may be present in raw groundwaters for drinking water production, along with high carbon dioxide (CO_2) concentrations and absence of molecular oxygen (O_2) (Worch, 2019). These parameters can usually be controlled by conventional groundwater treatment comprised of gas exchange and sand filtration, as shown in Figure I-1. This treatment scheme may be complemented by disinfection or hardness adjustion. Advanced treatment steps such as coagulation, oxidation, activated carbon filtration, ion exchange or membrane filtration can often be omitted in groundwater treatment.

Effects of NOM on Groundwater Treatment and Quality

Humic substances interact with inorganic and organic compounds in groundwater and affect various processes in drinking water treatment. E.g., oxidation of Fe(II) by oxygen (Osterwald, 2009) as well as by other oxidants (Knocke et al., 1992) is hampered in the presence of NOM. In combination with Fe(III), NOM may form negatively charged colloidal structures with size of 3–200 nm for carbon/iron molar ratios > 1.4 (Liao et al., 2017), which applies for humic-rich groundwaters presented in this work and elsewhere (Schulz, 2020). Such colloids complicate sand filtration and may increase iron concentration and turbidity of treated water (Krupińska, 2020). In advanced groundwater treatment exceeding aeration and sand filtration, NOM may cause fouling resistance in membrane filtration (Lee et al., 2005), compete for adsorption sites with trace organic compounds in activated carbon adsorption (Matsui et al., 2003) and with arsenic in ferric hydroxide adsorption (Saldaña-Robles et al., 2018). In chlorine-based disinfection processes, toxic trihalomethanes are formed (Hua and Reckhow, 2007). Moreover, chromophoric, i.e. light-absorbing NOM moieties decrease the efficacy of UV disinfection (Crittenden et al., 2012).

In addition to its impact on groundwater treatment processes, NOM, especially humic substances, induce color in raw and treated water (Crittenden et al., 2012). Water color is often compared to the color standard platinum-cobalt solution and thus specified in the unit mg L^{-1} Pt or measured spectrophotometrically as spectral absorbance coefficient e.g. at 436 nm (Kölle, 2010). For unit conversion between platinum-cobalt solutions and spectral absorbance measurements, the correlation color = 18.216 * 2.303 SAC_{440} – 0.209 was suggested, with the color in mg L^{-1} Pt and the spectral absorbance coefficient at 440 nm (SAC_{440}) in m^{-1} (Cuthbert and del Giorgio, 1992). For conversion to absorbance at 436 nm (SAC_{436}), the correlation $SAC_{440} = SAC_{436}\ e^{[-S(440\ nm\ -\ 436\ nm)]}$ may be used. The spectral slope S depends on the type of NOM. A value of S = 0.01688 nm^{-1}, derived from Quebec lake water, was found to be in the

middle of reported literature values (Cuthbert and del Giorgio, 1992). Using this value for S, the correlation of SAC_{436} in m^{-1} and color in mg L^{-1} Pt is color = 39.2 * SAC_{436} – 0.209. A value of SAC_{436} = 0.5 m^{-1} would then translate into approximately 19.4 mg L^{-1} Pt.

Visible color of water is limited by drinking water regulations in various countries e.g. 20 mg L^{-1} Pt in England and Wales (Water Supply (Water Quality) Regulations, 2016), 15 mg L^{-1} Pt in the United States (National Secondary Drinking Water Regulations, 1979) or SAC_{436} of 0.5 m^{-1} (previously 20 mg L^{-1} Pt) in Germany (Trinkwasserverordnung, 2001).

Enhanced NOM Removal in Drinking Water Treatment

Due to its interaction with different processes, NOM is altered and removed during drinking water treatment from groundwater. Up to of 30 % of groundwater DOC content is removed by biodegradation and adsorption in sand filters for iron and manganese removal (Korth, 2000; Korth et al., 2001). Partial NOM removal was also observed in lime softening depending on operating conditions (Coro and Laha, 2001; Russell et al., 2009). To enhance NOM removal in drinking water treatment from groundwater and surface water, several strategies have been tested and reviewed (Andersson et al., 2020; Kämmler et al., 2021; Kastl et al., 2016; Krzeminski et al., 2019; Ødegaard et al., 2010). At high water recovery rate and relatively low costs, NOM, particularly humic substances can be removed by flocculation in combination with conventional or membrane filtration (Köhler et al., 2016; Schulz, 2020; Wricke et al., 2016). Oxidation by permanganate (Hidayah and Yeh, 2018; Kämmler et al., 2021; Lu et al., 2015), ozone (Loeb et al., 2012; Tan and Johnson, 2001) or advanced oxidation processes (AOP) (Sillanpää et al., 2018) was also tested, with focus on decolorization. If high NOM removal rates are required, nanofiltration (Beyer et al., 2014; Dubowski et al., 2018) and ion exchange (Edgar and Boyer, 2021; Grefte et al., 2013; Hu and Boyer, 2017; Levchuk et al., 2018; Schulz et al., 2017) have been proved successful. Moreover, various novel NOM removal techniques have been introduced at bench-scale, including electrocoagulation (Särkkä et al., 2015) and electrosorption (Mantel et al., 2021).

2.2 Aquatic Ozone Chemistry

2.2.1 Kinetics of Ozonation, Secondary Oxidants and Matrix Effects

Ozone is a strong oxidant (oxidation potential E_0 = 2.08 V; Crittenden et al., 2012) and reacts readily with various compounds in water. Due to its reactivity, ozone is not stable in water and must therefore be used right after production. The rate of ozone degradation depends on physical and chemical water quality parameters, such as temperature, pH, type and concentration of dissolved organic matter (DOM), alkalinity, concentration of reduced inorganic species and turbidity (Elovitz et al., 2000; Gardoni et al., 2012; Park et al., 2001; von Gunten, 2003a; Westerhoff et al., 1999). Reactions of ozone and the water matrix may produce secondary oxidants such as the hydroxyl radical (•OH) and the carbonate radical ($CO_3^{\bullet-}$).

Ozone decay in water is often modeled as a two-step process consisting of an initial rapid drop in ozone concentration and a second phase that underlies first-order exponential decay kinetics (Kwon et al., 2017; Westerhoff et al., 1999). Ozone decay in the first phase, often referred to as instantaneous or immediate ozone demand (IOD) phase, is governed by the reaction of ozone with fast-reacting NOM moieties, such as phenols (Buffle et al., 2006a; Cho et al., 2003). IOD reactions occur within few seconds after ozone dosage (Buffle et al., 2006b; Buffle et al., 2006a; Cho et al., 2003; Kwon et al., 2017; Nöthe et al., 2009). Due to experimental limitations, the IOD is usually quantified as a concentration difference between ozone starting concentration and ozone concentration measured in the first sample taken. The definition of the IOD by practical rather than chemical aspects complicates comparability of IOD values between different studies, which have been suggesting IOD sampling times of up to 1 min (Kämmler et al., 2022; Shin et al., 2016; Westerhoff et al., 1999).

The IOD phase of ozone decay is followed by a secondary phase which can be modeled as first-order exponential decay with respect to ozone, with the decay rate k_{sec} (Equation 2-1) (von Gunten, 2003a). An increase of k_{sec}, i.e. faster ozone decay, was observed for increasing temperature, pH, alkalinity (Elovitz et al., 2000) and $SUVA_{254}$ (Westerhoff et al., 1999) and for decreasing specific ozone dose (Kämmler et al., 2022; Kwon et al., 2017).

$$c_{O_3}(t) = c_{O_3,t_0} e^{-k_{sec}t} \qquad \text{Equation 2-1}$$

c_{O_3}	Concentration of dissolved ozone	mg L^{-1}
c_{O_3,t_0}	Initial concentration of dissolved ozone	mg L^{-1}
k_{sec}	First-order rate constant for ozone decay	s^{-1}

2.2.2 Hydroxyl Radical and R_{ct}

In the course of ozonation, a chain of reactions of ozone and the water matrix may consume ozone and produce •OH. The oxidative potentials of •OH and ozone in water may be described by the integration of their concentrations over time. These time integrals are referred to as the ozone and the •OH exposure (Equation 2-2, Equation 2-3). The ratio of •OH to ozone concentrations, R_c, or the time integral of R_c, R_{ct} (Equation 2-4), are often applied to quantify the contribution of •OH to total oxidant exposure in water treatment (Elovitz and von Gunten, 1999; Yong and Lin, 2012).

$$ct = \int_0^\infty c_{O_3}(t)dt$$ Equation 2-2

$$[\bullet OH]_{dt} = \int_0^\infty c_{\bullet OH}(t)dt$$ Equation 2-3

$$R_{ct} = \int_0^\infty R_c\, dt = \int_0^\infty \frac{c_{\bullet OH}(t)}{c_{O_3}(t)}dt = \frac{[\bullet OH]_{dt}}{ct}$$ Equation 2-4

ct	Ozone exposure	mg L^{-1} min
$[\bullet OH]_{dt}$	Hydroxyl radical exposure	mg L^{-1} min
R_{ct}	Ratio of hydroxyl radical and ozone exposures	–
R_c	Ratio of hydroxyl radical and ozone concentrations	–

In DOM-free water, •OH formation is initiated by the reaction of ozone with the hydroxyl ion (OH^-) (Equation 2-5) (Gottschalk et al., 2010). A high pH value, i.e. a high concentration of OH^-, increases both ozone consumption and •OH formation. The consumption of ozone and production of •OH proceeds in a radical chain reaction without further consumption of OH^-.

$$O_3 + OH^- \rightarrow O_2^{\bullet -} + HO_2^{\bullet}$$ Equation 2-5

Different water constituents affect ozone and •OH production and consumption in water. These compounds may be classified as initiators, promoters and inhibitors of ozone decay (Staehelin and Hoigne, 1985; Yong and Lin, 2012). Initiators would consume ozone and ultimately form •OH radicals. Inhibitors would consume •OH and thereby stop the radical chain reaction. Thus, the ratio of initiation to inhibition capacity of a water matrix is equal to R_{ct}. Promoters combine features of both initiators and inhibitors and would consume •OH to ultimately form another •OH. This enhances both ozone and •OH decay equally (Yong and Lin, 2012). Examples of initiators, promoters and inhibitors and their impact on ozone decay kinetics are introduced in Table 2-2.

Table 2-2. Initiator, promoter and inhibitor of ozone decay concept (adapted from Yong and Lin, 2012)

Class	Example	Ozone decay rate	Ozone exposure	•OH exposure	R_{ct}
Initiator	OH^-, DOM	+	–	+	+
Promoter	Methanol, DOM	+	–	–	± 0
Inhibitor	t-BuOH, HCO_3^-, DOM	–	+	–	–

DOM may be considered an initiator, a promoter and an inhibitor simultaneously, due to the presence of various functional groups (Buffle and von Gunten, 2006; Staehelin and Hoigne, 1985; Yong and Lin, 2012). The initiating and promoting roles of DOM are dominant in natural waters, as indicated by a significant increase in ozone decay in presence of various types of NOM (Westerhoff et al., 1999). The •OH yield from reactions of ozone with DOM increases

with phenol content of DOM (Önnby et al., 2018). DOM-induced •OH production may be comparable to an AOP in the ozonation of DOM-rich water (Buffle et al., 2006a). •OH production from reactions of ozone typically peaks in the initial phase of ozonation due to reactions of phenolic compounds with ozone. However, DOM moieties that produce •OH by reaction with ozone are continuously formed in ozonation (Nöthe et al., 2009; von Sonntag and von Gunten, 2012). Due to the high •OH exposure in the initial phase of ozonation, R_{ct} decreases with increasing reaction time of ozone (Qi et al., 2016; Wang et al., 2021b; Yu et al., 2020). Similarly, R_{ct} decreases with increasing specific ozone dose, due to depletion of fast-reacting NOM moieties with high •OH production (Zimmermann et al., 2011).

Initiation of ozone decomposition by OH^- and inhibition by HCO_3^- implies that pH and alkalinity of natural waters also affect R_{ct} (Elovitz et al., 2000). Moreover, reaction temperature affects ozone reaction kinetics. At lower temperature, ozone decay and therefore NOM-initiated •OH production are slowed down. This results in higher ozone exposure and lower R_{ct}.

An alternative approach in illustrating the oxidant ratio in water is the $R_{OH,O3}$ concept which normalizes •OH exposure based on the consumed amount ozone rather than based on ozone exposure (Kwon et al., 2017). In contrast to R_{ct}, $R_{OH.O3}$ is independent of temperature and ozone dose and may therefore be a feasible parameter to model ozonation.

2.2.3 Ozonation in combination with H_2O_2 dosage

Ozonation in combination with H_2O_2 dosage is a well established water treatment technique. The reaction of H_2O_2 with ozone may accelerate ozone consumption and therefore decrease ozone exposure while the •OH yield is increased. The reaction takes place via the deprotonated form of H_2O_2 (HO_2^-) and other intermediates, but may be summarized using Equation 2-6 (Crittenden et al., 2012; Wert et al., 2007). The specific effects of H_2O_2 on ozone and •OH exposure strongly depend on water matrix characteristics and specific ozone dose (Acero and von Gunten, 2001; Wang et al., 2018c). Due to high •OH yield in the application of ozone/H_2O_2, it is considered an advanced oxidation process (AOP).

$$H_2O_2 + 2\ O_3 \rightarrow 2\ \bullet OH + 3\ O_2 \qquad \text{Equation 2-6}$$

2.3 Ozonation of Dissolved Organic Matter

2.3.1 Reaction Mechanisms

Ozone is electrophilic and reacts with various natural and industrial organic compounds. The major ozone-reactive NOM fraction are humic substances (HS) (Bose et al., 1994). HS contain various electron-rich moieties that are prone to reaction with ozone. Aromatic compounds are accessible for oxidation especially if “activated”, i.e. substituted with functional groups that increase electron density in the aromatic system. These functional groups include methoxy (-O-CH_3), hydroxy (-OH) and amino (-NH_2) groups (Hoigné and Bader, 1983; Mvula et al.,

2009; von Sonntag and von Gunten, 2012). Non-aromatic compounds with unsaturated carbon-carbon bonds (sp^2-hybridized), e.g. β-diketones or olefins, may also react readily with ozone (Houska et al., 2021).

In HS, phenolic (-OH activated aromatic) moieties are the major fraction of fast-reacting moieties, which is indicated by a significant loss of EDC at low ozone doses (Chon et al., 2015; Walpen et al., 2020). Thus, phenols are often used as model compounds to study reactions of HS and ozone. A major initial reaction mechanism of ozone and phenols is an electrophilic addition of ozone to the aromatic ring (von Sonntag and von Gunten, 2012). Alternatively, phenols may transfer an electron to ozone, resulting in a phenoxyl and an ozonide radical and ultimately producing •OH. At low ozone to substrate (phenol) ratio, various stable reaction products of ozone and phenol are formed. These include hydroquinone, catechol, 1,4-benzoquinone and cis,cis-muconic acid (Mvula and von Sonntag, 2003). All of these compounds may further react with ozone to form smaller organic compounds, e.g. organic acids (Ramseier and von Gunten, 2009). These reactions include cleavage of aromatic rings in phenol structures, e.g. by the Criegee mechanism. In consequence, the aromatic character of phenols is lost, as indicated by a substantial decrease in ultraviolet light absorbance at 254 nm (UV_{254}) (Wenk et al., 2013).

Various secondary oxidants are formed in the ozonation of phenol, including high amounts of hydroxyl radicals (•OH) (Mvula and von Sonntag, 2003). The combination of fast ozonation of phenols and concomitant •OH production results in high •OH concentration in the in the initial phase of HS ozonation (Buffle et al., 2006a). Both ozone consumption and •OH production are continuing due to reaction with phenol intermediates, after depletion of initial phenol concentration (Nöthe et al., 2009).

2.3.2 Reactivity of NOM with Ozone

The potential of NOM to consume ozone is highly variable and depends on molecular NOM features, e.g. type of substituents (von Sonntag and von Gunten, 2012). Table 2-3 summarizes NOM features that affect its reactivity toward ozone. Some of the bulk parameters given in Table 2-3.a show good correlation with each other, e.g., $SUVA_{254}$ and aromaticity (Weishaar et al., 2003), $SUVA_{254}$ and EDC (Walpen et al., 2016) or unsaturation and aromaticity (Westerhoff et al., 1999). Consequently, these parameters show good agreement in their impact on ozone-NOM reactivity. More generally, reactivity of NOM toward ozone was correlated with high electron density and high energy level of the highest occupied molecular orbital (HOMO) of NOM, as shown in Table 2-3.b (Naumov and von Sonntag, 2010). Bulk parameters like pH value may also affect the reactivity of NOM toward ozone (Table 2-3.a). In conclusion, sterically accessible, electron-rich NOM moieties are prone to oxidation by ozone, due to its electrophilic behaviour (Naumov and von Sonntag, 2010).

Table 2-3. Parameters that affect reactivity of NOM toward ozone. **(a)** Bulk parameters, **(b)** molecular-level information

Feature	Effect	Mechanism	Reference
a. Bulk parameters			
High pH, highly negative Mulliken charge	+	Deprotonation of phenols, increased nucleophilicity due to high electron density	Mvula and von Sonntag (2003), Naumov and von Sonntag (2010)
High $SUVA_{254}$	+	Reaction of ozone with electron-rich carbon-carbon double bonds	(Westerhoff et al., 1999)
High aromaticity / phenol content / EDC	+	Fast reaction of ozone with phenols	Önnby et al. (2018)
Low oxidation state (O:C ratio), low saturation (H:C ratio)	+	Increase in carbon-carbon double bonds	These and Reemtsma (2005)
b. Molecular-level information			
High content of carboxylic groups	–	Sterical shielding	These and Reemtsma (2005)
Low Gibbs free energy of adduct formation	+	Increasingly exergonic reactions	Naumov and von Sonntag (2010)
High energy of the highest occupied molecular orbital (HOMO)	+	Decreasing energy separation between HOMO of the electron donor and lowest unoccupied molecular orbital (LUMO) of the acceptor (ozone)	Naumov and von Sonntag (2010)

2.3.3 Effects of Ozonation on DOM properties

Oxidation by ozone and secondary oxidants involved in ozonation affects the character of NOM in various ways. A summary of NOM transformation by ozonation is given in Table 2-4. As explained above, ozonation significantly transforms molecular structure of NOM (Table 2-4.a). Changes in NOM molecular structure severely depend on ozone dose, as primary oxidation products may further react with ozone if it is present in sufficient concentration (Ramseier and von Gunten, 2009). Molecular weight, elemental composition, chemical bonds and functional groups are altered by ozonation. Conversion of phenolic compounds to quinonic moieties results in a decrease of EDC (Önnby et al., 2018). Oxidation of double-bonds and decreasing aromaticity result in significant decrease of bulk optical parameters such as UV and visible light (UV-vis) absorbance and fluorescence (Table 2-4.b). Typically, the reduction in absorbance is more pronounced at higher wavelengths, as quinonic ozonation products may still exhibit UV absorbance (Nöthe et al., 2009). This results in an increased spectral slope and absorbance ratio at 254 and 365 nm (E2:E3) (Leresche et al., 2021; Wenk et al., 2013). NOM transformation is also reflected in physical and chemical NOM properties (Table 2-4.c). These properties are associated with changes in molecular NOM structure. E.g., bioavailability may be related to an increase in low molecular-weight acids and aldehydes content (Wert et al., 2007).

Table 2-4. Overview of ozonation effects on **(a)** molecular NOM structure, **(b)** bulk NOM parameters, **(c)** physical and chemical NOM properties

Parameter	Effect	Reference
a. Changes in molecular NOM structure		
Average molecular weight	–	Swietlik et al. (2004)
O:C ratio	+	Remucal et al. (2020)
Unsaturation (oxygen subtracted double bond equivalents per carbon)	–	Phungsai et al. (2019)
Low molecular-weight organic acids and aldehydes content	+	Hammes et al. (2006), Ramseier and von Gunten (2009), Wert et al. (2007)
Phenol content	–	Önnby et al. (2018)
Aromaticity	–	Wenk et al. (2013)
b. Effects on bulk NOM parameters		
UV-vis absorbance	–	Li et al. (2017), Nanaboina and Korshin (2010), Leresche et al. (2019)
Fluorescence	–	Baghoth et al. (2011), Stylianou et al. (2018a)
Spectral slope, E2:E3 ratio	+	Leresche et al. (2021), Wenk et al. (2013)
EDC	–	Chon et al. (2015), Walpen et al. (2020)
c. Changes in physical and chemical NOM properties		
Bioavailability	+	Audenaert et al. (2013), Ramseier et al. (2011)
Hydrophilicity	+	Swietlik et al. (2004), Bose et al. (1994)
Carboxylic acidity	+	Bose et al. (1994)

Compared to ozone, •OH is less selective toward aromatic NOM moieties and is able to oxidize more saturated structures (Phungsai et al., 2019). This results in increased overall number of reactive DOM moieties in the presence of •OH (Remucal et al., 2020). In contrast to ozone, reactivity of •OH with DOM is more uniform across different types of DOM (von Sonntag and von Gunten, 2012; Westerhoff et al., 2007). However, reactivity of •OH with non-isolated wastewater DOM was positively correlated to $SUVA_{254}$ (Rosario-Ortiz et al., 2008). Reaction products of DOM and •OH are similar to those formed by reaction with ozone. However, slight differences may be found in more hydroxylated (i.e., introduction of OH) and decarboxylated (i.e., abstraction of CO_2) compounds after reaction with •OH (Remucal et al., 2020). Ozone is consumed more slowly in presence of an •OH scavenger, which may result in enhanced absorbance removal especially at wavelengths > 315 nm (Wenk et al., 2013). However, aromatic compounds with small ozone reactivity may be oxidized by •OH and thereby become activated for further oxidation by ozone (Leresche et al., 2021).

DOM may also be transformed by the carbonate radical ($CO_3^{\bullet-}$) which is produced in the ozonation of bicarbonate-containing water. Similarly to ozone, $CO_3^{\bullet-}$ is selectively reacting with

phenolic and aromatic NOM moieties and able to decrease UV-vis absorbance of DOM (Canonica et al., 2005; Yan et al., 2019).

2.4 Formation and Minimization of Bromate and Other Ozonation By-products

Transformation of organic and inorganic water constituents by ozone alters their chemical composition, physical features and therefore their toxicity. Several ozonation by-products have been reported for the ozonation of drinking water. The formation of these by-products requires sufficient ozone dose and presence of precursors, e.g. bromide or phenolic DOM. In presence of bromide, bromo-organic compounds may be formed from reaction of bromine (mainly $BrOH/BrO^-$) with phenolic DOM moieties (Heeb et al., 2014; Westerhoff et al., 1998). The resulting bromo-organic compounds may increase the toxicity of treated water (von Gunten, 2003b; Wu et al., 2019). Some groundwater resources may exhibit high levels of *N,N*-dimethylsulfamide, a degradation product of the fungicide tolylfluanide. In the ozonation of these waters, high concentrations of the presumed human carcinogen *N*-nitrosodimethylamine are formed (Krasner et al., 2013; Schmidt and Brauch, 2008). The most important ozonation by-product in bromide-containing waters is bromate, which often requires control strategies (von Gunten, 2018; von Sonntag and von Gunten, 2012).

2.4.1 Bromate Toxicology and Legislation

Bromate is a presumed human carcinogen and therefore its maximum concentration is regulated in drinking water. An upper-bound excess cancer lifetime risk of 10^{-5} was assigned to 2 µg L^{-1} bromate, i.e. one additional tumor is assumed in 10^5 persons with lifelong exposure to a bromate drinking water concentration of 2 µg L^{-1} (WHO, 2005). The world health organizsation (WHO) set a provisional guideline value (PGV) of 10 µg L^{-1} for bromate, due to technological and analytical challenges with the lower value of 2 µg L^{-1} (WHO, 2017). The range of worldwide bromate drinking water limits is in between 5 and 25 µg L^{-1} (WHO, 2018). Many countries have adapted 10 µg L^{-1} as bromate drinking water limit, which is therefore used as benchmark in this work (EU, 1998; Trinkwasserverordnung, 2001; USEPA, 2009).

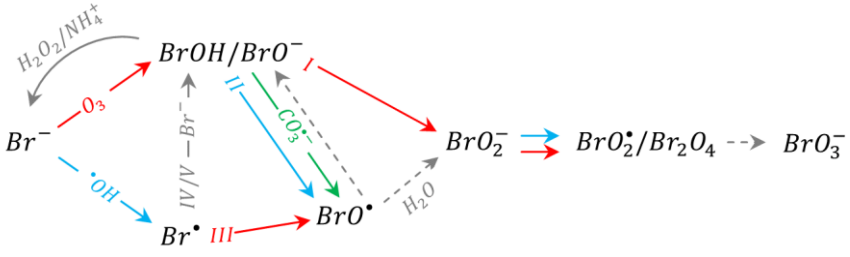

Figure 2-2. Bromate formation scheme according to Fischbacher et al. (2015), von Sonntag and von Gunten (2012) and von Gunten (2003b). Red arrows: oxidation by ozone. Blue arrows: oxidation by •OH. Major bromate formation pathways highlighted as I, II and III according to Song et al. (1997). I: direct; II: direct-indirect; III: indirect-direct. Bromate pathways IV and V indicate bromate formation by reduction of Br• and subsequent oxidation by ozone (IV) or •OH (V).

2.4.2 Formation of Bromate

The formation of bromate from bromide involves several steps and intermediate products. An overview of relevant reaction equations and rate constants is given in Table I-2. An overview on bromate formation pathways involving ozone, •OH and $CO_3^{\bullet-}$ is given in Figure 2-2. Initially, bromide must be oxidized by either ozone (direct oxidation) or •OH (indirect oxidation). Three major bromate formation pathways have been studied (Joshi et al., 2020; Song et al., 1997; Yang et al., 2019b). If bromide is directly oxidized by ozone in the first step, the intermediate BrOH/BrO^- may be oxidized by ozone, resulting in the direct bromate formation pathway (Figure 2-2, I). If BrOH/BrO^- is further oxidized by •OH, bromate formation occurs via the direct-indirect pathway (Figure 2-2, II). If bromide is initially oxidized by •OH, the intermediate Br• reacts with ozone to form BrO•, resulting in the indirect-direct bromate formation pathway (Figure 2-2, III). Br• may also be reduced by Br^-, partly producing BrOH in a cascade of reactions. This results in bromate formation pathways IV for BrOH/BrO^- oxidation by ozone or V for BrOH/BrO^- oxidation by •OH. The portion of bromate formed via these pathways, especially pathway IV, is minor but increases with bromide concentration (von Gunten, 2003b). Finally, all bromate formation pathways include the intermediate BrO_2^- which can be further oxidized by both ozone and the hydroxyl radical (Fischbacher et al., 2015). However, no attribution to a direct or indirect bromate formation pathway is commonly made for the oxidation of BrO_2^-. Figure 2-2 also highlights the impact of two bromate minimization strategies (H_2O_2 and NH_4^+ addition), which are discussed below.

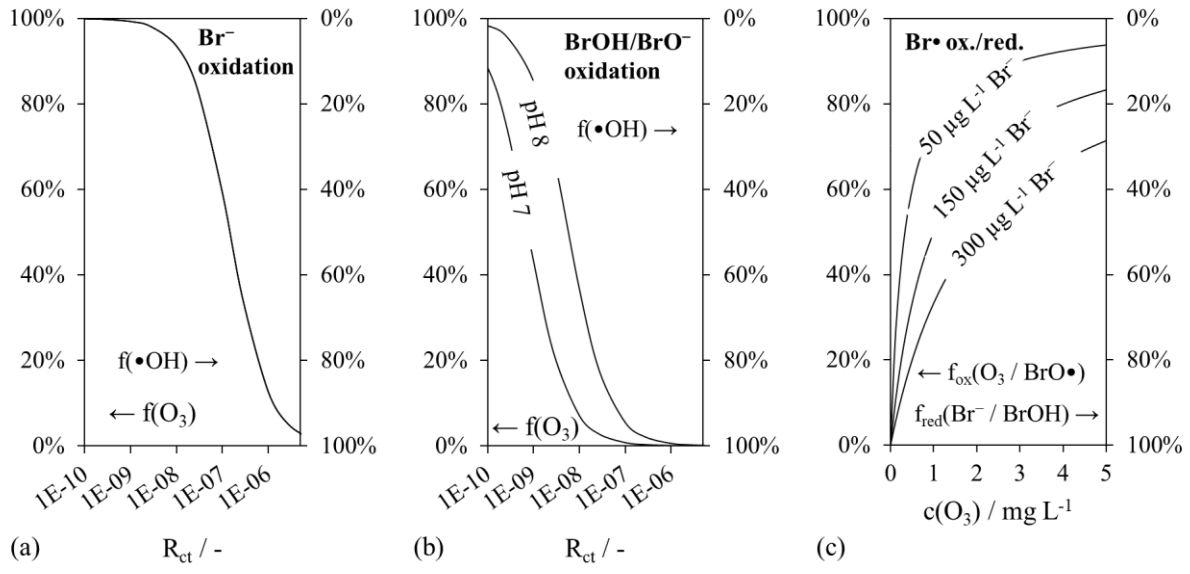

Figure 2-3. **(a)** Fractions of bromide oxidized by ozone, f(O_3), and by •OH, f(•OH). depending on R_{ct}.**(b)** Fractions of BrOH/BrO^- oxidized by ozone, f(O_3), and by •OH, f(•OH) relative to the total amount of BrOH/BrO^- oxidized by O_3 and •OH. **(c)** Fraction of Br• oxidized by O_3, f_{ox}(O_3 / BrO•) resulting in BrO• and fraction of Br• reduced by Br^-, f_{red}(Br^- / BrOH) resulting in BrOH relative to the total amount of Br• reacting with either O_3 or Br^-, depending on O_3 and Br^- concentrations. Fractions of Br• reduced by Br^-, but not resulting in BrOH were neglected. See Table I-2 for equations used.

The occurrence of bromate formation pathways depends on the concentrations of ozone, •OH and bromide. These are affected by ozonation and water matrix conditions, especially R_{ct} and pH. Based on the considerations of von Gunten (2003b), fractions of bromide (Br^-), bromine ($BrOH/BrO^-$) and Br• reacting with ozone, •OH and bromide were calculated for various concentration levels of relevant species. Calculation results are shown in Figure 2-3. Figure 2-3.a depicts the fractions of bromide reacting with ozone, $f(O_3)$ and the hydroxyl radical, f(•OH). Fractions are shown as a function of R_{ct}. R_{ct} values of $7 \cdot 10^{-10}$ to $4 \cdot 10^{-8}$ were reported for natural waters (Elovitz et al., 2000). Thus, for a wide range of water matrices, the oxidation of bromide by ozone dominates (Qi et al., 2016; Yu et al., 2020). However, R_{ct} may be significantly higher at low ozone doses or in the initial phase of ozonation (see section 2.2.1). After 350 ms reaction time, R_{ct} of approximately $2 \cdot 10^{-6}$ was measured (Buffle et al., 2006b). The large range of reported R_{ct} values results in calculated f(•OH) fractions of 0.5 % to 93 %. Especially at short reaction time, the indirect oxidation of bromide may be siginificant. Figure 2-3.b shows the oxidation of $BrOH/BrO^-$ to discriminate between direct $f(O_3)$ and direct-indirect f(•OH) bromate formation. Contribution of both oxidants may be expected for a range of pH values. At high R_{ct} values, i.e., high hydroxyl radical concentrations, f(•OH) may dominate. Figure 2-3.c shows the oxidation of Br• by ozone to BrO•, $f(O_3 \rightarrow BrO•)$ and the reduction by Br^- to BrOH $f(Br^- \rightarrow BrOH)$. The latter is only 1/6 of the Br• amount reduced by Br^- (Table I-2, Equation I-10).

For a specific example of water matrix conditions (pH 8, bromide 150 µg L^{-1}, dissolved ozone concentration 1.5 or 3 mg L^{-1}), fractions of bromate formation pathways discussed here are shown as function of R_{ct} in Figure I-2. Pathway II is dominating for a wide range of conditions, while pathway I becomes important at low R_{ct} values and pathway III at high R_{ct} values. Pathway IV contributes minimal bromate formation and pathway V is relevant at high R_{ct} values, similar to pathway III.

2.4.3 Bromate Minimization and Removal

Bromate has been identified as a problematic disinfection by-product in the early 1990s (Lim et al., 2022). Since then, several methods to abate bromate formation in ozonation processes have been reviewed for use in drinking water and wastewater treatment (Joshi et al., 2020; Soltermann et al., 2017; Song et al., 1997; von Gunten, 2003b; Yang et al., 2019b). The selective manipulation of reactions of ozone, •OH or bromate intermediates (mainly $BrOH/BrO^-$) has been tested by addition of different chemicals (Table 2-5.a). Ozonation in presence of H_2O_2 has been proposed, thereby turning the ozonation process into an AOP. This process is feasible if high •OH exposure is aspired, e.g. in micropollutant oxidation (Bourgin et al., 2017; Lekkerkerker-Teunissen et al., 2012). However, H_2O_2 addition may increase •OH-induced bromate formation, e.g. via the indirect-direct pathway (III) (Yu et al., 2020).

Table 2-5. Bromate minimization strategies in drinking water and wastewater treatment. Techniques, mechanisms and effects on bromate formation pathways (I – direct, II – direct-indirect, III – indirect-direct). **(a)** by dosing of chemicals. **(b)** by process optimization.

Technique	Mechanism	Pathways	Reference
a. Bromate minimization by addition of chemicals			
H_2O_2 addition	Reduction of ozone exposure (at increased •OH exposure), reduction of BrOH/BrO^- by H_2O_2	I, II	Bourgin et al. (2017), Lekkerkerker-Teunissen et al. (2012), von Gunten and Oliveras (1998)
pH reduction	Increasing protonation of BrOH/BrO^-, lower reaction rate of BrOH	I, II	Legube et al. (2004), Li et al. (2011), von Gunten (2003b)
NH_4^+ addition	Quenching of BrOH by NH_4^+	I, II	Pinkernell and von Gunten (2001), von Sonntag and von Gunten (2012)
HOCl + NH_4^+ addition	Quenching of BrOH by NH_4^+, quenching of •OH by NH_2Cl	I, II, III	Buffle et al. (2004)
NH_2Cl addition	Quenching of •OH by NH_2Cl	II, III	Ikehata et al. (2013)
b. Bromate minimization by process optimization			
Membrane ozonation with H_2O_2	Low transient dissolved ozone concentrations, ozone quenching by H_2O_2	n.a.	Merle et al. (2017)
Membrane ozonation without H_2O_2	Low dissolved ozone concentrations, ozone quenching by NOM	n.a.	Kämmler et al. (2022)
Optimization of contactor design	Reduction of ozone dosage	n.a.	Wols et al. (2010), Yang et al. (2017b)

Reduction of pH and addition of NH_4^+ both suppress bromate formation by slowing down the oxidation of BrOH/BrO^-. In case of pH reduction, BrOH is reacting slower than BrO^- with both ozone and •OH (von Gunten, 2003b). NH_4^+ quenches BrOH to form monobromamine (NH_2Br), which is then not available for further oxidation to bromate (von Sonntag and von Gunten, 2012). The direct-indirect bromate formation is not affected by NH_4^+ addition (Pinkernell and von Gunten, 2001). It was suggested to overcome this limitation by dosing NH_4^+ in combination with HOCl prior to ozonation (Buffle et al., 2004). This results in formation of NH_2Cl which exhibits high •OH scavenging potential. Bromate formation may therefore be suppressed via all three pathways in presence of NH_4^+ and HOCl.

Besides additional dosing effort, addition of other chemicals to an ozonation process is challenged by legal requirements and chemical effects that exceed suppression of bromate formation. The application of both NH_4^+ and NH_2Cl is currently restricted in Germany (Umweltbundesamt, 2021). NH_4^+ addition may decrease both bromate and organic bromine formation but increase formation of nitrogen-containing compounds with increased cytotoxicity (Wu et al., 2020). HOCl addition to water rich in DOM may produce toxic halo-organic compounds (von Sonntag and von Gunten, 2012). pH reduction and H_2O_2 addition affect the stabilities of

ozone and •OH. This may affect treatment goals and have complex effects on bromate formation (Ikehata et al., 2013; Tan et al., 1991; Yu et al., 2020).

Bromate formation may also be partly controlled by process optimization (Table 2-5.b). E.g., improved ozone distribution in reactors was observed to decrease ozone demand and thereby bromate formation (Yang et al., 2017b). Moreover, selective target compound removal over bromate formation was achieved by limiting dissolved ozone concentrations in membrane contactors, for both ozone/H_2O_2 (Merle et al., 2017) and ozone alone (Kämmler et al., 2022).

Bromate removal after formation has been reviewed as an alternative or in addition to bromate suppression strategies (Jahan et al., 2021; Xiao et al., 2017; Yang et al., 2019b). Proposed bromate removal techniques for drinking and wastewater treatment include ion exchange (Wiśniewski and Kabsch-Korbutowicz, 2010), chemical reduction (Gordon et al., 2002; Wang et al., 2018a), anaerobic microbial reduction (Liu et al., 2012; Wang et al., 2018b) or the reduction by fresh granular activated carbon (GAC) (Wang et al., 2021a; Yan et al., 2015). Among these techniques, the only process that is covered in literature on full-scale potable water treatment is GAC filtration. This post-treatment method may result in significant cost increase due to frequent reactivation requirements of GAC (Sobhani et al., 2012). Thus, the application of novel bromate suppression strategies remains important to improve the overall performance of ozonation processes.

2.5 Membrane Ozonation

2.5.1 Characteristics and Applications of Membrane Ozonation

Membrane ozonation is an ozone injection technology that may be used alternatively to established techniques, e.g. venturi injection or the use of bubble columns. Liquid and gas side are separated by a membrane, which allows the independent operation of their flow rates and prevents bubble formation (Figure 2-4.a). Further advantages of membrane ozonation include high specific surface area and compact design, modular design with high scale-up potential and the opportunity for off-gas recycling (Gottschalk et al., 2010; Schmitt et al., 2020). For specific operational conditions, bromate formation could be reduced in membrane ozonation, compared to batch experiments (Kämmler et al., 2022; Merle et al., 2017). These advantages of membrane ozonation need to outweigh possible disadvantages, which are mainly related to high costs and energy demand (Gottschalk et al., 2010). Despite the viability of membrane ozonation to treat drinking water was shown in laboratory studies (Jansen, 2005; Leiknes et al., 2005; Stylianou et al., 2018b; Zoumpouli, 2021), its large-scale implementation lacks coverage in literature (Bein et al., 2020).

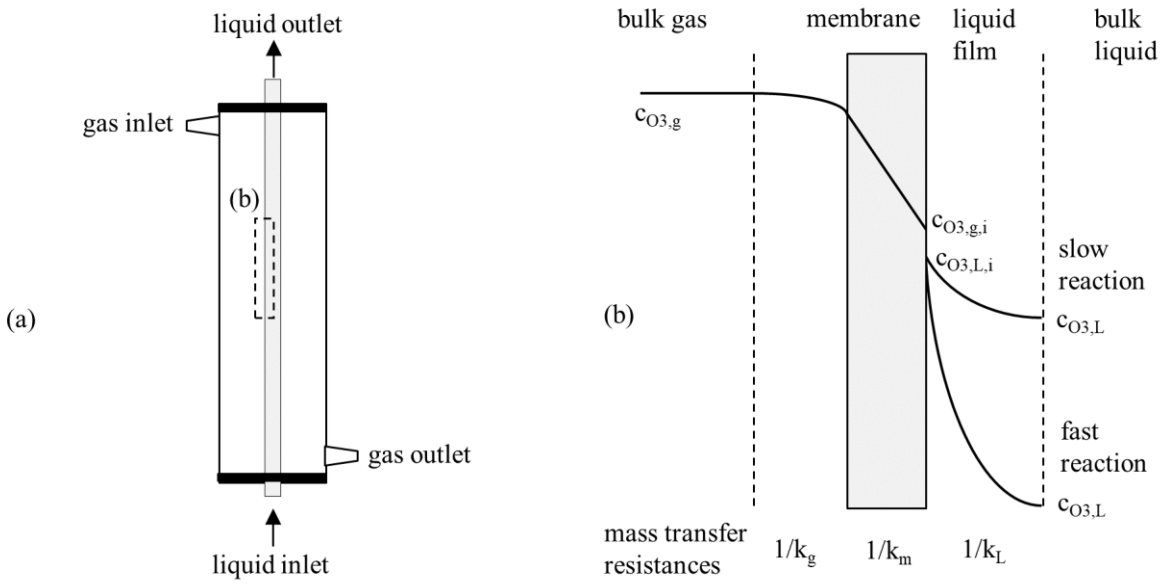

Figure 2-4. **(a)** Scheme of membrane ozonation in a single-tube contactor. **(b)** Scheme of ozone mass transfer with chemical reaction in a membrane tube. Abbreviations: $c_{O3,g}$: bulk ozone gas concentration; $c_{O3,g,i}$: interface ozone gas concentration; $c_{O3,L,i}$: interface ozone liquid concentration; $c_{O3,L}$: bulk ozone liquid concentration. Scheme adapted from Bein et al. (2020)

2.5.2 Mass Transfer in Membrane Ozonation

In membrane ozonation, Ozone has to overcome three major mass transfer resistances to dissolve in water (Figure 2-4.b): gas-side resistance (coefficient k_g), membrane resistance (coefficient k_m) and liquid-side resistance (coefficient k_L). Gas-side resistance is usually of minor importance (Berry et al., 2017). Membrane resistance depends hugely on the membrane material and thickness. While membranes made from porous polytetrafluoroethylene (PTFE) exhibit low mass transfer resistance, mass transfer in non-porous polydimethylsiloxane (PDMS) may be signicantly affected by membrane resistance (Bein et al., 2020). The driving force for ozone dissolution in water is the difference between Henry equilibrium and actual ozone concentration (Equation I-11). Ozone mass-transfer on the liquid side is the limiting step for many membrane ozonation applications (Pines et al., 2005). Different models have been applied to model ozone mass transfer at the gas-liquid interface in membrane contactors, including the surface renewal model, the penetration model and the film model (Jansen et al., 2005; Phattaranawik et al., 2005). The film model was developed by Lewis and Whitman (1924). The film theory assumes that bulk gas and bulk liquid are well-mixed. Gas and liquid are separated by thin films which are not part of bulk media. Mass transfer within the films is controlled by diffusion. Thus, it depends on film thickness.

Ozone mass transfer in the liquid film may occur concomitantly with chemical reaction, which is the case for membrane ozonation. The film model allows analytical determination of reaction conditions in the liquid film (Beltrán, 1995). The dimensionless Hatta number (Ha, Equation 2-7) is the ratio of ozone consumption rate to ozone mass transfer rate in the liquid film. With increasing Ha, the rate of ozone consumed in the liquid film to the rate of ozone transferred to

the bulk liquid increases (Charpentier, 1981). The liquid-side ozone mass transfer coefficient, k_L depends on flow-dynamic conditions in membrane ozonation. k_L and therefore overall mass transfer rate in membrane ozonation may be increased by increasing the liquid-side flow velocity (Zoumpouli et al., 2018).

$$Ha = \sqrt{\frac{d_L^2\, k_{sec}}{D_{O_3}}} = \frac{\sqrt{D_{O_3}\, k_{sec}}}{k_L}$$ Equation 2-7

d_L	Liquid film thickness	m
Ha	Hatta number	–
D_{O_3}	Diffusion coefficient of ozone in water	$m^2\ s^{-1}$
k_{sec}	First-order rate constant for ozone decay	s^{-1}
k_L	Liquid-side ozone mass transfer coefficient	$m\ s^{-1}$

2.6 Application of Ozonation-Biofiltration in Drinking Water Treatment

2.6.1 Ozone Applications

The use of ozone for drinking water treatment has been established for multiple purposes, as reviewed in detail elsewhere (Jekel, 2010; Lim et al., 2022; Loeb et al., 2012; von Gunten, 2018). In surface water treatment, ozonation was suggested used to improve coagulation and conventional filtration performance (Sadrnourmohamadi and Gorczyca, 2015; Winzenbacher, 2000) or to mitigate NOM-induced membrane fouling (Yu et al., 2018). Ozone was also suggested to reduce disinfection by-product formation potential in subsequent chlorine disinfection (De Vera et al., 2015; Rougé et al., 2020; Tubić et al., 2011) or as a disinfectant itself (Ding et al., 2019; Li et al., 2018). Ozone was applied to oxidize inorganic compounds such as Mn(II) (Gregory and Carlson, 2001) and to enhance biodegradation of trace organic contaminants (Gulde et al., 2021; Liu et al., 2021; Zoumpouli et al., 2019). The capacity of ozone to oxidize organic water constituents is frequently exploited to control sensory characteristics of water such as taste and odor (Beniwal et al., 2018; Fakioglu et al., 2021). Color removal by ozone has been established for the treatment of surface water (Krzeminski et al., 2019; Ødegaard et al., 2010). Moreover, color was succesfully removed (removal rate > 70 %) from groundwater in bench, pilot and full-scale studies (Table 2-6). However, the application of ozone in groundwater treatment may result in significant formation of the oxidation by-product bromate, which requires bromate minimization or removal strategies (Ikehata et al., 2013; Sobhani et al., 2012; Tyrovola and Diamadopoulos, 2005).

2.6.2 Biofiltration of Ozonated Water

The oxidation of NOM by ozone and secondary oxidants increases the concentration of biodegradable organic compounds. These compounds may be quantified as assimilable organic carbon (AOC) or biodegradable organic carbon (BDOC) and may enhance biological growth in drinking water distribution systems (Park et al., 2016; Ramseier et al., 2011).

Table 2-6. Case studies on ground•water decolorization by ozone

Plant type	Ozone dose / mg_{O3}/mg_{DOC}	Color removal	Bromate formation	Reference
Full-scale	3.8	92 %[1]	n.a.	Tan and Johnson (2001)
Pilot-scale	1–1.8	70–83 %	n.a.	Rittmann et al. (2002)
Full-scale	≈ 1	95 %	6 µg L^{-1} (use of catalytic carbon)	Sobhani et al. (2012)
Bench-scale	0.74	73 %	63 µg L^{-1} (w/o reduction strategy)	Ikehata et al. (2013)

Ozonation may also produce toxic, but biodegradable transformation products of trace organic contaminants, if present in raw water (Gulde et al., 2021; Zoumpouli et al., 2019). Thus, ozonation requires biological post-treatment to remove biodegradable compounds before drinking water distribution. The post-treatment step is often performed by biological filters (biofilters), which are convenient to operate. Biofilters allow establishment of high bacteria concentrations that are able to utilize biodegradable ozonation products efficiently (Lautenschlager et al., 2014).

Various studies on the effects of biofiltration on the quality of ozonated water have been made (Table 2-7). These effects include significant reduction of AOC, BDOC and DOC and small reduction in color. Moreover, biofiltration of ozonated water reduces the disinfection by-product formation potential in subsequent chlorination (De Vera et al., 2016). A comprehensive overview of the effects of biofiltration on ozonated drinking water is also given in Terry and Summers (2018).

AOC removal in ozonated water by biofiltration is often incomplete (Table 2-7). Especially slowly biodegradable DOC may remain in ozonated drinking water after biofiltration (Yavich et al., 2004). This may decrease the microbiological quality of ozonated-biofiltered water (van der Kooij et al., 1989).

Ozonation-biofiltration affects the bacterial composition of drinking water. Most bacteria abundant in raw water are inactivated by ozone. Bacterial composition of biofilter effluent waters therefore depends on bacterial composition within the biofilters (Lautenschlager et al., 2014). Due to high substrate availability in ozonated water, ozonation-biofiltration effluents may exhibit high bacterial cell counts (van der Kooij et al., 1989).

2.7 Gaps in Knowledge

As depicted in the previous chapters, effects of ozone on organic and inorganic water constituents have been intensively studied both in a general way and for specific compounds. However, theoretical application of these findings to complex natural water matrices is limited due to manifold interaction between water constitutents and the variety of NOM itself and must therefore be supplemented with empirical data. Moreover, reaction mechanisms hugely depend on the applied ozone dose and thus on the specific treatment target. The specific ozone application

of decolorization of groundwaters was tested in single-case studies, however with different outcomings regarding ozone dose, biological post-treatment effectivity and bromate formation (Table 2-6). To address these uncertainties, a comprehensive examination of ozonation-biofiltration to treat colored groundwater was done using different Northern German groundwater matrices, dosing methods and points, and bromate minimization strategies.

Table 2-7. Case studies on biofiltration of ozonated water. *Review paper

Water Matrix	Ozone dose / mg_{O3}/mg_{DOC}	Filter material	EBCT / min	Target compound / removal	Reference
Various 10–20 °C	n.a.	Various	10 (mean)	TOC 13 % (n = 32, median)	Terry and Summers (2018)*
2.9 mg_{DOC} L^{-1} 22 °C	1–1.8	Sand, GAC or anthracite	6–9	DOC 3–31 %	Rittmann et al. (2002)
2.5 mg_{DOC} L^{-1} 14±9 °C	n.a.	GAC operated for > 2 years	10.8	DOC 10–17 %	Liu et al. (2020)
4.7 mg_{DOC} L^{-1}	3.8	GAC	9	DOC 15 %, AOC 58 %	Tan and Johnson (2001)
4–5 mg_{DOC} L^{-1} 10–12 °C	0.5–1.2	Polyethylene carriers, expanded clay	6.2–48	Aldehydes, acetone, ketoacids > 80 %	Melin and Ødegaard (2000)
5.5 mg_{DOC} L^{-1} 10 °C	0.55	GAC + Sand	n.a.	AOC 59 %	van der Kooij et al. (1989)
≈ 2 mg_{DOC} L^{-1} 12 °C	≈ 0.7	GAC+Sand	n.a.	AOC 51 %	van der Kooij et al. (1989)
≈ 4 mg_{DOC} L^{-1}	≈ 0.25	Anthracite + sand	38	AOC 56 % (> 10 °C), 40 % ($\vartheta \leq 10$ °C)	Pharand et al. (2015)

3 Materials and Methods

3.1 Water Samples

Five natural groundwaters with elevated NOM content were used for the experiments conducted within this work. Groundwater samples stemmed from groundwater treatment plants in Northern Germany. Groundwater treatment plants A and C are rather small facilities on islands which use freshwater lenses as water resource. At these plants, water is mainly taken from rather small depths of < 15 m. Groundwater treatment plants B, D and E are located onshore and use groundwater mainly from higher depths, but also from shallow riverbank filtrate wells. An overview of processes used for the treatment of the groundwaters presented here is given in Table 3-1. All treatment plants use different gas exchange, sand filtration and deacidification steps for uptake of oxygen, removal of reduced species (e.g. CH_4, H_2S, Mn(II), Fe(II), NH_4^+) and pH adjustion. In addition, groundwater A is treated by coagulation with < 0.5 mg L^{-1} Al^{3+} for enhanced turbidity removal and by UV light for disinfection (Figure II-1). Groundwater E is flocculated with $Ca(OH)_2$ to reduce the high iron concentration of approximately 11 mg L^{-1} prior to filtration (Figure II-2).

Table 3-2 shows exemplary water quality analyses for the groundwater samples used in this study. Samples for water characterization and batch experiments were taken from the finished water reservoirs of the plants, i.e. after full treatment. The water samples exhibited high total organic carbon (TOC) concentrations of 3.5–6.1 mg L^{-1}, high specific UV absorbance values at 254 nm ($SUVA_{254}$) of 2.7–4.1 and variable specific spectral absorbance coefficient at 436 nm ($SSAC_{436}$) values of 0.09–0.34.

Table 3-1. Groundwater treatment plant information. GW – groundwater. *Advanced treatment implies processes exceeding gas exchange, sand filtration and deacidification

Groundwater	**A**	**B**	**C**	**D**	**E**
Treatment capacity / m^3 d^{-1}	1,200	120,000	4,800	14,000	12,000
Water resource	freshwater lense	GW + riverbank filtrate	freshwater lense	GW + riverbank filtrate	GW
Filter stages	1	1	2	2	2
Filter velocity / m h^{-1}	0.7–4.3	2–3	1.5-4	8–11 / 1.3–1.8	9.3–11
Advanced treatment steps	< 0,5 mg L^{-1} Al^{3+}, UV light	–	–	–	$Ca(OH)_2$ + polymer

Table 3-2. Water quality of groundwaters tested (samples taken from finished water reservoir after full treatment). Abbreviations: EC_{25} – electrical conductivity at 25 °C, $SSAC_{436}$ – specific spectral absorbance coefficient at 436 nm (SAC_{436}/DOC)

Groundwater	**A**	**B**	**C**	**D**	**E**
pH / -	7.8	7.6	8.0	7.7	7.8
EC_{25} / µS cm^{-1}	623	685	447	526	263
Total $alkalinity_{pH\ 4.3}$ / mmol L^{-1}	2.7	4.1	2.4	2.9	1.7
TOC / mg L^{-1}	4.8	5.2	3.5	6.2	6.1
DOC / mg L^{-1}	4.5	5.1	3.5	6.1	6.1
UV_{254} / m^{-1}	16.7	14.0	15.1	19.1	16.5
SAC_{436} / m^{-1}	0.90	0.41	1.20	0.64	0.54
$SUVA_{254}$ / L mg^{-1} m^{-1}	3.7	2.7	4.3	3.1	2.7
$SSAC_{436}$ / L mg^{-1} m^{-1}	0.2	0.08	0.34	0.10	0.09
UV_{254}/SAC_{436} / -	19	34	13	30	31
Iron / mg L^{-1}	<0.02	<0.03	0.06	0.01	0.10
Bromide / µg L^{-1}	330	110	180	70	90
Chloride / mg·L^{-1}	96	47	51	25	24
Nitrate / mg L^{-1}	3	3	2	1	4
Sulfate / mg L^{-1}	22	71	12	82	1

The concentration of particulate organic carbon (POC) in the treated groundwater samples was low. This is indicated by the small concentration differences between TOC and dissolved organic carbon (DOC) (Table 3-2, Figure II-3.a). The organic matrix in the groundwaters used here was further analysed by LC-OCD (see below for method description). Humic substances (HS) were the major NOM fraction found in the groundwaters with 59±4 % of the DOC concentration (Figure II-3.b). LC-OCD analysis of groundwater E was performed, succeeded by absorbance measurements at 254 and 436 nm and fluorescence emission measurement at 380 nm (Figure II-4). Absorbance was mainly induced by HS. Absorbance at 436 nm, i.e. color, showed a shift to smaller retention time, compared to the DOC peak. This indicates the preferred contribution of larger molecular weight HS to chromophoric structures and may be explained by more possible charge-transfer interactions between electron-donating and accepting HS moieties in larger molecules (Del Vecchio and Blough, 2004).

Organic water parameters were only slightly affected by the treatment applied to groundwaters presented here. Mean SAC_{436} removal was 3 % (-18–13 %, Figure II-5.a). Mean UV_{254} removal was 11 % (2–26 %, Figure II-5.b). Mean TOC removal was 10 % (3–21 %). TOC removal was therefore comparable to results of Korth (2000), who reported 7–27 % TOC abatement in conventional groundwater treatment.

3.2 Experimental Setups and Methods

3.2.1 Laboratory Batch Experiments

Experimental Setups

Two experimental setups were used to perform batch ozonation experiments (Figure 3-1). The first setup (Figure 3-1.a) was used for batch equilbrium experiments and consisted of a regular glass bottle containing a groundwater sample on a magnetic stirrer. For ozone stock solution addition, a 20 mL polypropylene/polyethylene syringe (Injekt Solo, B. Braun, Melsungen, DE) or a 60 mL model (HENKE-JECT, Henke Sass Wolf, Tuttlingen, DE) were used and connected to a polytetrafluoroethylene (PTFE) tube to enable submerged ozone dosing. After dosing, the bottle cap was remounted on the bottle. This setup allowed ozonation of multiple samples within short time as a sufficient number of sample bottles was available. The second setup (Figure 3-1.b) was used for batch kinetic experiments. It used a glass bottle with a side-socket, a PTFE septum, a needle (Sterican, B. Braun, Melsungen, DE) and a ball valve to dose ozone without removal of the bottle cap. Instead of a regular bottle cap, a commercial lab dispenser (Dispensette, Brand, Wertheim, DE) was mounted onto the sample bottle. The dispenser head was adjusted to a fixed volume (usually 3 mL) to allow withdrawal of consistent sample volumes. A PTFE tube was attached to the dispenser outlet to allow submerged dosing of ozone into prepared sampling vials.

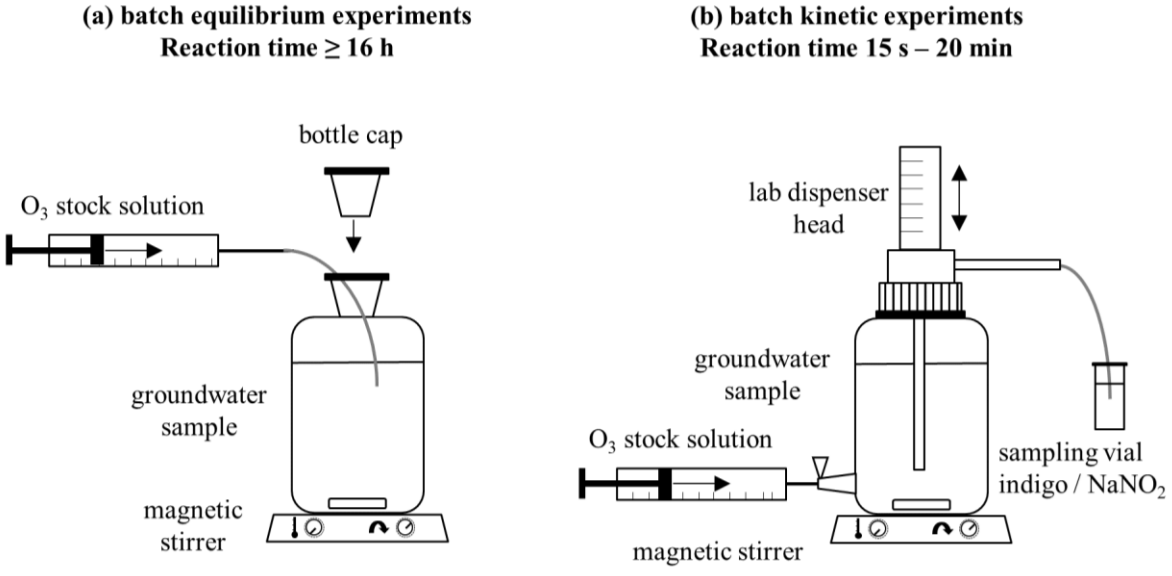

Figure 3-1. Experimental setups for batch ozonation experiments. **(a)** batch equilibrium setup, **(b)** batch kinetic setup.

Experimental Methods

Batch equilibrium experiments (Figure 3-1.a) were done at room temperature (≈ 20 °C). Groundwaters A, B, C, D and E (Table 3-2) were used for the experiments. Groundwater samples were taken out of the fridge at least some hours before experiments to allow adaptation to room temperature. Ozone stock solution was also prepared at room temperature (see below), yielding dissolved ozone concentrations of ≈ 15 mg L^{-1}. Groundwater sample volumes were between 170 and 200 mL, in 250 mL flasks. Groundwater C volume was 400 mL, in 500 mL flasks. Ozone was dosed to water samples at specific ozone doses of 0.1–1.0 mg_{O3}/mg_{TOC}. This resulted in varying total liquid volumes and dilution factors in the groundwater samples, with a maximum factor of approximately 1.4. Analytical results were multiplied with the individual dilution factors of the samples to improve their comparability. The ozone stock solution dosing time was up to approximately 30 s, depending on the stock solution volume required. Dosing was realized with the sample on the magnetic stirrer, which was set to moderately fast stirring speed. The sample was taken from the stirrer after approximately 30 s, and the next sample was ozonated. Experiments were usually done in triplicates. The samples were analyzed for TOC, UV_{254}, SAC_{436}, bromate concentration and LC-OCD. TOC, LC-OCD, UV_{254} and SAC_{436} measurements took place usually on the day after experimental procedure, which resulted in reaction times of at least 16–24 h. Complete ozone decay was assured by these reaction times and confirmed by the absence of characteristic ozone smell when opening sample bottles. Bromate measurements were done usually some weeks after the experiments. In between, samples were stored in closed bottles in the fridge. For batch experiments with some of the groundwaters presented here, additional information on materials and methods may be found in the original reference (groundwater C: Preda, 2019; groundwater D: Specker, 2019; groundwater E: Sellmann, 2020).

In addition to regular ozonation experiments, further ozonation experiments were performed with dosing of H_2O_2, right before ozone addition, to groundwater samples. Ozone/H_2O_2 experiments with groundwater A were performed at 0.25, 0.5 and 1.0 mg_{O3}/mg_{DOC} and H_2O_2/O_3 molar ratios of 0.5 and 2 mol_{H2O2}/mol_{O3} (Eberhard, 2021). These experiments were performed in an adapted form of the batch equilibrium experiments. After ozone addition, the sample flasks were opened at pre-defined time intervals (0.5, 1.5, 5, 30, 60 and 120 min, 1 d and 7 d) and aliquots for analysis were taken with a regular adjustable pipette (polypropylene tip) and immediately analyzed without further quenching. Analytical parameters were H_2O_2, SAC_{436} and dissolved ozone (see below for analytical procedures). After completion of reaction, i.e. > 7 d, bromate was determined in the samples. Further ozone/H_2O_2 experiments were performed with groundwater C (Preda, 2019) and groundwater E. No H_2O_2 or dissolved ozone measurements were made in these experiments and only one sample after complete ozone depletion (> 4 h) was analyzed. Specific ozone doses were fixed at 0.8 mg_{O3}/mg_{TOC} (groundwater C) or 1.14 mg_{O3}/mg_{TOC} (groundwater E). H_2O_2 was added at doses of 0.25, 0.5, 1, 2 and 5 mol_{H2O2}/mol_{O3}.

Groundwater C was also ozonated at varied pH (Preda, 2019). The sample pH was adjusted with 0.1 M HCl and 0.1 M NaOH, right before conduction of the experiment. Additional experiments with groundwater C (0.1–1.0 mg_{O3}/mg_{TOC}) were conducted at reduced sample temperatures of 8–10 °C and ozone stock solution temperatures of 12–15 °C, resulting in reaction temperatures of 10–11 °C (Preda, 2019). Multi-stage ozonation experiments were conducted with groundwater C (Preda, 2019). The specific ozone dose of 0.8 mg_{O3}/mg_{TOC} was split into 1, 2, 3, 4 or 5 aliquots, to mimic the equivalent number of ozonation stages. The aliquots were dosed to groundwater C in time intervals of 10±1 min to allow complete ozone decay before dosage of the next aliquot.

Batch kinetic experiments were performed using the setup depicted in Figure 3-1.b. These experiments were made to determine transient concentrations of ozone and other relevant species, before complete ozone consumption. Batch kinetic experiments were done with groundwater E to study reaction kinetics of ozone (Kämmler et al., 2022) and with groundwater A, at various total alkalinities (Bharadwaj, 2022). Ozone was added by submerged dosing to avoid ozone loss. The magnetic stirrer was applied for 30 s and then switched off. Sample volumes for batch kinetic experiments were chosen with respect to minimization of headspace and ozone volatilization. Only little ozone loss and decay were observed in a H_3PO_4 solution at pH 2, if stirring was stopped 30 s after ozone dosage (Figure II-7). Thus, it was assumed for simplification that ozone loss in the sample was entirely due to reaction with the water matrix. To determine transient ozone concentrations in the samples, indigo working solutions were prepared in 20 mL glass vials, with a volume of indigo stock solution + phosphate buffer + ultrapure water of 7 mL. The sample volume was set to 3 mL to obtain a final volume of 10 mL. Before withdrawal of every sample, the dispenser was rinsed twice to remove residual liquid from previous samplings. Indigo blind samples were obtained from the dispenser, with the exact volume as ozone-containing samples, but before ozone dosage. Molar absorbance coefficient of indigo for batch kinetic experiments with groundwater E was determined as 24787 M^{-1} cm^{-1}. This factor was determined by linear calibration according to DIN 38408-3 (2011). Ozone concentration measured by UV absorbance at 260 nm (molar absorbance coefficient of 3200 M^{-1} cm^{-1}, von Sonntag and von Gunten, 2012) was used as reference for indigo calibration. Absorbance coefficient for batch kinetic experiments with groundwater A was determined equivalently as 20870 M^{-1} cm^{-1} (Bharadwaj, 2022). The initial ozone concentration in batch kinetic experiments was determined from UV measurements at 260 nm, with the same procedure as described for batch equilibrium experiments.

In experiments with groundwater A, a second sampling vial filled with 6 mL of 8 mg L^{-1} sodium nitrite ($NaNO_2$) solution was used to quench ozone. Nitrite exhibits fast reaction rate with ozone ($k_{O3,NO2^-} = 3.7 \cdot 10^5$ M^{-1} s^{-1}, von Gunten, 2003a). $NaNO_2$ samples were taken right after ozone samples with a sample volume of 3 mL. $NaNO_2$-quenched samples were used for transient UV_{254}, SAC_{436} and bromate measurements. After completion of ozone decay, a non-quenched

sample was taken to determine UV_{254}, SAC_{436} and bromate and compared to quenched samples. $NaNO_2$-Samples were partly diluted in the analysis process (factor 3 for UV_{254} and SAC_{436} and factor 6 for bromate analysis). Results were multiplied with these dilution factors to allow comparison to non-quenched samples. Batch kinetic experiments were performed in duplicates.

Natural Groundwater Samples for Batch Experiments

Most batch experiments in this study were performed with the groundwater samples listed in Table 3-2. Batches of groundwater A and groundwater E with slight quality variation were used in some experiments with hydrogen peroxide (H_2O_2) (chapter 4.4) and under varied alkalinity and pH (chapter 4.3). Water quality of these samples is listed in the supplemental materials and methods (Table II-1 and Table II-2). Groundwater samples were sampled directly at the water treatment plants in 30 L batches and stored in the fridge after sampling. Experiments were performed several weeks after sampling. Stability of water quality was confirmed by regular analyses of TOC concentration, SAC_{436} and conductivity.

Materials and Chemicals

Ozone for batch experiments was produced from oxygen and dissolved in ultrapure water to obtain an ozone stock solution. The setup for ozone stock solution production was adapted from Zappatini and Götz (2015) and is shown in Figure II-6. An oxygen flow rate of 40–60 L h^{-1} was fed into an ozone generator (model 301.7, Sander, Uetze-Elze, DE). The ozone feed gas concentration was not measured but may be approximated as up to 100 g m^{-3} according to manufacturer's information. Polytetrafluoroethylene (PTFE) and partly silicone tubings were used for ozone gas transport. The ozone/oxygen mixture was washed in a glass bottle containing a buffer of 6 mM Na_2HPO_4 and 44 mM NaH_2PO_4 dissolved in ultrapure water to remove potential NO_x contamination. NO_x-free ozone/oxygen gas was then used to produce ozone stock solution by diffusion of gas bubbles in a glass bottle containing ultrapure water, under continuous stirring. For some experiments, the ozone stock solution was cooled during production to achieve higher dissolved ozone concentrations. An external ice-bath was used for cooling. The ozone stock solution bottle had a side-socket, equipped with a PTFE/silicone septum, a stainless steel syringe needle (Sterican, B. Braun, Melsungen, DE) and a ball valve (Luer Lock, B. Braun, Melsungen, DE) to withdraw ozone stock solution with a syringe. A 20 mL or a 60 mL syringe (described above) were connected to the ball valve with a Luer Lock connector to withdraw ozone stock solution from the bottle. The syringe was rinsed twice with ozonated water for conditioning of the material. Afterwards, ozone measurement or dosing to samples took place. For ozone dosing, a PTFE tube was mounted on a stainless steel needle and attached to the syringe via a Luer Lock connector. Ozone stock solution concentration was measured photometrically in a 1 cm quartz glass cuvette. The cuvette was rinsed twice with ozone stock solution and then filled carefully from bottom to top to minimize ozone leakage. The measurement was done with a Shimadzu UV-1601 instrument (Shimadzu, Kyoto, JP), at wavelength 260 nm. The

molar attenuation coefficient of ozone was assumed 3200 M^{-1} cm^{-1} (von Sonntag and von Gunten, 2012). Equilibration of dissolved ozone concentration in the stock solution was followed by repeated ozone concentration measurements. Ozone production was continued for the entire duration of the ozone dosing process, as usually more than one aliquot of stock solution was used. Another dissolved ozone concentration measurement was performed right after the ozone dosing process to ensure consistent ozone stock solution concentration.

Glassware used for batch experiments was washed in a laboratory machine (G 7783 MIELABOR, Miele & Cie., Gütersloh, DE). Prior to use, it was either rinsed with ultrapure water or burned at 550 °C to minimize glassware contamination by organic substances.

40 mL Glass bottles for AOC incubation were immersed in 1 % HCl overnight and subsequently rinsed with ultrapure water and burned at 550 °C before usage. Polypropylene bottle caps with PTFE/silicone septums were soaked in 100 g L^{-1} sodium persulfate, heated to 60 °C for 1 h and then rinsed thoroughly with ultrapure water.

Ultrapure water was produced with a Millipore Direct-Q 5 UV System (Merck, Darmstadt, DE) and obtained a quality of electrical conductivity at 25 °C 0.056 µS cm^{-1}, TOC concentration < 5 µg L^{-1} according to the system manufacturer.

Qualities and manufacturers of stock chemicals used are listed in Table II-3. Information on working solutions which were used in batch experiments is given below.

The H_2O_2 working solution had a concentration of 0.098 M and was prepared by 1:100 dilution of a 30 % H_2O_2 stock solution by ultrapure water. H_2O_2 working solutions were prepared on the day of use. For pH adjustion in batch experiments, 0.1 M NaOH and 0.1 M HCl working solutions were used. Adjustion of total alkalinity in groundwater A was done by dissolving $NaHCO_3$ in 1 L of the water sample. The $NaNO_2$ working solution for ozone quenching was prepared by dissolving 8 mg L^{-1} of $NaNO_2$ in ultrapure water. The indigo stock solution for ozone determination was made according to Bader and Hoigné (1981) by dissolving 600 mg L^{-1} of indigo trisulfonate in 20 mM H_3PO_4. The 20 mM H_3PO_4 solution was prepared by diluting 0.136 ml H_3PO_4 (ρ = 1.7, 85 %) up to 100 mL with ultrapure water. Indigo stock solution was stored in a glass bottle wrapped with aluminium foil in the fridge for maximum four months. Indigo working solution for dissolved ozone measurement was prepared from indigo stock solution, phosphate buffer and ultrapure water at volumes adapted from Bader and Hoigné (1981). Phosphate buffer for indigo working solutions was prepared according to Bader and Hoigné (1981) by diluting 31.7 g $NaH_2PO_4 \cdot 2\ H_2O$ (0.2 M) and 20.6 ml H_3PO_4 (ρ = 1.7, 85 %) up to 1000 mL with ultrapure water. The phosphate buffer was stored in a glass bottle in the fridge. Depending on the required sample volume and expected ozone concentration, the volume of indigo stock solution and the sampling flask size were determined. The phosphate buffer vol-

ume was 1/10 of the sampling flask volume. Ultrapure water was used to make up for the difference between sampling flask volume and the sum of indigo stock solution, buffer and sample volumes.

3.2.2 Small-scale Pilot Experiments

Experimental Setup

The small-scale pilot plant used in this work is depicted in Figure II-8 and Figure II-9. The plant was a custom-built ozonation plant based on the model PAP M 10 (Anseros, Tübingen, DE). The original plant was altered, e.g. equipped with extra sensors and a programmable logic controller (PLC). Instrumentational details on equipment used in the small-scale pilot plant are given in Table II-4.

The feed water unit consisted of a feed reservoir that steadily obtained water from the assigned inflow, which e.g. was the outlet of a full-scale water treatment plant. A floating valve was used to maintain a constant water level in the feed reservoir. Water volume in the feed reservoir was ≈ 30 L, resuting in an average hydraulic retention time of 10 min at a water flow rate of 180 L h^{-1}. The feed reservoir supplied continuous water flow to a feed pump. Feed water flow rate was adjusted manually by partly opening or closing a ball valve and measured by a magnetic flow meter (Picomag, Endress+Hauser, Reinach, CH). An oscillation in flow rate was observed, however usually in the range of < 5 %.

The ozonation unit consisted of a Venturi ozone injector that was mounted in a pipe loop. Ozone gas was supplied with a gauge pre-pressure of approximately 0.3–0.4 bar. A frequency-controlled injector pump was used to produce high flow rates in the loop, resulting in a gauge pressure of approximately 0 bar at the gas-side of the Venturi jet. Ozone feed gas flow rate was measured by a rotameter and controlled manually with a needle valve.

The ozonation unit was followed by a tube reactor (L = 10 m, D = 6 mm, Re ≈ 9000 at flow rate 180 L h^{-1} and 15 °C) for rapid mixing of ozone gas bubbles and water. A column reactor (15 L, D = 0.105 m, Re ≈ 500 at flow rate 180 L h^{-1} and 15 °C) with downward flow direction was used to enable a reaction time of approximately 5 min. The column reactor exhibited several sampling points that were used to measure ozone concentrations after different reaction times. An electrochemical ozone sensor (Orbisphere C1100, Hach, Loveland, US) was used for dissolved ozone measurements and for recording of the water temperature.

The effluent of the column reactor was connected to a filtration column (biofilter 1, Figure II-10). Feed water was distributed by an open overflow that was mounted in the center of the column. The hydraulic head was between approximately 5 and 45 cm. It was lowest right after filter backwash and increased over time. This implies hydraulic retention times of 2–21 min in the filter headspace at a flow rate of 10 L h^{-1}. The filter material consisted of a granular activated carbon (GAC) layer (GAC 830 Supra, Norit, Amersfoort, NL) of 0.4 m and a phonolithe (0.4–

0.8 mm, Hans G. Hauri Mineralstoffwerke, Bötzingen, DE) layer of 1.1 m. Different sampling points were available (between GAC and phonolithe layer and at the bottom of phonolithe layer, i.e. biofilter effluent). A second, identical filtration column (biofilter 2) was connected to the water influent pipe before the feed reservoir, i.e. it received non-ozonated water.

The small-scale pilot plant was equipped with different dosing points to allow the dosage of HCl, H_2O_2 and NH_4^+ (as $(NH_4)_2SO_4$). The standard dosing points were before the ozone injection loop. However one dosing point for H_2O_2 was also installed at the column reactor inlet, i.e. after ozone dosage. The same dosing pump was used for H_2O_2 and NH_4^+ dosage. However, both chemicals were never used simultaneously and the dosing tubes were rinsed in between, with ultrapure water. The H_2O_2 and NH_4^+ flow rates were controlled manually and adjusted by continuous weighing of the feed bottles. The HCl dosing pump was controlled by the PLC to allow the adjustment of a lower target pH. A pH electrode was used for in-line pH measurement and supplied the control value for the HCl dosing pump. The pH electrode was calibrated in regular intervals but usually showed a slightly smaller (~ 0.1 pH unit) value than withdrawn samples measured by a handheld device. pH values obtained by the in-line measurement were not corrected but used as recorded.

Construction materials in the small-scale pilot plant with contact to ozone gas were perfluoroalkoxy alkane (PFA) and polytetrafluoroethylene (PTFE). Ozone-containing water was in contact with rigid polyvinyl chloride (PVC) pipes, a stainless steel pump and PFA and silicon tubes.

Experimental Methods

Two kinds of experiments were conducted with the small-scale pilot plant. The first kind of experiments were ozonation experiments without biofiltration. These experiments were used to determine the effects of experimental conditions (e.g., ozone dosage, pH, H_2O_2, NH_4^+) on ozone reaction kinetics, decolorization and bromate formation. The second kind of ozonation experiments were performed in combination with subsequent biofiltration. Ozonation settings usually remained constant during these experiments.

Ozonation experiments at various specific ozone doses were performed at both groundwater treatment plants E (Sellmann, 2020) and A, without biological post-treatment of ozonated water. Ozone dose was varied by adjusting the ozone feed gas concentration, while other parameters were held constant. Experimental parameters are given in Table 3-3 and were slightly different at both treatment plants. Only small differences in experimental results with groundwater E were observed for a variety of feed water flow rate (100–180 L h^{-1}) and ozone gas concentration settings (5–30 g m^{-3}) (Figure III-21). Off-gas ozone concentration and gas flow rate, water flow rate and feed water TOC or DOC content were considered for specific ozone dose determination. Water samples were withdrawn from the reaction column, usually at half the height of the column. Sampling was preceded by an equilibration time of approximately 5 min to allow the exchange of the complete water volume of the reaction column. Minimization of residual

ozone escape or decay while sampling was aspired by using a custom sampling unit (Specker, 2019). The unit consisted of a 100 mL glass flask and a cap equipped with 4 mm inner diameter PTFE tubes as inlet and outlet. The inlet tube reached until right above the bottle bottom. On its second end, the inlet tube was connected to a ball valve at the reaction column. The outlet of the sampling cap was connected to the ozonation plant outlet collector. With this setup, the sampling bottle could be rinsed, from bottom to top, with several bottle volumes of ozonated water before removing the custom cap and exchanging with a regular bottle cap. Sampling bottles were completely filled to minimize ozone volatilization after sampling. Standard analytical parameters of ozonated samples were SAC_{436}, UV_{254} and bromate. Residual ozone concentrations were measured in some experiments by the electrochemical ozone sensor. The sensor inlet (4 mm inner diameter PTFE tube) was connected to the sampling port at the reaction column inlet. The sample flow rate was approximately 20 L h^{-1} (≈ 0.5 m s^{-1} in sampling tubes). The tube length was up to 2 m depending on the sampling port, which implies that retention time in the sampling tube was negligible (≈ 1 s). It was assumed that a well-mixed bulk water sample was taken, reflecting the average ozone concentration in the reaction column after the respective reaction time. Samples were usually taken in duplicates.

Dissolved ozone concentration was read from the instrument display, after equilibration of the value (usually after some minutes). The first measurement was made at the column reactor inlet. The measurement procedure was continued at the second sampling port, from top to bottom. Again, sufficient equilibration time was given for the sensor value. In total, five dissolved ozone concentration measurements were made for every pilot plant setting. Dissolved ozone concentrations measured by the online sensor showed good agreement with the indigo method (Figure III-22). The hydraulic retention time of ozonated water between ozone injection and the column reactor was determined by the use of a tracer and approximated as 30 s for a water flow rate of 150 L h^{-1} (Sellmann, 2020). For other flow rates, residence times were approximated proportionally. Between the sampling ports, residence time was determined as the ratio of reactor volume between the sampling ports and water flow rate.

Non-ozonated feed water samples were analyzed for TOC, DOC and bromide content, in addition to SAC_{436} and UV_{254}.

Ozonation experiments were partly conducted with addition of 0.2 M HCl to reduce the pH value of groundwater A before ozonation. HCl dosage was pH-controlled (see above for description of the setup). At every pH tested, two ozone doses were applied before pH was readjusted. Further experiments were done with dosage of 0.3 % H_2O_2 for both groundwater E (Sellmann, 2020) and groundwater A. These experiments started without H_2O_2 dosage, at a set ozone feed gas concentration. H_2O_2 dosage was then started and adjusted by measuring the weight loss of the H_2O_2 bottle over time. The H_2O_2 flow rate range was approximately 0.2–9 mL min^{-1}. With increasing H_2O_2 dose, the ozone off-gas concentration decreased, as H_2O_2 enhanced ozone decay. This was dealt with differently at groundwater treatment plants A and E:

At groundwater treatment plant A, the ozone feed gas concentration was slightly reduced to obtain a relatively constant specific ozone dose. At groundwater treatment plant E, the ozone feed gas concentration was held constant, which resulted in a concomitant increase in ozone dose with H_2O_2 dose. Experiments with dosage of NH_4^+ were performed with groundwater A. The 500 mg L^{-1} $(NH_4)_2SO_4$ was dosed with the same dosing equipment used for H_2O_2. The resulting NH_4^+ concentration in the feed water (0.79 mg L^{-1}) was obtained from a non-ozonated sample withdrawn from the reaction column. More detailed information on small-scale pilot ozonation experiments with groundwater E is given in Sellmann (2020).

Table 3-3. Experimental settings for experiments with varied ozone dose at groundwater treatment plants A and E. *Feed water flow rate for groundwater usually 180 L h^{-1} but lower for experiments with raw water and for experiments with subsequent biofiltration

Parameter	Groundwater A	Groundwater E
Feed water flow rate / L h^{-1}	100–180*	150
Feed gas flow rate / L h^{-1}	25	45
Feed gas ozone concentration / mg L^{-1}	4–38	4–25
Injector pump frequency / Hz	25	31.7

Biofiltration experiments with ozonated water started with virgin GAC and phonolithe at groundwater treatment plant E. The ozonation process was done as described above. After short conditioning with with non-ozonated water, the biofilter received ozonated water (20 L h^{-1}) as influent. A second identical biofilter received non-ozonated water to improve understanding of the biofiltration process. The feed flow rate of both biofilters was reduced later to 10 L h^{-1} as higher flow rates caused too high hydraulic resistance. This resulted in a filter velocity of 1.3 m h^{-1} and an empty-bed contact time (EBCT) of 71 min (19 min EBCT in the GAC layer and 52 min EBCT in the phonolithe layer). A constant ozone dose (in mg L^{-1}) was maintained by maintaining constant ozone feed gas concentration as well as constant feed gas and water flow rates. 0.33–0.46 mg_{O3}/mg_{TOC} were applied to treat groundwater E. The variation was due to a manual and intended increase in ozone feed gas concentration over time to improve decolorization efficacy. The absence of residual ozone in the biofilter influent was monitored by continuous measurement with the electrochemical ozone sensor. Pilot plant flow rates, e.g. for biofilter feed, were controlled daily by waterworks staff. Biofilter backwash was conducted manually when the hydraulic head of the filter was not sufficient to allow a flow rate of 10 L h^{-1} in the filter (approximately every four weeks). Pilot plant influent was used as backwash water. The backwash flow rate was 300 L h^{-1} (38 m h^{-1}) for approximately 5 min. Regular analytical parameters at groundwater treatment plant E were UV_{254}, SAC_{436}, TOC and bromate. Influent samples were also analyzed for bromide. For one set of samples, additional LC-OCD experiments were made and samples were taken for incubation to a laboratory for AOC, high nucleic-

acid (HNA) and low nucleic-acid (LNA) cell count and TOC measurements. AOC measurements were performed by incubating small-scale water samples at 30 °C, thereby enhancing growth of autochthonous bacteria. Ozonated samples were microfiltered (0.1 µm, Minisart, Sartorius, Göttingen, DE) and spiked with non-ozonated sample (10 vol%) as natural inoculum. Subsequently, total, high-nucleic-acid (HNA) and low-nucleic-acid (LNA) cell count were measured. After AOC measurement, TOC was measured in the same samples to examine TOC degradation during the incubation period.

After approximately nine months operating time at groundwater treatment plant E, the small-scale pilot plant was relocated to groundwater treatment plant A and operated with the same biofilter that was conditioned with groundwater E before. The second biofilter with non-ozonated water as feed was not used at groundwater treatment plant A. Ozonation-biofiltration experiments at groundwater treatment plant A were initially performed with aerated, flocculated and filtered water (sand filter effluent, Figure II-1, see below). Specific ozone doses for ozonation-biofiltration were 0.17–0.28 mg_{O3}/mg_{TOC} for groundwater A. The variation was due to a variation in influent quality for the small-scale pilot plant. Sampling for groundwater A started after five months of conditioning time. After two weeks of sampling, the influent water quality for the pilot plant was switched to aerated water (see below). It was conditioned for one week before another sampling period of two weeks started. Analytical parameters at groundwater treatment plant A were UV_{254}, SAC_{436}, TOC and bromate. Influent samples were also analyzed for bromide, conductivity and pH. In some samples, LC-OCD analyses were made.

Natural Groundwater Samples for Small-scale Pilot Experiments

Small-scale pilot experiments were conducted at groundwater treatment plants A and E, mainly with finished groundwater taken directly from the water treatment plant outlets. At groundwater treatment plant A, additional experiments were performed with three different non- or semi-treated water qualities. The first additional quality was raw water, i.e. water treatment plant influent (Figure II-1). The second additional quality was aerated water after ammonia removal, i.e. from the pressure side of sand filter pumps, but before dosage of coagulant (Figure II-1). The third additional water quality was aerated, flocculated and filtered water, which was taken from the effluent of sand filters (Figure II-1). Small-scale pilot experiments were done at different dates and partly run for several weeks. Water quality over time was relatively stable in groundwater E but underlied seasonal changes in groundwater A due to low well depth. Specific water qualities used for experiments are highlighted in the experiments and presented in Table II-1 (groundwater A) and Table II-2 (groundwater E).

Chemicals

Oxygen was produced by pressure swing adsorption (SEP 100, Anseros, Tübingen, DE). This oxygen concentrator was used at groundwater treatment plant E. The system was replaced by

another instrument (Everflo, Philips Respironics, Murrysville, US) for experiments at ground-water treatment plant A. The 0.3 % H_2O_2 solution for small-scale pilot experiments was prepared by diluting 9.01 mL L^{-1} 30 % H_2O_2 with ultrapure water. The solution was prepared on the day of use. The 500 mg L^{-1} NH_4^+ solution was prepared by dissolving 1835 mg L^{-1} $(NH_4)_2SO_4$ in ultrapure water. The solution was prepared four days before and cooled until use. The HCl solution used for small-scale pilot experiments had a concentration of approximately 0.2 M and was prepared by dilution a 1 M HCl solution with deionized water.

3.2.3 Membrane Ozonation Experiments

Experimental Setups

Membrane ozonation experiments were performed with two different membrane ozonation contactors. The first membrane contactor was a small lab-scale contactor comprised of a single polydimethylsiloxane (PDMS) fiber in a glass tube (schematic drawing Figure 3-2.a, picture Figure II-11.a). The second contactor was a multi-tube half-commercial scale contactor comprised of 490 PTFE fibers in a stainless steel housing (schematic drawing Figure 3-2.b, picture Figure II-11.b). Both membrane contactor setups were connected to an influent tank and an effluent tank. Ozone feed gas was produced with a commercial ozone generator (BMT 803N, BMT Messtechnik, Berlin, DE) from oxygen (99.5 %, BOC, Guildford, UK) and analyzed for ozone (BMT 964, BMT Messtechnik). Ozone off-gas concentration was measured with a second BMT 964 analyzer. Ozone gas flow rate was measured with a rotameter and was assumed identical for feed and off-gas. Water flow rate was measured gravimetrically (single-tube) or volumetrically (multi-tube). Water flow direction was upward, inside the membrane fibers, while ozone gas flow direction was downward, outside the membrane fibers but inside the housing. In the multi-tube contactor, the flow direction could be inverted by changing the gas-flow direction to upward. Technical specifications of the membrane ozonation contactors are summarized in Table II-5.a. Additional information on the membrane ozonation contactors is given elsewhere (Kämmler et al., 2022; Zoumpouli, 2021).

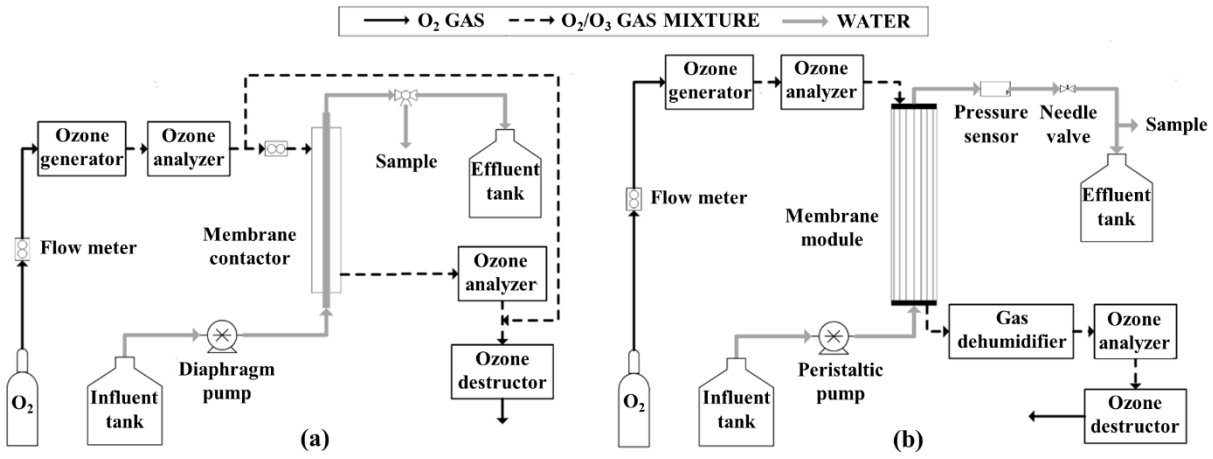

Figure 3-2. **(a)** single-tube PDMS membrane ozonation setup, **(b)** multi-tube PTFE membrane ozonation setup. Figure taken from Kämmler et al. (2022).

Experimental Methods

Membrane ozonation experiments with both contactors were conducted by applying different feed water flow rates and ozone feed gas concentrations. In the single-tube contactor, feed water flow rates were 1.2, 2.6, 5.0 and 9.7 mL min^{-1} at ozone feed gas concentrations of 25, 50, 100 and 200 g m^{-3}, yielding a total of 16 experimental settings. In the multi-tube contactor, feed water flow rates were 400, 680 and 920 mL min^{-1} at ozone feed gas concentrations of 25, 35, 50 and 70 g m^{-3}, yielding a total of twelve experimental settings. Flow-dynamic parameters for the experimental settings are listed in Table II-5.b. Each experimental setting was equilibrated for 10 min (single-tube contactor) or 4 min (multi-tube contactor) before sampling. Samples were taken from sampling valves mounted after the contactor outlets. The scope of analyses comprised dissolved ozone, UV_{254}, SAC_{436} and bromate. Feed water samples were also analyzed for TOC, DOC and bromide. Residual dissolved ozone at the membrane contactor outlets was measured by the indigo method (Bader and Hoigné, 1981). Two samples were taken for ozone measurement. UV_{254}, SAC_{436} and bromate were determined from another sampling bottle without ozone quenching agent. Cylindrical glass bottles were filled carefully from bottom to top, with a tube submerged below the water level to minimize ozone loss. Two sampling bottles were filled for each experimental setting. These samples were analyzed after approximately one week. Samples were stored dark and cool in between. Membrane ozonation experiments were performed at room temperature, which was 16 °C.

Natural Groundwater Sample Used for Membrane Ozonation Experiments

Membrane ozonation experiments were performed with a batch of groundwater E ($E.1_F$).

3.3 Analytical Methods

Analytical methods used in this work are described below.

pH of water samples was measured with a handheld pH device (pH 320, WTW, Weilheim, DE). The instrument was calibrated by two-point calibration before use.

Electrical conductivity at 25 °C was measured with a handheld device (LF 340, WTW, Weilheim, DE).

Total alkalinity was determined as the amount (in mmol L^{-1}) of HCl needed to reduce the sample pH to 4.3. 100 mL of water sample were used for alkalinity measurement and was stirred with a magnetic stirrer at moderate speed. 0.1 M HCl was added manually with a burette. The pH was continuously measured by a handheld device. When pH approached 4.3, HCl was added dropwise and stirring was stopped prior to pH measurements for more precise pH determination.

Dissolved ozone in ozone stock solution was measured by UV absorbance at 260 nm (molar absorbance coefficient of 3200 M^{-1} cm^{-1}, von Sonntag and von Gunten, 2012). Dissolved ozone in groundwater samples was measured by the indigo method (Bader and Hoigné, 1981). For

details see description of the respective experimental procedure. Both UV measurements at 260 nm and indigo measurements at 600 nm were made in a 1 cm quartz glass cuvette in a Shimadzu UV-1601 photometer (Shimadzu, Kyoto, JP).

UV_{254} and SAC_{436} measurements were made in a 5 cm quartz glass cuvette in another spectrophotometer (Hach Lange DR 5000, Hach, Loveland, US). The same instrument and cuvette were used for wavelength scans. Increment for wavelength scans was 0.5 nm, range 190–700 nm. Spectrophotometric samples were pre-filtered by a 0.45 µm polypropylene membrane filter (VWR International, Radnor, US). A 20 mL polypropylene/polyethylene syringe (Injekt Solo, B. Braun, Melsungen, DE) was used for filtration. Syringe and filter were pre-rinsed with approximately 20 mL of sample before an aliquot was measured.

Bromate concentration was measured by ion chromatography (Eco IC, Metrohm, Herisau, CH) with post-column reaction of bromate and potassium iodide to triiodide in presence of ammonium heptamolybdate. Triiodide was detected by UV absorbance at 352 nm. The method is described in ISO 11206 (2011). A Metrohm ASupp16 column and a sulfuric acid eluent were used for bromate determination. The limit of quantification obtained by this system was 1.5 µg L^{-1} bromate.

Bromide concentration was measured by the same ion chromatography as bromate, however with a Metrohm ASupp5 column and carbonate eluent. Bromide was detected by UV absorbance measurement at 205 nm.

TOC and DOC (after 0.45 µm filtration) were analyzed as non-purgeable organic carbon by the TOC analyser TOC-L (Shimadzu Corp., Kyoto, JP) using combustion catalytic oxidation at 680 °C, coupled with a nondispersive infrared sensor.

LC-OCD-UVD analysis was performed with 0.45 µm filtered samples on a column packed with Toyopearl HW 50 S resin (Tosoh Bioscience, Tokyo, JP) using a phosphate buffer of 2.38 g L^{-1} KH_2PO_4 and 1.33 g L^{-1} $Na_2HPO_4 \cdot 2\ H_2O$ as mobile phase. A Grätzel thin-film UV reactor was used to convert organic carbon to CO_2 after removal of inorganic carbon by acidification. The system was coupled with an infrared CO_2 detector (Ultramat 6, Siemens, München, DE) and a UV detector working at 254 nm (UV-M II, Pharmacia Biotech, Uppsala, SE). A 2 mL sample aliquot was used for chromatography. A 0.2 mL aliquot was used as bypass sample to determine bulk DOC content and UV absorbance. LC-OCD-UVD analysis is described elsewhere in more detail (Huber et al., 2011). NOM fractions were calculated from peak analysis in the software ChromCalc (DOC-Labor Dr. Huber, Karlsruhe, DE).

It should be noted that small amounts of HS may be found in the LMWA fraction (Huber et al., 2011). The mathematical procedure used by the software ChromCalc to distinguish LMWA and low molecular-weight HS is based on UV absorbance of the LMWA fraction. UV absorbance is significantly reduced by ozonation, which could result in overestimation of LMWA yield by ozonation. Thus, all NOM moieties eluting with the LMWA fraction were assigned

LMWA. The downside of this procedure is an overestimation of LMWA contents of non-ozonated water samples. Thus, LMWA concentrations corrected by HS content for non-ozonated water samples are given in the captions of respective figures.

Calibration of the OCD signal was made indiviually for each sample by normalizing the bypass DOC concentration in the respective sample to DOC concentration measured with the TOC-L analyzer. LC-OCD chromatograms were plotted from LC-OCD-UVD raw data in Microsoft Excel (Microsoft, Redmond, US).

Some LC-OCD-UVD samples were measured in another laboratory (TZW Dresden), with a similar setup. The setup was equipped with additional detectors: a photodiode array detector for absorbance measurement at 436 nm (Varian ProStar 335) and a fluorescence detector (474, Waters, Milford, USA) set at excitation wavelength of 365 nm and emission wavelength of 480 nm to measure humic fluorescence. This setup was used for the data shown in Figure II-4.

Residual H_2O_2 in groundwater samples was determined with a commercial H_2O_2 test kit (118789, Merck, Darmstadt, DE). A 1 cm cuvette was used, resulting in a measuring range of 0.03–6 mg L^{-1} H_2O_2. This method was tested in detail and found to successfully reflect H_2O_2 concentration in a non-ozonated, natural groundwater sample (4.6 mg_{DOC} L^{-1}) (Eberhard, 2021).

NH_4^+ in groundwater was determined with a commercial test kit (LCK 304, Hach, Loveland, US) and a photometer (DR3900, Hach, Loveland, US). The measuring range was 0.015–2 mg L^{-1} NH_4-N.

AOC was measured with a procedure adapted from Hammes and Egli (2005). Initially, total cell count (TCC, see below for method) was measured in water samples, without filtration or other sample pre-treatment. The measurement was made maximum one day after sampling. Samples were cooled at approximately 4–8 °C until measurement. After the initial TCC measurement, 15 aliquots (20 mL each) of every water sample were transferred to 40 mL glass bottles which were closed immediately. Ozonated samples partly showed no viable cells and were therefore filtered (0.1 µm) and inoculated with non-ozonated water sample (1:10) before preparing the aliquots for AOC measurement. The samples were put on a horizontal shaker and agitated moderately fast at a temperature of 30 °C. After 3 d, 7 d, 14 d, 21 d and 28 d, three aliquots of every sample were taken from the shaker and analyzed for TCC. Mean TCC values were obtained from the three aliquots. AOC was calculated from the difference between initial TCC and maximum mean TCC during the incubation period. The correlation of 10^{-7} μg_{AOC} $cell^{-1}$ (Hammes et al., 2006) was used to convert information from TCC measurements into AOC values.

TCC was measured according to Ho et al. (2020) by flow cytometry with a CyFlow SL instrument (Partec, Münster, DE). Samples were stained with SYBR Green I and incubated for 13 min at 37 °C in the dark. Measurement was performed using a bluediode pumped solid-state laser (20 mW) at 488 nm. The result was a red and green fluorescence intensity plot which was

processed with the software FloMax (Partec, Münster, DE). Instrument calibration was done with fluorescent 3 µm beads (Sysmex, Kobe, JP). Background scattering of the measurement was identified by measurement of a filtered (0.1 µm) sample of a natural "evian" mineral water (Danone, Paris, FR) and comparison to non-filtered "evian" water. The TCC gate was defined manually based on these measurements. Within the TCC gate, two clusters of bacteria were defined: high nucleic-acid (HNA) and low nucleic-acid (LNA) cells. HNA and LNA clusters were defined manually, based on "evian" water measurements.

3.4 Data Analysis and Calculations

Data analysis was usually done in Microsoft Excel. Some fittings were done in Origin (Originlab, Northampton, US), which is noted in figure captions in this case. If more than one sample was available for analysis, mean value and standard deviation (uncorrected estimator) were calculated from the data and are usually shown in figures.

Measured parameters were in some cases used indirectly to calculate other values. Calculation procedures are described below.

The immediate ozone demand (IOD) was calculated as the difference between dosed ozone concentration and the first sample measured. For batch samples, this was after 15 s for most experiments. In small-scale pilot experiments, the IOD time was 25 s for most experiments. IOD times are mentioned in figure captions.

Ozone exposure was calculated from dissolved ozone concentration measurements obtained at different time steps. First-order ozone decay was assumed. The calculation procedure is described in the appendix, pp. LII.

Ozone mass transfer calculations in membrane ozonation included calculation of membrane, liquid-side and overall mass transfer coefficients for both membrane contactors. The calculation procedures were presented in detail in a previous publication (Kämmler et al., 2022). Results of these calculations are a function of water flow velocity and membrane material and are presented in Table II-5.b.

Hatta number (Ha, Equation 2-7) calculation for membrane ozonation experiments was based on the film theory (Charpentier, 1981). It was calculated from the ozone diffusivity in water (D_{O3}), the first-order ozone decay rate for the secondary phase of ozonation (k_{sec}) and the liquid-side ozone mass transfer coefficient (k_L). D_{O3} is constant at a specific temperature ($1.56 \cdot 10^{-9}$ $m^2\ s^{-1}$ at 16 °C, Johnson and Davis, 1996). k_L was obtained from ozone mass transfer calculations (see above). k_{sec} was obtained from kinetic batch experiments with groundwater E at 16 °C, at specific ozone doses of 0.5, 1.0 and 1.5 mg_{O3}/mg_{DOC}. The exponential function $k_{sec} = 0.0024\ s^{-1} + 0.3\ s^{-1} \exp(-3.8\ mg_{DOC}\ mg_{O_3}^{-1} * specific\ ozone\ dose\ [mg_{O_3} mg_{DOC}^{-1}])$ was fitted in Origin to obtain a correlation of specific ozone dose and k_{sec} (Kämmler et al., 2022). The function was also used to extrapolate k_{sec} for specific ozone doses lower than 0.5 or higher

than 1.5 mg_{O3}/mg_{DOC}. To obtain specific ozone doses for membrane ozonation, it was assumed that UV_{254} reduction rates in membrane and batch ozonation were equal at the same specific ozone dose. By this, specific ozone doses for membrane ozonation could be interpolated from data from batch equilibrium experiments at 0.1–1.5 mg_{O3}/mg_{DOC}. The procedure is described in detail in Kämmler et al. (2022). Note that by the procedure described here, ozone decay rate in the membrane contactors may be slightly underestimated as ozone decay was not completed at the reactor outlet for some samples and might have been faster in the initial phase of ozonation.

4 Laboratory Batch Ozonation

This chapter comprises results of laboratory batch ozonation experiments using different natural, organic-rich groundwaters that exhibited high residual color after full treatment (SAC_{436} 0.41–1.2 m^{-1}). Laboratory batch experiments were performed at Hamburg University of Technology. Results for some of the groundwaters were presented elsewhere before. These groundwaters include groundwater C (Preda, 2019), groundwater D (Specker, 2019), groundwater E (Sellmann, 2020), groundwater A with H_2O_2 dosage (Eberhard, 2021) and groundwater A at varied alkalinity (Bharadwaj, 2022). An excerpt of the results shown here was presented before in Kämmler et al. (2020) and Kämmler et al. (2021).

4.1 Effects of Ozonation on Groundwater NOM from Different Sources

4.1.1 Impact of Ozonation on Groundwater NOM Fractions and Concentration

The effect of ozonation on groundwater natural organic matter (NOM) fractions is highlighted by LC-OCD-UVD analysis. This technique yields information about NOM size distribution due to an increase in retention time with decreasing molecular size (Huber et al., 2011). Information on molecular size and fractions is supplemented by concomitant UV analysis to detect chromophoric NOM groups. Ozonation induced concentration changed in all NOM fractions that were detected by LC-OCD. These concentration changes, relative to the non-ozonated sample, are shown in a boxplot diagram that comprises information from experiments with five different humic-rich groundwater samples (Figure 4-1).

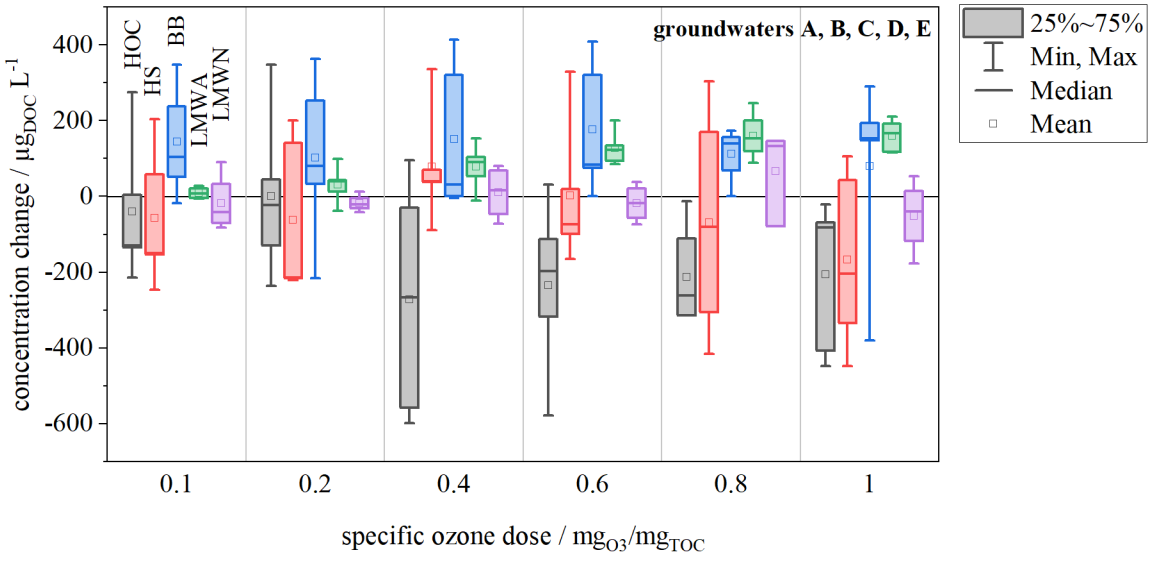

Figure 4-1. Organic carbon concentration changes (difference to non-ozonated samples) in NOM fractions of groundwaters A, B, C, D (Table 3-2) and E.1_F (Table II-2) due to ozonation shown as boxplots. Determination of fractions by LC-OCD: HOC – hydrophobic organic carbon, HS – humic substances, BB – building blocks, LMWA – low molecular-weight acids, LMWN – low molecular-weight neutrals. No humic substances in LMWA fraction assumed. n = 5 groundwater samples, no data for groundwater E at 0.8 mg_{O3}/mg_{TOC}. Exclusion of groundwater B for LMWN (clear outlier, Figure III-3) Dilution effect ozone stock solution considered by multiplication with dilution factor.

Individual LC-OCD results for the groundwater samples used are shown in Figure III-1 (groundwater A), Figure III-3 (groundwater B), Figure III-5 (groundwater C), Figure III-7 (groundwater D) and Figure III-9 (groundwater E). Biopolymers were detected at negligible concentrations (< 50 μg_{DOC} L^{-1}) and therefore excluded from diagrams. Part of NOM, the hydrophobic organic carbon (HOC) fraction, is not eluted from the chromatographic column within analysis time and is therefore not detected by LC-OCD-UVD. However, its concentration may be calculated from the difference of OCD signal from the chromatographic column effluent and a sample aliquot that by-passes the column. Overall, the content of HOC showed only small changes at specific ozone doses < 0.4 mg_{O3}/mg_{TOC} but decreased significantly at higher ozone doses (Figure 4-1). Reduction of HOC aligns with the results of other authors (Loganathan et al., 2022; Zietzschmann et al., 2015).

The humic substances (HS) fraction did not show systematic increase or decrease in ozonation but large variance depending on the groundwater used (Figure 4-1). This is different from other studies which observed a decrease in humic substance concentration of up to 20 % at similar specific ozone doses (Beniwal et al., 2018; Li et al., 2017). However, a right-shift in peak retention time of HS (fraction I) was induced by ozonation, as it is exemplarily shown in the LC-OCD-UVD chromatograms of groundwater A (Figure 4-2). This implies a decrease in average molecular weight of HS (Huber et al., 2011), which was expected due to previous research (Swietlik et al., 2004). Moreover, the right-shift in retention time indicates a transient continuum of NOM transformation products that are produced by ozonation. The composition changes with ozone dose. Similarly, it has been shown for smaller organic molecules (phenols) that ozonation produces a variety of products that may be broken down stepwise to smaller molecules with increasing oxidant dose (Ramseier and von Gunten, 2009).

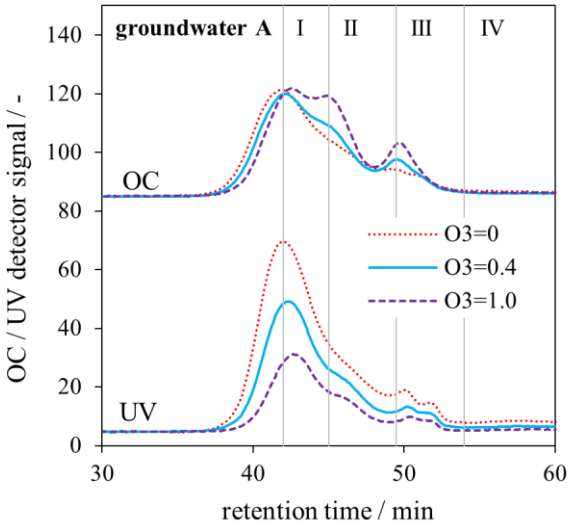

Figure 4-2. LC-OCD-UVD diagram of groundwater A. Specific ozone doses 0 (blind sample), 0.4 and 1.0 mg_{O3}/mg_{TOC}. ϑ = 20 °C, DOC 4.5 mg L^{-1}, pH 7.8. Top: organic carbon (OC) signal, bottom: ultraviolet (UV) signal. I – humic substances, II – building blocks, III – low molecular-weight acids and humic substances, IV – low molecular-weight neutrals. Dilution by ozone stock solution considered by multiplication with dilution factor

Groundwaters B (Figure III-2) and D (Figure III-6) showed similar chromatograms as groundwater A. Contrarily, a decrease in HS peak retention time, i.e. increase in average molecular weight was observed for groundwater C (Figure III-4) and groundwater E (Figure III-8). It was hypothesized that ozonation may transform hydrophobic, high molecular-weight, non-chromatographable NOM to HS detectable by LC-OCD (Kämmler et al., 2022). This could have resulted in a decrease of HS peak retention time.

Building blocks (BB, fraction II) and low molecular-weight acids (LMWA, fraction III) are formed by ozonation (Figure 4-1, Figure 4-2). Unlike the HOC and HS fractions, BB and LMWA formation showed clear increase and less variance across the groundwaters tested (Figure 4-1). An increase of BB and LMWA peaks was previously observed by other authors (Beniwal et al., 2018; Stylianou et al., 2018a).

The effect of ozonation on low molecular-weight neutrals (LMWN, fraction IV) was small and did not show clear results regarding increase or decrease (Figure 4-1). LMWN content of non-ozonated groundwater B was a clear outlier (Figure III-3). No consistent trends were also observed in the analysis of various LC-OCD-UVD chromatograms of ozonated groundwaters (Figure 4-2, Figure III-2, Figure III-4, Figure III-6 and Figure III-8). Similar to the results here, different effects of ozonation on LMWN were reported previously. Both a decrease in LMWN (Stylianou et al., 2018a; Zietzschmann et al., 2015) and an increase in LMWN (Stylianou et al., 2018a) were reported. This supports that effects of ozonation on LMWN may vary with water composition or experimental conditions.

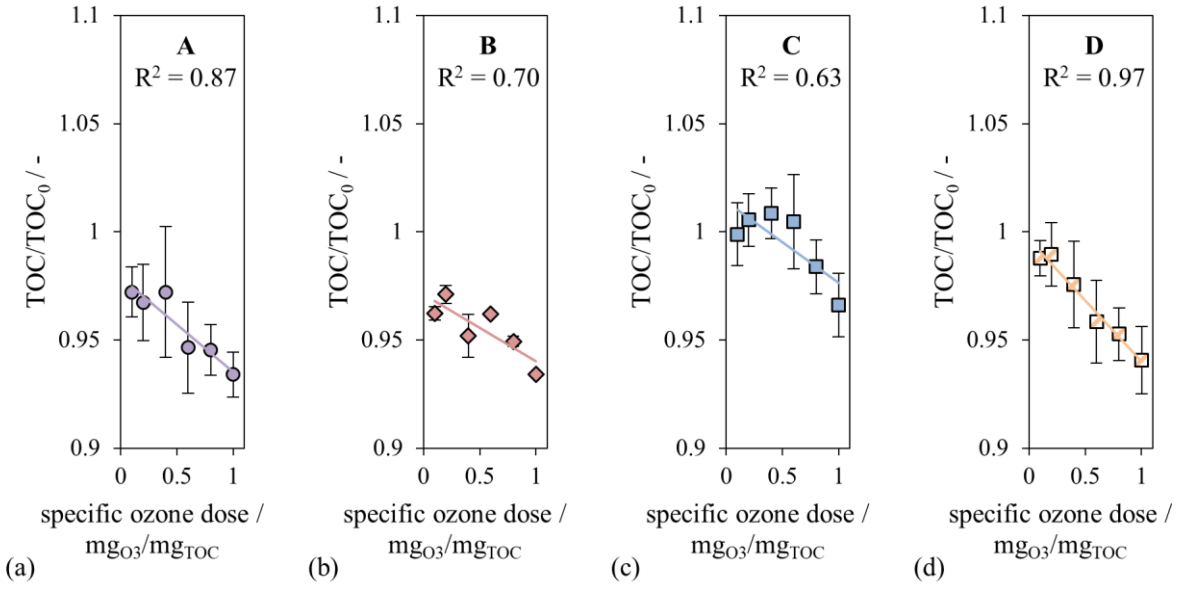

Figure 4-3. TOC in batch ozonation of **(a)** groundwater A, **(b)** groundwater B, **(c)** groundwater C and **(d)** groundwater D; no data for groundwater E. ϑ = 20 °C, TOC_0 3.5–6.2 mg L^{-1}, pH 7.6–8.0 (Table 3-2)

The UV signal of LC-OCD-UVD was decreased proportionally to specific ozone dose, as the chromatograms in the bottom part of Figure 4-2 depict. The UV absorbance abatement was observed for all NOM fractions, including those that showed increase in OC concentration, as BB and LMWA. Consequently, the bulk specific UV_{254} absorption ($SUVA_{254}$) was reduced significantly in all groundwater samples (Figure III-10). It was observed previously that ozonation selectively reduces UV absorbance of types of NOM (Wenk et al., 2013).

Despite its transformative impact on all major NOM fractions, ozonation of groundwater with 0.1 to 1.0 mg_{O3}/mg_{TOC} decreased the total organic carbon (TOC) concentration of groundwaters only by << 10 % (Figure 4-3). At ozone doses of < 0.5 mg_{O3}/mg_{TOC} (see below), the reduction in TOC was < 5 %. Reduction of TOC content implies decarboxylation reactions, which in turn require significant pre-oxidation of NOM (Nöthe et al., 2009). Ozone doses used here may therefore have been too small to induce significant TOC removal.

4.1.2 Impact of Ozonation on Bulk Spectroscopic NOM properties

Ozonation reduced light absorption of the water samples within the whole UV-visible spectrum and proportionally to specific ozone dose (Figure 4-4.a). For all groundwaters except groundwater E, absorbance abatement increased with wavelength. This is highlighted by the increased ratio UV_{254}/SAC_{436} with specific ozone dose (Figure 4-4.b). Similarly, the ratio of absorbance at 254 and 365 nm (E2:E3) was observed to increase with specific ozone dose (Remucal et al., 2020). A stronger decrease in absorbance at higher wavelength was also observed in the ozonation of NOM isolates (Wenk et al., 2013) and wastewater DOM (Li et al., 2017; Nanaboina and Korshin, 2010). This may partly be due to the fact that transformation products of NOM may still exhibit UV absorbance (Nöthe et al., 2009; Önnby et al., 2018). An explanation may also be attempted on a molecular level: low energy separation for intramolecular charge transfer interaction was positively correlated with large molecular size and absorbance at high wavelengths (Del Vecchio and Blough, 2004), and also with reactivity toward ozone (Naumov and von Sonntag, 2010). Thus, chromophores absorbing at high wavelengths may react preferentially with ozone. This is fully consistent with the observation that molecular weight is decreased by ozonation (chapter 4.1.1).

Groundwater E showed a decrease in the ratio of UV_{254}/SAC_{436} at specific ozone doses of 0.1 and 0.2 mg_{O3}/mg_{TOC}, which was different from other groundwaters tested (Figure 4-4.b). As LC-OCD chromatograms of ozonated groundwater E (Figure III-8) suggest, the humics peak shifted to shorter retention time, i.e. larger molecular weight at 0.4 mg_{O3}/mg_{TOC} and also at lower ozone doses (not shown). This may indicate the formation of high-molecular, chromophoric NOM by ozonation, as it was discussed in detail in Kämmler et al. (2022). These effects were only visible at small ozone doses. At specific ozone doses > 0.2 mg_{O3}/mg_{TOC}, UV_{254}/SAC_{436} increased in groundwater E similarly to the other samples.

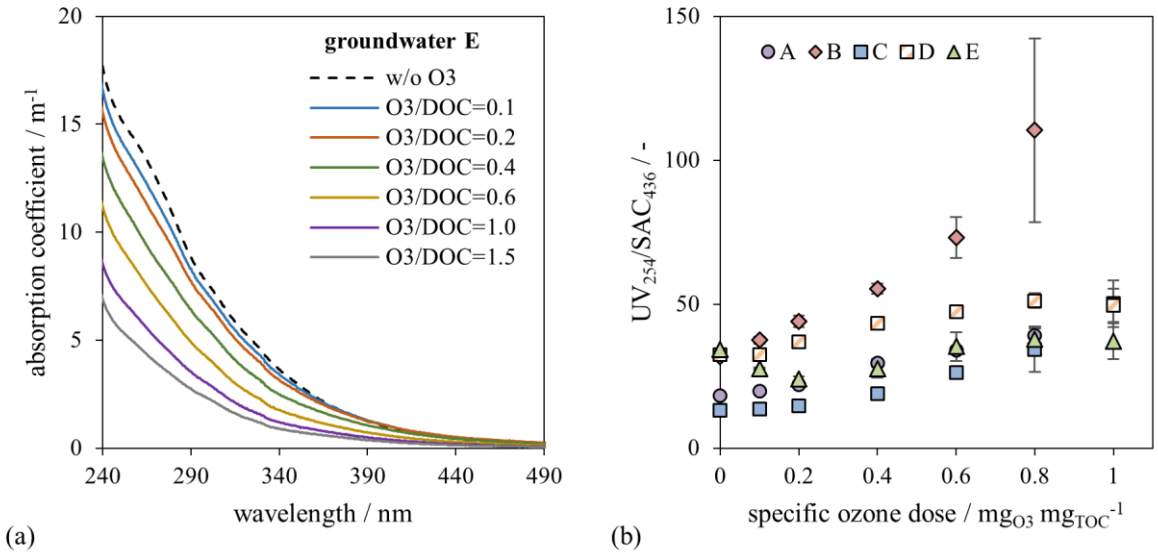

Figure 4-4. **(a)** Impact of specific ozone (in mg_{O3}/mg_{TOC}) on the absorption spectrum of groundwater $E.1_F$ (Kämmler et al., 2022). ϑ = 16 °C, pH 8.1, DOC 5.6 mg L^{-1}; a. spectral absorption coefficients / m^{-1}, **(b)** ratio UV_{254}/SAC_{436} as a function of specific ozone dose for different groundwaters. ϑ = 20 °C, TOC_0 3.5–6.2 mg L^{-1}, $UV_{254,0}$ 14.0–19.1 m^{-1}, SAC_{436} 0.41–1.2 m^{-1}, pH 7.6–8.0 (Table 3-2).

The effect of specific ozone dose on UV_{254} and SAC_{436} in humic-rich groundwater is further illustrated in Figure 4-5. Results are given as relative concentrations. A comprehensive overview of batch ozonation results for all groundwater samples is given in Table III-1. The left side of Figure 4-5 shows the relative decrease of UV_{254} (Figure 4-5.a) and SAC_{436} (Figure 4-5.c) versus specific ozone dose, i.e. ozone dose normalized to the groundwater TOC concentration. On the right side of Figure 4-5, UV_{254} (Figure 4-5.b) and SAC_{436} (Figure 4-5.d) are displayed versus the UV_{254}-specific ozone dose (O_3/UV_{254}), i.e. ozone dose normalized to the groundwater UV_{254} absorption. Ozonation resulted in reduction in both UV_{254} and visible (SAC_{436}) light absorption, as explained above.

Groundwaters C and E exhibit a lower rate of UV_{254} removal than other groundwaters, at comparable specific ozone dose (Figure 4-5.a). For groundwater C, which exhibits the highest $SUVA_{254}$, i.e. ratio of UV_{254} to DOC content of the groundwaters tested (Table 3-2), this may be explained by lower O_3/UV_{254} ratios than other waters at a particular specific ozone dose. If UV_{254} removal is plotted against UV_{254}-specific ozone dose (Figure 4-5.b), groundwater C is in line with most other groundwaters tested. Similar UV_{254} abatement trends in different groundwaters suggest that similar reaction mechanisms took place in the groundwaters tested here. As no reactive inorganic species as Fe(II) were present in the samples used here, it is assumed that reactions of ozone with NOM were consuming the major part of ozone. Similarly, it was observed for wastewater ozonation that DOM controls the consumption of ozone (Buffle et al., 2006a).

The fact that groundwater E seemed to be an outlier with lower UV_{254} removal seems less intuitive. SAC_{436} of ozonated groundwater E was also higher than that of other groundwaters and

even exceeded the initial SAC_{436} (Figure 4-5.c and d). The increase in SAC_{436} might be associated with the formation of high-molecular HS from hydrophobic NOM moieties (see chapter 4.1.1 and Kämmler et al., 2022). These HS may have contained additional phenolic moieties. If phenolic moieties are ozonated, quinonic moieties such as benzoquinones are produced, which exhibit strong UV absorbance coefficients (Nöthe et al., 2009; Önnby et al., 2018). This mechanism may have increased the overall UV_{254} of ozonated groundwater E. However, the higher UV_{254} of groundwater E may also be due to overestimation of specific ozone dose in this sample as it also showed unexpectedly low bromate formation (chapter 4.2).

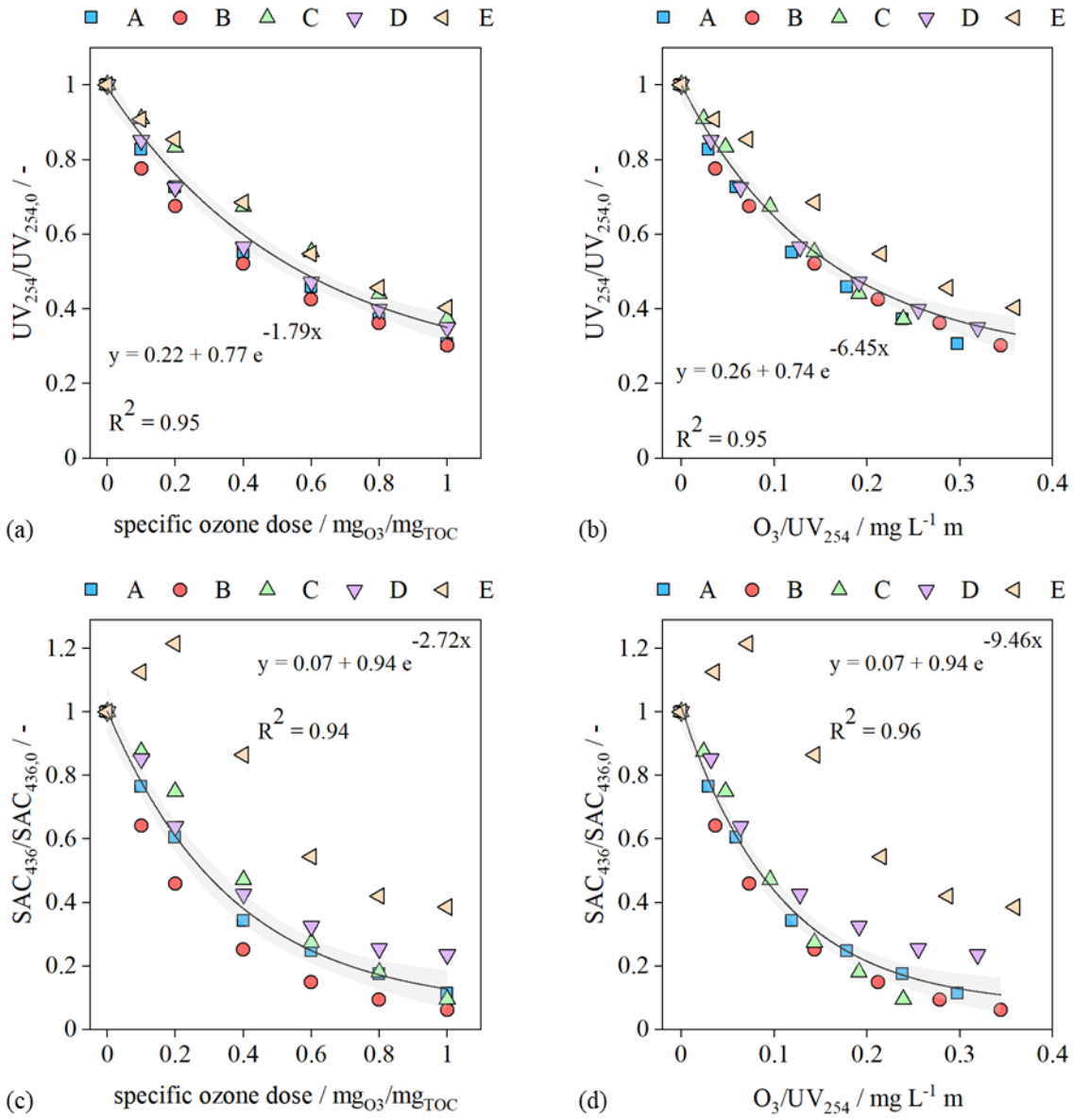

Figure 4-5. Correlation of UV_{254} and SAC_{436} in groundwater ozonation with TOC-specific ozone dose and UV_{254}-specific ozone dose (O_3/UV_{254}) with exponential fittings and 95 % confidence intervals. Origin fittings (Originlab, Northampton, US; groundwater E not included in SAC_{436} fittings). Experimental conditions: ϑ = 20 °C, TOC_0 3.5–6.2 mg L^{-1}, $UV_{254,0}$ 14.0–19.1 m^{-1}, SAC_{436} 0.41–1.2 m^{-1}, pH 7.6–8.0 (Table 3-2). **(a)** relative residual UV_{254} absorbance versus TOC-specific ozone dose. **(b)** relative residual UV_{254} absorbance versus UV_{254}-specific ozone dose; **(c)** relative residual SAC_{436} absorbance versus TOC-specific ozone dose; **(d)** relative residual SAC_{436} absorbance versus UV_{254}-specific ozone dose.

At comparable specific ozone dose, reduction in SAC_{436} was more pronounced than in UV_{254} for all groundwaters tested (Figure 4-5.c and d), as discussed above and also highlighted by an increase in the UV_{254}/SAC_{436} ratio by ozonation (Figure 4-4.b). Results for SAC_{436} abatement by ozonation look slightly more scattered than for UV_{254} (Figure 4-5.c and d). This is not quite reflected in the correlation coefficients as groundwater E was a clear outlier for SAC_{436} and hence not included in the SAC_{436} but in the UV_{254} fittings. The scattering may partly be due to the fact that values for SAC_{436} were more than a magnitude smaller than for UV_{254} (Table 3-2) and therefore more prone to experimental and analytical errors. Moreover, the decrease in SAC_{436} showed poor correlation with the SAC_{436}-specific ozone dose O_3/SAC_{436}, as it is shown in Figure III-11. In fact, SAC_{436} reduction decreased with increasing UV_{254}/SAC_{436} ratio (Figure III-11). This indicates a competition between UV_{254} absorbing and SAC_{436} absorbing moieties for ozone.

In conclusion, ozonation of groundwater NOM has little effect on concentrations of HS and TOC. However, molecular structure of NOM is altered by loss of hydrophobicity and decrease in molecular weight. BB and LMWA are formed at higher concentrations with increasing ozone dose. Chromophoric NOM features are significantly depleted by ozonation, particularly those with high wavelength absorption. UV_{254} absorbing moieties seem to be a major ozone consumer and therefore predict SAC_{436} reduction by ozonation better than DOC content of groundwater.

4.2 Bromate Formation in Groundwater Ozonation

Reaction of bromide with ozone and secondary oxidants, such as the hydroxyl radical (•OH), may produce the ozonation by-product bromate (von Gunten, 2003b; Yang et al., 2019b). The groundwaters examined in this work exhibit bromide concentrations of 70–330 µg L^{-1} (Table 3-2). The WHO proposed a bromate drinking water limit of 10 µg L^{-1} that was adopted by many countries while a health-based value of 2 µg L^{-1} was also suggested, but rendered unrealistic due to technical and analytical constraints (WHO, 2017).

Figure 4-6.a displays bromate concentrations that were measured in ozonated groundwater samples. At specific ozone doses < 0.4 mg_{O3}/mg_{TOC}, bromate concentrations were smaller than 10 µg L^{-1} in all groundwaters tested. SAC_{436} removal rates were up to 70 % at 0.4 mg_{O3}/mg_{TOC} (Figure 4-5.c). However, 10 µg L^{-1} bromate were exceeded at specific ozone doses between 0.4 and 0.8 mg_{O3}/mg_{TOC} in every groundwater tested (Figure 4-6.a). Moreover, Figure 4-6.a depicts a clear dependence of bromate formation on raw water bromide concentration. Under the conditions shown here, i.e. ozonation of aerated, filtrated natural groundwater samples at pH 7.6–8.0, applicable ozone doses are limited by bromate formation to 0.2–0.4 mg_{O3}/mg_{TOC} depending on the specific raw water quality (Kämmler et al., 2021). However, higher ozone doses may be applicable in raw water samples with lower bromide concentrations than shown here or in treatment schemes that apply bromate minimization or removal strategies.

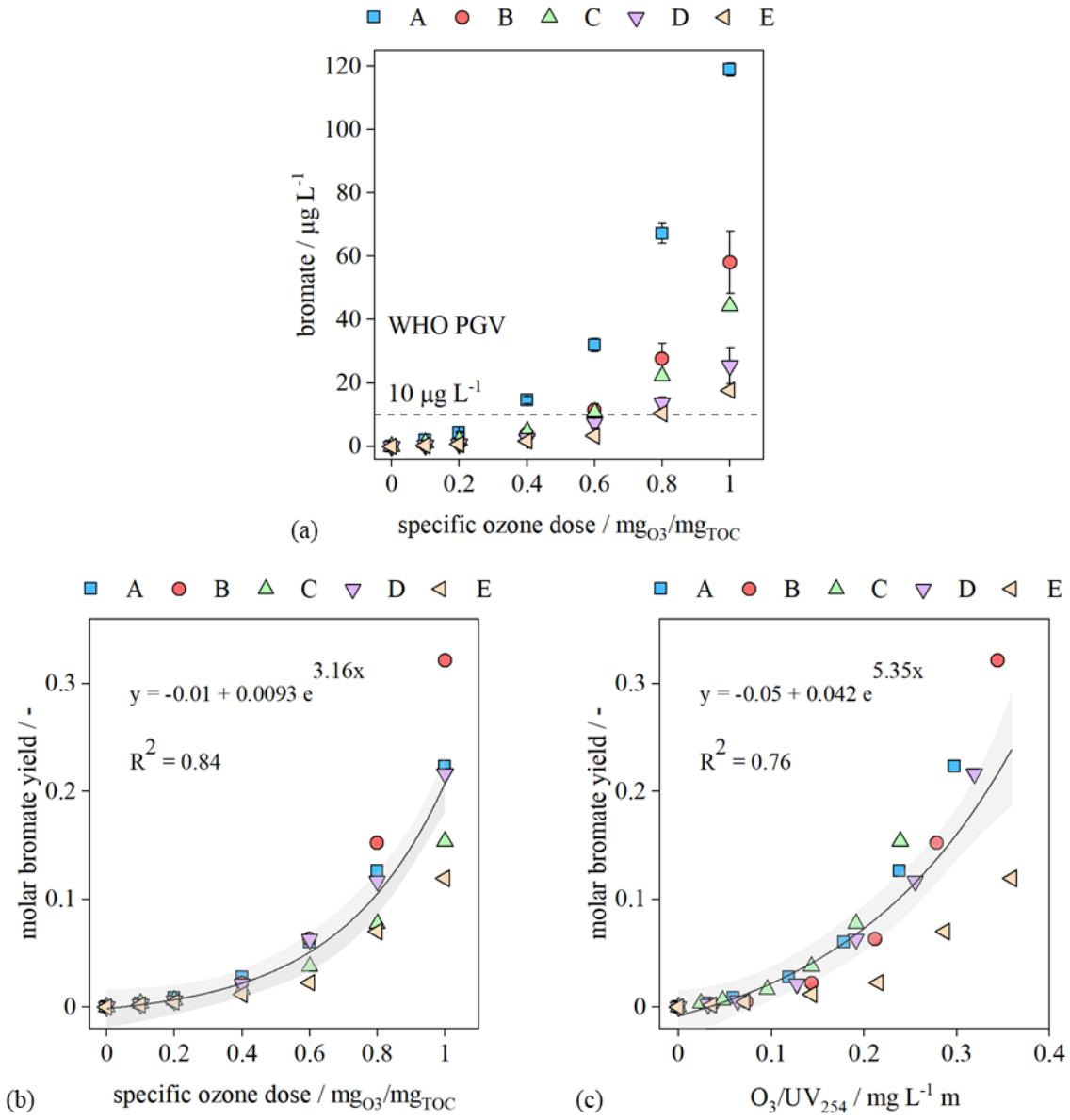

Figure 4-6. **(a)** Bromate concentrations in ozonated groundwater samples and world health organization provisional guideline value (WHO PGV) for bromate (WHO, 2017). Origin fittings (Originlab, Northampton, US). **(b)** Molar bromate yield versus TOC-specific ozone dose and **(c)** Molar bromate yield versus UV_{254}-specific ozone dose (O_3/UV_{254}) with exponential fittings and 95 % confidence intervals. Experimental conditions: ϑ = 20 °C, TOC_0 3.5–6.2 mg L^{-1}, pH 7.6–8.0 (Table 3-2).

To compare bromate formation in different groundwater samples, the molar bromate yield may be used which normalizes bromate formation to the initial bromide content of the water sample. Relationships of molar bromate yield and bromate concentrations are schematized in Figure III-12. For the groundwaters used here, bromate concentrations of 2 and 10 µg L^{-1} imply molar bromate yields of 0.4–1.7 % (2 µg L^{-1}) or 1.9–8.5 % (10 µg L^{-1}). Thus, acceptable molar bromate yields in groundwater ozonation are significantly below 10 %. Considering both the potential carcinogenic effect of bromate and regulatory limits, a maximum molar bromate yield of ~ 1 % may be considered acceptable in different waters, as a rule of thumb.

Molar bromate yield at a particular specific ozone dose is lower in groundwater samples C and E (Figure 4-6.b). In groundwater C, this may be due to the high aromaticity ($SUVA_{254}$ = 4.3 L mg^{-1} m^{-1}). If ozone dose is normalized to the sample UV_{254} absorbance, which reflects aromaticity, the correlation to molar bromate yield is similar for groundwater C as for groundwaters A, B and D (Figure 4-6.c). The lower bromate formation in groundwater E co-occurred with lower UV_{254} removal, at comparable ozone dose (Figure 4-5.a and b). This may be due to increased consumption of ozone by additional NOM moieties that were formed during the ozonation process, as indicated by increasing SAC_{436} (Figure 4-5.c and d). However, this may also indicate overestimation of specific ozone dose.

The mechanisms for bromate formation depend strongly on transient concentrations of ozone and hydroxyl radicals (•OH) as these are the main oxidants that produce bromate in ozonation processes (chapter 2.4). Bromate formation pathways may not be clearly identified for the data shown here, as information on •OH or the ratio of •OH to ozone exposure (R_{ct}) is not available. However, bromate formation pathways may be assessed by previous literature findings on R_{ct} and bromate formation pathways. It was observed that R_{ct} values peak in different water matrices both in the initial phase of ozonation and at small ozone doses (Buffle et al., 2006a; Wang et al., 2021b; Yu et al., 2020). Reported literature values for R_{ct} were as high as $1.3 \cdot 10^{-7}$ for wastewater (pH 7–7.2) at 0.41 mg_{O3}/mg_{DOC} (Zimmermann et al., 2011) and up to approximately $5 \cdot 10^{-7}$ for lake water (pH 6.9) at 0.23 mg_{O3}/mg_{C} (Shin et al., 2016). For the experiments shown here, a variation in R_{ct} with specific ozone dose is expected despite lack of analytical data. An R_{ct} value of 10^{-7} may be used to roughly approximate bromate formation pathways at low specific ozone doses (e.g., < 0.5 mg_{O3}/mg_{TOC}), which are realistic in groundwater treatment (see above). Figure I-2 shows theoretical portions of bromate formation pathways for a hypothetical, but realistic groundwater sample with pH 8 and 150 µg L^{-1} bromide, at 1.5 and 3 mg L^{-1} ozone. For the water samples used here (DOC 3.5–6.1 mg L^{-1}), 1.5 mg_{O3} L^{-1} may approximate low ozone doses. At $R_{ct} \approx 10^{-7}$, bromate formation pathways would range in the order II > III > V > I > IV (Figure I-2). At lower ozone doses (i.e., higher R_{ct}), indirect-direct bromate formation (pathway 3) may become more important while at higher ozone doses, bromate formation is shifted toward the direct-direct pathway (Figure I-2). However, it is expected that for typical groundwater decolorization conditions, direct-indirect and indirect-direct bromate formation are of major importance, due to relatively low applicable ozone doses. This should be considered when selecting appropriate bromate strategies for groundwater ozonation.

Figure 4-7 depicts molar bromate yield versus relative UV_{254} reduction (Figure 4-7.a) and relative SAC_{436} reduction (Figure 4-7.b). After strong initial reduction of UV_{254} and SAC_{436} at low bromate yield, bromate formation increased drastically for UV_{254} reduction of more than ≈ 30 % or SAC_{436} reduction of more than ≈ 50 %. This was reported similarly for wastewater ozonation, where an abrupt increase in bromate formation from UV_{254} reduction of 32 % was observed

(Chon et al., 2015). The correlation of exponential fitting is significantly better for UV_{254} reduction ($R^2 = 0.97$, Figure 4-7.a) than for SAC_{436} reduction ($R^2 = 0.73$, Figure 4-7.b). This may be a consequence of the generally more consistent reaction of UV_{254} toward ozonation, as shown in Figure 4-5 and discussed above. Slight variation between different water matrices may be due to different water matrix composition of the groundwater sample used, such as type of NOM, pH, alkalinity and bromide concentration. These parameters affect bromate formation significantly, due to their interaction with ozone and •OH (Song et al., 1996).

The exponential increase in bromate yield with UV_{254} reduction co-occurs with an increase in both •OH and ozone exposure, as these are the major oxidants involved in bromate formation (chapter 2.4). •OH exposure increases linearly with ozone consumption (Kwon et al., 2017) and with specific ozone dose (Lee et al., 2013). Conversely, the required amount of ozone to reduce UV_{254} by another unit increases with increasing degree of UV_{254} reduction (Figure 4-5). Thus, •OH exposure may show correlation beyond linearity with UV_{254} reduction. The increase in ozone exposure with ozone dose may be even more enhanced than in •OH exposure, due to depletion of ozone-reactive NOM moieties (Lee et al., 2013). Therefore, as UV_{254} abatement is a viable indicator of •OH and ozone exposure, it may approximate bromate formation in the ozonation of different water matrices (Chon et al., 2015; Li et al., 2017; Walpen et al., 2020). The results shown here suggest that this is also applicable for groundwater ozonation.

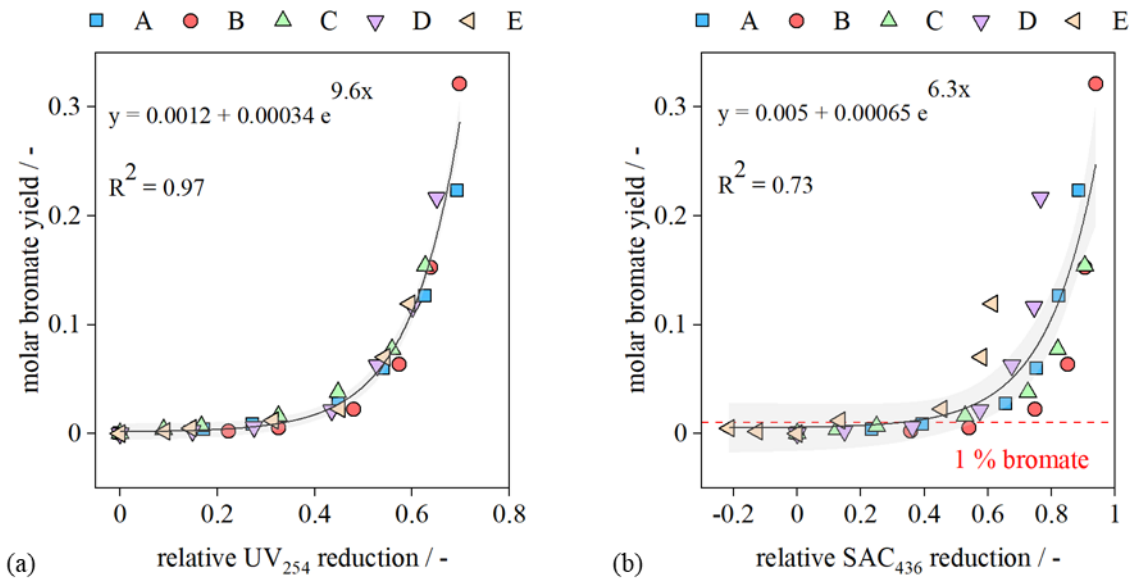

Figure 4-7. **(a)** molar bromate yield (percentage of raw water bromide turned into bromate) as a function of relative UV_{254} reduction ($1\text{-}UV_{254}/UV_{254,0}$); **(b)** molar bromate yield as a function of relative SAC_{436} reduction ($1\text{-}SAC_{436}/SAC_{436,0}$), molar bromate yield of 1 % highlighted with dashed line. Origin fittings (Originlab, Northampton, US). Exponential fittings include all groundwater samples with 95 % confidence interval. Experimental conditions: $\vartheta = 20$ °C, TOC_0 3.5–6.2 mg L^{-1}, pH 7.6–8.0 (Table 3-2).

4.3 Water Matrix Effects on NOM Degradation and Bromate Formation

4.3.1 Effect of Alkalinity

Ozonation of water A (total alkalinity 2.7 mmol L^{-1}) was performed at increased alkalinities of 3.15 and 3.6 mmol L^{-1} at constant pH of 8.1. Ozone doses of 0.5 and 1.0 mg_{O3}/mg_{DOC} were used. Experiments shown in this section were produced within a student project work at Hamburg University of Technology and partly presented in alternative form previously (Bharadwaj, 2022).

Figure 4-8 illustrates the ozone consumption parameters ozone exposure (ct), immediate ozone demand (IOD) and ozone decay rate for the secondary phase of ozonation (k_{sec}) for alkalinities of 2.7–3.6 mM and specific ozone doses of 0.5 and 1.0 mg_{O3}/mg_{DOC}. Variation of these parameters was more pronounced for different ozone doses than for different alkalinities (note the logarithmic axis scale). Most significantly, ct increased by more than a magnitude when the ozone dose was increased from 0.5 to 1.0 mg_{O3}/mg_{DOC}. The IOD increased only slightly, as it mainly reflects fast-reacting NOM moieties which are finite (Nöthe et al., 2009). The decrease in k_{sec} with ozone dose by about one magnitude was expected (Kwon et al., 2017). It may also be explained by more enhanced degradation of fast-reacting NOM moieties at 1.0 mg_{O3}/mg_{DOC}, resulting in lower reaction rates with ozone.

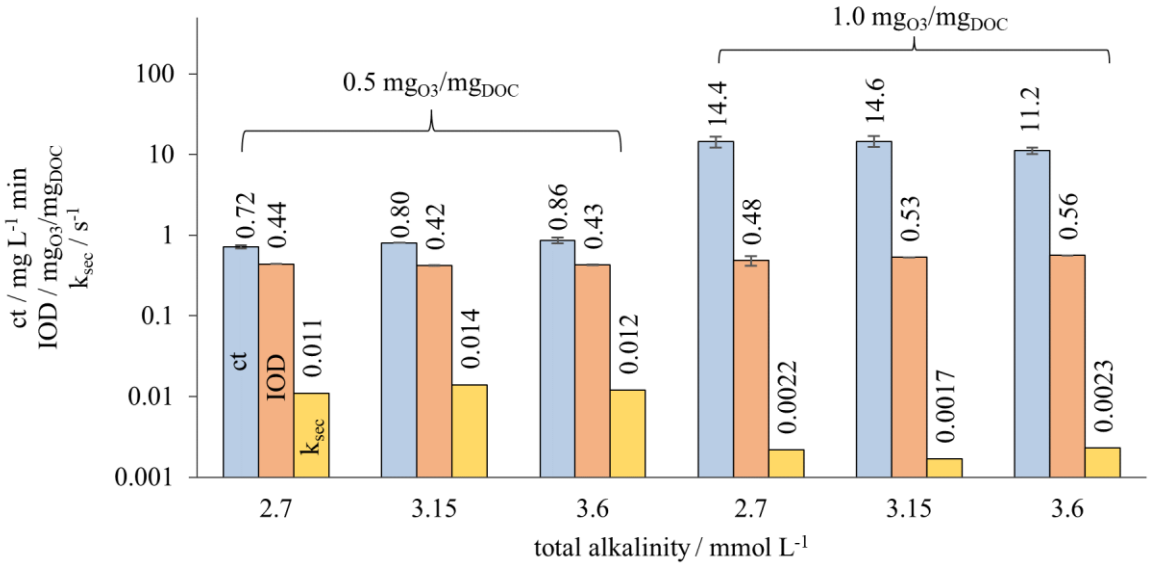

Figure 4-8. Effect of alkalinity on ozone exposure (ct), immediate ozone demand after 30 s (IOD) and secondary reaction rate of ozone (k_{sec}) in humic-rich groundwater at different alkalinities and ozone doses. Finished groundwater $A.5_F$ (Table II-1), pH 8.1, DOC 4.5 mg L^{-1}, $\vartheta \approx 19$ °C. Data with permission from Bharadwaj (2022)

The effect of alkalinity on ct, IOD and k_{sec} was less pronounced than the effect of ozone dose (Figure 4-8). A slight increase in ct with alkalinity at 0.5 mg_{O3}/mg_{DOC} was observed. This was also reported for different water matrices in previous studies and ascribed to the quenching of hydroxyl radicals (•OH) by bicarbonate and carbonate. Ozone decay is slowed down in this

case (Elovitz et al., 2000; Kim et al., 2020; Yang et al., 2019a). However, alkalinity had no clear effect on ct at 1.0 mg_{O3}/mg_{DOC}. Due to the strong dependence of ct on ozone dose, it may be assumed that the ozone dose in the 1.0 mg_{O3}/mg_{DOC} and 3.6 mM total alkalinity sample was slightly lower than supposed. This is supported by an increased IOD for this sample, which may result from overestimation of initial ozone concentration. For the other samples, at both ozone doses, IOD and also k_{sec} did not show significant variaton or trend with increased alkalinity. Contrarily, it was reported that IOD and k_{sec} slightly decrease with alkalinity (Elovitz et al., 2000; Kim et al., 2020). However, generally smaller alkalinities were used in the studies mentioned above compared to the current study. Effects of alkalinity on ozone reaction kinetics were found to level out at higher alkalinity (Elovitz et al., 2000). This could have resulted in only small effects of alkalinity on ct, IOD and k_{sec} in the experiments shown here. These effects could have been overlaid by small experimental or analytical errors.

Figure 4-9 shows the effects of alkalinity on SAC_{436}, UV_{254} and bromate formation in final, non-quenched samples of groundwater A. UV_{254} reduction was enhanced at 1.0 mg_{O3}/mg_{DOC} compared to 0.5 mg_{O3}/mg_{DOC}, as expected. In contrast, SAC_{436} reduction was comparable at 1.0 and 0.5 mg_{O3}/mg_{DOC}. As samples were diluted and actually measured absorbance values for SAC_{436} were quite low in the samples presented here (as low as 0.15 m^{-1} in non-quenched samples and 0.02 m^{-1} in quenched samples, measured in a 5 cm cuvette), the unexpectedly high SAC_{436} at 1.0 mg_{O3}/mg_{DOC} may be due to measurement inaccuracy. Actually measured UV_{254} values were >> 1 m^{-1} in all samples and may therefore be more resilient against analytical errors.

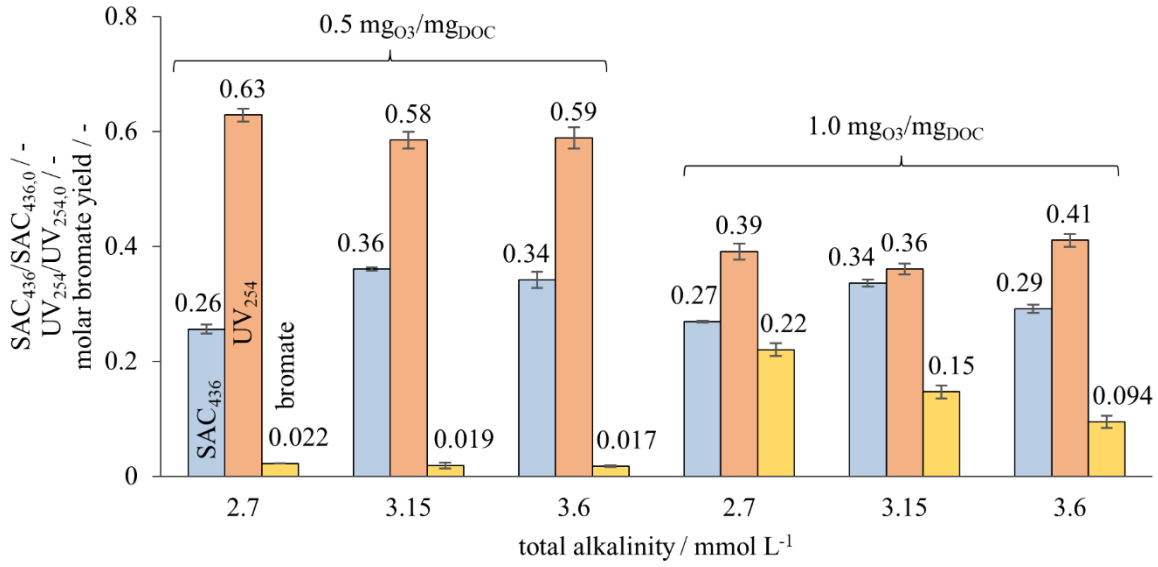

Figure 4-9. Effects of alkalinity and specific ozone dose on relative residual color ($SAC_{436}/SAC_{436,0}$), relative residual UV absorbance ($UV_{254}/UV_{254,0}$) and molar bromate yield in the ozonation of finished groundwater $A.5_F$ (Table II-1), pH 8.1, DOC 4.5 mg L^{-1}, $\vartheta \approx 19$ °C. Non-quenched samples after complete ozone decomposition are shown. Data with permission from Bharadwaj (2022)

Samples that obtained the same ozone dose of both 0.5 or 1.0 mg_{O3}/mg_{DOC} did not show a clear trend regarding UV_{254} and SAC_{436} reduction, that could be ascribed to alkalinity in these non-quenched samples. Results for SAC_{436} in quenched samples, as function of ct, are shown in Figure III-13. At 0.5 mg_{O3}/mg_{DOC}, SAC_{436} removal efficacy increased with decreasing alkalinity (Figure III-13.a). However, no clear effects of alkalinity on SAC_{436} at 1 mg_{O3}/mg_{DOC} (Figure III-13.b) and on UV_{254} (Figure III-14) were discernible.

Reactions of •OH and bicarbonate produce carbonate radicals ($CO_3^{\bullet-}$), which are secondary oxidants of ozone-based processes (von Sonntag and von Gunten, 2012). $CO_3^{\bullet-}$ and ozone are both selective oxidants which is indicated by correlation of their reaction rate constants with NOM aromaticity (Westerhoff et al., 1999; Yan et al., 2019). In contrast, •OH is less selective (von Sonntag and von Gunten, 2012; Westerhoff et al., 2007). Thus, it may also oxidize non-activated aromatic moieties recalcitrant to ozone (Leresche et al., 2021). A combination of •OH and ozone oxidation may therefore enhance the overall absorbance abatement by ozonation (Wenk et al., 2013). The increased scavenging of •OH by bicarbonate presumably decreased the activation of aromatic moieties by •OH. Conversely, oxidation of chromphores by $CO_3^{\bullet-}$ might not interact specifically with ozonation, as both oxidants are similarly selective. This could result in decreased SAC_{436} reduction at increased alkalinity, i.e. increased •OH scavenging. However, as no consistent effects of alkalinity on absorbance were discernible for part of the results shown here, overall effects of alkalinity on NOM absorbance abatement by ozonation may be small.

An increase in SAC_{436} in final, non-quenched samples compared to previous samples was observed (Figure III-13). This was not observed for UV_{254} (Figure III-14). This phenomenon was not expected and highlights the need for further investigation of the effect of reaction time on SAC_{436}.

Bromate formation in final non-quenched samples was reduced at increased alkalinities of 3.15 and 3.6 mmol L^{-1} at specific ozone doses of both 0.5 mg_{O3}/mg_{DOC} and 1.0 mg_{O3}/mg_{DOC} (Figure 4-9). This was also observed for quenched samples which were used to depict molar bromate yield as a function of ct in Figure III-15.

It was assumed in chapter 4.2 that bromate formation pathways in groundwater ozonation depend on specific ozone dose, but comprise oxidation of $BrOH/BrO^-$ by •OH (direct-indirect, pathway II) or oxidation of bromide by •OH (indirect-direct, pathway III) for many typical conditions. $CO_3^{\bullet-}$, which increasingly substitutes •OH at increasing alkalinity, may not oxidize bromide but $BrOH/BrO^-$ (Yang et al., 2019b; Yang et al., 2019a). Due to the latter and an increase in ct, an increase in bromate formation with alkalinity was observed in other studies (Freer, 2020; Li et al., 2011; Song et al., 1996). However, similar to the results shown here, a decrease in bromate formation with increasing alkalinity was observed in a study using moderate ozone doses of 0.5 and 1.0 mg_{O3}/mg_{DOC} (Glaze et al., 1993). At these relatively low ozone doses, the indirect-direct bromate formation is not assumed the major bromate formation

pathway, but may contribute significantly to bromate formation (chapter 4.2). This may have reduced bromate formation at increased alkalinity for the results shown here. Moreover, $CO_3^{\bullet-}$ is a selective oxidant for chromophoric NOM moieties (Yan et al., 2019). For the water sample presented here, with high content of chromophores, reaction with NOM might have consumed $CO_3^{\bullet-}$ and reduced its availability for oxidation of BrOH/BrO^-.

In summary, ozonation at increased alkalinity resulted in a decrease in bromate formation. For some of the experimental settings used here, results also indicate that this advantage might be compensated by higher SAC_{436} values at increased alkalinity.

4.3.2 Effect of pH

The effect of groundwater pH on SAC_{436} removal and bromate formation was analyzed in batch experiments using groundwater C (Preda, 2019). pH was adjusted with dosage of 0.1 M HCl or 0.1 M NaOH right before the experiments to avoid further changes in pH due to uptake or release of CO_2. Alkalinity was not adjusted and would therefore decrease with pH.

With increasing pH, ozone exposure generally decreases, which was considered to be mainly due to faster ozone decomposition by deprotonated phenolic DOM moieties (Audenaert et al., 2013; Buffle et al., 2006a). •OH exposure was observed to be independent of pH over a wide pH range (pH 6–9) in decarbonated lake water, i.e. without •OH scavenger. This results in higher R_{ct} values at higher pH (Elovitz et al., 2000). However, a slight increase in •OH yield with pH was reported for various NOM isolates at a similar pH range (pH 7–9), in presence of •OH scavenger (Önnby et al., 2018). Based on these references, an increase in pH induces a decrease in ozone exposure, at constant or increased •OH exposure and increased R_{ct}.

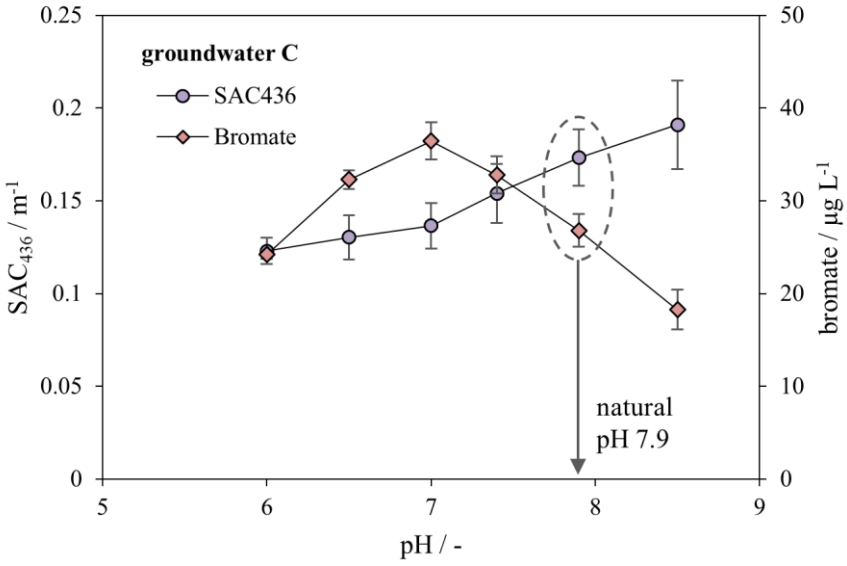

Figure 4-10. Effect of pH on SAC_{436} and bromate concentration after ozonation of groundwater C with 0.8 mg_{O3}/mg_{TOC}. pH adjusted from natural pH of 7.9 by addition of HCl or NaOH. DOC 3.5 mg L^{-1}, 21 °C

A consistent trend for decreasing SAC_{436} with pH was observed in the ozonation of groundwater C at 0.8 mg_{O3}/mg_{TOC} (Figure 4-10). UV_{254} was also abated more effectively at lower pH (Figure III-16.a). Enhanced UV_{254} abatement at lower pH was observed previously for the ozonation of NOM isolates at pH 7 and 11 (Remucal et al., 2020). This could be due to increased ozone exposure at lower pH. However, the effect of increased ozone exposure may partly be outweighed by slower reactions of DOM and ozone at lower pH (Audenaert et al., 2013). Another potential reason for more intensive chromophore abatement at lower pH may be found in pH-dependent reaction pathways of ozone and DOM. For the ozonation of phenol, which is incorporated in reactive NOM moieties, a dependence of product yield on pH was reported (Mvula and von Sonntag, 2003). At lower pH values, the yield of *cis,cis*-muconic acid increases compared to other reaction products. The yield of *cis,cis*-muconic acid is associated with ring cleavage reactions of NOM, which results in effective abatement of chromophores (Wenk et al., 2013). This indicates that at lower pH, reactions of NOM and ozone which induce reduction of UV-vis absorbance may be favored. Note that UV-vis absorbance of NOM generally decreases with pH (Dryer et al., 2008). This could result in a slight overestimation of the effects of pH on the ozonation of chromophores.

An increase in UV_{254}/SAC_{436} was observed with decreasing pH (Figure III-16.b). Similarly, slightly higher E2:E3 was observed in ozonation at pH 7 compared to pH 11 (Remucal et al., 2020). This could be due to competition of different kinds of NOM reactions, as described above.

The range of bromate concentration and SAC_{436} for pH 6–8.5 is illustrated in Figure 4-10. Bromate formation peaks at pH 7 and would decrease from there both at lower and higher pH. The lowest bromate concentration was measured at pH 8.5. At lower pH, the decisive bromate intermediate BrOH/BrO^- (pK_a = 8.8) is increasingly protonated, i.e. present in BrOH form. BrOH has lower reaction rates than BrO^- with both ozone ($k_{BrOH,O3}$ = 0, $k_{BrO^-,O3}$ 100 M^{-1} s^{-1}) and •OH ($k_{BrOH,•OH} = 2 \cdot 10^9$ M^{-1} s^{-1}, $k_{BrO^-,•OH} = 4.5 \cdot 10^9$ M^{-1} s^{-1}) (von Gunten, 2003b). The lower reactivity of BrOH would slow down bromate formation via the direct-direct and the direct-indirect pathways, as BrOH is a key intermediate in both (Figure 2-2). Additionally, BrOH may be increasingly consumed by NOM at lower pH and would therefore not be available for further oxidation (Song et al., 1997; von Gunten, 2003b). As a consequence of these bromate-minimizing effects, linear decrease in bromate concentration with pH was observed at constant ozone exposure (Legube et al., 2004). However, if the ozone dose is held constant at reduced pH, as in the experiments shown here, ozone exposure would increase, at constant or slightly lower •OH exposure (Elovitz et al., 2000; Önnby et al., 2018). This may enhance the oxidation of both bromide and Br• by ozone and increase bromate formation via the direct-indirect and the indirect-direct pathways (Figure 2-2). In the experiment shown in Figure 4-10, an increase in bromate formation with decreasing pH was observed between pH 8.5 and 7. Increased ozone exposure at lower pH might have outweighed slower oxidation of BrOH in this

pH range. Similarly, a pH reduction from 8.0 to 7.1 did not result in significant bromate control in the ozonation of another colored groundwater (Ikehata et al., 2013). However, below pH 7, a decrease in bromate formation was observed, which is assumed to be due to negligible concentrations of BrO^- below pH 7 (14 % of BrOH/BrO^- is present as BrO^- at pH 8 while only 1.6 % at pH 7 and 0.16 % at pH 6 for pK_a = 8.8). Moreover, total •OH yield may have been lower, at lower pH (Önnby et al., 2018), which would reduce bromate formation also via the indirect-direct pathway. Due to accumulation of BrOH at low pH values, bromo-organic compounds may be formed, which are an undesired by-product of ozonation (Song et al., 1997; von Gunten, 2003b).

It should be noted that alkalinity was reduced along with the pH due to increasing protonation of carbonate species. As bromate formation in groundwater ozonation may be enhanced at lower alkalinity (chapter 4.3.1), the variation in bromate formation shown might not be entirely due to variation in pH.

Overall, ozonation at lower pH results in enhanced absorbance degradation, but may also result in higher bromate formation, at constant ozone dose. However, higher absorbance reduction at lower pH may allow a reduction of ozone dose and therefore result in a beneficial tradeoff between color reduction and bromate formation. E.g., the ozonation of groundwater C at pH 6 with 0.8 mg_{O3}/mg_{TOC} resulted in SAC_{436} = 0.12 m^{-1} and 24 µg L^{-1} bromate (Figure 4-10) while ozonation with 1.0 mg_{O3}/mg_{TOC} at pH 7.9 resulted in SAC_{436} = 0.11 and 44 µg L^{-1} bromate (Figure 4-5, Figure 4-6.a).

4.3.3 Effect of Temperature

Most batch experiments shown in this work were performed at room temperature of the laboratory, which was ~ 20 °C. However, temperature in groundwater treatment plants may be lower. To improve the predictability of batch experiments for practical conditions, an additional set of experiments was conducted with groundwater C at reduced temperature of 10 °C (Preda, 2019).

The impact of different ozone doses on SAC_{436} and bromate, at 10 °C and 20 °C, is shown in Figure 4-11.a (SAC_{436}) and Figure 4-11.b (bromate). SAC_{436} reduction was similar at 10 °C and 20 °C for specific ozone doses of 0.1 and 1.0 mg_{O3}/mg_{TOC} (Figure 4-11.a). For ozone doses in between, SAC_{436} was lower at 10 °C. Bromate concentration was lower at 10 °C for the lowest specific ozone dose of 0.1 mg_{O3}/mg_{TOC} but higher for specific ozone doses > 0.1 mg_{O3}/mg_{TOC} (Figure 4-11.b). Thus, an increase in both SAC_{436} reduction and bromate formation was observed for most specific ozone doses, except 0.1 mg_{O3}/mg_{TOC}.

Generally, a two- to threefold decrease in reaction rate, depending on the specific reaction, may be expected for a temperature decrease of 10 °C (Blumenthal et al., 2006). Thus, ozone decay at lower temperature is slowed down. In fact, for a temperature decrease of 10 °C, a duplication of ozone exposure was observed (Elovitz et al., 2000). The •OH exposure was observed to depend on the consumed amount of ozone and not the ozone exposure and thus be independent

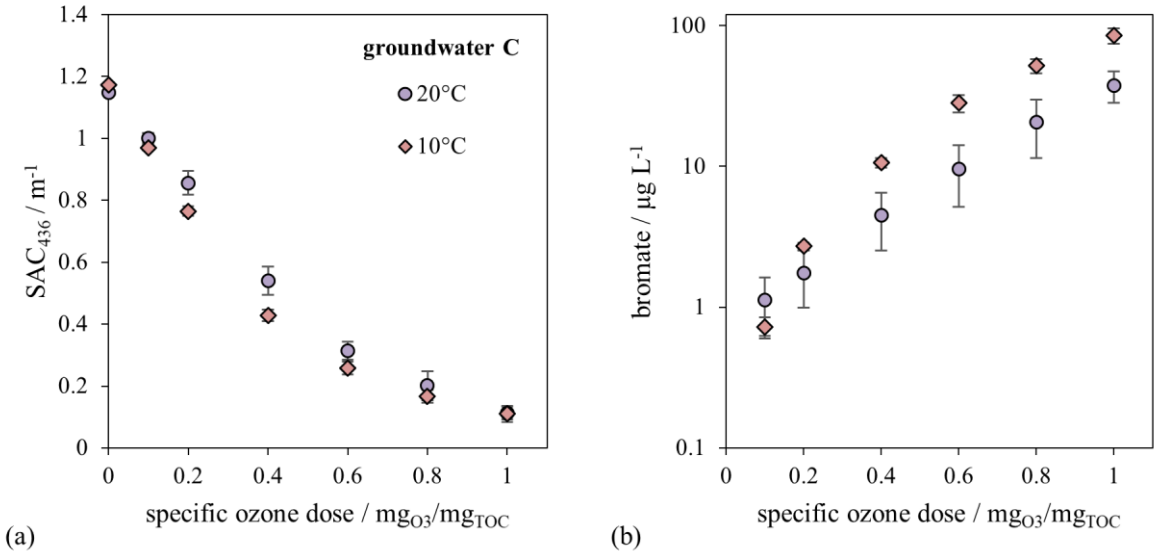

Figure 4-11. Effect of sample temperature on **(a)** SAC_{436} and **(b)** bromate concentration as a function of specific ozone dose after ozonation of groundwater C. Note logarithmic scaling of **(b).** pH 8.0, DOC 3.5 mg L^{-1}

of temperature (Elovitz et al., 2000; Kwon et al., 2017). However, contrary observations were made in other studies. Both an increase (Shin et al., 2016) and a decrease (Kim et al., 2020) in •OH exposure with temperature were observed in other studies, at constant ozone dose. Predictability of •OH exposure in the experiments presented here is hampered by these contrary literature findings.

As DOM is a major ozone consumer in water (Audenaert et al., 2013), it may be expected that the slower ozone decay at lower temperature is governed by slower reaction rates of DOM with ozone. However, lower SAC_{436} values were obtained at lower temperature (Figure 4-11.a). Thus, it may be hypothesized that reaction rates of chromophoric DOM moieties with ozone are less affected by temperature than other moieties. This could result in a more selective ozonation of chromophores. Moreover, •OH yield from ozonation could have decreased at lower temperature (Shin et al., 2016), which would slow down ozone consumption by radical chain reactions and therefore increase the availabilily of ozone for direct reactions with chromophoric DOM. However, as •OH exposure was not measured in the experiments shown here and contrary literature findings were made on its temperature-dependence (see above), this interpretation of lower residual SAC_{436} at lower temperature lacks verification.

Bromate formation is slowed down at lower temperature, if the ozone exposure is held constant (Legube et al., 2004). This may be due to both decreased reaction rates of bromate intermediates and lower •OH exposure, due to slower ozone consumption. However, at constant ozone dose, as in the experiments shown here, ozone exposure is expected to increase at lower temperature (Elovitz et al., 2000). This may have outweighed slower rates of bromate formation reactions. In fact, an increase in bromate formation was observed at lower temperature, at specific ozone doses > 0.1 mg_{O3}/mg_{TOC} (Figure 4-11.b). Only for the lowest ozone dose of 0.1 mg_{O3}/mg_{TOC},

bromate formation was lower at 10 °C compared to 20 °C. It is hypothesized that ozone consumption by bromate intermediates was outcompeted by chromophoric DOM, at low ozone dose. At higher ozone dose, chromophoric DOM may have been increasingly depleted and bromate formation increased due to higher ozone exposure. An alternative explanation for lower bromate formation at 10 °C and 0.1 mg_{O3}/mg_{TOC} implies that •OH exposure could have decreased with temperature (Shin et al., 2016). At low ozone doses, i.e. high R_{ct} values, the contribution of •OH to bromate formation, e.g. in the indirect-direct pathway, is high (Figure I-2). However, this explanation remains unverified, as •OH was not measured and literature findings on the effect of temperature on •OH are contrary (see above).

Figure III-17 depicts the trade-off between UV_{254} (Figure III-17.a) and SAC_{436} (Figure III-17.b) reduction and bromate formation. For low UV_{254} and SAC_{436} reduction, i.e., relative reduction smaller than 30–40 %, bromate formation was lower at 10 °C while higher bromate formation at 10 °C was observed for high UV_{254} and SAC_{436} reduction. In combination with different literature findings regarding the effect of temperature on •OH exposure, this highlights the need to perform ozonation laboratory experiments under realistic conditions, which include realistic temperature.

4.4 Bromate Minimization Techniques in Batch Ozonation

As it was shown in the previous chapters, ozonation of humic-rich groundwaters may produce bromate concentrations beyond regulatory limits, i.e. 10 µg L^{-1} in many countries (WHO, 2018). At natural groundwater conditions regarding pH, alkalinity, bromide concentration and DOC content, the 10 µg L^{-1} bromate limit was exceeded in five tested groundwaters at specific ozone doses between 0.4 and 0.8 mg_{O3}/mg_{TOC} (Figure 4-6.a). Thus, the control of bromate formation in groundwater ozonation may either allow the use of higher ozone doses or help to further minimize bromate concentrations.

4.4.1 Effects of the Combined O_3/H_2O_2 Process

The application of ozone in combination with H_2O_2 for the treatment of colored groundwater was tested in batch experiments (see below) as well as in small-scale pilot experiments (chapter 5.3). For batch experiments, groundwater A was ozonated at 0.25, 0.5 and 1.0 mg_{O3}/mg_{DOC}. Ozonation was performed without H_2O_2 (0 mol_{H2O2}/mol_{O3}) and with H_2O_2 added directly prior to ozone at H_2O_2/O_3 molar ratios of 0.5 and 2.0. Concentrations of dissolved ozone, H_2O_2 and SAC_{436} were measured at times 0.5, 1.5 and 5 min (ozone) or 5, 30, 60, 120 min, 1 d and 7 d (SAC_{436}, H_2O_2) while bromate was only measured once, several days after completion of the experiment. A comprehensive overview on the effects of H_2O_2 on the decolorization of groundwater by ozone is given in Figure 4-12. Dissolved ozone was detected only in two samples, at specific ozone doses of 0.5 and 1 mg_{O3}/mg_{DOC} in samples without dosage of H_2O_2 (Figure 4-12.d and g). Thus, ozone exposure could not be calculated accurately for the experiments. It was observed previously that H_2O_2 decreases ozone exposure significantly (Wang et al., 2018c).

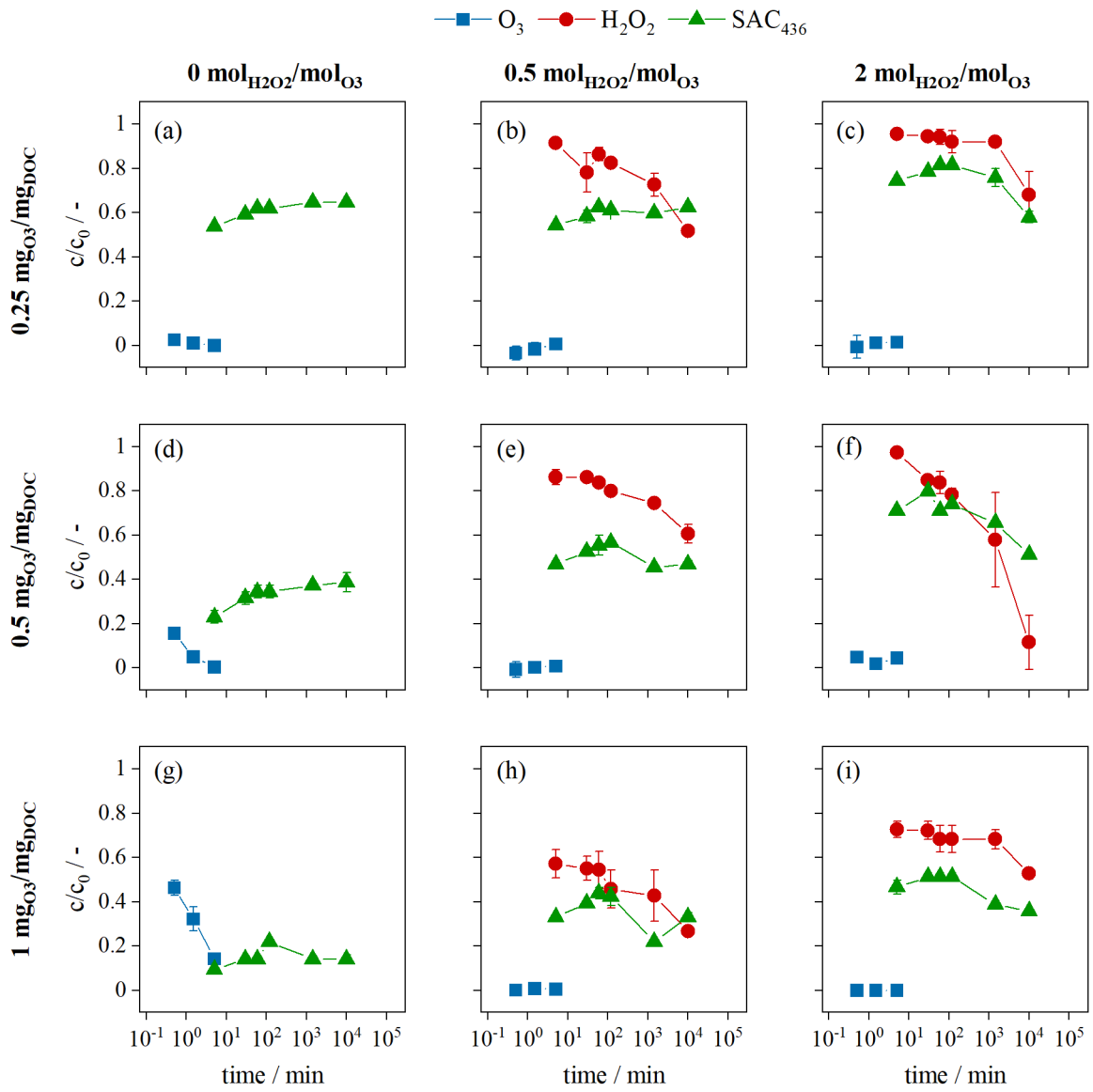

Figure 4-12. Dissolved ozone, SAC_{436} and H_2O_2 relative concentrations over time (logarithmic scale) in batch experiments with groundwater A.6$_F$ (Table II-1) at varying ozone and H_2O_2 doses. **(a)** 0.25 mg_{O3}/mg_{DOC}, 0 mol_{H2O2}/mol_{O3}; **(b)** 0.25 mg_{O3}/mg_{DOC}, 0.5 mol_{H2O2}/mol_{O3}; **(c)** 0.25 mg_{O3}/mg_{DOC}, 2 mol_{H2O2}/mol_{O3}; **(d)** 0.5 mg_{O3}/mg_{DOC}, 0 mol_{H2O2}/mol_{O3}; **(e)** 0.5 mg_{O3}/mg_{DOC}, 0.5 mol_{H2O2}/mol_{O3}; **(f)** 0.5 mg_{O3}/mg_{DOC}, 2 mol_{H2O2}/mol_{O3}; **(g)** 1 mg_{O3}/mg_{DOC}, 0 mol_{H2O2}/mol_{O3}; **(h)** 1 mg_{O3}/mg_{DOC}, 0.5 mol_{H2O2}/mol_{O3}; **(i)** 1 mg_{O3}/mg_{DOC}, 2 mol_{H2O2}/mol_{O3}; results from Eberhard (2021). Experimental conditions: pH 8.4, DOC 4.6 mg L^{-1}, $\vartheta \approx 20$ °C

The rate of ozone consumption by H_2O_2 depends on H_2O_2 concentration and, due to the initiation by reaction with HO_2^-, on pH. It may be calculated based on the assumptions of von Sonntag and von Gunten (2012) (pK_a (H_2O_2, HO_2^-) = 11.8, $k_{HO2^-,O3} = 9.6 \cdot 10^6$ M^{-1} s^{-1}). For the experiments presented in this chapter, i.e., at H_2O_2 doses of 12–192 µM and pH 8.4, pseudo-first-order reaction rate constants of ozone decay by reaction with H_2O_2 in the range of 0.046–0.73 s^{-1} may be assumed. This is in the range of ozone decay in DOM-rich waters. E.g., first-order ozone decay rates between 0.3 and 0.4 s^{-1} were measured in DOM-rich wastewater at pH 8 for the initial phase of reaction (Buffle et al., 2006a). Thus, H_2O_2 may significantly enhance ozone decay even in organic-rich waters, if present at sufficient concentration.

Residual amounts of H_2O_2 > 50 % were measured in all samples withdrawn at the first time step of 5 min, at all H_2O_2 doses tested (Figure 4-12). Slightly higher H_2O_2 residuals were measured at 2 mol_{H2O2}/mol_{O3} than at 0.5 mol_{H2O2}/mol_{O3} which may be expected due to higher initial H_2O_2 concentrations. However, high residual amounts of ozone were also measured at 0.5 mol_{H2O2}/mol_{O3} (Figure 4-12.b, e and h), which is the stoichiometric ratio of the reaction of ozone with H_2O_2 (Equation 2-6) and should result in complete H_2O_2 consumption if ozone reacted exclusively with H_2O_2.

As discussed above, H_2O_2 and DOM may react with ozone at similar rates, which predisposes both to compete for ozone. In wastewater ozonation, the reaction of ozone with DOM was reported to be dominant at low ozone or H_2O_2 doses (Buffle et al., 2006a). Thus, residual H_2O_2 was reported to exceed consumed H_2O_2 at low H_2O_2 doses in wastewater ozonation (Hübner et al., 2015). The portion of ozone reacting with H_2O_2, quantified as H_2O_2-induced hydroxyl radical yield, was observed to become more significant with increasing ozone dose, due to depletion of fast-reacting DOM moieties (Pocostales et al., 2010). This may be the reason for a decrease of residual H_2O_2 concentration at 1 mg_{O3}/mg_{DOC}, compared 0.5 mg_{O3}/mg_{DOC} (e.g., Figure 4-12.e and h). Likewise, a minor increase in total consumed H_2O_2 at 0.5 mg_{O3}/mg_{DOC} (Figure 4-12.e) was measured, compared to 0.25 mg_{O3}/mg_{DOC}. This is not reflected in the relative residual concentrations given, however total initial H_2O_2 concentration increased with ozone dose, at constant H_2O_2/O_3 ratio. After ozone depletion, H_2O_2 consumption in the water samples continued. In some samples, especially at the lowest ozone dose of 0.25 mg_{O3}/mg_{TOC}, high residual concentrations of H_2O_2 were still measured in the last aliquot that was withdrawn after seven days. In large-scale application of ozone/H_2O_2, removal of H_2O_2 after ozonation may therefore be necessary to address H_2O_2 drinking water limits.

For all ozone and H_2O_2 doses tested, SAC_{436} decreased proportionally to ozone dose (Figure 4-12). In samples with H_2O_2 addition, 5-min SAC_{436} residuals increased with H_2O_2 dose at 0.5 and 1 mg_{O3}/mg_{DOC} (Figure 4-12.e, f, h and i). At 0.25 mg_{O3}/mg_{DOC}, a similar pattern was observed for the increase of H_2O_2 dose from 0.5 to 2 mol_{H2O2}/mol_{O3} (Figure 4-12.b and c).

As discussed above, the addition of H_2O_2 to an ozonation process shifts oxidant exposure from ozone to •OH (Wang et al., 2018c). This is also indicated in the results shown here, as residual ozone concentrations were only measured in samples without H_2O_2 (Figure 4-12.d and g). In comparison to ozone, •OH is less selective in oxidizing aromatic DOM structures (Remucal et al., 2020; Wenk et al., 2013). This may explain the increase in SAC_{436} with H_2O_2 dose. A decrease in decolorization efficacy in the presence of H_2O_2 was also observed in a pilot study for groundwater decolorization using ozone (Tan et al., 1991). Similarly, in surface water treatment, UV_{254} abatement (Stylianou et al., 2018a) and humic substances removal (Beniwal et al., 2018) were less effective in the presence of H_2O_2 than without. Contrarily, higher $SUVA_{254}$ abatement in drinking water by ozone in combination with H_2O_2, compared to ozone alone, was reported (Phungsai et al., 2019). This suggests that the efficacy of absorbance abatement by

ozone/H_2O_2 treatment may depend on water characteristics or experimental conditions. Moreover, at H_2O_2/O_3 molar ratios exceeding the stoichiometric ratio of 0.5 mol_{H2O2}/mol_{O3}, the hydroxyl radical exposure might have been decreased due to scavenging of •OH by H_2O_2 (Glaze et al., 1987; Gottschalk, 1996; von Sonntag and von Gunten, 2012). This would reduce the total oxidant exposure in the samples, which is expected to result in high residual SAC_{436} values.

At the lowest ozone dose of 0.25 mg_{O3}/mg_{DOC}, SAC_{436} after ozone depletion was similar in the sample without H_2O_2 and at 0.5 mol_{H2O2}/mol_{O3} (Figure 4-12.a and b). This indicates a low impact of H_2O_2 on ozone exposure at low doses of both H_2O_2 and ozone, due to high initial reaction rates of DOM and ozone (Pocostales et al., 2010). Unexpectedly, in samples without H_2O_2 (Figure 4-12.a, d and g), SAC_{436} reached a minimum at 5 min after which it increased and reached a plateau at 90 min reaction time. This phenomenon was observed similarly in chapter 4.3.1. After ozone depletion, SAC_{436} decay continued at all ozone doses tested. Thus, it is assumed that the residual H_2O_2 levels caused oxidation of chromophoric NOM moieties.

The effect of H_2O_2 addition in combination with ozonation on bromate formation is depicted in Figure 4-13. Results are shown relative to bromate concentrations in ozonated samples without H_2O_2 dosage. A plot of molar bromate yield as function of specific ozone dose is given in supplemental Figure III-18. The effect of H_2O_2 addition on bromate reduction was largely dependent on ozone and H_2O_2 doses. At 0.25 mg_{O3}/mg_{DOC}, addition of H_2O_2 resulted in insignificant reduction in bromate by 10±15 % and 1±2 % for H_2O_2 doses of 0.5 and 2 mol_{H2O2}/mol_{O3} compared to non-H_2O_2 ozonation. At 0.5 mg_{O3}/mg_{DOC}, bromate formation was reduced by 30±4 % and 38±9 % while bromate was most significantly reduced by 66±0 % and 88±2 % at 1 mg_{O3}/mg_{DOC}.

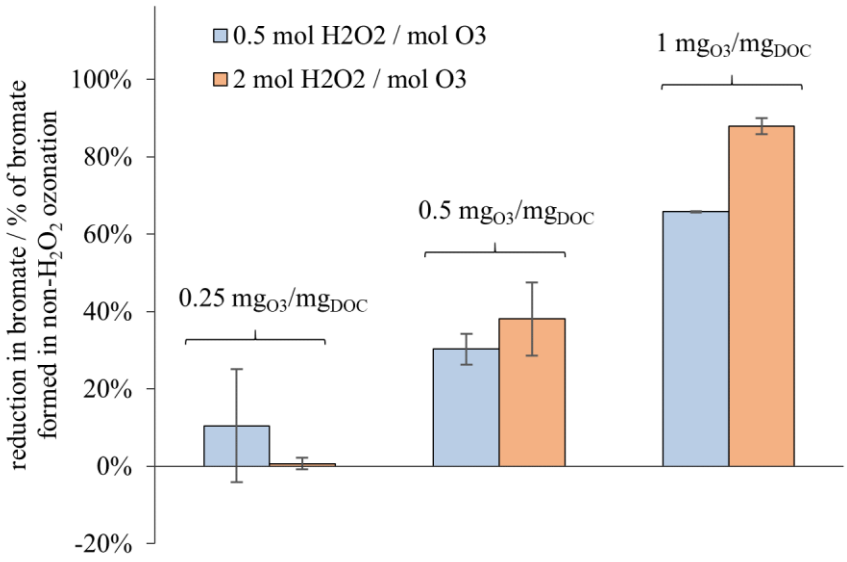

Figure 4-13. Reduction in bromate formation (as percentage of non-H_2O_2 ozonated samples) in batch experiments with groundwater $A.6_F$ (Table II-1) at varying ozone and H_2O_2 doses. Results adapted from Eberhard (2021). Experimental conditions: pH 8.4, DOC 4.6 mg L^{-1}, $\vartheta \approx 20$ °C

The addition of H_2O_2 decreases direct reaction of ozone with bromate intermediates and may therefore reduce bromate formation, especially via the direct-direct but also via other pathways (Soltermann et al., 2017). Moreover, H_2O_2 reduces the bromate intermediate BrOH to bromide (von Gunten and Oliveras, 1997), which would abate bromate formation via both the direct-direct and the direct-indirect pathways. Diametrically, bromate formation involving oxidation by the hydroxyl radical is enhanced in the presence of H_2O_2. This is evidenced in the presence of ammonia, which abates bromate formation via the direct-direct and the direct-indirect pathways (Pinkernell and von Gunten, 2001; Wu et al., 2020). H_2O_2 addition escalates bromate formation under these conditions due to an increased hydroxyl radical yield (Hofmann and Andrews, 2006). Consequently, the bromate minimization impact of H_2O_2 depends on specific reaction conditions. H_2O_2 was successfully applied to reduce bromate formation at relatively high ozone doses (> 0.5 mg_{O3}/mg_C) in the ozonation of surface water (Bourgin et al., 2017; Yu et al., 2020) and wastewater (Lee et al., 2016). High ozone doses imply low R_{ct} values (Shin et al., 2016), at which molecular ozone contributes significantly to bromate formation (Figure I-2). Under these conditions, H_2O_2 may mitigate bromate formation, as it is shown for ozone doses of 0.5 and 1 mg_{O3}/mg_{DOC} in Figure 4-13. However, the enhancement of hydroxyl radical-involved bromate formation by H_2O_2 may also exceed the reduction in ozone-involved bromate formation, resulting in a net increase in bromate concentration. This was observed for relatively low ozone dose in one out of three surface waters (Yu et al., 2020) and in specific wastewater matrices (Lee et al., 2016).

The production of hydroxyl radicals from ozone and H_2O_2 reaches a maximum at approximately 0.5 mol_{H2O2}/mol_{O3}, while both ozone exposure and BrOH concentration are still controlled at higher H_2O_2 doses. Thus, the ability of H_2O_2 to reduce bromate formation increases with H_2O_2 dose (von Gunten and Hoigne, 1994; von Gunten and Oliveras, 1998). High H_2O_2 doses may reduce bromate formation at a variety of experimental conditions including low ozone doses (Lekkerkerker-Teunissen et al., 2012; Soltermann et al., 2017). This could also be observed at 2 mol_{H2O2}/mol_{O3}, which resulted in higher bromate abatement than 0.5 mol_{H2O2}/mol_{O3} (Figure 4-13). Excessive H_2O_2 dosing may increase the operational costs of groundwater treatment. Moreover, maximum dosing and residual concentrations of H_2O_2 need to be considered (in Germany, 17 mg L^{-1} and 0.1 mg L^{-1}, respectively (Umweltbundesamt, 2021)).

In conclusion, the application of ozone in combination with H_2O_2 decreased bromate formation but also increased residual SAC_{436}. The impact of H_2O_2 increased both with ozone dose and with H_2O_2 dose. Figure III-19 is a comprehension of SAC_{436} versus bromate values for the ozone and H_2O_2 tested here. As SAC_{436} showed further decrease after ozone consumption, values after one hour (Figure III-19.a) and seven days (Figure III-19.b) are depicted. The value obtained after one hour should be more realistic for practical application as it is assumed that H_2O_2 would be removed after ozone depletion and would therefore not be available for further reaction. After one hour (Figure III-19.a), bromate formation was similar or higher when H_2O_2

was applied, at comparable SAC_{436}. SAC_{436}/bromate combinations obtained after reaction time of one week (Figure III-19.b) do not reveal a beneficial combination of ozone and H_2O_2 as all values are described by similar graphs. For both reaction times, the application of H_2O_2 in combination with ozone did not significantly improve the trade-off between decolorization and bromate formation beyond the effect of reduction in specific ozone dose.

To examine the effects of ozonation in combination with H_2O_2 dosage in other groundwaters, additional experiments with groundwaters C and E were performed, at one ozone dose each (0.8 and 1.14 mg_{O3}/mg_{TOC}). A similar trade-off between bromate minization and SAC_{436} increase was observed in these groundwaters, indicating similar mechanisms as discussed above for groundwater A. (Figure III-20).

4.4.2 Multi-stage Ozone Dosage

Experiments with multi-stage ozone dosage, i.e. partitioning of the total ozone dose into smaller aliquots, were performed with groundwater C (Preda, 2019). The specific ozone dose of 0.8 mg_{O3}/mg_{TOC} was added to the water sample in 1–5 aliquots. This procedure was supposed to mimic multi-stage ozonation with different number of stages. Equilibration time between the dosing steps was 10 min to allow complete ozone depletion in between.

Figure 4-14 illustrates the effect of different number of ozone stock solution aliquots on SAC_{436} and bromate obtained in the final sample. With increasing number of aliquots, SAC_{436} decreased. Similar to the results shown here, enhanced reduction of UV_{254} was observed when ozone was added in a multi-step procedure to NOM isolates at neutral pH (Lienhard and Sontheimer, 1979).

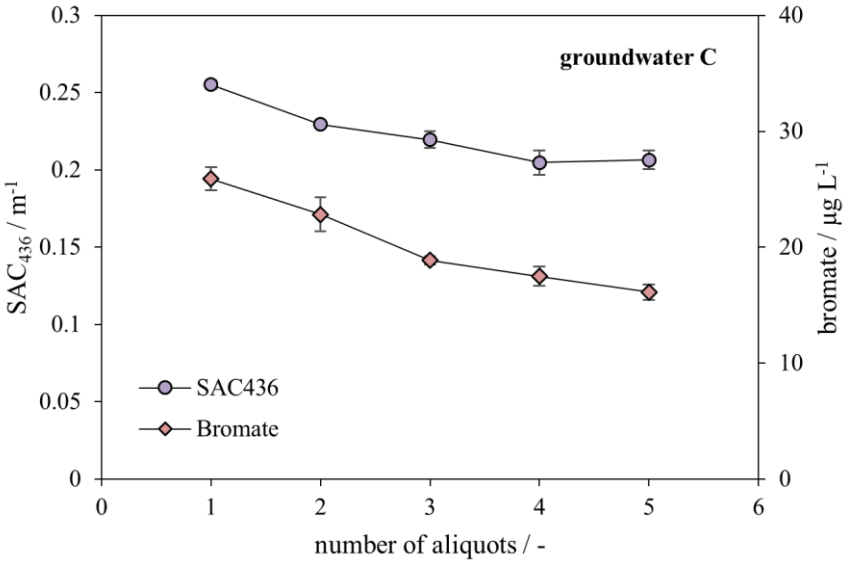

Figure 4-14. Effect of partitioned dosing of ozone on SAC_{436} and bromate. Stock solution volume to apply specific ozone dose of 0.8 mg_{O3}/mg_{TOC} was partitioned into 1, 2, 3, 4 or 5 aliquots dosed in 10 min intervals. Results adapted from Preda (2019). pH 8.0, DOC 3.5 mg L^{-1}, 21 °C

The use of smaller ozone doses changes ozone/NOM ratios. It has been shown that reaction products of ozone and phenols vary depending on the ozone/phenol ratio due to competition of different reactants for ozone (Mvula and von Sonntag, 2003). It is plausible that this competition kinetic approach also applies for NOM. As chromophoric NOM moieties show high reaction rates with ozone (Westerhoff et al., 1999), they could be oxidized preferentially, at limited ozone availability. This would result in enhanced removal of absorbance, e.g. of SAC_{436}. It is also viable that a shift in reaction conditions of NOM implies a change in •OH yield. At lower •OH yield, direct ozonation of chromophores may be enhanced. In the same study cited above (Lienhard and Sontheimer, 1979), no difference in UV_{254} reduction between single-step and multi-step ozone dosage was observed at pH 2. At pH 2, the •OH yield of NOM ozonation is significantly lower than at neutral pH (Önnby et al., 2018). Generally, a decrease in •OH yield would also decrease the maximum potential of •OH yield reduction. Contrawise, at neutral pH, a high overall •OH yield would allow more significant reduction in •OH yield. Note that no effects of pH on •OH yield were reported elsewhere (Mvula and von Sonntag, 2003). Due to this contradiction and the lack of •OH measurements for the results presented here, the explanation of higher absorbance removal due to lower •OH yield must remain hypothetical.

Similar to SAC_{436}, bromate concentrations in ozonated samples decreased with increasing number of dosing steps (Figure 4-14). The discussion on the effect of ozone limitation on SAC_{436} removal may also explain the effect on bromate. If NOM moieties with high ozone reaction rates preferentially consume ozone at low ozone dosing concentrations, this may reduce ozone availability for direct reaction with bromide and BrOH. Moreover, if •OH yield is reduced, this would also decrease bromate formation.

Despite uncertainties about the underlying mechanisms, multi-stage ozone dosage resulted in clear improvements in both SAC_{436} removal and bromate minimization. Thus, it is considered a viable option for optimization of the ozonation-biofiltration process with regard to bromate minimization. If multi-stage ozonation is combined with an intermittent biological degradation step, e.g. biofiltration, biodegradable organic compounds may be removed before the next ozonation stage. These compounds are therefore not consuming ozone in the subsequent ozonation stage. Higher overall DOC removal rates were reported for multi-stage ozonation with intermittent biodegradation (Nishijima et al., 2003; Yasui and Miyaji, 1992). Intermittent biodegradation could also allow the reduction of overall ozone dose. This would further reduce the formation of bromate and other ozonation by-products.

5 Small-scale Pilot Ozonation-biofiltration

This chapter presents results of small-scale pilot experiments for groundwater decolorization at groundwater treatment plants A and E. Both plants produce drinking water with visible color (SAC_{436}) around (groundwater E, $SAC_{436} \approx 0.5\ m^{-1}$) or above (groundwater A, $SAC_{436} \approx 0.8$–$0.9\ m^{-1}$) the German drinking water limit of $0.5\ m^{-1}$ (Trinkwasserverordnung, 2001). The small-scale pilot plant is schematized in Figure II-8 and described in chapter 3.2.2. A first set of experiments focussed on ozonation under different operating conditions, comparison to batch experiments and bromate minimization strategies (H_2O_2 or ammonia addition, pH depression). A second set of experiments focussed on the effects of combined ozonation and biofiltration. For most experiments conducted, finished drinking water was used, however, additional experiments were conducted with raw water and aerated, non-filtrated raw water at groundwater treatment plant A. Part of the results shown here for groundwater treatment plant E were elaborated within a Master's thesis at Hamburg University of Technology (Sellmann, 2020). Moreover, excerpts of the results shown here were presented before in Kämmler et al. (2021).

5.1 Comparison to Batch Experiments

Small-scale pilot experiments were performed with water samples similar to those that were used for batch ozonation experiments (chapter 4). Thus, results of small-scale pilot and batch ozonation obtained with groundwaters A and E were compared. Data for groundwater samples were shown and discussed previously in chapter 4.1. Small-scale pilot experiments were performed on other days than sampling for batch experiments was done, which resulted in slightly different water quality, e.g. higher temperature and pH in batch experiments due to sample adaptation to atmospheric conditions during transport and storage.

Generally, groundwater E showed lower decolorization performance than groundwater A (Figure 5-1.a), which was discussed for batch experiments before (Figure 4-5.c, chapter 4.1). For both groundwaters A and E, a lower ozone dose was needed for SAC_{436} reduction in batch than in pilot ozonation. A similar pattern was obtained for UV_{254} reduction in groundwater A while UV_{254} reduction in groundwater E was comparable in batch and pilot experiments (Figure 5-1.b). Bromate formation was similar for batch and pilot ozonation in groundwater A while pilot ozonation of groundwater E resulted in significantly higher bromate formation than batch ozonation at ozone doses above 0.5 mg_{O3}/mg_{TOC} (Figure 5-1.c). To exclude the possibility that different patterns obtained by pilot and batch ozonation result from systematic error regarding ozone dose in one of the ozonation setups, UV_{254} reduction was plotted against bromate formation (Figure 5-1.d). By this, ozonation results may be discussed independently of ozone dose. For both groundwaters A and E, molar bromate yield was smaller in pilot than in batch ozonation for relative UV_{254} reduction of up to approximately 30–40 %. For higher UV_{254} reduction, bromate formation was clearly enhanced in pilot experiments.

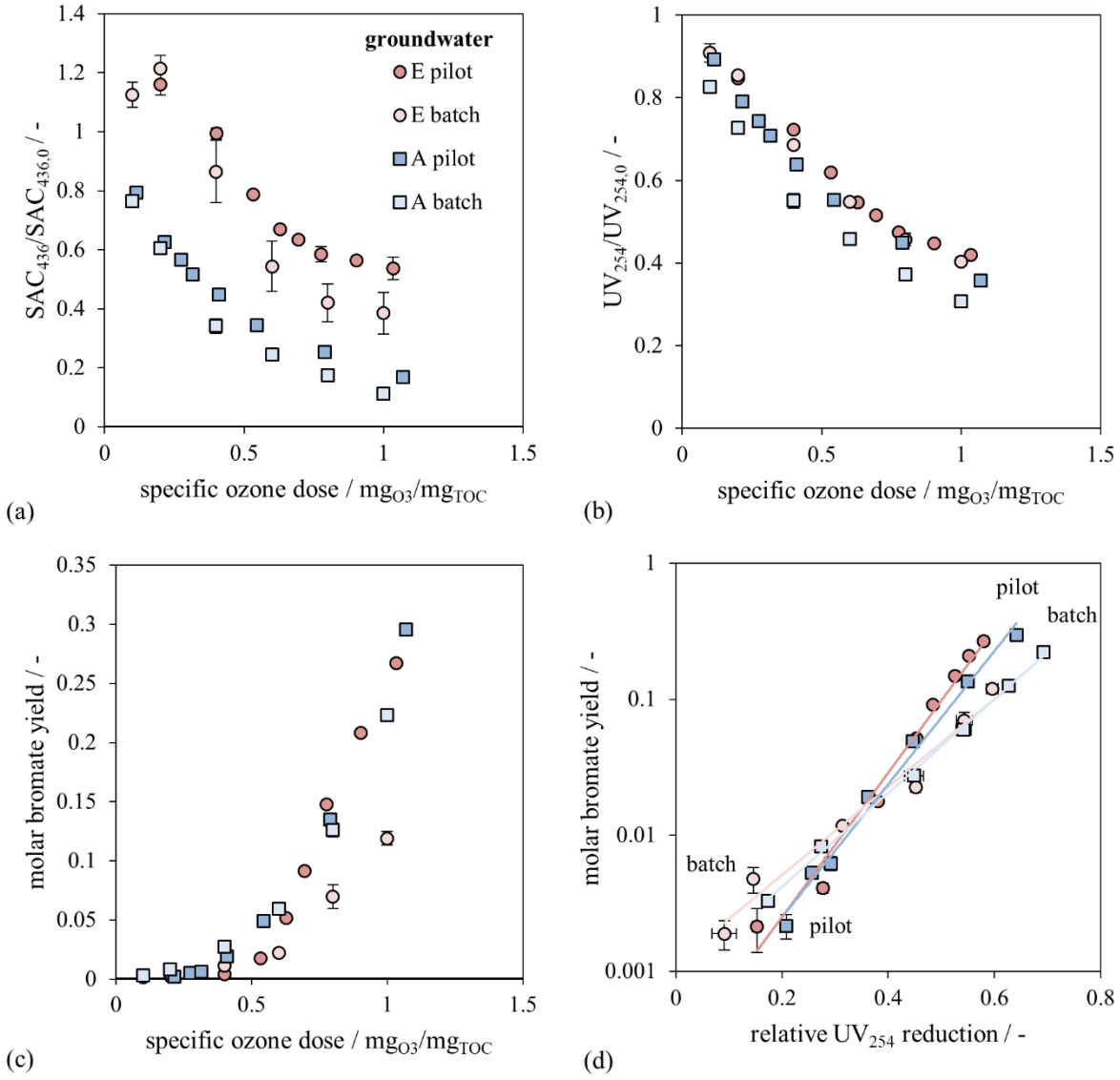

Figure 5-1. Results of of small-scale pilot experiments compared to batch ozonation for groundwaters A and E. **(a)** Relative residual SAC_{436} versus specific ozone dose; **(b)** relative residual UV_{254} versus specific ozone dose; **(c)** molar bromate yield versus specific ozone dose; **(d)** molar bromate yield (logarithmic scale) versus relative UV_{254} reduction ($1-UV_{254}/UV_{254,0}$) Experimental data and exponential fits ($y = a \cdot \exp(b \cdot x)$). Fitting parameters: a = 0.0002, b = 12.2, R^2 = 0.98 (E pilot); a = 0.0012, b = 7.4, R^2 = 0.97 (E batch); a = 0.0003, b = 11.3, R^2 = 0.99 (A pilot); a = 0.0009, b = 7.9, R^2 = 1.0 (A batch). Experimental conditions: 13 °C, 5.7 mg_{TOC} L^{-1}, pH 8.0 (E pilot); 20 °C, 5.9 mg_{TOC} L^{-1}, pH 7.8 (E batch); 15±1 °C, 4.5 mg_{TOC} L^{-1}, pH 7.6 (A pilot); 20 °C, 4.6 mg_{TOC} L^{-1}, pH 7.8 (A batch). Water samples used: Groundwater A and E for batch experiments (Table 3-2), Groundwater $A.1_F$ (Table II-1) and $E.1_F$ (Table II-2) for pilot experiments.

The coincidence of this phenomenon in both groundwaters suggests that this pattern may be due to reaction conditions in pilot and batch ozonation. E.g., a major difference between both ozonation setups is in dosing mechanisms, i.e. addition of ozone stock solution in batch experiments and ozone gas venturi injection in pilot experiments. Similarly, it was observed that bromate formation in batch ozonation may either be lower or higher than in membrane ozone/H_2O_2 application (Merle et al., 2017; Stylianou et al., 2018b) and in membrane ozonation (Kämmler et al., 2022) depending on the operating conditions. An alternative explanation may be the higher temperature of 20 °C in batch ozonation compared to 13–16 °C in pilot ozonation.

This could also have resulted in lower bromate formation, similar to the batch ozonation of groundwater C at 10 °C and 20 °C (Figure 4-11, Figure III-17). To interpret the results obtained in this study, it should be noted that realistic ozone doses for groundwater decolorization are in the range of 0.2–0.4 mg_{O3}/mg_{TOC} and result in molar bromate yield of ≈ 0.01 (chapter 4.1). In this range, batch and pilot ozonation resulted in similar combination of UV_{254} reduction and molar bromate yield (Figure 5-1.d). However, the congruence of results shown here with larger plants or other ozone dosing systems is not suppositional and warrants further research.

5.2 Ozone Decay and Reaction Kinetics in Organic-rich Groundwater

Ozone decay kinetics were examined in groundwaters A and E in small-scale pilot experiments. Dissolved ozone measurements were made with an online sensor at different sampling ports mounted on a column reactor (Figure II-8). A correlation to reaction time was made by dividing reactor volume and water flow rate.

Figure 5-2.a depicts ozone decay kinetics in groundwater A as relative logarithmic plot. From the first data point measured, i.e. after the immediate ozone demand (IOD) phase, ozone decay was exponential, which appears as linear plot for logarithmic values. Linear slopes shown in Figure 5-2.a were used to calculate the first-order ozone decay rate constant k_{sec}. k_{sec} values in the range of $1.7 \cdot 10^{-3}$ s^{-1} to $1.7 \cdot 10^{-2}$ s^{-1} were measured in groundwater A and decreased with specific ozone dose. k_{sec} for other experiments, e.g. with groundwater E, are listed in Table III-2. k_{sec} in groundwater E was faster than in groundwater A (up to $4.7 \cdot 10^{-2}$ s^{-1} at 0.5 mg_{O3}/mg_{DOC}, Figure III-23.a). Lower k_{sec} values in the range of $2.7 \cdot 10^{-4}$ s^{-1} to $1.5 \cdot 10^{-2}$ s^{-1} were reported for natural waters and NOM isolates (Elovitz et al., 2000; Kwon et al., 2017; Shin et al., 2016; Westerhoff et al., 1998).

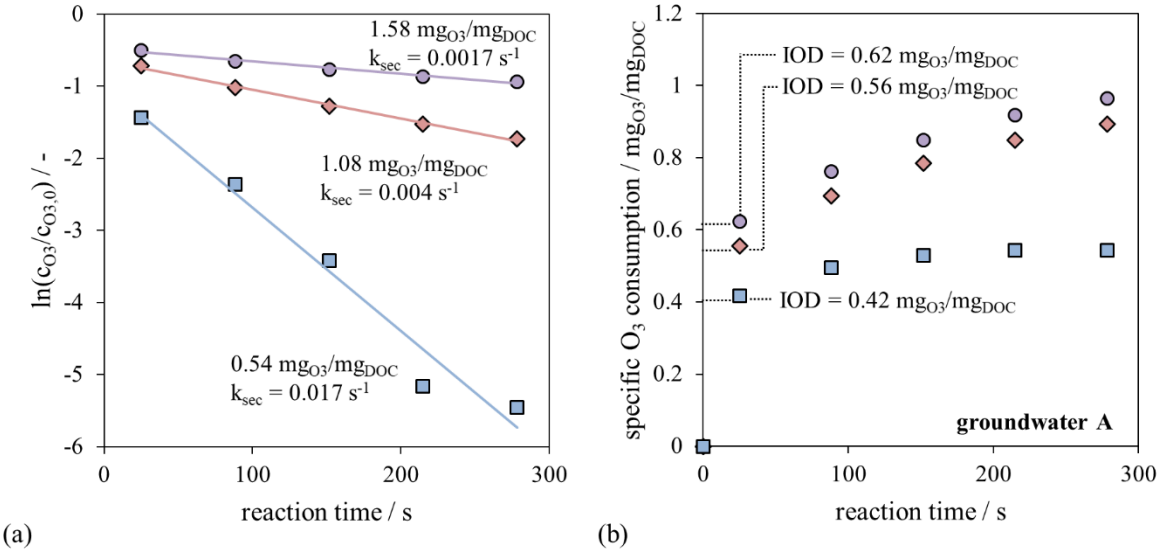

Figure 5-2. Reaction kinetics of ozone in finished groundwater $A.1_F$ (Table II-1). Experimental conditions: ϑ = 14 °C, DOC 4.5 mg L^{-1}, pH 7.7. **(a)** logarithmic relative ozone decay kinetics plotted as $\ln(c_{O3}/c_{O3,0})$, R^2 = 0.98, 1.00 and 0.97 for 1.58, 1.08 and 0.54 mg_{O3}/mg_{DOC}. **(b)** Specific ozone consumption (normalized to influent sample DOC concentration) with immediate ozone demand (IOD) after 25 s.

Similar to the groundwaters used here, k_{sec} in wastewater ozonation may exhibit values of up to $3.1 \cdot 10^{-2}$ s^{-1} (Nöthe et al., 2009). The high ozone decay-rates in the samples used here may be due to their relatively high $SUVA_{254}$ (Table 3-2) (Westerhoff et al., 1999). Moreover, NOM from highly reduced environments may be rich in lignin-like material (Kölle, 2010) and exhibit high electron donating capacity (EDC) (Walpen et al., 2018). Generally, this could indicate a high content of phenolic compounds in reduced groundwaters (Aeschbacher et al., 2012). Phenols exhibit high reaction rates with ozone (Houska et al., 2021), which could explain the high k_{sec} in groundwaters used here. Within the groundwaters A and E, higher k_{sec} in groundwater E indicates that the composition of NOM moieties may be different. Groundwater E exhibits low sulfate concentration (1 mg L^{-1}, Table 3-2). This indicates that groundwater E is highly reduced (Kölle, 2010), which could in turn imply a high phenol content (Walpen et al., 2018). Moreover, total alkalinity of groundwater E is low (Table 3-2), which implies low •OH scavenging by carbonate and bicarbonate and therefore enhanced ozone consumption (Elovitz et al., 2000).

Figure 5-2.b depicts specific ozone consumption, i.e., consumed ozone amount per initial DOC concentration, versus reaction time. At the lowest ozone dose of 0.5 mg_{O3}/mg_{DOC}, ozone was completely consumed at well below 300 s. At 1 and 1.5 mg_{O3}/mg_{DOC}, ozone consumption increased in very similar way after the IOD phase, which consumed slightly more ozone at 1.5 mg_{O3}/mg_{DOC}. The IOD increased with specific ozone dose and was in the range of 0.42–0.62 mg_{O3}/mg_{DOC} for groundwater A. This was only slightly lower than the IOD in groundwater E (0.46–0.67 mg_{O3}/mg_{DOC}, Figure III-23.b). Specific IOD values in natural waters were reported in the range of 0.15 to 0.5 mg_{O3}/mg_{DOC} while ozonation of more aromatic and reactive NOM isolates may result in IOD values of up to 1 mg_{O3}/mg_{DOC} (Cho et al., 2003; Kwon et al., 2017; Park et al., 2001; Shin et al., 2016). Similar to k_{sec}, the IOD in organic-rich groundwater is therefore in the upper range of reported literature values.

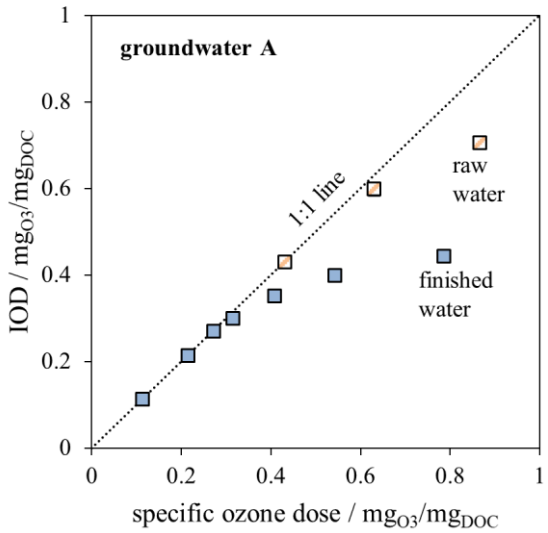

Figure 5-3. Immediate ozone demand (IOD) after 25 s reaction time in raw groundwater ($A.1_R$) and finished groundwater ($A.1_F$). 14–17 °C, DOC 4.5 mg L^{-1}, pH 7.6 (finished), DOC 6.1 mg L^{-1}, pH 7.8 (raw) (Table II-1)

Figure 5-3 shows the IOD for raw groundwater A compared to finished, i.e., aerated, coagulated and filtered groundwater A. The IOD in raw water was increased compared to finished water. Reduced inorganic species in anoxic groundwater, e.g. Fe^{2+}, H_2S and NO_2^- exhibit reaction rates with ozone in the 10^5 M^{-1} s^{-1} range (von Gunten, 2003a). Resulting half-life times of these species, even at a low ozone concentration of 1 mg L^{-1}, are ≤ 1 s, which is fast enough to allow significant oxidation of inorganic compounds within the IOD phase. For the groundwater tested here, mainly H_2S may be expected from the water supplier's regular analyses. Moreover, the raw water shown exhibited slightly higher pH (7.7 versus 7.6, Table II-1) and higher $SUVA_{254}$ (3.9 versus 3.2 L mg^{-1} m^{-1}), which may have increased its reactivity with ozone (Westerhoff et al., 1999).

Dissolved ozone concentration measurements from the ozonation of groundwater A at pilot-scale were used to calculate the ozone exposure at different specific ozone doses of 0.11–1.07 mg_{O3}/mg_{DOC}. Figure 5-4 depicts the effects of ozone exposure (ct) on (a) residual SAC_{436}, (b) residual UV_{254} and (c) molar bromate yield. SAC_{436} and UV_{254} decreased rapidly to approximately 50 % and 70 % of initial values at ct << 1 mg L^{-1} min. At higher ozone exposition, SAC_{436} and UV_{254} reduction was increasingly ineffective. This was expected based on the dependence of absorbance reduction on specific ozone dose (Figure 4-5). Bromate yield increased with ozone exposure (Figure 5-4.c and d) as expected based on the contribution of ozone in direct and direct-indirect bromate formation (Figure 2-2). The initial increase in bromate concentration was more enhanced than at higher ozone exposure, which is indicated by the steeper slope of the first datapoints given. This may be due to disproportionally high R_{ct} values at low ozone exposure (Buffle et al., 2006a).

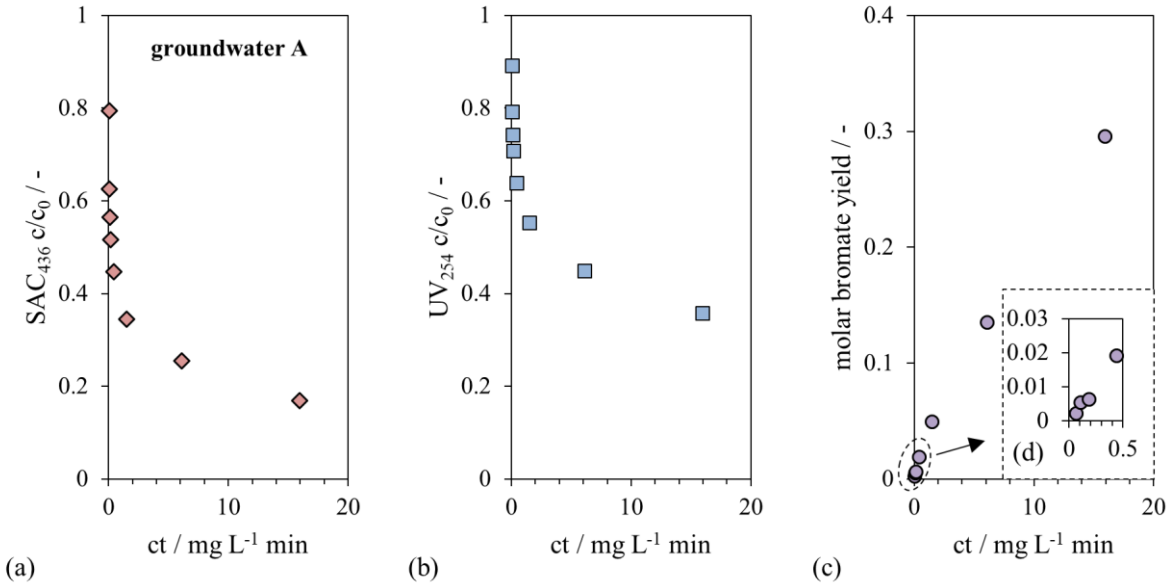

Figure 5-4. impact of ozone exposure (ct) on **(a)** residual SAC_{436}, **(b)** residual UV_{254} and **(c)** molar bromate yield in the ozonation of finished groundwater $A1_F$ (small-scale pilot). **(d)** showing molar bromate yield (y-axis) versus ct (x-axis) for ct < 0.5 mg L^{-1} min. Results obtained from experiments with specific ozone dose of 0.11–1.07 mg_O/mg_{DOC}. ϑ = 14–17 °C, DOC 4.5 mg L^{-1}, pH 7.6 (see Table II-1 for details)

Overall, ozone consumption in organic-rich groundwaters is fast due to high reactivity of NOM. This indicates high content of reactive NOM moieties, e.g. phenols, which is also suggested by the fact that organic-rich groundwaters may be highly reduced. IOD values of ~ 0.5 mg_{O3}/mg_{DOC} have been measured. SAC_{436} and UV_{254} show high removal rates at low ozone exposure and smaller rates at later stage. Formation of bromate was observed even at low ozone exposure, presumably due to high R_{ct} values.

5.3 Biofiltration of Ozonated Water

5.3.1 General Performance

Ozonation experiments with subsequent biofiltration were conducted at groundwater treatment plants A and E. Maximum applicable ozone doses with regard to bromate formation were determined in pre-experiments. Specific ozone doses for ozonation-biofiltration were 0.33–0.46 mg_{O3}/mg_{TOC} (groundwater E) or 0.17–0.28 mg_{O3}/mg_{TOC} (groundwater A). Feed gas concentrations were determined after initial ozonation experiments as process settings with good color removal but low bromate formation. The biofilter was usually operated at 10 L h^{-1}, i.e. filter velocity of 1.3 m h^{-1} and empty-bed contact time (EBCT) of 71 min. At groundwater treatment plant E, finished water was used as the small-scale pilot plant influent. Measuring data from the start-up at groundwater treatment plant E phase is presented in Figure III-26. After approximately 40–50 days operation, SAC_{436}, UV_{254} and TOC in the biofilter effluent equilibrated after low initial values due to GAC adsorption (Terry and Summers, 2018).

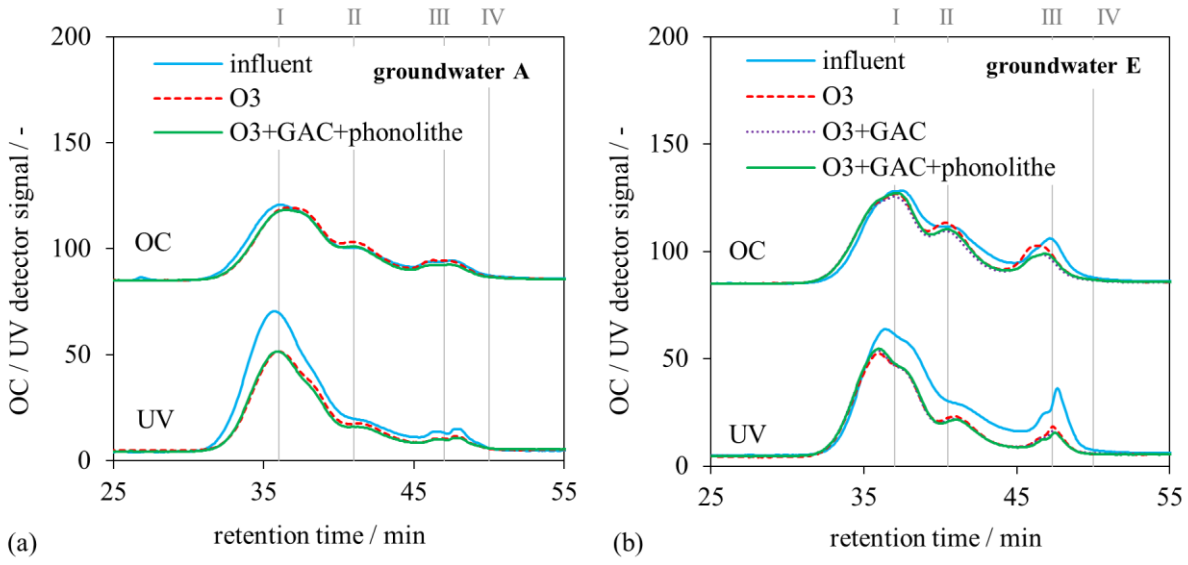

Figure 5-5. LC-OCD-UVD tracking of ozonation-biofiltration in groundwater treatment. **(a)** groundwater $A.4_A$ (aerated groundwater before coagulation and filtration), TOC 4.0 mg L^{-1}, 0.28 mg_{O3}/mg_{TOC}, pH 7.9, 16 °C. **(b)** groundwater $E.2_F$ (finished drinking water), TOC 6.3 mg L^{-1}, 0.36 mg_{O3}/mg_{TOC}, pH 7.8, 15 °C. EBCT 71 min for (a) and (b). Samples: O3 (ozonation effluent/biofilter influent), O3+GAC (effluent of granular activated carbon (GAC)), O3+GAC+phonolithe (biofilter effluent after ozonation, GAC and phonolithe filtration). LC-OCD-UVD fractions (Huber et al., 2011): I – humic substances, II – building blocks, III – low molecular-weight acids and humic substances, IV – low molecular-weight neutrals

Figure 5-5 shows the impact of ozonation-biofiltration on LC-OCD-UVD fractions of groundwater A (Figure 5-5.a) and groundwater E (Figure 5-5.b) for a single representative sampling day. Ozonation affected the organic carbon (OC) composition of humic substances (HS, fraction I), building blocks (BB, fraction II) and low molecular-weight acids (LMWA, fraction III) and reduced the UV absorbance of all NOM fractions, as discussed in detail in chapter 4.1. The impact of ozonation on the OC signal was more significant in groundwater E, which may be due to the slightly higher specific ozone dose used (0.36 mg_{O3}/mg_{TOC} while 0.28 mg_{O3}/mg_{TOC} for groundwater A).

Biofiltration (GAC + phonolithe) decreased the concentrations of BB and LMWA and resulted in lower OC signal intensities than in the plant influent. This is assumed to be due to bacterial processing, as these NOM fractions are small enough to enter GAC pores (Velten et al., 2011) and well biodegradable (Lautenschlager et al., 2014). A slight decrease in UV signal was induced by biofiltration, mainly in BB and LMWA fractions but also in smaller HS fractions (Figure 5-5.a). However, the decrease of UV was smaller than of OC.

For groundwater E, an additional LC-OCD sample was taken from a sampling point between the GAC and phonolithe filter layers (Figure 5-5.b). However, no differences were discernible between LC-OCD-UVD analyses of GAC and GAC/phonolithe filtered water. Therefore it is assumed that most significant biofiltration processes occurred in the GAC layer. This may be due to an empty-bed contact time (EBCT) of 19 min in the GAC layer, which may suffice for removal of biodegradable compounds (Melin and Ødegaard, 2000; Terry and Summers, 2018).

The impact of ozonation in combination with biofiltration on bulk NOM parameters and bromate concentration in groundwaters E and A is depicted in Figure 5-6. SAC_{436} and UV_{254} were reduced significantly by ozonation in groundwater E (Figure 5-6.b). GAC filtration resulted in further decrease of both SAC_{436} (mean overall removal rate of 39 %) and UV_{254} (mean overall removal rate of 47 %). Note that the preferred removal of UV_{254} over SAC_{436} by ozonation was only observed for groundwater E, among five groundwaters tested (chapter 4.1.2). Phonolithe filtration had minor impact on SAC_{436} and UV_{254} (GAC + phonolithe). Data scattering of groundwater A samples was more enhanced as plant influent was obtained directly from sand filter effluent, with alternating wells in use. Similar to groundwater E, biofiltration of groundwater A resulted in further decrease of SAC_{436} and UV_{254} (mean overall removal rates of 45 % for SAC_{436} and 27 % for UV_{254}, Figure 5-6.a). Color removal in biofiltration of ozone-treated water was observed previously in another study, for different filter materials (Rittmann et al., 2002). As removal of UV absorbance was mainly due to removal of biodegradable fractions (BB and LMWA, Figure 5-5.b), it is viable that the additional absorbance removal in biofiltration was due to biodegradation. However, adsorptive processes may occur in biologically active GAC filters over a long time period and may also induce absorbance removal (Terry and Summers, 2018).

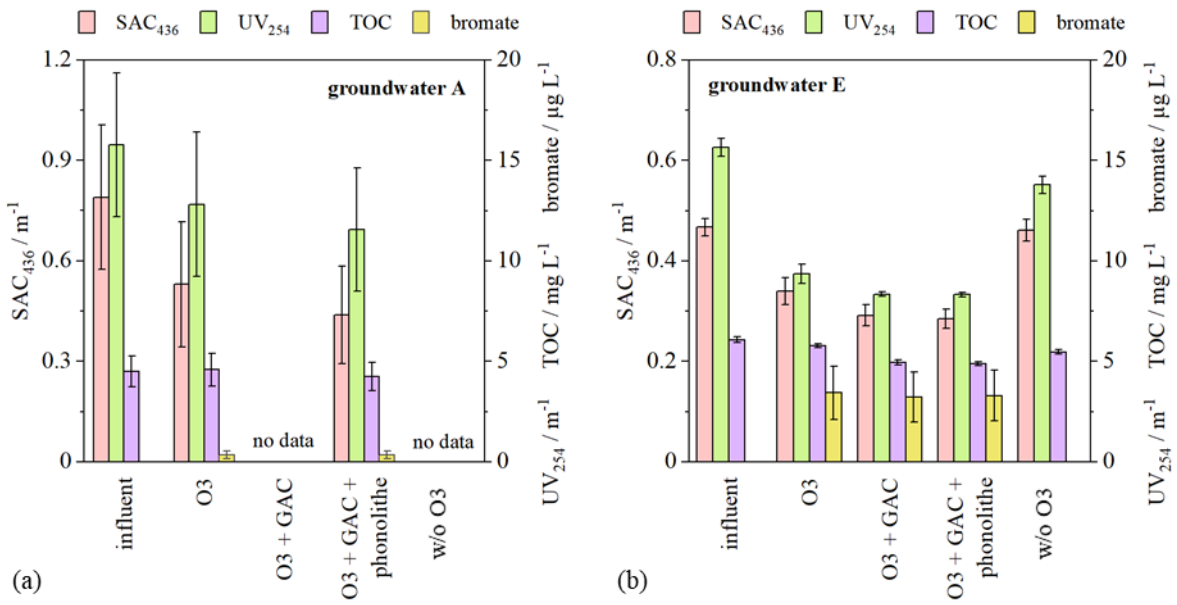

Figure 5-6. Small-scale ozonation-biofiltration results for **(a)** groundwater A after aeration, coagulation and filtration, specific ozone dose = 0.22±0.03 mg_{O3}/mg_{TOC}, EBCT 71 min, pH 7.6–7.9, 15–16 °C, n = 5 samples, bromate below limit of quantification (LOQ) of 1.5 µg L^{-1} in one sample (approximation: 0.5 · LOQ) and below limit of detection (LOD) of 0.5 µg L^{-1} in four samples (approximation: 0.5 · LOD); **(b)** finished groundwater E, specific ozone dose 0.38±0.06 mg_{O3}/mg_{TOC}, EBCT 35–71 min, pH 7.6–7.9, 15–16 °C, n = 6 samples (SAC_{436}, UV_{254}, TOC) n = 3 samples (bromate); Sample abbreviations: O3 = ozonation effluent; O3 + GAC = ozonation effluent filtered by granular activated carbon (GAC); O3 + GAC + phonolithe: ozonation effluent filtered by GAC and phonolithe; w/o O3: effluent from second, identical biofilter with non-ozonated water as influent. Note different y-axis scaling of (a) and (b).

TOC concentration of groundwater E showed minor decrease in ozonation (5 % of initial concentration) but was further decreased in GAC and phonolithe filtration to a total of 19 % reduction (Figure 5-6.b). Approximately 10 % TOC reduction were also obtained by biofiltration of non-ozonated groundwater E (Figure 5-6.b, Figure III-26.d), while SAC_{436} was marginally affected (Figure 5-6.b, Figure III-26.c). In groundwater A, TOC concentration increased slightly in the ozonation stage by 2 %, which may be due to experimental or analytical error. An overall TOC reduction of 6 % was achieved by ozonation, GAC and phonolithe filtration of groundwater A. The lower TOC reduction efficacy compared to groundwater E may partly be due to lower ozone dose. However, TOC removal in both groundwaters by ozonation-biofiltration lies well within the range reviewed by Terry and Summers (2018) (TOC removal rate 3–47 %, median 15 %, n = 72).

Bromate concentration in groundwater E was approximately 3 µg L^{-1} after ozonation and stayed << 10 µg L^{-1} in all samples measured. In the start-up phase with virgin GAC, partial bromate removal in the GAC layer was observed (Figure III-26.e). This may be due to chemical reduction of bromate which occurs in virgin activated carbon but not at later stage (Huang and Chen, 2004). Increased ozone dose was applied to improve SAC_{436} removal but resulted in bromate formation ~ 10 µg L^{-1} (Figure III-26.e). Thus, increase in ozone dose and therefore color removal were constrained by bromate formation in this case, without bromate minimization strategies. Bromate concentration in groundwater A was below the limit of quantification

(1.5 µg L^{-1}) in all samples measured. A slight increase in ozone dose and therefore bromate formation may therefore be acceptable to improve decolorization efficacy for groundwater A.

Ozonation-biofiltration was performed with an additional water quality at groundwater treatment plant A, i.e. aerated water before coagulant addition and filtration (Figure III-25). Results were similar to finished, i.e. aerated, coagulated and filtered groundwater E. This was expected as only low differences in relevant water quality parameters (TOC, UV_{254}, SAC_{436}, bromide) were measured between these water qualities.

In conclusion, removal of SAC_{436} and UV_{254} mainly occurred in ozonation and to some extent in biofiltration. Biofiltration resulted in more enhanced TOC removal than ozonation alone and concomitantly reduced UV_{254} and SAC_{436}. Ozonation-biofiltration resulted in SAC_{436} removal of 39 % in groundwater E (SAC_{436} < 0.3 m^{-1}) and 45 % in groundwater A (SAC_{436} < 0.5 m^{-1}). Bromate formation was controlled << 10 µg L^{-1} for both groundwaters, however limited the application of higher ozone doses and decolorization rates. Groundwater A (high bromide content) and groundwater E (color increase at low ozone dose) may be considered difficult for ozonation-biofiltration. For other groundwaters used in this work, higher decolorization rates of up to 70 % may be expected, based on results of batch experiments (chapter 4.2).

5.3.2 Microbiological Characterization of the Ozonation-Biofiltration Process

Biological growth potential and microbiological stability of ozonated-biofiltered water were assessed by measurement of assimilable organic carbon (AOC). AOC is the increase of carbon mass incorporated in bacterial cells (Hammes and Egli, 2005; Ross et al., 2013; van der Kooij et al., 1982). Thus, total cell count (TCC) was measured at different points of the small-scale pilot plant right after sampling. Samples were then incubated at 30 °C, with regular measurements of TCC. AOC was quantified by indirect determination of changes in bacterial biomass (10^{-7} μg_{AOC} $cell^{-1}$, Hammes et al., 2006). Moreover, incubated samples were analyzed for their content of low nucleic-acid (LNA) and high nucleic-acid (HNA) cells and for their TOC concentration. Initial TCC (after sampling) were $1.56 \cdot 10^5$ cells mL^{-1} (ozonation influent), $2.74 \cdot 10^5$ cells mL^{-1} (O_3 + GAC) and $2.41 \cdot 10^5$ cells mL^{-1} (O_3 + GAC + phonolithe), indicating bacterial regrowth within the biofilter. The ozonated sample (O_3) showed a high degree of inactive cells and was therefore filtered (0.1 µm) and inoculated (1:10) with ozonation influent. High cell counts in biofilter effluents reflect high biological activity (van der Kooij et al., 1989).

Figure 5-7 depicts AOC concentrations in groundwater E for batch ozonation at varying specific ozone doses and for small-scale pilot ozonation with subsequent biofiltration. For batch ozonation, a strong correlation between AOC and specific ozone dose was observed. Similarly, a linear correlation of AOC and ozone dose was reported for low ozone doses of up to approximately 1 mg_{O3}/mg_{DOC} (van der Kooij et al., 1989). Despite dilution by ozone stock solution (factor 1.04–1.43), AOC after ozonation showed good agreement between batch and small-scale pilot ozonation. Good agreement of AOC data was previously observed between batch

tests and full-scale treatment (Hammes et al., 2006). Ozonation in the small-scale pilot plant with 0.36 mg_{O3}/mg_{TOC} increased the AOC concentration significantly from 41 to 185 µg L^{-1} (Figure 5-7). Increased AOC may stimulate growth of bacteria, including pathogens, in ozonated water (Park et al., 2016). Biofiltration resulted in reduction of AOC from 185 µg L^{-1} to 55 µg L^{-1} in the GAC layer and to 48 µg L^{-1} in the phonolithe layer. The overall removal of AOC in biofiltration was 74 %, which is slightly higher than the 40–59 % AOC removal observed in other studies (Pharand et al., 2015; Tan and Johnson, 2001; van der Kooij et al., 1989).

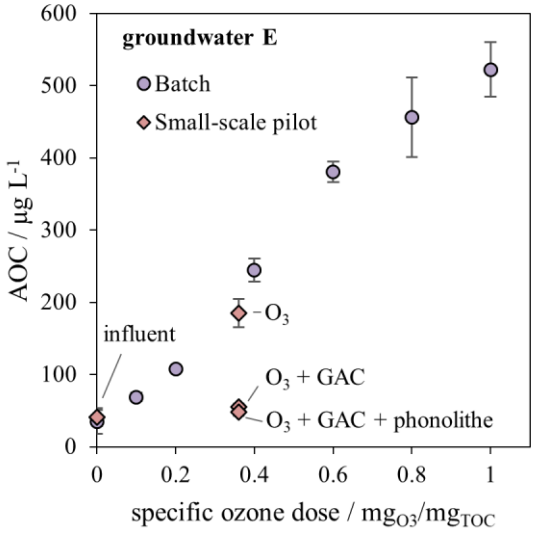

Figure 5-7. AOC levels after batch and small-scale pilot ozonation of groundwater E and effect of biofiltration (GAC + phonolithe) on AOC. Batch: pH 7.8, TOC 6.1 mg L^{-1}, 20 °C (Table 3-2). Pilot: 0.36 mg_{O3}/mg_{TOC}, pH 7.8, TOC 6.3 mg L^{-1}, 15 °C, EBCT 71 min. Sample abbreviations: O_3 = ozonation effluent, O_3 + GAC = ozonation effluent filtered by granular activated carbon (GAC), O_3 + GAC + phonolithe: ozonation effluent filtered by GAC and phonolithe. Dilution of batch samples by addition of ozone stock solution balanced by multiplication with dilution factor. AOC determination by flow cytometric cell counting (correlation 10^{-7} μg_{AOC} $cell^{-1}$, Hammes et al., 2006). Standard deviations show incubation aliquots (n = 3) obtained from the same original sample. Batch results adapted from Sellmann (2020)

During the incubation of small-scale pilot samples, a decrease of TOC compared to non-incubated samples was measured in all samples (Figure 5-8). TOC decrease was most significant in the initial phase but was proceeding for the whole incubation period of 28 d. Ozonated (Figure 5-8.b) and biofiltered (Figure 5-8.a and b) samples showed enhanced TOC decrease compared to the influent sample (Figure 5-8.a). Decrease of TOC concentration in incubation may serve as indicator for biodegradable dissolved organic carbon (BDOC), similarly to incubation methods described elsewhere (Gregorich et al., 2003; McDowell et al., 2006). Note that TOC and DOC were similar in the water sample used here and may therefore approximate each other with reasonable accuracy (Table 3-2). The initial rapid TOC reduction in all samples was accompanied by rapid increase in HNA cells (Figure 5-8). HNA cells contain elevated concentrations of nucleic acid compared to LNA cells (Prest et al., 2013). Moreover, HNA cells exhibit relatively high growth rates and biochemical activity (Jie et al., 2017; Park et al., 2016). This might explain the rapid increase of HNA count in all samples.

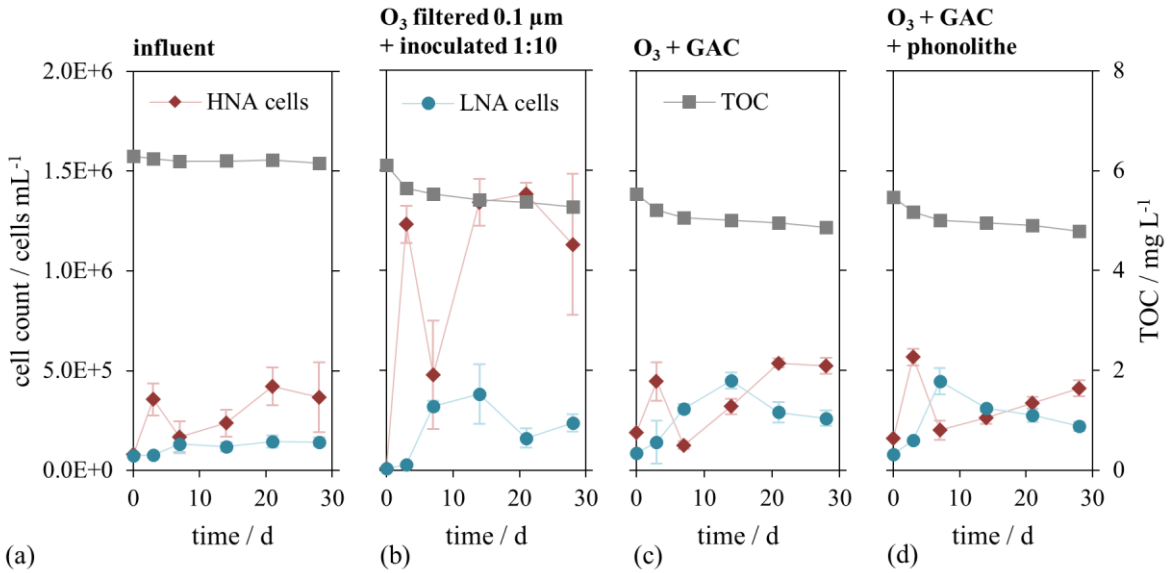

Figure 5-8. Incubation (30 °C) of small-scale pilot samples from different sampling points. **(a)** influent, **(b)** ozonation effluent (0.36 mg_{O3}/mg_{TOC}), filtered and inoculated 1:10 with influent sample, **(c)** ozonation effluent filtered by granular activated carbon (GAC), **(d)** ozonation effluent filtered by GAC and phonolithe. Influent water quality: pH 7.8, DOC 6.3 mg L^{-1}. Biofiltration conditions: EBCT = 71 min, ϑ = 14 °C (filter influent). HNA – high-nucleic-acid bacteria, LNA – low-nucleic-acid bacteria.

The maximum HNA count in the ozonated sample (Figure 5-8.b) exceeded maximum HNA counts in the influent (Figure 5-8.a) and biofiltered (Figure 5-8.c and d) samples by factors 2.4–3.3. Cell counts in the ozonated sample may even be slightly underestimated as the incubation flasks contained 10 vol% influent sample to stimulate bacterial growth. High HNA counts in ozonated water may indicate relatively high bacterial regrowth and contamination potential in the ozonated sample (Prest et al., 2013). This is also highlighted by increased concentrations of building blocks and low molecular-weight acids in the ozonation effluent compared to the influent sample (Figure 5-5.b) and from higher AOC (Figure 5-7).

Similar HNA counts and growth patterns were observed in both biofilter samples (Figure 5-8.c and d). Maximum HNA counts were only slightly elevated compared to the influent sample (Figure 5-8.a). As error bars for standard deviation are overlapping, HNA regrowth in biofiltered samples is not considered significantly higher than in the influent sample. This suggests resilience of ozonated-biofiltered groundwater against rapid bacterial regrowth.

LNA growth was delayed compared do HNA growth in all samples (Figure 5-8), due to lower growth rate of LNA bacteria (Schuster et al., 2022; Wang et al., 2009). LNA cell counts in the incubated influent sample exceeded the initial count only slightly (Figure 5-8.a). LNA cell counts in ozonated (Figure 5-8.b) and ozonated-biofiltered (Figure 5-8.c and d) samples were significantly higher than in the influent sample and showed similar growth patterns. Similar to the incubation experiments shown here, it was observed that the LNA cell count increased in slow sand filters (0.2–0.5 m/h) after ozonation and GAC filtration, while the HNA cell count remained constant after initial increase (Lautenschlager et al., 2014). Thus, ozonated-biofiltered

water may still be prone to slow LNA regrowth, while HNA regrowth would not proceed significantly after biofiltration. The scope of bacteria occurring in natural waters may adapt to varying nutrient availability by intra- and interspecific differentiation (Egli, 2010; Kundu et al., 2020). The slow increase in LNA cell count with concomitant slow TOC degradation in the later incubation stage suggests that LNA bacteria utilized more recalcitrant carbon sources than HNA. Similar to the results shown here, an increase in TCC in ozonated-biofiltered water was observed in water distribution systems, associated with decrease in AOC. This was associated with a potential risk of microbial contamination of ozonated-biofiltered water and the need for subsequent disinfection (van der Kooij et al., 1989).

LNA and HNA cells were assumed to contribute equally to AOC, despite different cell size (Hammes and Egli, 2005). The increased LNA count, compared to the influent sample, is a major reason for slightly higher AOC concentrations in ozonated and biofiltered samples (Figure 5-7). Maximum cell counts were observed at times > 7 d for all samples presented here except ozonation effluent. In contrast, incubation times < 10 d were suggested for flow-cytometric AOC determination (Elhadidy et al., 2016; Hammes and Egli, 2005). Thus, the AOC incubation method used here (30 °C for 28 d) may overestimate rapidly available AOC.

In conclusion, HNA cells dominated the initial phase of NOM biodegradation, along with TOC reduction in ozonated and ozonated-biofiltered samples. AOC concentration and HNA yield in the ozonated sample were higher than in ozonated-biofiltered samples, suggesting a reduction of rapid regrowth potential by biofiltration. However, increased LNA yield was observed both in ozonated and in ozonated-biofiltered samples. LNA growth was slower than HNA growth and resulted in steady TOC degradation during the degradation experiment. The potential of increased LNA growth in ozonated water indicates the need for further research regarding microbial contamination of ozonated water and applicable control measures.

5.4 Effect of Bromate Minimization Techniques

5.4.1 Dosage of Hydrogen Peroxide

Ozonation in combination with dosage of hydrogen peroxide (H_2O_2) was tested in small-scale pilot experiments with groundwater A, at specific ozone doses of 0.26 and 0.51 mg_{O3}/mg_{DOC}. At 0.51 mg_{O3}/mg_{DOC}, bromate yield decreased with H_2O_2 dose (Figure 5-9.a). At 0.26 mg_{O3}/mg_{DOC}, the effect of H_2O_2 on bromate yield was marginal. Ozone dose-dependent bromate minimization efficacy of H_2O_2 was shown previously for batch experiments (Figure 4-13) and discussed in chapter 4.4.

Only small effects of H_2O_2 dose on SAC_{436} were observed at both 0.26 and 0.51 mg_{O3}/mg_{DOC} (Figure 5-9.b). For 0.26 mg_{O3}/mg_{DOC}, this accords with the results of batch ozonation at 0.25 mg_{O3}/mg_{DOC} for the last sample taken after seven days (Figure 4-12.a–c). Similarly, the time between sampling and measurement was approximately one week for the results shown in Figure 5-9. At 0.5 mg_{O3}/mg_{DOC}, an increase of residual SAC_{436} with H_2O_2 dose was observed in

batch experiments (Figure 4-12.d–f). This seems to contradict the results for 0.51 mg_{O3}/mg_{DOC} shown in Figure 5-9.b. However, H_2O_2 and SAC_{436} showed relatively slow equilibration kinetics in ozonated groundwater (Figure 4-12). This may induce differences in SAC_{436} due to variation in reaction time or sample storage conditions (temperature, UV light).

From the observations made in Figure 4-12 it is expected that SAC_{436} was initially, i.e. minutes to hours after ozone depletion, higher than shown in Figure 5-9.b. This is further supported by a SAC_{436} decrease of approximately 20 % in a non-ozonated sample that received 8.7 mg L^{-1} H_2O_2 (Figure 5-9.b). This is the maximum H_2O_2 dose that was used in the experiments presented here (at 0.51 mg_{O3}/mg_{DOC} and 5 mol_{H2O2}/mol_{O3}). In conclusion, it is not expected that H_2O_2 dosage significantly improved the trade-off between bromate minimization and decolorization, at realistic reaction times.

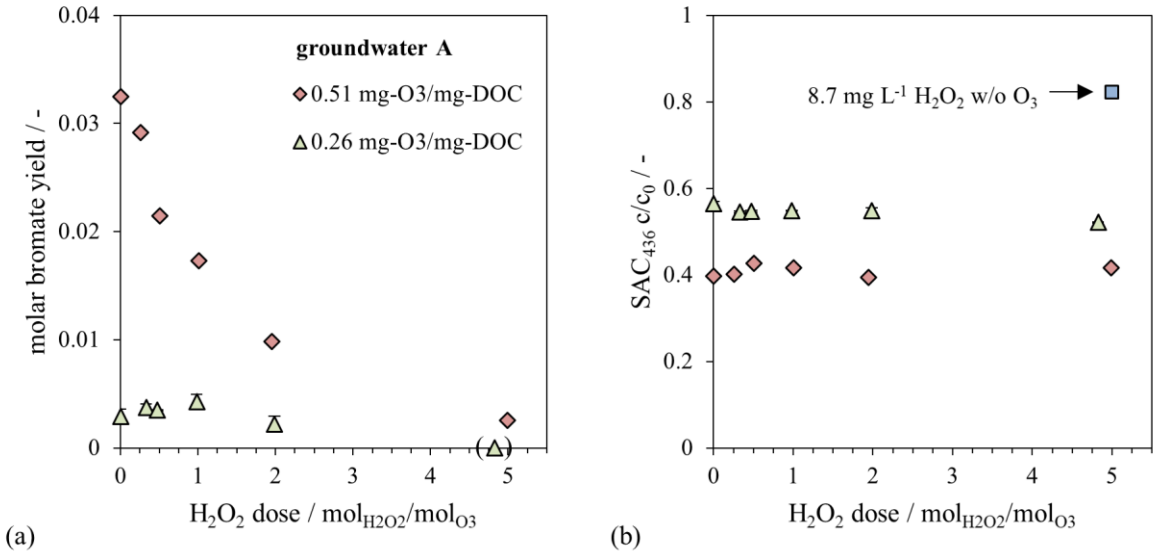

Figure 5-9. Small-scale pilot ozonation of groundwater $A.3_F$ in combination with H_2O_2 dosage. Effect of H_2O_2 dose on **(a)** molar bromate yield and **(b)** residual SAC_{436}. Experimental conditions: ϑ = 15 °C, pH 7.6, DOC = 4.9 mg L^{-1} (see Table II-1 for details), specific ozone doses 0.51 and 0.26 mg_{O3}/mg_{DOC}. Samples measured one week after experiment with residual H_2O_2 reacting in the sampling vials. Bromate analysis at 0.26 mg_{O3}/mg_{DOC} and 5 mol_{H2O2}/mol_{O3} was hampered by high residual H_2O_2 concentration and is therefore enclosed in brackets.

Further experimental studies on ozonation in combination with H_2O_2 dosage were performed in small-scale pilot experiments with groundwater E (Sellmann, 2020). H_2O_2 was dosed either before ozone addition (pre-ozone H_2O_2 dosing) or approximately 30 s after ozone addition (post-ozone H_2O_2 dosing). The inlet ozone gas concentration was held constant during the experiments after a specific ozone dose of 1.1 mg_{O3}/mg_{TOC} was initially set, without H_2O_2 dosage. In pre-ozone H_2O_2 dosing experiments, ozone mass transfer to the water was enhanced, which resulted in lower ozone off-gas concentration and an increase in ozone dose with H_2O_2 dose.

Figure 5-10.a depicts bromate formation in pre- and post-ozone H_2O_2 dosing. Both dosing strategies decreased bromate formation proportionally to H_2O_2 dose, as observed also for groundwater A (Figure 5-9.a) and in batch ozonation of groundwater E (Figure III-20.b).

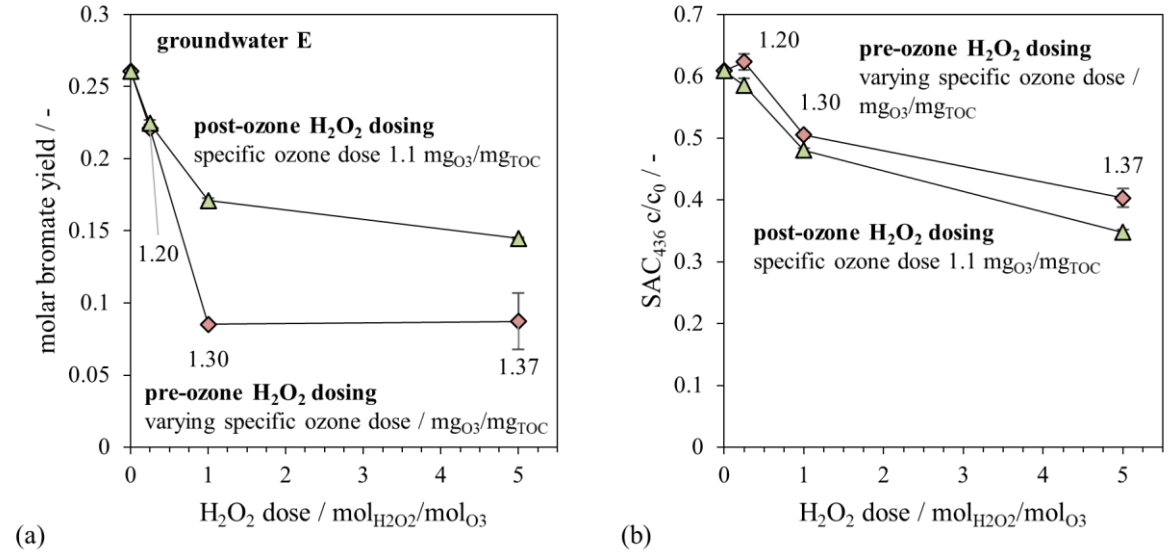

Figure 5-10. Ozonation of groundwater E.1$_F$ in combination with H_2O_2 dosage. ϑ = 14 °C, DOC 5.6 mg L^{-1}, pH 8.0. H_2O_2 dosing before ozone addition (pre-ozone H_2O_2 dosing, ozone dose 1.1 mg_{O3}/mg_{TOC}) or 30 s after H_2O_2 dosing (post-ozone H_2O_2 dosing, ozone dose 1.1–1.37 mg_{O3}/mg_{TOC}, see data labels). **(a)** molar bromate yield, **(b)** relative residual SAC_{436} (measured four days after the experiment). Data adapted from Sellmann (2020)

Despite higher ozone dose, pre-ozone H_2O_2 dosing resulted in significantly lower bromate formation compared to post-ozone H_2O_2 dosing. Although the ozone exposure was not determined for these experiments, significantly higher ozone exposure may be expected for post-ozone H_2O_2 dosing. This might have resulted in increased bromate formation compared to pre-ozone H_2O_2 dosing.

The impact of pre- and post-ozone H_2O_2 dosing on SAC_{436} is shown in Figure 5-10.b. Post-ozone H_2O_2 dosing resulted in slightly lower SAC_{436} than pre-ozone H_2O_2 dosing, which may be due to higher ozone exposure. Pre-ozone H_2O_2 dosing resulted in lower SAC_{436} than without H_2O_2 dosing, at 1 and 5 mol_{H2O2}/mol_{O3}. This was not observed in batch ozonation of groundwater E at similar but constant ozone dose (Figure III-20.b) and may therefore be due to the variation of ozone dose within the experiment.

In conclusion, small-scale pilot results on ozonation in combination with H_2O_2 dosage support the findings that were made in batch ozonation (4.4), i.e. bromate minimization efficacy increases with ozone and H_2O_2 doses. A trade-off between decolorization and bromate was not observed in small-scale pilot experiments, but may be expected at shorter reaction times. The dosing of H_2O_2 subsequently to ozone may result in lower residual color, however bromate yield was increased compared to pre-ozone H_2O_2 dosing.

5.4.2 Dosage of Hydrochloric Acid

Ozonation at reduced pH was performed in small-scale pilot experiments with groundwater A. Natural pH was 7.6, which was reduced to pH values between 6.5 and 7.5 by continuous, pH-controlled dosage of hydrochloric acid (HCl) (≈ 0.2 M) to the feed water right before ozone addition. Two specific ozone doses were used (0.5 and 0.25 mg_{O3}/mg_{DOC}).

Figure 5-11.a shows the effect of pH on molar bromate yield in groundwater A. Bromate concentration peaked at pH 7.5 for both ozone doses tested. Similar bromate concentrations were measured at pH 6.5, 7 and 7.6. This is comparable to the results obtained in batch ozonation of groundwater C, which resulted in only small variaton in bromate formation between pH 6.5 and 7.5 (Figure 4-10). Diverging from the results shown here, bromate formation in groundwater C peaked at pH 7.5. This small difference may be specific for the groundwaters used or due to the higher specific ozone dose used for groundwater C (0.8 mg_{O3}/mg_{TOC}). Theoretical background of the effect of pH on bromate formation was discussed in chapter 4.3.

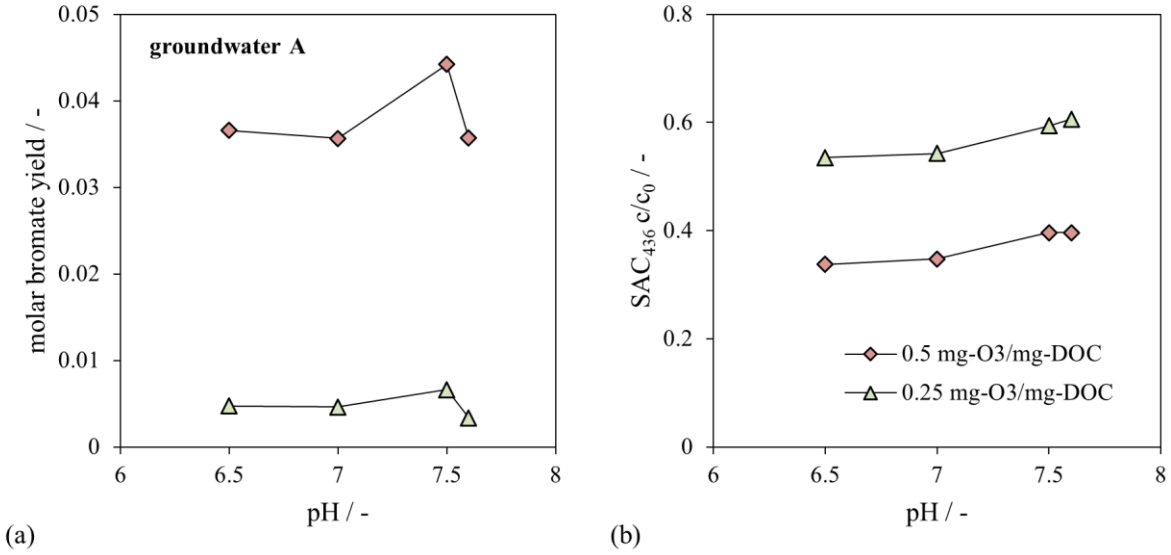

Figure 5-11. Ozonation of groundwater $A.3_F$ at natural pH 7.6 and at reduced pH 6.5–7.5. **(a)** molar bromate yield, **(b)** relative residual SAC_{436}. pH adjustment by dosage of hydrochloric acid. Θ = 14–15 °C, DOC 4.9 mg L^{-1} (see Table II-1 for details)

Figure III-24.a shows bromate formation as a function of ozone exposure for the results presented here. At comparable ozone exposure, bromate formation increased in the order pH 6.5 < 7.0 < 7.6 < 7.5. An increase of bromate concentration with pH was observed before (Legube et al., 2004). Thus, the results were expected apart from higher bromate formation at pH 7.5 compared to pH 7.6. However, differences in both ozone exposure and pH were marginal between pH 7.5 and pH 7.6. Therefore it is not possible to exclude experimental or analytical error as reason for higher bromate formation at pH 7.5 than at pH 7.6, at comparable ozone exposure.

Figure 5-11.b depicts the effect of pH on SAC_{436} reduction in groundwater A. At both ozone doses tested, residual SAC_{436} decreased with pH. This is comparable to the results obtained with groundwater C at 0.8 mg_{O3}/mg_{TOC} and suggests that this effect is independent of water sample used and specific ozone dose.

5.4.3 Dosage of Ammonia

Ozonation in combination with dosage of ammonia (NH_4^+) was performed in small-scale pilot experiments with groundwater A. Ammonia is currently not allowed as additive for drinking

water treatment in Germany (Umweltbundesamt, 2021), but may occur naturally in anaerobic groundwaters. E.g., the ammonia concentration in raw groundwater A.1$_R$ was 0.87 mg L^{-1} (Table II-1). It was hypothesized that the ozonation of raw water may result in lower bromate formation compared to finished groundwater, due to its ammonia content. To test this hypothesis, the raw water ammonia concentration was mimicked by ammonia addition to the feed of finished groundwater A. The resulting feed ammonia concentration was 0.79 mg L^{-1}. At this concentration, major impact of ammonia on bromate minimization may be expected (Pinkernell and von Gunten, 2001).

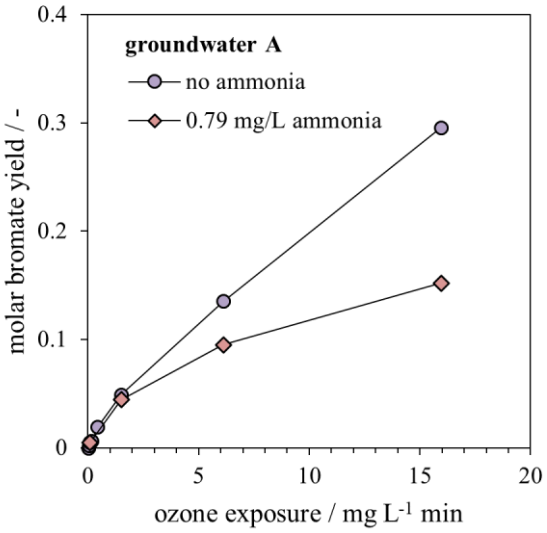

Figure 5-12. Effect of ammonia spiking (0.79 mg L^{-1}) on bromate formation in the ozonation of groundwater A.1$_F$. ϑ = 14–17 °C, pH 7.6, DOC 4.5 mg L^{-1}. Specific ozone doses 0.25, 0.5, 0.75 and 1.0 mg$_{O3}$/mg$_{DOC}$ in ammonia-spiked groundwater; Additional data points for non-spiked groundwater at 0.1, 0.2, 0.3 and 0.4 mg$_{O3}$/mg$_{DOC}$ (data previously shown in Figure 5-4.c and d)

Figure 5-12 shows bromate yield in finished groundwater A with and without dosage of ammonia. At ozone exposure > 5 mg L^{-1} min, which involves ozone doses of 0.75 and 1.0 mg$_{O3}$/mg$_{DOC}$, bromate concentrations in ammonia-spiked water were 30 % and 49 % lower than in the absence of ammonia. Similarly, a maximum reduction in bromate yield of 50 % by ammonia was suggested, due to quenching of the bromate intermediate BrOH by ammonia (von Sonntag and von Gunten, 2012). At ozone exposure < 2 mg L^{-1} min, no significant differences in bromate formation were observed in the presence and in the absence of ammonia. Similar to the reults shown here, no bromate minimization by ammonia was observed for ozone exposure < 2 mg L^{-1} min in Lake Zürich water (Pinkernell and von Gunten, 2001). This was attributed to significant impact of indirect-bromate formation, i.e. without BrOH intermediate, at low ozone exposure. It is viable that the effect of ammonia on bromate formation also depends on the type of NOM. In the ozonation of Suwanee River NOM, which exhibits unusually high reaction rates with ozone (Kwon et al., 2017; von Sonntag and von Gunten, 2012), no inhibitory effect of ammonia on bromate formation was observed even at 1 mg$_{O3}$/mg$_{DOC}$ (Wu et al., 2020). Therefore, results shown here may not be quantitatively comparable to other groundwaters.

Only minor and inconsistent effects of ammonia on the reduction of SAC_{436} and UV_{254} by ozonation were observed (data not shown). The limited effect of ammonia on bromate minimization, especially at low ozone exposure, implies only minor impact on bromate formation at realistic ozone doses both for naturally occuring ammonia and ammonia spiking. Enhanced bromate reduction may be possible in the combination of ammonia and chlorine or chloramine addition (Buffle et al., 2004; Ikehata et al., 2013). Like ammonia, chloramine is currently not allowed for use in drinking water treatment in Germany (Umweltbundesamt, 2021).

5.5 Ozonation of Different Feed Water Qualities

To test the potential of integrating ozonation-biofiltration into groundwater treatment, small-scale pilot experiments at groundwater treatment plant A were performed with feed water obtained from different treatment steps. Water qualities used were raw water (before mineralization tank, Figure II-1), aerated water (after mineralization, before polyaluminium hydroxylchloride addition and sand filtration, Figure II-1) and aerated, flocculated, filtered water (AFF, sand filter effluent). Compared to raw water, aerated water contained no hydrogen sulfide and ammonia. Beyond that, AFF water contained lower TOC, SAC_{436} and UV_{254} levels (Table II-1).

The effects of feed water quality on ozonation kinetics and results were analyzed. A comprehensive overview of results obtained with different feed water qualities is given in Table III-3. Figure 5-13.a depicts relative UV_{254} removal for various specific ozone doses in the ozonation of different feed water qualities. UV_{254} removal patterns were similar for aerated water and AFF water. Other than that, UV_{254} removal in raw water was less pronounced compared to other feed water qualities. This may be due to increased content of H_2S in non-aerated raw water, which consumes ozone fast enough to compete with NOM ozonation (chapter 5.2).

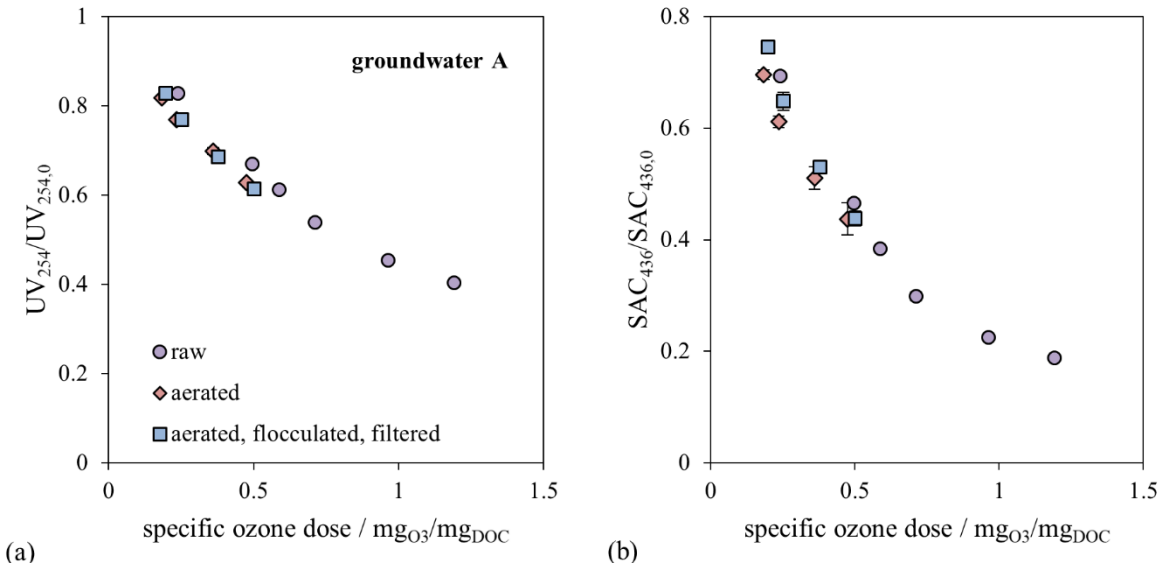

Figure 5-13. Relative reduction of **(a)** UV_{254} and **(b)** SAC_{436} versus specific ozone dose. Water samples used: Raw groundwater ($A.2_R$, 14 °C, 5.2 mg_{DOC} L^{-1}, pH 7.8), aerated groundwater ($A.2_A$, 14 °C, 5.2 mg_{DOC} L^{-1}, pH 7.7) and aerated, flocculated (0.2 mg L^{-1} Al) and sand-filtered groundwater ($A.2_F$, 14 °C, 4.9 mg_{DOC} L^{-1}, pH 7.7) (see Table II-1 for water quality details)

SAC_{436} reduction efficacy by ozonation of different feed water qualities showed only slight variation and ranged in the order aerated > AFF > raw (Figure 5-13.b). The lower SAC_{436} removal in raw water may be expected from the presence of inorganic substances (see above). Aerated water exhibited lower UV_{254}/SAC_{436} ratio than AFF water, as UV_{254}/SAC_{436} increased during coagulation and sand filtration (Table II-1). It was shown that SAC_{436} removal efficacy increased with decreasing UV_{254}/SAC_{436} ratio (Figure III-11). This might explain the higher SAC_{436} removal efficacy of ozone in aerated water compared to AFF water.

Bromate formation was lowest in raw water both as a function of specific ozone dose (Figure 5-14.a) and of UV_{254} reduction (Figure 5-14.b). Lower bromate formation in raw water may partly be due to lower ozone exposure, at comparable specific ozone dose (Figure III-27.a). However, bromate formation in raw water was also lower than in the other feed waters, at comparable ozone exposure (Figure III-28). This may be due to the ammonia content of 0.54 mg L^{-1} in raw water (Table II-1). The presence of ammonia reduces bromate formation via BrOH (see chapter 5.4). Bromate formation in aerated water was slightly lower than in AFF water, at comparable specific ozone dose (Figure 5-14.a) or UV_{254} reduction (Figure 5-14.b). Aerated water exhibited higher $SUVA_{254}$ than AFF water (Table II-1), which implies high reactivity with ozone (Westerhoff et al., 1999). This reduced ozone exposure in aerated water (Figure III-27.a) and therefore resulted in lower bromate concentration compared to AFF water. At comparable ozone exposure, bromate formation in aerated water was higher than in AFF water (Figure III-28.b). In aerated water, more ozone was consumed than in AFF water, at comparable ozone exposure. This may have resulted in increased •OH radical yield (Kwon et al., 2017) and thereby increased bromate formation in aerated water.

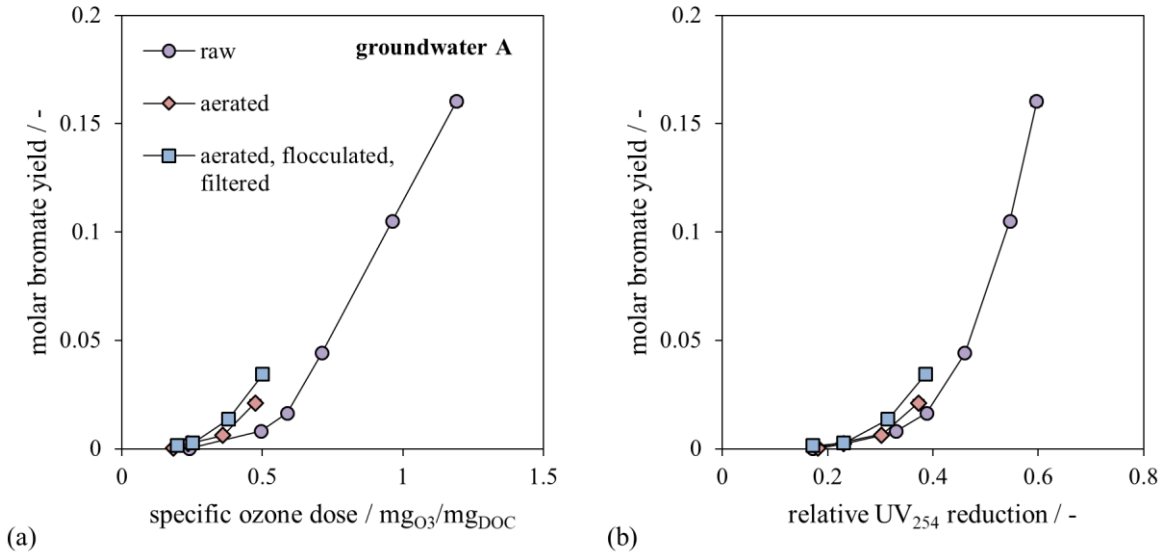

Figure 5-14. Molar bromate yield versus **(a)** specific ozone dose and **(b)** relative UV_{254} reduction ($1-UV_{254}/UV_{254,0}$) for raw groundwater ($A.2_R$, 14 °C, 5.2 mg_{DOC} L^{-1}, pH 7.8), aerated groundwater ($A.2_A$, 14 °C, 5.2 mg_{DOC} L^{-1}, pH 7.7) and aerated, flocculated (0.2 mg L^{-1} Al) and sand-filtered groundwater ($A.2_F$, 14 °C, 4.9 mg_{DOC} L^{-1}, pH 7.7) (see Table II-1 for water quality details)

As various effects on SAC_{436} and bromate formation were observed for the different water qualities used here, a comprehensive overview of bromate concentrations and SAC_{436} is given in Figure III-29. The AFF sample showed the lowest bromate formation, at comparable SAC_{436}. However, the initial SAC_{436} in the AFF sample was smaller than in other samples due to prior flocculation and filtration. Aerated and raw water exhibited the same initial SAC_{436} value. Bromate formation was similar at low SAC_{436} abatement. At the highest ozone dose used for aerated water, bromate formation was higher than in raw water, which may be due to the effect of ammonia in raw water.

In conclusion, only small water quality differences in UV and color degradation and bromate formation were obtained for the ozonation of feed water from different locations of groundwater treatment plant A. Thus, location of ozonation-biofiltration may be flexibly considered within the treatment scheme, with respect to water quality. Slightly less ozone was needed for SAC_{436} reduction in water pre-treated with aeration, coagulation and sand filtration. This is assumed to result in lower •OH yield and therefore lower bromate formation. However, the comparison between coagulated and non-coagulated water is biased, as less ozone for the same overall color removal may also be needed in a hypothetical process with coagulation positioned after ozonation. The ammonia content of raw water improved the trade-off between decolorization and bromate formation only at high ozone doses, compared to aerated water. In other groundwaters than used here, high Fe(II) and Mn(II) concentrations may hamper the ozonation of raw water due to low Fe(III) filtration performance and permanganate formation (DVGW, 2005; Reisz et al., 2008; von Gunten, 2003a).

6 Membrane Ozonation

Membrane ozonation experiments were performed with groundwater E using two different contactors: a single-tube contactor with a dense polydimethylsiloxane (PDMS) membrane and a multi-tube contactor with 490 porous polytetrafluoroethylene (PTFE) fibers. Membrane ozonation experiments were performed at University of Bath (UK), in cooperation with Garyfalia Zoumpouli. Additional batch ozonation experiments were performed at Hamburg University of Technology as a benchmark for water quality obtained by membrane ozonation. Results presented in this section were previously published, in adapted form (Kämmler et al., 2022; Zoumpouli, 2021).

6.1 Ozone Mass Transfer in Membrane Ozonation

The ozone dose in membrane ozonation was adjusted by varying hydraulic retention time (HRT) and ozone feed gas concentration ($c_{O3,g}$). Ozone dose could not be measured directly due to low concentration difference between feed and outlet gas streams. Thus, results were compared based on dissolved ozone concentration (c_{O3}) at the membrane contactor outlet and UV_{254} reduction. c_{O3} for all experimental settings and both membrane contactors are shown in Figure 6-1. c_{O3} in both membrane contactors were severely below Henry equilibrium concentrations. This indicates the occurrence of ozone mass transfer throughout the entire module length, due to the existence of a driving force. For the single-tube contactor, c_{O3} were in the range 0.0–6.4 mg L^{-1} for $c_{O3,g}$ of 25–200 g m^{-3}. Similar results were obtained with the multi-tube contactor (0.0–7.2 mg L^{-1}) for lower $c_{O3,g}$ of 25–70 g m^{-3}. The higher ozone gas concentration needed in the single-tube contactor to obtain the same dissolved ozone concentration may be explained by its different mass transfer characteristics (see below).

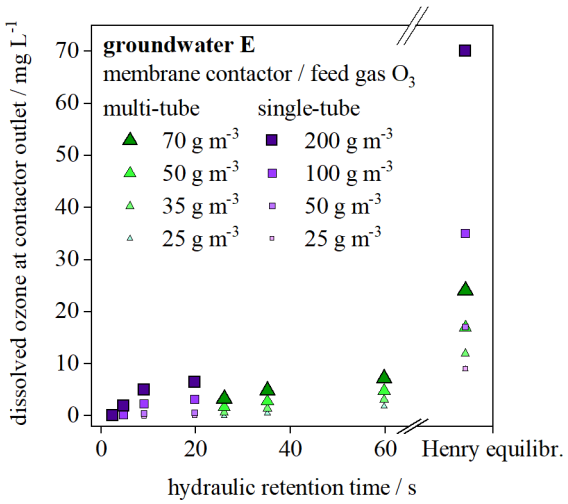

Figure 6-1. Ozonation of groundwater E.1_F (Table II-2) by membrane ozonation. Dissolved ozone concentrations at the contactor outlets for various feed gas ozone concentrations and hydraulic retention times. Experimental conditions: ϑ 16 °C, pH 8.0, DOC 5.6 mg L^{-1}. Henry equilibrium concentration given for 16 °C according to Carell Morris (1988). Results adapted from Kämmler et al. (2022)

Ozone mass transfer in membrane contactors is determined by various parameters including the overall mass transfer coefficient, ozone solubility in the membrane material, specific surface area, liquid flow velocity and contactor length (Equation I-11, Equation I-12, Berry et al., 2017). The single-tube contactor exhibited slightly larger overall mass transfer coefficient and lower ozone solubility in the membrane (Table II-5), which would imply slightly higher ozone flux per unit volume (Equation I-11). However, flow velocities were higher than in the multi-tube contactor, at significantly shorter module length. This resulted in lower HRT in the single-tube contactor. Moreover, the single-tube fiber diameter was larger, implying a lower specific surface area (Table II-5). Despite high ozone flux, these features of the single-tube contactor have hampered the attainment of higher dissolved ozone concentrations (Equation I-12). Thus, higher ozone gas concentrations were necessary to apply sufficient dissolved ozone concentrations in the single-tube contactor. The discussion on ozone mass transfer in the membrane contactors used here is extended in previous publications (Kämmler et al., 2022; Zoumpouli et al., 2018; Zoumpouli, 2021).

Figure 6-2.a depicts c_{O3} obtained by membrane ozonation versus relative UV_{254} reduction, as a proxy for ozone dose. For both membrane contactors, no ozone was measured at the contactor outlets for relative UV_{254} reduction ≤ 0.2. This indicates significant reaction of ozone within the membrane contactors. For the single-tube contactor, due to its low HRT, this implies ozone consumption within seconds, in the time range of the immediate ozone demand (IOD) (chapter 2.2.1). At increasing UV_{254} reduction, i.e. higher ozone dose and increasing depletion of fast-reacting NOM moieties, c_{O3} increased. This was similar in both membrane ozonation contactors.

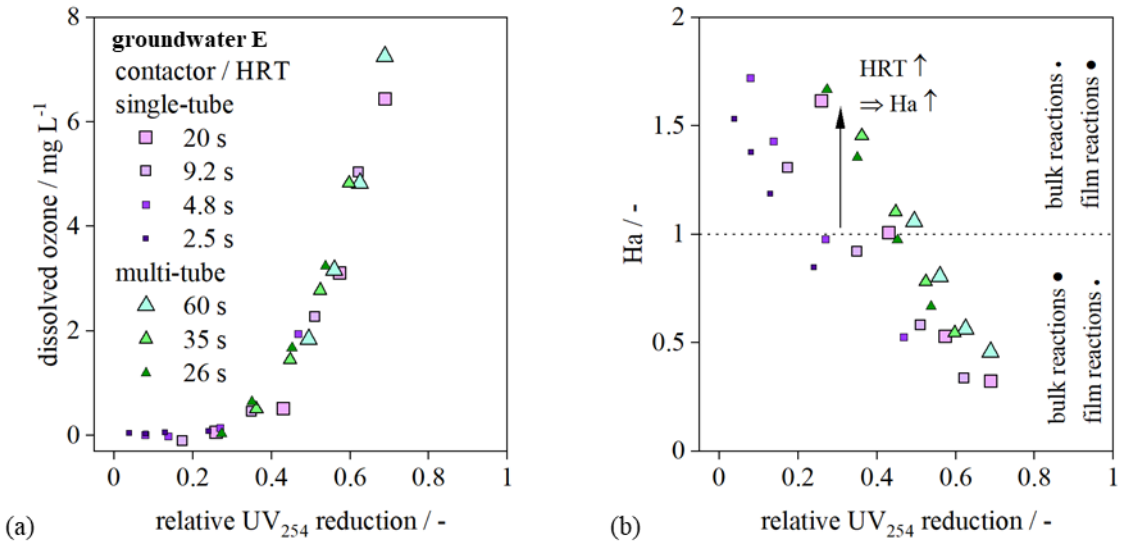

Figure 6-2. Ozonation of groundwater E.1$_F$ (Table II-2) using two different membrane contactors at varying hydraulic retention time (HRT). Correlation between relative UV_{254} reduction and **(a)** dissolved ozone concentration, **(b)** Hatta number (Ha). Experimental conditions: ϑ 16 °C, pH 8.0, DOC 5.6 mg L^{-1}. Results adapted from Kämmler et al. (2022)

The Hatta number (Ha) gives insight into the location of ozone consumption in membrane contactors (chapter 2.5). Figure 6-2.b depicts Ha of membrane ozonation versus relative UV_{254} reduction. Ha ranged from 0.31 to 1.72 in the membrane contactors. This is in the moderately fast reaction regime and indicates ozone consumption both in the liquid film and in the bulk liquid (Charpentier, 1981). At Ha = 1, the amount of ozone reacting in the liquid film equals ozone consumption in bulk liquid. At Ha > 1, ozone consumption in the liquid film dominates while ozone consumption in the bulk is dominant at Ha < 1 (Leiknes et al., 2005). Ha in the moderately fast regime were also obtained in the ozonation of drinking water NOM concentrate (2.7 mg_{DOC} L^{-1}) at comparable flow-dynamic conditions (i.e., Reynolds number < 100 for most experiments) (Leiknes et al., 2005). This indicates the results presented here are applicable to other NOM-rich waters. Ha decreased for increasing UV_{254} reduction, at constant HRT, i.e. at constant flow-dynamic conditions (Figure 6-2.b). This decrease in Ha is due to decreasing ozone decay rate with increasing depletion of ozone-reactive NOM moieties (Jansen et al., 2005). Moreover, Ha increased with increasing HRT, at constant UV_{254} reduction. This is due to higher liquid-side mass transfer resistance at lower HRT (Bein et al., 2020; Zoumpouli et al., 2018). This implies that by variation of HRT and $c_{O3,g}$, the location of main ozone consumption within the membrane contactors may be adjusted.

6.2 Decolorization and Bromate Control in Membrane Ozonation

Figure 6-3.a depicts relative SAC_{436} reduction versus relative UV_{254} reduction for membrane ozonation and, as a benchmark, for batch ozonation. At relative UV_{254} reduction < 0.3, SAC_{436} increased compared to the initial concentration, which resulted in negative removal rates. The reason for the increase in SAC_{436} was discussed in detail in chapter 4.1 and in Kämmler et al. (2022). For practical reasons, comparison of decolorization efficacy between different ozonation setups is limited to positive values of SAC_{436} reduction. This was observed at relative UV_{254} reduction above 0.3, i.e. to specific ozone doses of approximately 0.4 mg_{O3}/mg_{DOC} in batch ozonation. Under these conditions, SAC_{436} removal was slightly enhanced in single-tube membrane and in batch ozonation, compared to multi-tube ozonation. Ozone distribution in the multi-tube contactor was from a single central baffle, combined with small space between fibers (Figure II-12). This may have resulted in higher ozone dose in fibers closer to the center. In these fibers, ozone may have been consumed by reactions with NOM degradation products, after depletion of fast-reacting NOM moieties, particularly phenols. Such degradation products include quinones (Mvula and von Sonntag, 2003; Önnby et al., 2018), which exhibit significant UV_{254} absorbance. The ongoing oxidation of quinonic NOM reaction products may have resulted in more selective UV_{254} over SAC_{436} removal in the multi-tube contactor. SAC_{436} degradation in the single-tube contactor was more scattered than in the multi-tube contactor (Figure 6-3.a). This may be due to a higher range of flow-dynamic conditions in the single-tube contactor (Table II-5.b). However, no clear patterns of different HRT were discernible. Thus, SAC_{436} removal is considered relatively resilient against changes in flow-dynamic conditions in the single-tube contactor.

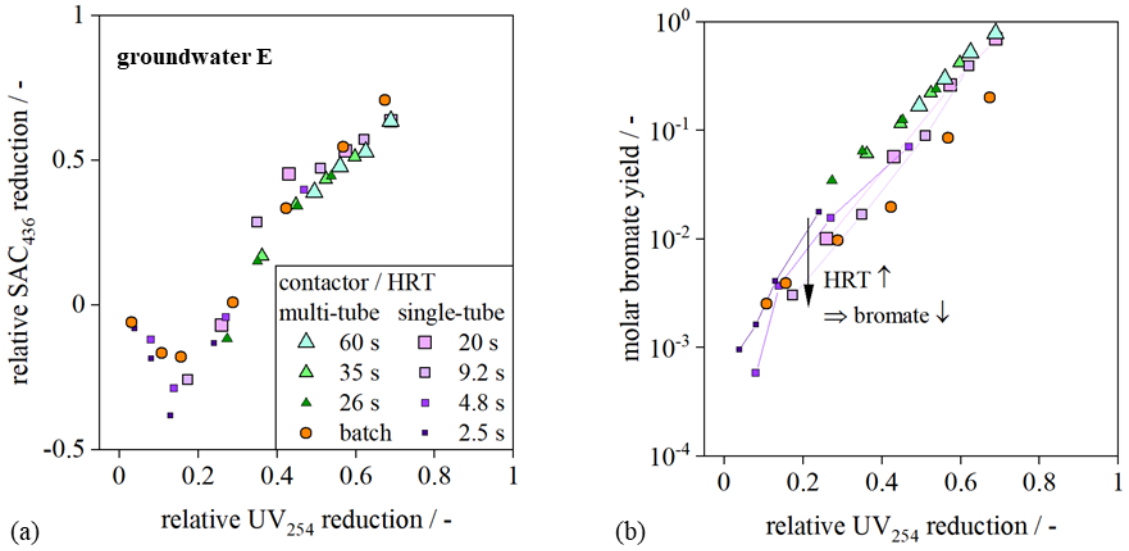

Figure 6-3. Comparison of batch and membrane ozonation using two different membrane contactors at varying hydraulic retention time (HRT). Correlation between relative UV_{254} reduction and **(a)** relative SAC_{436} reduction, **(b)** molar bromate yield. Experimental conditions: groundwater $E.1_F$ (Table II-2), ϑ 16 °C, pH 8.0, DOC 5.6 mg L^{-1}. Results adapted from Kämmler et al. (2022)

Figure 6-3.b shows bromate yield obtained by membrane and batch ozonation. In the multi-tube contactor, bromate yield was significantly higher than in batch and single-tube ozonation. Similarly as for SAC_{436} removal, this may be due to ozone accumulation in some membrane fibers. These fibers would receive higher ozone exposure than others, which would increase bromate formation drastically.

Single-tube ozonation resulted in lower or similar bromate formation compared to batch ozonation for relative UV_{254} removal of up to 0.2 (Figure 6-3.b). This coincided with $c_{O3} \approx 0$ (Figure 6-2.a) and Ha > 1 (Figure 6-2.b). However, at higher UV_{254} removal rate, bromate formation in single-tube ozonation resulted in significantly higher bromate formation than batch ozonation. Similar to the interpretation of higher bromate formation and lower SAC_{436} removal in the multi-tube contactor, higher bromate formation in membrane ozonation may be explained by competition kinetics and spatially varying ozone concentration. In membrane ozonation, ozone concentrations closer to the membrane surface may significantly exceed concentrations in the center (Berry et al., 2017; Schmitt et al., 2020). This could result in excessive oxidation of NOM and increasing availability of ozone for bromate formation at locations closer to the membrane surface. Similar to the results shown here, higher bromate formation in membrane ozonation in combination with H_2O_2 dosage was observed (Stylianou et al., 2018b). In the same study, it was found that a decrease in membrane diameter decreased differences between membrane and batch ozonation, which was attributed to more uniform oxidant distribution within the membrane fibers. This supports the hypothesis that spatial variation in ozone concentration affects bromate formation in membrane ozonation.

It was found that bromate formation in membrane ozonation in combination with H_2O_2 dosage decreased with decreasing $c_{O3,g}$, at constant target compound removal (Merle et al., 2017; Stylianou et al., 2018b). This accords with the single-tube ozonation results presented here: A decrease in bromate yield was observed with increasing HRT, at comparable UV_{254} removal (Figure 6-3.b). Note that an increase in HRT at constant UV_{254} removal was combined with a decrease in $c_{O3,g}$ for the results shown here. The effect of HRT on bromate formation was only visible at low UV_{254} removal, i.e. < 0.4. In this range, Ha was > 1 (Figure 6-2.b), indicating the liquid film as the main reaction zone. Under this condition, c_{O3} and therefore ozone exposure could be kept low, which is demonstrated by low c_{O3} at the contactor outlet, at low UV_{254} removal rates (Figure 6-2.a). Similarly, lower bromate formation at lower $c_{O3,g}$ in ozonation with H_2O_2 dosing was attributed to a decrease in c_{O3} by Merle et al. (2017). This was explained by time-expansion of the dosing process. The use of Ha to explain low ozone exposure in membrane ozonation may be an alternative approach to explain the effect of HRT and $c_{O3,g}$ on bromate formation. Moreover, H_2O_2 and NOM may affect bromate formation in membrane ozonation similarly, as both exhibit high ozone quenching rates (chapter 4.4.1).

In conclusion, flow-dynamic conditions, $c_{O3,g}$ and Ha affect bromate formation in membrane ozonation significantly. This may result in higher bromate formation than in batch ozonation but may also be utilized to control bromate formation, if ozonation is conducted at high Ha. High Ha is aspired to allow rapid ozone consumption by NOM and reduce ozone exposure of bromate intermediates. Moreover, module design apparently affects SAC_{436} removal and bromate formation in membrane ozonation. Inhomogeneous ozone distribution between different membrane fibers seemed to affect results.

7 Conclusions and Outlook

7.1 Characteristics of Ozonation-biofiltration for Groundwater Decolorization

Organic-rich groundwaters used in this work present a characteristic composition. These waters usually exhibit high concentrations of highly conjugated chromophoric natural organic matter (NOM), measured as total organic carbon (TOC, 3.5–6.1 mg L^{-1}), ultraviolet light absorbance (UV_{254}, 14.0–16.7 m^{-1}) or visible light absorbance/color (SAC_{436}, 0.41–1.2 m^{-1}). Moreover, the groundwaters used were characterized by relatively high pH of 7.5–8.1 and relatively high content of bromide (70–330 µg L^{-1}). Different groundwaters exhibit similar reaction behaviour with ozone (O_3), yet with high dependence on specific ozone dose, i.e. ozone dose normalized to the dissolved organic carbon (DOC) content of groundwater (chapter 4). A specific ozone dose of up to approximately 0.5 mg_{O3}/mg_{DOC} is consumed rapidly, i.e. within approximately 30 seconds, in different organic-rich groundwaters, due to fast reaction rates of ozone with highly conjugated NOM (chapter 5.2). At such conditions, further referred to as "low ozone dose" conditions, characteristic reaction conditions are present in groundwater (Table 7-1.a), In particular low ozone exposure (< 1 mg_{O3} L^{-1} min) and presumably high ratios of hydroxyl radical (•OH) to ozone exposure (R_{ct}) (Buffle et al., 2006a; Önnby et al., 2018). At high specific ozone doses (0.5–1.0 mg_{O3}/mg_{DOC}), ozone exposure increases significantly due to depletion of fast-reacting NOM moieties. Concomitantly, a decrease in R_{ct} is presumed.

7.2 Reassessment of Objects of Research

7.2.1 Transformation of Groundwater NOM by Ozonation-biofiltration at Typical Decolorization Conditions

The examination of this object of research must be initiated by the definition of typical decolorization conditions. It has been discussed in chapter 4 that bromate formation was the limiting factor in groundwater decolorization. The applicable ozone dose may be slightly but not significantly increased by available bromate minimization or removal strategies (see below). Under this premise, typical decolorization conditions for groundwater imply specific ozone doses < 0.5 mg_{O3}/mg_{DOC}, referred to as "low ozone doses" (Table 7-1). Note that most effects of ozonation on NOM transformation are highly dose-dependent and may also vary between very low and moderately low ozone doses.

Ozonation at typical decolorization conditions changes NOM composition, analyzed by liquid chromatography coupled with organic carbon detection (LC-OCD, chapter 4.1.1): humic substances (HS) are only slightly affected in concentration but undergo a shift to smaller molecular weight. The molecular-weight shift of NOM progresses into smaller fractions such as building blocks and low molecular-weight acids. Small NOM fractions show enhanced biodegradation potential, which is indicated by an increase in assimilable organic carbon (AOC), particularly at high, but also at small ozone doses (Table 7-1.b). NOM mineralization results in slight reduction (< 5 %) of TOC by ozonation alone, i.e. without biofiltration.

Table 7-1. Summary of ozonation-biofiltration in organic-rich groundwater. Effects of low and high ozone doses on **(a)** ozone reaction kinetics, **(b)** organic water quality parameters, **(c)** bromate formation and impact of •OH and **(d)** bromate minimization strategies. ○ = no or adverse effect, ● = low, ●● = medium, ●●● = high, **n.a.** = not available / not tested. *Not measured within this work, therefore based on assumptions. **H_2O_2 addition reduces efficacy of decolorization

	Low ozone dose (< 0.5 mg_{O3}/mg_{DOC})	**High ozone dose (0.5–1.0 mg_{O3}/mg_{DOC})**
a. Ozone reaction kinetics		
Ozone decay rate k_{sec}	●●●	●●
Ozone exposure	●	●●
R_{ct}*	●●●	●●
b. Removal and formation of organic parameters		
Color (SAC_{436}) removal	●●	●●●
UV_{254} removal	●	●●
TOC removal	○ – ●	●
AOC formation	● – ●●	●● – ●●●
c. Bromate formation and impact of •OH		
Total bromate	● – ●●	●●●
•OH-induced bromate*	●●●	●●
d. Effect of bromate minimization strategies		
H_2O_2**	○ – ●●	●● – ●●●
NH_4^+	○ – ●	●●
pH reduction (pH 6–6.5)	●	●
Multi-stage dosing	**n.a.**	●●
Membrane ozonation	● – ●●	○

NOM transformation continues in post-ozonation biofiltration by GAC/phonolithe (chapter 5.3). Building blocks and low molecular-weight organic acids concentrations are reduced in biofiltration, due to biological degradation. Chromophoric, i.e. light-absorbing properties of NOM were quantified as UV_{254} and SAC_{436}. Low ozone doses, especially in combination with biofiltration, may lead to significant but incomplete reduction of SAC_{436} and UV_{254} (Table 7-1.b). Biofiltration results in slightly enhanced reduction of SAC_{436}, UV_{254} and TOC. Overall removal rates for NOM bulk parameters in small-scale pilot ozonation-biofiltration were 40–

50 % for SAC_{436}, 25–45 % for UV_{254} and 6–19 % for TOC, for two water samples tested. Among the five groundwater samples tested, these two samples showed the most difficult reaction behavior with ozone (groundwater A due to high bromide content, groundwater E due to increase in SAC_{436} at low ozone doses). Thus, for other water samples used for experiments without biofiltration in this work, maximum removal rates may be estimated slightly higher as up to 70 % for SAC_{436}, up to 50 % for UV_{254} and up to 20 % for TOC.

7.2.2 By-product Formation and Minimization in Groundwater Ozonation

Several ozonation by-products may complicate ozonation, including bromo-organic compounds, transformation products of trace organic contaminants, biodegradable organic compounds and bromate (von Gunten, 2018). The formation of bromo-organic compounds is low at low ozone doses (Legube, 1996), which were identified as typical decolorization conditions (see above). In the absence of trace organic compounds, relevant ozonation by-products in groundwater decolorization are biodegradable organic compounds and bromate. The formation of both were observed in the ozonation of groundwater (chapter 5.3.2, chapter 4.2, Table 7-1.c).

Biodegradable organic compounds, quantified as assimilable organic carbon (AOC), are significantly, but not completely removed in biofiltration (chapter 5.3.2). This coincides with reduction in TOC concentration, and in growth potential for high nucleic-acid (HNA) cells. This may reduce the risk of pathogenic contamination of ozonated-biofiltered water. However, low nucleic-acid (LNA) cells may grow in ozonated-biofiltered water, under incubation conditions at 30 °C. The consequences of this for microbial safety of drinking water remain an important object of research.

In contrast to AOC, post-ozonation removal strategies for bromate are associated with high costs and effort (chapter 2.4). Thus, different available bromate minimization strategies (e.g. H_2O_2, NH_4^+ or HCl dosing, multi-stage ozonation and membrane ozonation) have been examined with regard to their efficacy in groundwater decolorization (chapters 4.4, 5.4 and 6.1). All bromate minimization techniques tested have only little effect on bromate minimization, without affecting the main treatment target of decolorization (Table 7-1.d). H_2O_2 and NH_4^+ addition, which mainly mitigate bromate formation that is initiated by reaction of bromide with molecular ozone, are rather ineffective in the presence of low ozone and high •OH concentrations. Reduction of pH shows only small improvement in the trade-off between decolorization and bromate formation. Small reduction in bromate formation for low ozone dose settings was observed for multi-stage ozonation (chapter 4.4.2) and for membrane ozonation, depending on process settings (chapter 6).

Ozonation of organic-rich groundwaters presumably results in high concentrations of hydroxyl radicals (•OH) which contribute to bromate formation especially at low ozone doses, i.e. for typical decolorization conditions (Table 7-1.c). Quenching of •OH could therefore be a viable

strategy to reduce bromate formation in groundwater decolorization. No specific •OH quenching strategies were tested in this work. •OH quenching strategies covered by literature (Buffle et al., 2004; Ikehata et al., 2013) are based on NH_2Cl and therefore restricted for use in drinking water production in Germany (Umweltbundesamt, 2021). It was observed for some experimental conditions in chapter 4.3.1 that groundwater decolorization may be less efficient at increased alkalinity, i.e. in presence of •OH-quenching bicarbonate ions. This may be due to an important contribution of •OH to decolorization mechanisms. Thus, the development of practically feasible bromate minimization strategies based on •OH quenching remains a challenge. Note that an increased ozone dose, in case of successful bromate reduction, may result in increased concentrations of other ozonation by-products, such as AOC. Thus, the control of ozone dose remains most important to limit bromate formation in groundwater decolorization.

7.2.3 Applicability and Integration Potential of Ozonation-biofiltration into Groundwater Treatment

The applicability of ozone in groundwater treatment depends on the ozone dose available. As described above, the ozone dose is limited by the bromate formation potential of a groundwater. Certain groundwater qualities may allow higher ozone dose and are therefore more addressable by ozone. Most importantly, low bromide concentrations reduce the by-product formation potential regarding bromate and also bromo-organic compounds. As ozone decay in groundwater is decisively controlled by UV light absorbing NOM moieties (chapter 4.1.2), groundwaters with low UV_{254}/SAC_{436} ratio may exhibit higher relative SAC_{436} reduction at comparable ozone dose. An increase in groundwater alkalinity reduced bromate formation, presumably due to •OH quenching in groundwater A (chapter 4.3.1). Despite the necessity for this effect to be confirmed in other organic-rich groundwater matrices, it might indicate the application potential of ozonation in high-alkalinity waters. Moreover, these waters usually exhibit lower pH than low-alkalinity waters (after adjusting the calcium carbonate equilibrium). A lower pH may improve the decolorization – bromate formation trade-off slightly (chapters 4.3.2 and 5.4.2). In raw waters containing high CO_2 concentrations, ozone application may be beneficial before CO_2 removal to utilize lower pH and higher bicarbonate concentration. Ammonia in raw water may reduce bromate formation slightly if higher ozone doses are applied, but not at low ozone doses (chapter 5.5).

Ozonation of different feed water qualities of groundwater A was performed to examine the integration of ozonation-biofiltration into groundwater treatment at different positions. It was shown that differences in final water quality obtained were minor and render ozonation-biofiltration generally flexible regarding its positioning in groundwater treatment train. Given the complexity of water resources and existing treatment schemes, the most advantageous positioning of ozonation-biofiltration may therefore be determined by other, more practical reasons. E.g., it might be feasible to apply ozonation-biofiltration after removal of iron and manganese by Fe(II) and Mn(II) filtration, as these processes allow higher filter velocities than Fe(III) and

Mn(IV) filtration (DVGW, 2005). Moreover, oxidation of iron and manganese reduces the pH value which may be beneficial regarding bromate formation in ozonation.

7.3 Outlook

This work presents a comprehensive overview of the application ozonation-biofiltration for the treatment of organic-rich groundwaters. The possibility to treat different groundwater matrices with low ozone doses was shown in batch and small-scale pilot experiments. This may help increase the scope of groundwater resources eligible for drinking water treatment and regionally decrease water stress.

The application of ozonation-biofiltration for groundwater decolorization is mainly limited by bromate formation. Thus, the development or improvement of bromate minimization or removal strategies compatible with decolorization could improve the overall performance of the process. The development of methods that induce •OH quenching and process-based options (multi-stage ozonation, membrane ozonation) seems most favorable from the current perspective of process understanding. Bromate minimization strategies need to be applicable particularly at low ozone doses to avoid the trade-off of bromate against other ozonation by-products. Overall toxicity measurements, e.g. bioassays might be helpful to exclude the presence of toxic ozonation by-products other than bromate in ozonation-biofiltration treated water.

Mechanistic understanding of organic-rich groundwater ozonation could be enhanced by determining •OH exposure and its effects on decolorization and on bromate formation.

Further research should consider the impact of remaining AOC and LNA growth potential after ozonation-biofiltration on microbial drinking water quality. This might influence the requirements of biofiltration systems that follow ozonation of groundwater.

Practical aspects of ozonation-biofiltration in groundwater, especially its interaction with other treatment processes and the concomitant oxidation of inorganic species (e.g. iron, manganese, ammonia), highlight the need for further pilot studies and various water qualities. These studies should also benchmark ozonation-biofiltration economically, e.g. by assessing the optimization potential of biofilter operational parameters.

Further research on ozonation-biofiltration should also include the comparison to other processes viable for NOM removal and decolorization, e.g. coagulation, nanofiltration, or ion exchange. Comparison should include water quality differences, integration potential into groundwater treatment and economical and environmental aspects.

References

Acero, J.L., von Gunten, U., 2001. Characterization of Oxidation processes: ozonation and the AOP O3/H2O2. Journal - American Water Works Association 93 (10), 90–100.

Aeschbacher, M., Graf, C., Schwarzenbach, R.P., Sander, M., 2012. Antioxidant Properties of Humic Substances. Environmental Science & Technology 46 (9), 4916–4925.

Aeschbacher, M., Sander, M., Schwarzenbach, R.P., 2010. Novel electrochemical approach to assess the redox properties of humic substances. Environ. Sci. Technol. 44 (1), 87–93.

Aiken, G.R., McKnight, D.M., Thorn, K.A., Thurman, E.M., 1992. Isolation of hydrophilic organic acids from water using nonionic macroporous resins. Organic Geochemistry 18 (4), 567–573.

Andersson, A., Lavonen, E., Harir, M., Gonsior, M., Hertkorn, N., Schmitt-Kopplin, P., Kylin, H., Bastviken, D., 2020. Selective removal of natural organic matter during drinking water production changes the composition of disinfection by-products. Environ. Sci.: Water Res. Technol. 6 (3), 779–794.

Audenaert, W.T.M., Vandierendonck, D., van Hulle, S.W.H., Nopens, I., 2013. Comparison of ozone and HO· induced conversion of effluent organic matter (EfOM) using ozonation and UV/H2O2 treatment. Water Research 47 (7), 2387–2398.

Bader, H., Hoigné, J., 1981. Determination of ozone in water by the indigo method. Water Research 15 (4), 449–456.

Baghoth, S.A., Sharma, S.K., Amy, G.L., 2011. Tracking natural organic matter (NOM) in a drinking water treatment plant using fluorescence excitation-emission matrices and PARAFAC. Water Research 45 (2), 797–809.

Bein, E., Zucker, I., Drewes, J.E., Hübner, U., 2020. Ozone membrane contactors for water and wastewater treatment: A critical review on materials selection, mass transfer and process design. Chemical Engineering Journal, 127393.

Beltrán, F.J., 1995. Theoretical Aspects Of The Kinetics Of Competitive Ozone Reactions In Water. Ozone: Science & Engineering 17 (2), 163–181.

Benecke, J., 2018. Gypsum scaling during reverse osmosis desalination − characterization and effects of natural organic matter. Dissertation, Hamburg.

Beniwal, D., Taylor-Edmonds, L., Armour, J., Andrews, R.C., 2018. Ozone/peroxide advanced oxidation in combination with biofiltration for taste and odour control and organics removal. Chemosphere 212, 272–281.

Berry, M., Taylor, C., King, W., Chew, Y., Wenk, J., 2017. Modelling of Ozone Mass-Transfer through Non-Porous Membranes for Water Treatment. Water 9 (7), 452.

Beyer, F., Rietman, B.M., Zwijnenburg, A., van den Brink, P., Vrouwenvelder, J.S., Jarzembowska, M., Laurinonyte, J., Stams, A.J., Plugge, C.M., 2014. Long-term performance and fouling analysis of full-scale direct nanofiltration (NF) installations treating anoxic groundwater. Journal of Membrane Science 468, 339–348.

Bharadwaj, A., 2022. Experimental study of pH and alkalinity effects on bromate formation and groundwater decolourisation by ozonation. Project Work, Hamburg.

Blumenthal, G., Linke, D., Vieth, S., 2006. Chemie: Grundwissen für Ingenieure, 1. Aufl. ed. Chemie in der Praxis. Teubner, Wiesbaden.

Boretti, A., Rosa, L., 2019. Reassessing the projections of the World Water Development Report. npj Clean Water 2 (1), 133.

Bose, P., Bezbarua, B.K., Reckhow, D.A., 1994. Effect Of Ozonation On Some Physical and Chemical Properties Of Aquatic Natural Organic Matter. Ozone: Science & Engineering 16 (2), 89–112.

Bourgin, M., Borowska, E., Helbing, J., Hollender, J., Kaiser, H.-P., Kienle, C., McArdell, C.S., Simon, E., von Gunten, U., 2017. Effect of operational and water quality parameters on conventional ozonation and the advanced oxidation process O3/H2O2: Kinetics of micropollutant abatement, transformation product and bromate formation in a surface water. Water Research 122, 234–245.

Buffle, M.-O., Galli, S., von Gunten, U., 2004. Enhanced bromate control during ozonation: the chlorine-ammonia process. Environmental Science & Technology 38 (19), 5187–5195.

Buffle, M.-O., Schumacher, J., Meylan, S., Jekel, M., von Gunten, U., 2006a. Ozonation and Advanced Oxidation of Wastewater: Effect of O3 Dose, pH, DOM and HO• -Scavengers on Ozone Decomposition and HO• Generation. Ozone: Science & Engineering 28 (4), 247–259.

Buffle, M.-O., Schumacher, J., Salhi, E., Jekel, M., von Gunten, U., 2006b. Measurement of the initial phase of ozone decomposition in water and wastewater by means of a continuous quench-flow system: application to disinfection and pharmaceutical oxidation. Water Research 40 (9), 1884–1894.

Buffle, M.-O., von Gunten, U., 2006. Phenols and amine induced HO* generation during the initial phase of natural water ozonation. Environ. Sci. Technol. 40 (9), 3057–3063.

Buxton, G.V., Dainton, F.S., 1968. The radiolysis of aqueous solutions of oxybromine compounds; the spectra and reactions of BrO and BrO2. Proc. R. Soc. Lond. A 304 (1479), 427–439.

Canonica, S., Kohn, T., Mac, M., Real, F.J., Wirz, J., von Gunten, U., 2005. Photosensitizer method to determine rate constants for the reaction of carbonate radical with organic compounds. Environ. Sci. Technol. 39 (23), 9182–9188.

Carell Morris, J., 1988. The Aqueous Solubility of Ozone - a Review. Ozone News (1), 14–16.

Charpentier, J.-C., 1981. Mass-Transfer Rates in Gas-Liquid-Absorbers and Reactors, in: Drew, T.B., Cokelet, G.R., Hoopes Jr., J.W., Vermeulen, T. (Eds.), Advances in Chemical Engineering, 11 ed. Advances in chemical engineering 11.1981. Academic Press, New York.

Chen, J., Gu, B., LeBoeuf, E.J., Pan, H., Dai, S., 2002. Spectroscopic characterization of the structural and functional properties of natural organic matter fractions. Chemosphere 48 (1), 59–68.

Chen, W., Westerhoff, P., Leenheer, J.A., Booksh, K., 2003. Fluorescence excitation-emission matrix regional integration to quantify spectra for dissolved organic matter. Environ. Sci. Technol. 37 (24), 5701–5710.

Chen, W., Yu, H.-Q., 2021. Advances in the characterization and monitoring of natural organic matter using spectroscopic approaches. Water Research 190, 116759.

Cho, M., Kim, H., Cho, S.H., Yoon, J., 2003. Investigation of Ozone Reaction in River Waters Causing Instantaneous Ozone Demand. Ozone: Science & Engineering 25 (4), 251–259.

Chon, K., Salhi, E., von Gunten, U., 2015. Combination of UV absorbance and electron donating capacity to assess degradation of micropollutants and formation of bromate during ozonation of wastewater effluents. Water Research 81, 388–397.

Coro, E., Laha, S., 2001. Color removal in groundwater through the enhanced softening process. Water Research 35 (7), 1851–1854.

Crittenden, J.C., Trussell, R.R., Hand, D.W., Howe, K.J., Tchobanoglous, G., 2012. MWH's Water Treatment. John Wiley & Sons, Inc, Hoboken, NJ, USA.

Cuthbert, I.D., del Giorgio, P., 1992. Toward a standard method of measuring color in freshwater. Limnol. Oceanogr. 37 (6), 1319–1326.

De Vera, G.A., Keller, J., Gernjak, W., Weinberg, H., Farré, M.J., 2016. Biodegradability of DBP precursors after drinking water ozonation. Water Research 106, 550–561.

De Vera, G.A., Stalter, D., Gernjak, W., Weinberg, H.S., Keller, J., Farré, M.J., 2015. Towards reducing DBP formation potential of drinking water by favouring direct ozone over hydroxyl radical reactions during ozonation. Water Research 87, 49–58.

Del Vecchio, R., Blough, N.V., 2004. On the Origin of the Optical Properties of Humic Substances. Environmental Science & Technology 38 (14), 3885–3891.

DIN 38408-3, 2011. Deutsche Einheitsverfahren zur Wasser-, Abwasser- und Schlammuntersuchung – Gasförmige Bestandteile (Gruppe G) – Teil 3: Bestimmung von Ozon (G 3).

Ding, W., Jin, W., Cao, S., Zhou, X., Wang, C., Jiang, Q., Huang, H., Tu, R., Han, S.-F., Wang, Q., 2019. Ozone disinfection of chlorine-resistant bacteria in drinking water. Water Research 160, 339–349.

Dingemans, M., Dewulf, J., van Hecke, W., van Langenhove, H., 2008. Determination of ozone solubility in polymeric materials. Chemical Engineering Journal 138 (1-3), 172–178.

Dryer, D.J., Korshin, G.V., Fabbricino, M., 2008. In situ examination of the protonation behavior of fulvic acids using differential absorbance spectroscopy. Environ. Sci. Technol. 42 (17), 6644–6649.

Dubowski, Y., Greenberg-Eitan, R., Rebhun, M., 2018. Removal of Trihalomethane Precursors by Nanofiltration in Low-SUVA Drinking Water. Water 10 (10), 1370.

DVGW, 2005. Arbeitsblatt W 223-1: Enteisenung und Entmanganung; Teil 1: Grundsätze. Wirtschafts- und Verlagsgesellschaft Gas und Wasser mbH, Bonn.

Eberhard, O., 2021. Auswirkung der Ozonung mit Wasserstoffperoxid-Dosierung auf huminstoffbedingte Färbung und Bromatgehalt von Grundwasser. Project Work, Hamburg.

Edgar, M., Boyer, T.H., 2021. Removal of natural organic matter by ion exchange: Comparing regenerated and non-regenerated columns. Water Research 189, 116661.

Egli, T., 2010. How to live at very low substrate concentration. Water Research 44 (17), 4826–4837.

Elhadidy, A.M., van Dyke, M.I., Peldszus, S., Huck, P.M., 2016. Application of flow cytometry to monitor assimilable organic carbon (AOC) and microbial community changes in water. Journal of microbiological methods 130, 154–163.

Elovitz, M.S., von Gunten, U., 1999. Hydroxyl Radical/Ozone Ratios During Ozonation Processes. I. The Rct Concept. Ozone: Science & Engineering 21 (3), 239–260.

Elovitz, M.S., von Gunten, U., Kaiser, H.-P., 2000. Hydroxyl Radical/Ozone Ratios During Ozonation Processes. II. The Effect of Temperature, pH, Alkalinity, and DOM Properties. Ozone: Science & Engineering 22 (2), 123–150.

EU, 1998. Council Directive 98/83/EC of 3 November 1998 on the quality of water intended for human consumption.

Fakioglu, M., Gulhan, H., Ozgun, H., Ersahin, M.E., Ozturk, I., 2021. Removal of Taste and Odor Causing Compounds from Drinking Water Sources by Peroxone Process: Laboratory and Pilot Scale Studies. Ozone: Science & Engineering 43 (6), 527–537.

Fischbacher, A., Löppenberg, K., von Sonntag, C., Schmidt, T.C., 2015. A New Reaction Pathway for Bromite to Bromate in the Ozonation of Bromide. Environmental Science & Technology 49 (19), 11714–11720.

Fließ, R., Baumeister, C., Gudera, T., Hergesell, M., Kopp, B., Neumann, J., Posselt, M., 2021. Auswirkungen des Klimawandels auf das Grundwasser und die Wasserversorgung in Süddeutschland. Grundwasser - Zeitschrift der Fachsektion Hydrogeologie 26 (1), 33–45.

Freer, R., 2020. Reaction-kinetic Modeling of the Ozonation of Groundwaters for Drinking Water Treatment. Master's Thesis, Hamburg.

Frimmel, F.H., 1998. Characterization of natural organic matter as major constituents in aquatic systems. Journal of Contaminant Hydrology 35 (1-3), 201–216.

Gardoni, D., Vailati, A., Canziani, R., 2012. Decay of Ozone in Water: A Review. Ozone: Science & Engineering 34 (4), 233–242.

Glaze, W.H., Kang, J.-W., Chapin, D.H., 1987. The Chemistry of Water Treatment Processes Involving Ozone, Hydrogen Peroxide and Ultraviolet Radiation. Ozone: Science & Engineering 9 (4), 335–352.

Glaze, W.H., Weinberg, H.S., Cavanagh, J.E., 1993. Evaluating the Formation of Brominated DBPs During Ozonation. Journal - American Water Works Association 85 (1), 96–103.

Gleeson, T., Cuthbert, M., Ferguson, G., Perrone, D., 2020. Global Groundwater Sustainability, Resources, and Systems in the Anthropocene. Annu. Rev. Earth Planet. Sci. 48 (1), 431–463.

Gordon, G., Gauw, R.D., Emmert, G.L., Walters, B.D., Bubnis, B., 2002. Chemical Reduction Methods for Bromate Ion Removal. Journal - American Water Works Association 94 (2), 91–98.

Gottschalk, C., 1996. Oxidation organischer Mikroverunreinigungen in natürlichen und synthetischen Wässern mit Ozon und Ozon/Wasserstoffperoxid. Dissertation, Berlin.

Gottschalk, C., Libra, J.A., Saupe, A., Libra, J.A. (Eds.), 2010. Ozonation of water and waste water: A practical guide to understanding ozone and its applications, 2., completely rev. and updated edition ed. Wiley-VCH, Weinheim.

Grefte, A., Dignum, M., Cornelissen, E.R., Rietveld, L.C., 2013. Natural organic matter removal by ion exchange at different positions in the drinking water treatment lane. Drink. Water Eng. Sci. 6 (1), 1–10.

Gregorich, E., Beare, M., Stoklas, U., St-Georges, P., 2003. Biodegradability of soluble organic matter in maize-cropped soils. Geoderma 113 (3-4), 237–252.

Gregory, D., Carlson, K.H., 2001. Ozonation Of Dissolved Manganese In The Presence Of Natural Organic Matter. Ozone: Science & Engineering 23 (2), 149–159.

Gulde, R., Clerc, B., Rutsch, M., Helbing, J., Salhi, E., McArdell, C.S., von Gunten, U., 2021. Oxidation of 51 micropollutants during drinking water ozonation: Formation of transformation products and their fate during biological post-filtration. Water Research 207, 117812.

Haag, W.R., Hoigne, J., 1983. Ozonation of bromide-containing waters: kinetics of formation of hypobromous acid and bromate. Environ. Sci. Technol. 17 (5), 261–267.

Hammes, F., Salhi, E., Köster, O., Kaiser, H.-P., Egli, T., von Gunten, U., 2006. Mechanistic and kinetic evaluation of organic disinfection by-product and assimilable organic carbon (AOC) formation during the ozonation of drinking water. Water Research 40 (12), 2275–2286.

Hammes, F.A., Egli, T., 2005. New method for assimilable organic carbon determination using flow-cytometric enumeration and a natural microbial consortium as inoculum. Environ. Sci. Technol. 39 (9), 3289–3294.

Heeb, M.B., Criquet, J., Zimmermann-Steffens, S.G., von Gunten, U., 2014. Oxidative treatment of bromide-containing waters: formation of bromine and its reactions with inorganic and organic compounds--a critical review. Water Research 48, 15–42.

Helms, J.R., Stubbins, A., Ritchie, J.D., Minor, E.C., Kieber, D.J., Mopper, K., 2008. Absorption spectral slopes and slope ratios as indicators of molecular weight, source, and photobleaching of chromophoric dissolved organic matter. Limnol. Oceanogr. 53 (3), 955–969.

Hidayah, E.N., Yeh, H.H., 2018. Effect of Permanganate Preoxidation to Natural Organic Matter and Disinfection by-Products Formation Potential Removal. J. Phys.: Conf. Ser. 953, 12218.

Ho, J., Nocker, A., Bendinger, B., West, S., Tiehm, A., 2020. Weiterentwicklung und Validierung der Durchflusszytometrie als schnelle Detektionsmethode für Bakterien in Roh- und Trinkwasser: DVGW W201703.

Hofmann, R., Andrews, R.C., 2006. Impact of H2O2 and (bi)carbonate alkalinity on ammonia's inhibition of bromate formation. Water Research 40 (18), 3343–3348.

Hoigné, J., Bader, H., 1983. Rate constants of reactions of ozone with organic and inorganic compounds in water—I. Water Research 17 (2), 173–183.

Houska, J., Salhi, E., Walpen, N., von Gunten, U., 2021. Oxidant-reactive carbonous moieties in dissolved organic matter: Selective quantification by oxidative titration using chlorine dioxide and ozone. Water Research 207, 117790.

Hu, Y., Boyer, T.H., 2017. Integrated bicarbonate-form ion exchange treatment and regeneration for DOC removal: Model development and pilot plant study. Water Research 115, 40–49.

Hua, G., Reckhow, D.A., 2007. Characterization of disinfection byproduct precursors based on hydrophobicity and molecular size. Environ. Sci. Technol. 41 (9), 3309–3315.

Huang, W.J., Chen, L.Y., 2004. Assessing the effectiveness of ozonation followed by GAC filtration in removing bromate and assimilable organic carbon. Environmental technology 25 (4), 403–412.

Huber, S.A., Balz, A., Abert, M., Pronk, W., 2011. Characterisation of aquatic humic and non-humic matter with size-exclusion chromatography--organic carbon detection--organic nitrogen detection (LC-OCD-OND). Water Research 45 (2), 879–885.

Hübner, U., Zucker, I., Jekel, M., 2015. Options and limitations of hydrogen peroxide addition to enhance radical formation during ozonation of secondary effluents. Journal of Water Reuse and Desalination 5 (1), 8–16.

Ikehata, K., Wang, L., Nessl, M.B., Komor, A.T., Cooper, W.J., McVicker, R.R., 2013. Effect of Ammonia and Chloramine Pretreatment during the Ozonation of a Colored Groundwater with Elevated Bromide. Ozone: Science & Engineering 35 (6), 438–447.

ISO 11206, 2011. Water quality - Determination of dissolved bromate - Method using ion chromatography (IC) and post column reaction (PCR) (ISO 11206:2011). Beuth Verlag GmbH, Berlin 13.060.50. doi:10.31030/1972886.

Jahan, B.N., Li, L., Pagilla, K.R., 2021. Fate and reduction of bromate formed in advanced water treatment ozonation systems: A critical review. Chemosphere 266, 128964.

Jansen, R., 2005. Ozonation of humic substances in a membrane contactor: Mass transfer, product characterization and biodegradability. s.n.], Twente.

Jansen, R., Rijk, J.W. de, Zwijnenburg, A., Mulder, M., Wessling, M., 2005. Hollow fiber membrane contactors—A means to study the reaction kinetics of humic substance ozonation. Journal of Membrane Science 257 (1-2), 48–59.

Jardine, P.M., McCarthy, J.F., Weber, N.L., 1989. Mechanisms of Dissolved Organic Carbon Adsorption on Soil. Soil Sci. Soc. Am. j. 53 (5), 1378–1385.

Jekel, M., 2010. Ozone in Drinking-Water Treatment, in: Gottschalk, C., Libra, J.A., Saupe, A., Libra, J.A. (Eds.), Ozonation of water and waste water. A practical guide to understanding ozone and its applications, 2., completely rev. and updated edition ed. Wiley-VCH, Weinheim.

Jennings, M., Abdulla, H., Stubbins, A., Sun, L., Wang, R., Mopper, K., 2018. A dissolved organic carbon (DOC) analyzer capable of detecting sub-μM DOC differences in natural fresh waters: A proof of concept study. Limnol. Oceanogr. Methods 16 (5), 309–321.

Jie, L., Zhipeng, Z., Cuihong, C., Peilin, C., Yingying, W., 2017. In-situ features of LNA and HNA bacteria in branch ends of drinking water distribution systems. Journal of Water Supply: Research and Technology-Aqua 66 (5), 300–307.

Johnson, P.N., Davis, R.A., 1996. Diffusivity of Ozone in Water. Journal of Chemical & Engineering Data 41 (6), 1485–1487.

Joshi, R., Ratpukdi, T., Knutson, K., Bhatnagar, A., Khan, E., 2020. Bromate formation control by enhanced ozonation: A critical review. Critical Reviews in Environmental Science and Technology, 1–46.

Kaiser, K., Kalbitz, K., 2012. Cycling downwards – dissolved organic matter in soils. Soil Biology and Biochemistry 52, 29–32.

Kämmler, J., Plume, S., Wendler, B., Wricke, B., Ernst, M., 2021. Einsatzmöglichkeiten und Einsatzgrenzen von Verfahren zur Verringerung unerwünschter DOC-Anteile (Entfärbung) in huminstoffreichen Grundwässern. Abschlussbericht W 201719, Bonn.

Kämmler, J., Wendler, B., Ernst, M., 2020. Entfärbung huminstoffreicher Grundwässer mittels Ozonung. energie | wasser-praxis (12), 60–63.

Kämmler, J., Zoumpouli, G.A., Sellmann, J., Chew, J., Wenk, J., Ernst, M., 2022. Decolorization and control of bromate formation in membrane ozonation of humic-rich groundwater. Water Research, 118739.

Kastl, G., Sathasivan, A., Fisher, I., 2016. A selection framework for NOM removal process for drinking water treatment. Desalination and Water Treatment 57 (17), 7679–7689.

Kellerman, A.M., Dittmar, T., Kothawala, D.N., Tranvik, L.J., 2014. Chemodiversity of dissolved organic matter in lakes driven by climate and hydrology. Nature communications 5, 3804.

Kim, M.S., Cha, D., Lee, K.-M., Lee, H.-J., Kim, T., Lee, C., 2020. Modeling of ozone decomposition, oxidant exposures, and the abatement of micropollutants during ozonation processes. Water Research 169, 115230.

Kläning, U.K., Wolff, T., 1985. Laser Flash Photolysis of HClO, ClO−, HBrO, and BrO− in Aqueous Solution. Reactions of Cl- and Br-Atoms. Berichte der Bunsengesellschaft für physikalische Chemie 89 (3), 243–245.

Knocke, W.R., Conley, L., van Benschoten, J.E., 1992. Impact of dissolved organic carbon on the removal of iron during water treatment. Water Research 26 (11), 1515–1522.

Köhler, S.J., Lavonen, E., Keucken, A., Schmitt-Kopplin, P., Spanjer, T., Persson, K., 2016. Upgrading coagulation with hollow-fibre nanofiltration for improved organic matter removal during surface water treatment. Water Research 89, 232–240.

Kölle, W., 2010. Wasseranalysen - richtig beurteilt: Grundlagen, Parameter, Wassertypen, Inhaltsstoffe, Grenzwerte nach Trinkwasserverordnung und EU-Trinkwasserrichtlinie ; mit CD-ROM, 3., aktualisierte und erw. Aufl. ed. Wiley-VCH-Verl., Weinheim.

Korth, A., 2000. Biologischer Abbau organischer Wasserinhaltsstoffe aus reduziertem Grundwasser in Schnellfiltern zur Enteisenung, Nitrifikation und Entmanganung. Dissertation. Veröffentlichungen aus dem Technologiezentrum Wasser Karlsruhe. TZW, Hamburg.

Korth, A., Bendinger, B., Czekalla, C., Wichmann, K., 2001. Biodegradation of NOM in Rapid Sand Filters for Removing Iron and Manganese. Acta hydrochim. hydrobiol. 29 (5), 289–295.

Krasner, S.W., Mitch, W.A., McCurry, D.L., Hanigan, D., Westerhoff, P., 2013. Formation, precursors, control, and occurrence of nitrosamines in drinking water: a review. Water Research 47 (13), 4433–4450.

Krupińska, I., 2020. Impact of the Oxidant Type on the Efficiency of the Oxidation and Removal of Iron Compounds from Groundwater Containing Humic Substances. Molecules (Basel, Switzerland) 25 (15).

Krzeminski, P., Vogelsang, C., Meyn, T., Köhler, S.J., Poutanen, H., Wit, H.A. de, Uhl, W., 2019. Natural organic matter fractions and their removal in full-scale drinking water treatment under cold climate conditions in Nordic capitals. Journal of environmental management 241, 427–438.

Kundu, K., Weber, N., Griebler, C., Elsner, M., 2020. Phenotypic heterogeneity as key factor for growth and survival under oligotrophic conditions. Environmental microbiology 22 (8), 3339–3356.

Kwon, M., Kye, H., Jung, Y., Yoon, Y., Kang, J.-W., 2017. Performance characterization and kinetic modeling of ozonation using a new method: ROH,O3 concept. Water Research 122, 172–182.

Lankes, U., Lüdemann, H.-D., Frimmel, F.H., 2008. Search for basic relationships between "molecular size" and "chemical structure" of aquatic natural organic matter--answers from 13C and 15N CPMAS NMR spectroscopy. Water Research 42 (4-5), 1051–1060.

Lankes, U., Müller, M.B., Weber, M., Frimmel, F.H., 2009. Reconsidering the quantitative analysis of organic carbon concentrations in size exclusion chromatography. Water Research 43 (4), 915–924.

Lautenschlager, K., Hwang, C., Ling, F., Liu, W.-T., Boon, N., Köster, O., Egli, T., Hammes, F., 2014. Abundance and composition of indigenous bacterial communities in a multi-step biofiltration-based drinking water treatment plant. Water Research 62, 40–52.

Lee, S., Cho, J., Elimelech, M., 2005. Combined influence of natural organic matter (NOM) and colloidal particles on nanofiltration membrane fouling. Journal of Membrane Science 262 (1-2), 27–41.

Lee, Y., Gerrity, D., Lee, M., Bogeat, A.E., Salhi, E., Gamage, S., Trenholm, R.A., Wert, E.C., Snyder, S.A., von Gunten, U., 2013. Prediction of micropollutant elimination during ozonation of municipal wastewater effluents: use of kinetic and water specific information. Environ. Sci. Technol. 47 (11), 5872–5881.

Lee, Y., Gerrity, D., Lee, M., Gamage, S., Pisarenko, A., Trenholm, R.A., Canonica, S., Snyder, S.A., von Gunten, U., 2016. Organic Contaminant Abatement in Reclaimed Water by UV/H2O2 and a Combined Process Consisting of O3/H2O2 Followed by UV/H2O2: Prediction of Abatement Efficiency, Energy Consumption, and Byproduct Formation. Environ. Sci. Technol. 50 (7), 3809–3819.

Leenheer, J.A., 1981. Comprehensive approach to preparative isolation and fractionation of dissolved organic carbon from natural waters and wastewaters. Environ. Sci. Technol. 15 (5), 578–587.

Leenheer, J.A., Croué, J.-P., 2003. Characterizing Aquatic Dissolved Organic Matter. Environ. Sci. Technol. 37 (1), 18A-26A.

Legube, B., 1996. A Survey of Bromate Ion in European Drinking Water. Ozone: Science & Engineering 18 (4), 325–348.

Legube, B., Parinet, B., Gelinet, K., Berne, F., Croue, J.-P., 2004. Modeling of bromate formation by ozonation of surface waters in drinking water treatment. Water Research 38 (8), 2185–2195.

Leiknes, T., Phattaranawik, J., Boller, M., von Gunten, U., Pronk, W., 2005. Ozone transfer and design concepts for NOM decolourization in tubular membrane contactor. Chemical Engineering Journal 111 (1), 53–61.

Lekkerkerker-Teunissen, K., Knol, A.H., van Altena, L.P., Houtman, C.J., Verberk, J., van Dijk, J.C., 2012. Serial ozone/peroxide/low pressure UV treatment for synergistic and effective organic micropollutant conversion. Separation and Purification Technology 100, 22–29.

Leresche, F., McKay, G., Kurtz, T., von Gunten, U., Canonica, S., Rosario-Ortiz, F.L., 2019. Effects of Ozone on the Photochemical and Photophysical Properties of Dissolved Organic Matter. Environ. Sci. Technol. 53 (10), 5622–5632.

Leresche, F., Torres-Ruiz, J.A., Kurtz, T., von Gunten, U., Rosario-Ortiz, F.L., 2021. Optical properties and photochemical production of hydroxyl radical and singlet oxygen after ozonation of dissolved organic matter. Environ. Sci.: Water Res. Technol. 7 (2), 346–356.

Levchuk, I., Rueda Márquez, J.J., Sillanpää, M., 2018. Removal of natural organic matter (NOM) from water by ion exchange - A review. Chemosphere 192, 90–104.

Lewis, W.K., Whitman, W.G., 1924. Principles of Gas Absorption. Ind. Eng. Chem. 16 (12), 1215–1220.

Li, J., Zou, L., Guo, L., Ji, J., 2011. Pilot study on bromate reduction in ozonation of water with low carbonate alkalinities by carbon dioxide. Journal of Environmental Sciences 23 (9), 1491–1496.

Li, L., Zhu, C., Xie, C., Shao, C., Yu, S., Zhao, L., Gao, N., 2018. Kinetics and mechanism of Pseudoanabaena cell inactivation, 2-MIB release and degradation under exposure of ozone, chlorine and permanganate. Water Research 147, 422–428.

Li, W.-T., Cao, M.-J., Young, T., Ruffino, B., Dodd, M., Li, A.-M., Korshin, G., 2017. Application of UV absorbance and fluorescence indicators to assess the formation of biodegradable dissolved organic carbon and bromate during ozonation. Water Research 111, 154–162.

Liao, P., Li, W., Jiang, Y., Wu, J., Yuan, S., Fortner, J.D., Giammar, D.E., 2017. Formation, Aggregation, and Deposition Dynamics of NOM-Iron Colloids at Anoxic-Oxic Interfaces. Environmental Science & Technology 51 (21), 12235–12245.

Lienhard, H., Sontheimer, H., 1979. Influence of Process Conditions on the Effect of Ozone Treatment of Organic Substances in the Water. Ozone: Science & Engineering 1 (1), 61–72.

Lim, S., Shi, J.L., von Gunten, U., McCurry, D.L., 2022. Ozonation of Organic Compounds in Water and Wastewater: A Critical Review. Water Research, 118053.

Liu, J., Yu, J., Li, D., Zhang, Y., Yang, M., 2012. Reduction of bromate in a biological activated carbon filter under high bulk dissolved oxygen conditions and characterization of bromate-reducing isolates. Biochemical Engineering Journal 65, 44–50.

Liu, Z., Demeestere, K., van Hulle, S., 2021. Comparison and performance assessment of ozone-based AOPs in view of trace organic contaminants abatement in water and wastewater: A review. Journal of Environmental Chemical Engineering 9 (4), 105599.

Liu, Z., Lompe, K.M., Mohseni, M., Bérubé, P.R., Sauvé, S., Barbeau, B., 2020. Biological ion exchange as an alternative to biological activated carbon for drinking water treatment. Water Research 168, 115148.

Loeb, B.L., Thompson, C.M., Drago, J., Takahara, H., Baig, S., 2012. Worldwide Ozone Capacity for Treatment of Drinking Water and Wastewater: A Review. Ozone: Science & Engineering 34 (1), 64–77.

Loganathan, P., Kandasamy, J., Jamil, S., Ratnaweera, H., Vigneswaran, S., 2022. Ozonation/adsorption hybrid treatment system for improved removal of natural organic matter and organic micropollutants from water - A mini review and future perspectives. Chemosphere 296, 133961.

Lu, Z., Lin, T., Chen, W., Zhang, X.B., 2015. Influence of KMnO4 preoxidation on ultrafiltration performance and membrane material characteristics. Journal of Membrane Science 486, 49–58.

Malcolm, R.L., MacCarthy, P., 1992. Quantitative evaluation of XAD-8 and XAD-4 resins used in tandem for removing organic solutes from water. Environment International 18 (6), 597–607.

Mantel, T., Jacki, E., Ernst, M., 2021. Electrosorptive removal of organic water constituents by positively charged electrically conductive UF membranes. Water Research 201, 117318.

Mao, J.-D., Hu, W.-G., Schmidt-Rohr, K., Davies, G., Ghabbour, E.A., Xing, B., 2000. Quantitative Characterization of Humic Substances by Solid-State Carbon-13 Nuclear Magnetic Resonance. Soil Science Society of America Journal 64 (3), 873–884.

Matilainen, A., Gjessing, E.T., Lahtinen, T., Hed, L., Bhatnagar, A., Sillanpää, M., 2011. An overview of the methods used in the characterisation of natural organic matter (NOM) in relation to drinking water treatment. Chemosphere 83 (11), 1431–1442.

Matsui, Y., Fukuda, Y., Inoue, T., Matsushita, T., 2003. Effect of natural organic matter on powdered activated carbon adsorption of trace contaminants: characteristics and mechanism of competitive adsorption. Water Research 37 (18), 4413–4424.

McDonough, L.K., Rutlidge, H., O'Carroll, D.M., Andersen, M.S., Meredith, K., Behnke, M.I., Spencer, R.G., McKenna, A.M., Marjo, C.E., Oudone, P., Baker, A., 2020a. Characterisation of shallow groundwater dissolved organic matter in aeolian, alluvial and fractured rock aquifers. Geochimica et Cosmochimica Acta 273 (D4), 163–176.

McDonough, L.K., Santos, I.R., Andersen, M.S., O'Carroll, D.M., Rutlidge, H., Meredith, K., Oudone, P., Bridgeman, J., Gooddy, D.C., Sorensen, J.P.R., Lapworth, D.J., MacDonald, A.M., Ward, J., Baker, A., 2020b. Changes in global groundwater organic carbon driven by climate change and urbanization. Nature communications 11 (1), 1279.

McDowell, W.H., Zsolnay, A., Aitkenhead-Peterson, J.A., Gregorich, E.G., Jones, D.L., Jödemann, D., Kalbitz, K., Marschner, B., Schwesig, D., 2006. A comparison of methods to determine the biodegradable dissolved organic carbon from different terrestrial sources. Soil Biology and Biochemistry 38 (7), 1933–1942.

Melin, E., Ødegaard, H., 2000. The effect of biofilter loading rate on the removal of organic ozonation by-products. Water Research 34 (18), 4464–4476.

Merle, T., Pronk, W., von Gunten, U., 2017. MEMBRO 3 X, a Novel Combination of a Membrane Contactor with Advanced Oxidation (O 3 /H 2 O 2) for Simultaneous Micropollutant Abatement and Bromate Minimization. Environ. Sci. Technol. Lett. 4 (5), 180–185.

Möhler, F., Wiesner, C., Ruhland, A., 2021. Auswirkungen des Klimawandels und Anpassungsstrategien für das Wasserwerk Colbitz in Sachsen-Anhalt. Grundwasser - Zeitschrift der Fachsektion Hydrogeologie 26 (1), 47–60.

Mostofa, K.M.G., Liu, C., Vione, D., Mottaleb, M.A., Ogawa, H., Tareq, S.M., Yoshioka, T., 2013. Colored and Chromophoric Dissolved Organic Matter in Natural Waters, in: Mostofa, K.M., Yoshioka, T., Mottaleb, A., Vione, D. (Eds.), Photobiogeochemistry of Organic Matter, vol. 39. Environmental Science and Engineering. Springer Berlin Heidelberg, Berlin, Heidelberg, pp. 365–428.

Mvula, E., Naumov, S., von Sonntag, C., 2009. Ozonolysis of lignin models in aqueous solution: anisole, 1,2-dimethoxybenzene, 1,4-dimethoxybenzene, and 1,3,5-trimethoxybenzene. Environ. Sci. Technol. 43 (16), 6275–6282.

Mvula, E., von Sonntag, C., 2003. Ozonolysis of phenols in aqueous solution. Organic & biomolecular chemistry 1 (10), 1749–1756.

Nanaboina, V., Korshin, G.V., 2010. Evolution of absorbance spectra of ozonated wastewater and its relationship with the degradation of trace-level organic species. Environ. Sci. Technol. 44 (16), 6130–6137.

National Secondary Drinking Water Regulations, 1979. Code of Federal Regulations Part 143.

Naumov, S., von Sonntag, C., 2010. Quantum Chemical Studies on the Formation of Ozone Adducts to Aromatic Compounds in Aqueous Solution. Ozone: Science & Engineering 32 (1), 61–65.

Niehues, B., Merkel, W., 2021. Die Wasserversorgung im Jahr 2020 - Stressindikatoren und Ergebnisse der zweiten Online-Umfrage des DVGW. energie | wasser-praxis (8), 38–44.

Nishijima, W., Fahmi, Mukaidani, T., Okada, M., 2003. DOC removal by multi-stage ozonation-biological treatment. Water Research 37 (1), 150–154.

Nöthe, T., Fahlenkamp, H., von Sonntag, C., 2009. Ozonation of Wastewater: Rate of Ozone Consumption and Hydroxyl Radical Yield. Environmental Science & Technology 43 (15), 5990–5995.

Ødegaard, H., Østerhus, S., Melin, E., Eikebrokk, B., 2010. NOM removal technologies – Norwegian experiences. Drink. Water Eng. Sci. 3 (1), 1–9.

Önnby, L., Salhi, E., McKay, G., Rosario-Ortiz, F.L., von Gunten, U., 2018. Ozone and chlorine reactions with dissolved organic matter - Assessment of oxidant-reactive moieties by optical measurements and the electron donating capacities. Water Research 144, 64–75.

Osburn, C.L., Morris, D.P., Thorn, K.A., Moeller, R.E., 2001. Chemical and optical changes in freshwater dissolved organic matter exposed to solar radiation. Biogeochemistry 54 (3), 251–278.

Osterwald, A., 2009. Einfluss von gelöstem organischen Kohlenstoff (DOC) auf die Eisen(II)-Oxidation bei der Grundwasseraufbereitung. Dissertation. Berichte aus der Verfahrenstechnik. Shaker, Hamburg.

Pace, M.L., Reche, I., Cole, J.J., Fernández-Barbero, A., Mazuecos, I.P., Prairie, Y.T., 2012. pH change induces shifts in the size and light absorption of dissolved organic matter. Biogeochemistry 108 (1-3), 109–118.

Park, H.-S., Hwang, T.-M., Kang, J.-W., Choi, H., Oh, H.-J., 2001. Characterization of raw water for the ozone application measuring ozone consumption rate. Water Research 35 (11), 2607–2614.

Park, J.W., Kim, H.-C., Meyer, A.S., Kim, S., Maeng, S.K., 2016. Influences of NOM composition and bacteriological characteristics on biological stability in a full-scale drinking water treatment plant. Chemosphere 160, 189–198.

Parsi, Z., Hartog, N., Górecki, T., Poerschmann, J., 2007. Analytical pyrolysis as a tool for the characterization of natural organic matter—A comparison of different approaches. Journal of Analytical and Applied Pyrolysis 79 (1-2), 9–15.

Payment, P., Locas, A., 2011. Pathogens in water: value and limits of correlation with microbial indicators. Ground water 49 (1), 4–11.

Peuravuori, J., Pihlaja, K., 1997. Molecular size distribution and spectroscopic properties of aquatic humic substances. Analytica Chimica Acta 337 (2), 133–149.

Pharand, L., van Dyke, M.I., Anderson, W.B., Yohannes, Y., Huck, P.M., 2015. Full-Scale Ozone-Biofiltration: Seasonally Related Effects on NOM Removal. Journal - American Water Works Association 107 (8), E425-E435.

Phattaranawik, J., Leiknes, T., Pronk, W., 2005. Mass transfer studies in flat-sheet membrane contactor with ozonation. Journal of Membrane Science 247 (1-2), 153–167.

Phungsai, P., Kurisu, F., Kasuga, I., Furumai, H., 2019. Molecular characteristics of dissolved organic matter transformed by O3 and O3/H2O2 treatments and the effects on formation of unknown disinfection by-products. Water Research 159, 214–222.

Pines, D.S., Min, K.-N., Ergas, S.J., Reckhow, D.A., 2005. Investigation of an Ozone Membrane Contactor System. Ozone: Science & Engineering 27 (3), 209–217.

Pinkernell, U., von Gunten, U., 2001. Bromate Minimization during Ozonation: Mechanistic Considerations. Environmental Science & Technology 35 (12), 2525–2531.

Plummer, N., Glynn, P.D., 2013. Radiocarbon dating in groundwater systems, in: , Isotope Methods for Dating Old Groundwater. International Atomic Energy Agency, Vienna, Austria, pp. 33–89.

Pocostales, J.P., Sein, M.M., Knolle, W., von Sonntag, C., Schmidt, T.C., 2010. Degradation of ozone-refractory organic phosphates in wastewater by ozone and ozone/hydrogen peroxide (peroxone): the role of ozone consumption by dissolved organic matter. Environ. Sci. Technol. 44 (21), 8248–8253.

Preda, L., 2019. Laboratory experiments: Decolorization of drinking water by ozone under different operating conditions. Bachelor's Thesis, Hamburg.

Prest, E.I., Hammes, F., Kötzsch, S., van Loosdrecht, M.C.M., Vrouwenvelder, J.S., 2013. Monitoring microbiological changes in drinking water systems using a fast and reproducible flow cytometric method. Water Research 47 (19), 7131–7142.

Qi, S., Mao, Y., Lv, M., Sun, L., Wang, X., Yang, H., Xie, Y.F., 2016. Pathway fraction of bromate formation during O_3 and O_3/H_2O_2 processes in drinking water treatment. Chemosphere 144, 2436–2442.

Ramseier, M.K., Peter, A., Traber, J., von Gunten, U., 2011. Formation of assimilable organic carbon during oxidation of natural waters with ozone, chlorine dioxide, chlorine, permanganate, and ferrate. Water Research 45 (5), 2002–2010.

Ramseier, M.K., von Gunten, U., 2009. Mechanisms of Phenol Ozonation—Kinetics of Formation of Primary and Secondary Reaction Products. Ozone: Science & Engineering 31 (3), 201–215.

Reemtsma, T., These, A., Springer, A., Linscheid, M., 2008. Differences in the molecular composition of fulvic acid size fractions detected by size-exclusion chromatography-on line Fourier transform ion cyclotron resonance (FTICR-) mass spectrometry. Water Research 42 (1-2), 63–72.

Reisz, E., Leitzke, A., Jarocki, A., Irmscher, R., von Sonntag, C., 2008. Permanganate formation in the reactions of ozone with Mn(II): a mechanistic study. Journal of Water Supply: Research and Technology-Aqua 57 (6), 451–464.

Remucal, C.K., Salhi, E., Walpen, N., von Gunten, U., 2020. Molecular-Level Transformation of Dissolved Organic Matter during Oxidation by Ozone and Hydroxyl Radical. Environmental Science & Technology 54 (16), 10351–10360.

Riedel, T., 2019. Temperature-associated changes in groundwater quality. Journal of Hydrology 572, 206–212.

Ritchie, J.D., Perdue, E.M., 2003. Proton-binding study of standard and reference fulvic acids, humic acids, and natural organic matter. Geochimica et Cosmochimica Acta 67 (1), 85–96.

Rittmann, B.E., Stilwell, D., Garside, J.C., Amy, G.L., Spangenberg, C., Kalinsky, A., Akiyoshi, E., 2002. Treatment of a colored groundwater by ozone-biofiltration: pilot studies and modeling interpretation. Water Research 36 (13), 3387–3397.

Rosario-Ortiz, F.L., Mezyk, S.P., Doud, D.F.R., Snyder, S.A., 2008. Quantitative correlation of absolute hydroxyl radical rate constants with non-isolated effluent organic matter bulk properties in water. Environ. Sci. Technol. 42 (16), 5924–5930.

Ross, P.S., Hammes, F., Dignum, M., Magic-Knezev, A., Hambsch, B., Rietveld, L.C., 2013. A comparative study of three different assimilable organic carbon (AOC) methods: results of a round-robin test. Water Supply 13 (4), 1024–1033.

Rougé, V., von Gunten, U., Allard, S., 2020. Efficiency of pre-oxidation of natural organic matter for the mitigation of disinfection byproducts: Electron donating capacity and UV absorbance as surrogate parameters. Water Research 187, 116418.

Russell, C.G., Lawler, D.F., Speitel, G.E., Katz, L.E., 2009. Effect of softening precipitate composition and surface characteristics on natural organic matter adsorption. Environ. Sci. Technol. 43 (20), 7837–7842.

Rutlidge, H., McDonough, L.K., Oudone, P., Andersen, M.S., Meredith, K., Chinu, K., Peterson, M., Baker, A., 2021. Characterisation of groundwater dissolved organic matter using LC-OCD: Implications for water treatment. Water Research 188, 116422.

Sadrnourmohamadi, M., Gorczyca, B., 2015. Effects of ozone as a stand-alone and coagulation-aid treatment on the reduction of trihalomethanes precursors from high DOC and hardness water. Water Research 73, 171–180.

Saldaña-Robles, A., Damian-Ascencio, C.E., Guerra-Sanchez, R.J., Saldaña-Robles, A.L., Saldaña-Robles, N., Gallegos-Muñoz, A., Cano-Andrade, S., 2018. Effects of the presence of organic matter on the removal of arsenic from groundwater. Journal of Cleaner Production 183, 720–728.

Särkkä, H., Vepsäläinen, M., Sillanpää, M., 2015. Natural organic matter (NOM) removal by electrochemical methods — A review. Journal of Electroanalytical Chemistry 755, 100–108.

Schmidt, C.K., Brauch, H.-J., 2008. N,N-dimethylsulfamide as precursor for N-nitrosodimethylamine (NDMA) formation upon ozonation and its fate during drinking water treatment. Environ. Sci. Technol. 42 (17), 6340–6346.

Schmitt, A., Mendret, J., Roustan, M., Brosillon, S., 2020. Ozonation using hollow fiber contactor technology and its perspectives for micropollutants removal in water: A review. Science of the Total Environment 729, 138664.

Schulz, M., 2020. Entfernung natürlicher organischer Stoffe durch die Verfahrenskombination Flockung-Ultrafiltration bei der Aufbereitung reduzierter Grundwässer. Dissertation, Hamburg.

Schulz, M., Winter, J., Wray, H., Barbeau, B., Bérubé, P., 2017. Biologically active ion exchange (BIEX) for NOM removal and membrane fouling prevention. Water Supply 17 (4), 1178–1184.

Schuster, J., Huber, J., Stumme, J., Grieb, A., Ernst, M., 2022. Combining real-time fluorescence spectroscopy and flow cytometry to reveal new insights in DOC and cell characterization of drinking water. Front. Environ. Chem. 3, 1.

Sellmann, J., 2020. Praxisversuche zur Entfärbung von Trinkwasser mittels Ozon. Master's Thesis, Hamburg.

Shin, J., Hidayat, Z.R., Lee, Y., 2016. Influence of Seasonal Variation of Water Temperature and Dissolved Organic Matter on Ozone and OH Radical Reaction Kinetics During Ozonation of a Lake Water. Ozone: Science & Engineering 38 (2), 100–114.

Sillanpää, M., 2015. General Introduction. Chapter 1, in: Sillanpää, M. (Ed.), Natural organic matter in water. Characterization and treatment methods. Butterworth-Heinemann, Oxford, England.

Sillanpää, M., Matilainen, A., Lahtinen, T., 2015. Characterization of NOM. Chapter 2, in: Sillanpää, M. (Ed.), Natural organic matter in water. Characterization and treatment methods. Butterworth-Heinemann, Oxford, England.

Sillanpää, M., Ncibi, M.C., Matilainen, A., 2018. Advanced oxidation processes for the removal of natural organic matter from drinking water sources: A comprehensive review. Journal of environmental management 208, 56–76.

Sobhani, R., McVicker, R., Spangenberg, C., Rosso, D., 2012. Process analysis and economics of drinking water production from coastal aquifers containing chromophoric dissolved organic matter and bromide using nanofiltration and ozonation. Journal of environmental management 93 (1), 209–217.

Soltermann, F., Abegglen, C., Tschui, M., Stahel, S., von Gunten, U., 2017. Options and limitations for bromate control during ozonation of wastewater. Water Research 116, 76–85.

Song, R., Donohoe, C., Minear, R., Westerhoff, P., Ozekin, K., Amy, G., 1996. Empirical modeling of bromate formation during ozonation of bromide-containing waters. Water Research 30 (5), 1161–1168.

Song, R., Westerhoff, P., Minear, R., Amy, G., 1997. Bromate minimization during ozonation. Journal - American Water Works Association 89 (6), 69–78.

Specker, J., 2019. NOM Transformation and Bromate Formation during Ozonation of Humic-Rich Groundwaters in Laboratory and Pilot Experiments. Master's Thesis, Hamburg.

Staehelin, J., Hoigne, J., 1985. Decomposition of ozone in water in the presence of organic solutes acting as promoters and inhibitors of radical chain reactions. Environ. Sci. Technol. 19 (12), 1206–1213.

Statistisches Bundesamt, 2019. Öffentliche Wasserversorgung und öffentliche Abwasserentsorgung - Öffentliche Wasserversorgung. Fachserie 19, Reihe 2.1.1, 2016.

Stylianou, S.K., Katsoyiannis, I.A., Ernst, M., Zouboulis, A.I., 2018a. Impact of O3 or O3/H2O2 treatment via a membrane contacting system on the composition and characteristics of the natural organic matter of surface waters. Environmental science and pollution research international 25 (13), 12246–12255.

Stylianou, S.K., Katsoyiannis, I.A., Mitrakas, M., Zouboulis, A.I., 2018b. Application of a ceramic membrane contacting process for ozone and peroxone treatment of micropollutant contaminated surface water. Journal of Hazardous Materials 358, 129–135.

Swietlik, J., Dabrowska, A., Raczyk-Stanisławiak, U., Nawrocki, J., 2004. Reactivity of natural organic matter fractions with chlorine dioxide and ozone. Water Research 38 (3), 547–558.

Tan, L., Amy, G., Rigby, M., Renna, J., Kemp, K., 1991. Ozonation of Colored Groundwater Pilot-Scale and Full-Scale Experiences. Ozone: Science & Engineering 13 (1), 109–125.

Tan, L., Johnson, W., 2001. Removing Organic Color and By-Products from Groundwater with Ozone and Pressurized Biologically-Active Filtration. Ozone: Science & Engineering 23 (5), 393–400.

Terry, L.G., Summers, R.S., 2018. Biodegradable organic matter and rapid-rate biofilter performance: A review. Water Research 128, 234–245.

These, A., Reemtsma, T., 2005. Structure-dependent reactivity of low molecular weight fulvic acid molecules during ozonation. Environ. Sci. Technol. 39 (21), 8382–8387.

Thurman, E.M., 1985. Organic Geochemistry of Natural Waters. Springer Netherlands, Dordrecht.

Thurman, E.M., Wershaw, R.L., Malcolm, R.L., Pinckney, D.J., 1982. Molecular size of aquatic humic substances. Organic Geochemistry 4 (1), 27–35.

Trinkwasserverordnung, 2001. Trinkwasserverordnung in der Fassung der Bekanntmachung vom 10. März 2016 (BGBl. I S. 459), die zuletzt durch Artikel 1 der Verordnung vom 22. September 2021 (BGBl. I S. 4343) geändert worden ist: TrinkwV.

Tubić, A., Agbaba, J., Dalmacija, B., Perović, S.U., Klašnja, M., Rončević, S., Ivančev-Tumbas, I., 2011. Removal of Natural Organic Matter from Groundwater Using Advanced Oxidation Processes at a Pilot Scale Drinking Water Treatment Plant in the Central Banat Region (Serbia). Ozone: Science & Engineering 33 (4), 267–278.

Twardowski, M.S., Boss, E., Sullivan, J.M., Donaghay, P.L., 2004. Modeling the spectral shape of absorption by chromophoric dissolved organic matter. Marine Chemistry 89 (1-4), 69–88.

Tyrovola, K., Diamadopoulos, E., 2005. Bromate formation during ozonation of groundwater in coastal areas in Greece. Desalination 176 (1), 201–209.

Umweltbundesamt, 2021. Bekanntmachung der Liste der Aufbereitungsstoffe und Desinfektionsverfahren gemäß § 11 der Trinkwasserverordnung (23. Änderung): §-11-Liste.

UN, 2015. Resolution adopted by the General Assembly on 25 September 2015. Transforming our world: the 2030 Agenda for Sustainable Development.

UN Water, 2022. Groundwater making the invisible visible. The United Nations world water development report 2022. UNESCO, Paris.

UNESCO, 2019. Leaving no one behind. The United Nations world water development report 2019. UNESCO, Paris.

USEPA, 2009. National Primary Drinking Water Regulations.

van der Kooij, D., Hijnen, W., Kruithof, J.C., 1989. The Effects of Ozonation, Biological Filtration and Distribution on the Concentration of Easily Assimilable Organic Carbon (AOC) in Drinking Water. Ozone: Science & Engineering 11 (3), 297–311.

van der Kooij, D., Visser, A., Hijnen, W., 1982. Determining the concentration of easily assimilable organic carbon in drinking water. Journal - American Water Works Association 74 (10), 540–545.

Velten, S., Knappe, D.R.U., Traber, J., Kaiser, H.-P., von Gunten, U., Boller, M., Meylan, S., 2011. Characterization of natural organic matter adsorption in granular activated carbon adsorbers. Water Research 45 (13), 3951–3959.

von Gunten, U., 2003a. Ozonation of drinking water: Part I. Oxidation kinetics and product formation. Water Research 37 (7), 1443–1467.

von Gunten, U., 2003b. Ozonation of drinking water: Part II. Disinfection and by-product formation in presence of bromide, iodide or chlorine. Water Research 37 (7), 1469–1487.

von Gunten, U., 2018. Oxidation Processes in Water Treatment: Are We on Track? Environ. Sci. Technol. 52 (9), 5062–5075.

von Gunten, U., Hoigne, J., 1994. Bromate Formation during Ozonization of Bromide-Containing Waters: Interaction of Ozone and Hydroxyl Radical Reactions. Environmental Science & Technology 28 (7), 1234–1242.

von Gunten, U., Oliveras, Y., 1997. Kinetics of the reaction between hydrogen peroxide and hypobromous acid: Implication on water treatment and natural systems. Water Research 31 (4), 900–906.

von Gunten, U., Oliveras, Y., 1998. Advanced Oxidation of Bromide-Containing Waters: Bromate Formation Mechanisms. Environ. Sci. Technol. 32 (1), 63–70.

von Sonntag, C., von Gunten, U., 2012. Chemistry of Ozone in Water and Wastewater Treatment: From Basic Principles to Applications. IWA Publishing, London.

Wagner, M., Schmidt, W., Imhof, L., Grübel, A., Jähn, C., Georgi, D., Petzoldt, H., 2016. Characterization and quantification of humic substances 2D-Fluorescence by usage of extended size exclusion chromatography. Water Research 93, 98–109.

Walpen, N., Getzinger, G.J., Schroth, M.H., Sander, M., 2018. Electron-Donating Phenolic and Electron-Accepting Quinone Moieties in Peat Dissolved Organic Matter: Quantities and Redox Transformations in the Context of Peat Biogeochemistry. Environ. Sci. Technol. 52 (9), 5236–5245.

Walpen, N., Houska, J., Salhi, E., Sander, M., von Gunten, U., 2020. Quantification of the electron donating capacity and UV absorbance of dissolved organic matter during ozonation of secondary wastewater effluent by an assay and an automated analyzer. Water Research 185, 116235.

Walpen, N., Schroth, M.H., Sander, M., 2016. Quantification of Phenolic Antioxidant Moieties in Dissolved Organic Matter by Flow-Injection Analysis with Electrochemical Detection. Environ. Sci. Technol. 50 (12), 6423–6432.

Wang, F., Salgado, V., Van der Hoek, Jan Peter, van Halem, D., 2018a. Bromate Reduction by Iron(II) during Managed Aquifer Recharge: A Laboratory-Scale Study. Water 10 (4), 370.

Wang, F., van Halem, D., Ding, L., Bai, Y., Lekkerkerker-Teunissen, K., Van der Hoek, Jan Peter, 2018b. Effective removal of bromate in nitrate-reducing anoxic zones during managed aquifer recharge for drinking water treatment: Laboratory-scale simulations. Water Research 130, 88–97.

Wang, F., Zhang, L., Wei, L., Van der Hoek, Jan Peter, 2021a. Removal of Hydrogen Peroxide Residuals and By-Product Bromate from Advanced Oxidation Processes by Granular Activated Carbon. Water 13 (18), 2460.

Wang, H., Zhan, J., Yao, W., Wang, B., Deng, S., Huang, J., Yu, G., Wang, Y., 2018c. Comparison of pharmaceutical abatement in various water matrices by conventional ozonation, peroxone (O3/H2O2), and an electro-peroxone process. Water Research 130, 127–138.

Wang, Y., Hammes, F., Boon, N., Chami, M., Egli, T., 2009. Isolation and characterization of low nucleic acid (LNA)-content bacteria. The ISME journal 3 (8), 889–902.

Wang, Y., Man, T., Zhang, R., Yan, X., Wang, S., Zhang, M., Wang, P., Ren, L., Yu, J., Li, C., 2021b. Effects of organic matter, ammonia, bromide, and hydrogen peroxide on bromate formation during water ozonation. Chemosphere 285, 131352.

Wangersky, P.J., 1993. Dissolved organic carbon methods: a critical review. Marine Chemistry 41 (1-3), 61–74.

Water Supply (Water Quality) Regulations, 2016. Water, England and Wales. 2016 No. 614.

Weishaar, J.L., Aiken, G.R., Bergamaschi, B.A., Fram, M.S., Fujii, R., Mopper, K., 2003. Evaluation of specific ultraviolet absorbance as an indicator of the chemical composition and reactivity of dissolved organic carbon. Environmental Science & Technology 37 (20), 4702–4708.

Wenk, J., Aeschbacher, M., Salhi, E., Canonica, S., von Gunten, U., Sander, M., 2013. Chemical oxidation of dissolved organic matter by chlorine dioxide, chlorine, and ozone: effects on its optical and antioxidant properties. Environmental Science & Technology 47 (19), 11147–11156.

Wert, E.C., Rosario-Ortiz, F.L., Drury, D.D., Snyder, S.A., 2007. Formation of oxidation byproducts from ozonation of wastewater. Water Research 41 (7), 1481–1490.

Westerhoff, P., Aiken, G., Amy, G., Debroux, J., 1999. Relationships between the structure of natural organic matter and its reactivity towards molecular ozone and hydroxyl radicals. Water Research 33 (10), 2265–2276.

Westerhoff, P., Mezyk, S.P., Cooper, W.J., Minakata, D., 2007. Electron pulse radiolysis determination of hydroxyl radical rate constants with Suwannee River fulvic acid and other dissolved organic matter isolates. Environ. Sci. Technol. 41 (13), 4640–4646.

Westerhoff, P., Song, R., Amy, G., Minear, R., 1998. NOM's role in bromine and bromate formation during ozonation. Journal - American Water Works Association 90 (2), 82–94.

WHO, 2005. Bromate in Drinking-water. Background document for development of WHO Guidelines for Drinking-water quality: WHO/SDE/WSH/05.08/78.

WHO, 2017. Guidelines for drinking-water quality, Fourth edition incorporating the first addendum ed. World Health Organization, Geneva.

WHO, 2018. A global overview of national regulations and standards for drinking-water quality. World Health Organization, Geneva.

Winzenbacher, R., 2000. Untersuchungen zum Filtrationsprozess mit geringen Mengen an Fe(III)-Salzen bei der Aufbereitung von Oberflächenwasser. Dissertation, Berlin.

Wiśniewski, J.A., Kabsch-Korbutowicz, M., 2010. Bromate removal in the ion-exchange process. Desalination 261 (1-2), 197–201.

Wols, B.A., Hofman, J., Uijttewaal, W., Rietveld, L.C., van Dijk, J.C., 2010. Evaluation of different disinfection calculation methods using CFD. Environmental Modelling & Software 25 (4), 573–582.

Wong, S., Hanna, J.V., King, S., Carroll, T.J., Eldridge, R.J., Dixon, D.R., Bolto, B.A., Hesse, S., Abbt-Braun, G., Frimmel, F.H., 2002. Fractionation of natural organic matter in drinking water and characterization by 13C cross-polarization magic-angle spinning NMR spectroscopy and size exclusion chromatography. Environ. Sci. Technol. 36 (16), 3497–3503.

Worch, E., 2019. Drinking water treatment: An introduction. De Gruyter Graduate. De Gruyter, Berlin, Boston.

Wricke, B., Bornmann, K., Plume, S., 2016. Einfluss des DOC auf die Aufbereitung von Talsperrenwasser: Abschlussbericht zum Teilprojekt 3 des BMBF-Forschungsvorhabens „Belastung von Trinkwassertalsperren durch gelösten organischen Kohlenstoff: Prognose, Vorsorge, Handlungsempfehlungen (TALKO)". W 201204. DVGW – German Technical and Scientific Association for Gas and Water (Ed.), Bonn.

Wu, Q.-Y., Yang, L.-L., Zhang, X.-Y., Wang, W.-L., Lu, Y., Du, Y., Lu, Y., Hu, H.-Y., 2020. Ammonia-Mediated Bromate Inhibition during Ozonation Promotes the Toxicity Due to Organic Byproduct Transformation. Environ. Sci. Technol. 54 (14), 8926–8937.

Wu, Q.-Y., Zhou, Y.-T., Li, W., Zhang, X., Du, Y., Hu, H.-Y., 2019. Underestimated risk from ozonation of wastewater containing bromide: Both organic byproducts and bromate contributed to the toxicity increase. Water Research 162, 43–52.

Xiao, Q., Yu, S., Li, L., Wang, T., Liao, X., Ye, Y., 2017. An overview of advanced reduction processes for bromate removal from drinking water: Reducing agents, activation methods, applications and mechanisms. Journal of Hazardous Materials 324 (Pt B), 230–240.

Yan, H., Du, X., Li, P., Yu, S., Tang, Y., 2015. Adsorption of Bromate From Aqueous Solutions by Modified Granular Activated Carbon: Batch and Column Tests. Ozone: Science & Engineering 37 (4), 357–370.

Yan, M., Korshin, G.V., Claret, F., Croué, J.-P., Fabbricino, M., Gallard, H., Schäfer, T., Benedetti, M.F., 2014. Effects of charging on the chromophores of dissolved organic matter from the Rio Negro basin. Water Research 59, 154–164.

Yan, S., Liu, Y., Lian, L., Li, R., Ma, J., Zhou, H., Song, W., 2019. Photochemical formation of carbonate radical and its reaction with dissolved organic matters. Water Research 161, 288–296.

Yang, J., Dong, Z., Jiang, C., Liu, H., Li, J., 2019a. Quantitatively assessing the role played by carbonate radicals in bromate formation by ozonation. Journal of Hazardous Materials 363, 428–438.

Yang, J., Dong, Z., Jiang, C., Wang, C., Liu, H., 2019b. An overview of bromate formation in chemical oxidation processes: Occurrence, mechanism, influencing factors, risk assessment, and control strategies. Chemosphere 237, 124521.

Yang, J., Li, J., Dong, W., Ma, J., Yang, Y., Li, J., Yang, Z., Zhang, X., Gu, J., Xie, W., Cang, Y., 2017a. Enhancement of bromate formation by pH depression during ozonation of bromide-containing water in the presence of hydroxylamine. Water Research 109, 135–143.

Yang, J., Li, J., Zhu, J., Dong, Z., Luo, F., Wang, Y., Liu, H., Jiang, C., Yuan, H., 2017b. A novel design for an ozone contact reactor and its performance on hydrodynamics, disinfection, bromate formation and oxidation. Chemical Engineering Journal 328, 207–214.

Yasui, H., Miyaji, Y., 1992. A Novel Approach to Removing Refractory Organic Compounds in Drinking Water. Water Science and Technology 26 (7-8), 1503–1512.

Yavich, A.A., Lee, K.-H., Chen, K.-C., Pape, L., Masten, S.J., 2004. Evaluation of biodegradability of NOM after ozonation. Water Research 38 (12), 2839–2846.

Yong, E.L., Lin, Y.-P., 2012. Incorporation of initiation, promotion and inhibition in the Rct concept and its application in determining the initiation and inhibition capacities of natural water in ozonation. Water Research 46 (6), 1990–1998.

Yu, J., Wang, Y., Wang, Q., Wang, Z., Zhang, D., Yang, M., 2020. Implications of bromate depression from H2O2 addition during ozonation of different bromide-bearing source waters. Chemosphere 252, 126596.

Yu, W., Liu, T., Crawshaw, J., Liu, T., Graham, N., 2018. Ultrafiltration and nanofiltration membrane fouling by natural organic matter: Mechanisms and mitigation by pre-ozonation and pH. Water Research 139, 353–362.

Zappatini, A., Götz, C., 2015. Testverfahren zur Beurteilung der Behandelbarkeit von Abwasser mit Ozon: Anleitung zur Durchführung der Laborversuche. Verband Schweizer Abwasser- und Gewässerschutzfachleute.

Zehavi, D., Rabani, J., 1972. Oxidation of aqueous bromide ions by hydroxyl radicals. Pulse radiolytic investigation. J. Phys. Chem. 76 (3), 312–319.

Zietzschmann, F., Mitchell, R.-L., Jekel, M., 2015. Impacts of ozonation on the competition between organic micro-pollutants and effluent organic matter in powdered activated carbon adsorption. Water Research 84, 153–160.

Zimmermann, S.G., Wittenwiler, M., Hollender, J., Krauss, M., Ort, C., Siegrist, H., von Gunten, U., 2011. Kinetic assessment and modeling of an ozonation step for full-scale municipal wastewater treatment: micropollutant oxidation, by-product formation and disinfection. Water Research 45 (2), 605–617.

Zoumpouli, G.A., 2021. Micropollutant degradation, product formation and mass transfer in ozonation water treatment. Dissertation, Bath.

Zoumpouli, G.A., Baker, R., Taylor, C.M., Chippendale, M.J., Smithers, C., Xian, S.H., Mattia, D., Chew, Y.M.J., Wenk, J., 2018. A Single Tube Contactor for Testing Membrane Ozonation. Water 10 (1416).

Zoumpouli, G.A., Scheurer, M., Brauch, H.-J., Kasprzyk-Hordern, B., Wenk, J., Happel, O., 2019. COMBI, continuous ozonation merged with biofiltration to study oxidative and microbial transformation of trace organic contaminants. Environ. Sci.: Water Res. Technol. 5 (3), 552–563.

Appendix I. Supplemental Theoretical Background

Table I-1. Frequent NOM characterization methods

Method groups	Examples	Target NOM features	References
Elemental composition analyses	Dissolved organic carbon (DOC)	Bulk concentration of organic carbon	Jennings et al. (2018), Wangersky (1993)
	Mass spectrometry	Elemental composition	Parsi et al. (2007), Reemtsma et al. (2008)
	Radiocarbon dating	Age of NOM	Plummer and Glynn (2013)
Spectroscopic analyses	Light absorbance	Chromophores, spectral slope	Del Vecchio and Blough (2004), Twardowski et al. (2004)
	Fluorescence	Fluorophores	Chen et al. (2003), Chen and Yu (2021)
	Carbon-13 nuclear magnetic resonance	Functional groups	Mao et al. (2000), Wong et al. (2002)
	Fourier-transform infrared	Atomic bonds	Chen et al. (2002)
Chemical tests	Electron donating capacity	Redox properties	Aeschbacher et al. (2012), Walpen et al. (2020)
	Oxidative titration	Oxidant-reactive moieties (phenols, β-diketones, amines, olefins)	Houska et al. (2021)
	Potentiometric titration	Proton-binding properties	Ritchie and Perdue (2003)
Biological tests	Incubation	Bioavailability	Hammes and Egli (2005), McDowell et al. (2006)
Fractionation and separation	Membrane fractionation	Size distribution	Benecke (2018), Lankes et al. (2008)
	Resin fractionation (XAD, ion exchange)	Hydrophobicity, acidic or basic moieties	Aiken et al. (1992), Malcolm and MacCarthy (1992)
	Chromatographic fractionation	Size distribution, charge	Huber et al. (2011), Lankes et al. (2009), Wagner et al. (2016)

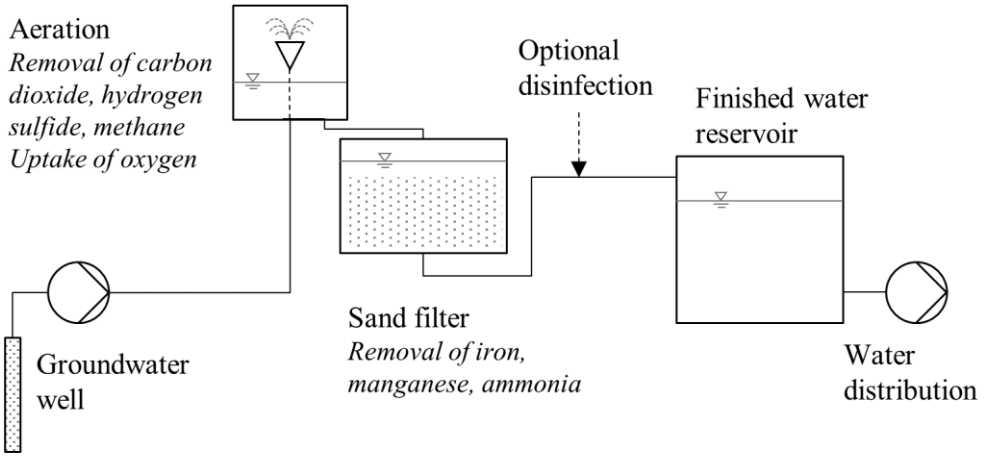

Figure I-1. Conventional treatment of groundwater, adapted from Worch (2019)

Table I-2. Bromate formation via ozone and hydroxyl radical. Subset of reactions and rate constants to identify bromate formation pathways. *Rate constant applicable for pH 6–9

Equation	Rate constant	Equation	Reference
Oxidation of Br^-			
$Br^- + O_3 \rightarrow BrO^- + O_2$	160 M^{-1} s^{-1}	Equation I-1	Haag and Hoigne (1983)
$Br^- + {}^{\bullet}OH \rightarrow Br^{\bullet} + OH^-$	$1.1 \cdot 10^9$ M^{-1} s^{-1}	Equation I-2	Yang et al. (2017a)*
Oxidation of BrOH/BrO^-			
$BrOH \leftrightarrow BrO^- + H^+$	pK_a = 8.8	Equation I-3	Haag and Hoigne (1983)
$BrO^- + O_3 \rightarrow BrO_2^- + O_2$	100 M^{-1} s^{-1}	Equation I-4	Haag and Hoigne (1983)
$BrO^- + {}^{\bullet}OH \rightarrow BrO^{\bullet} + OH^-$	$4.5 \cdot 10^9$ M^{-1} s^{-1}	Equation I-5	Buxton and Dainton (1968)
$BrOH + {}^{\bullet}OH \rightarrow BrO^{\bullet} + H_2O$	$2 \cdot 10^9$ M^{-1} s^{-1}	Equation I-6	Kläning and Wolff (1985)
Oxidation/Reduction of Br•			
$Br^{\bullet} + O_3 \rightarrow BrO^{\bullet} + O_2$	$1.5 \cdot 10^8$ M^{-1} s^{-1}	Equation I-7	von Gunten and Oliveras (1998)
$Br^{\bullet} + Br^- \rightarrow Br_2^{\bullet -}$	$\approx 10^{10}$ M^{-1} s^{-1}	Equation I-8	Zehavi and Rabani (1972)
$2\ Br_2^{\bullet -} \rightarrow Br^- + Br_3^{\bullet -}$	$2 \cdot 10^9$ M^{-1} s^{-1}	Equation I-9	von Gunten (2003b)
$Br_3^{\bullet -} + H_2O \rightarrow BrOH + 2\ Br^- + H^+$	n.a.	Equation I-10	von Gunten (2003b)

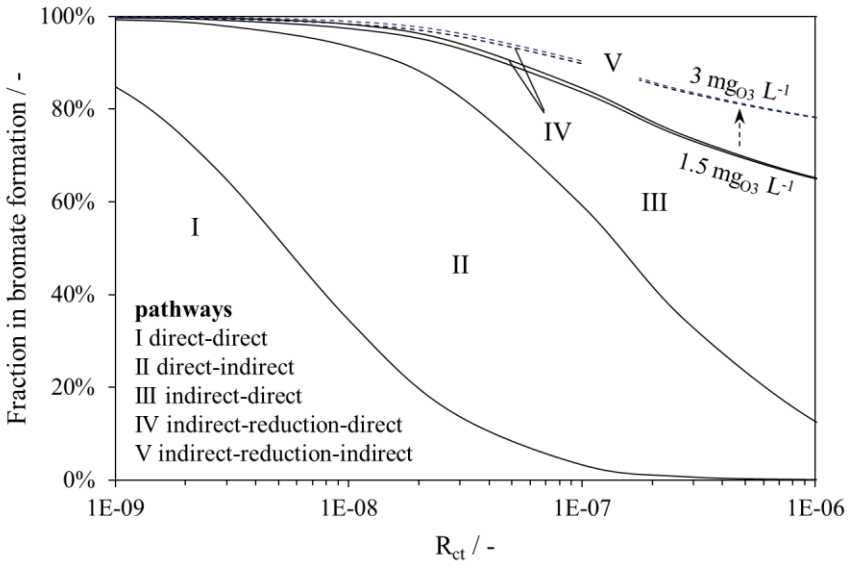

Figure I-2. Example for theoretical bromate formation pathways at pH 8, 150 µg L^{-1} bromide and ozone concentrations of 1.5 mg_{O3} L^{-1} (solid line) or 3 mg_{O3} L^{-1} (dotted line). Calculations according to Table I-2, attribution to pathways according to Figure 2-2. Direct oxidation by ozone, indirect oxidation by •OH, reduction means formation of BrOH by reaction of Br• with Br^- (Equation I-8, Equation I-9, Equation I-10). Dotted line highlighes shift in pathway III (bromate formation via pathway IV is marginal at 3 mg_{O3} L^{-1})

In membrane ozonation, the mass flux of ozone through the membrane N may be calculated by using Equation I-11. The concentration change of dissolved ozone per unit length in a membrane fiber $\frac{dc_L}{dx}$ may be calculated from Equation I-12 (Berry et al., 2017).

$$N = K_L\left(\frac{c_g}{S} - H \cdot c_L\right) \qquad \text{Equation I-11}$$

$$\frac{dc_L}{dx} = N\frac{a}{u_{L,mean}} \qquad \text{Equation I-12}$$

N	Mass flux of ozone	g m^{-2} s^{-1}
K_L	Overall ozone mass transfer coefficient	m s^{-1}
c_g	Ozone gas concentration	g m^{-3}
S	Solubility of ozone in the membrane material	–
H	Henry coefficient	–
c_L	Ozone liquid concentration	g m^{-3}
x	Length in direction of flow	m
a	Specific surface area of membrane per unit volume of liquid	m^{-1}
$u_{L,mean}$	Mean liquid velocity	m s^{-1}

Appendix II. Supplemental Materials and Methods

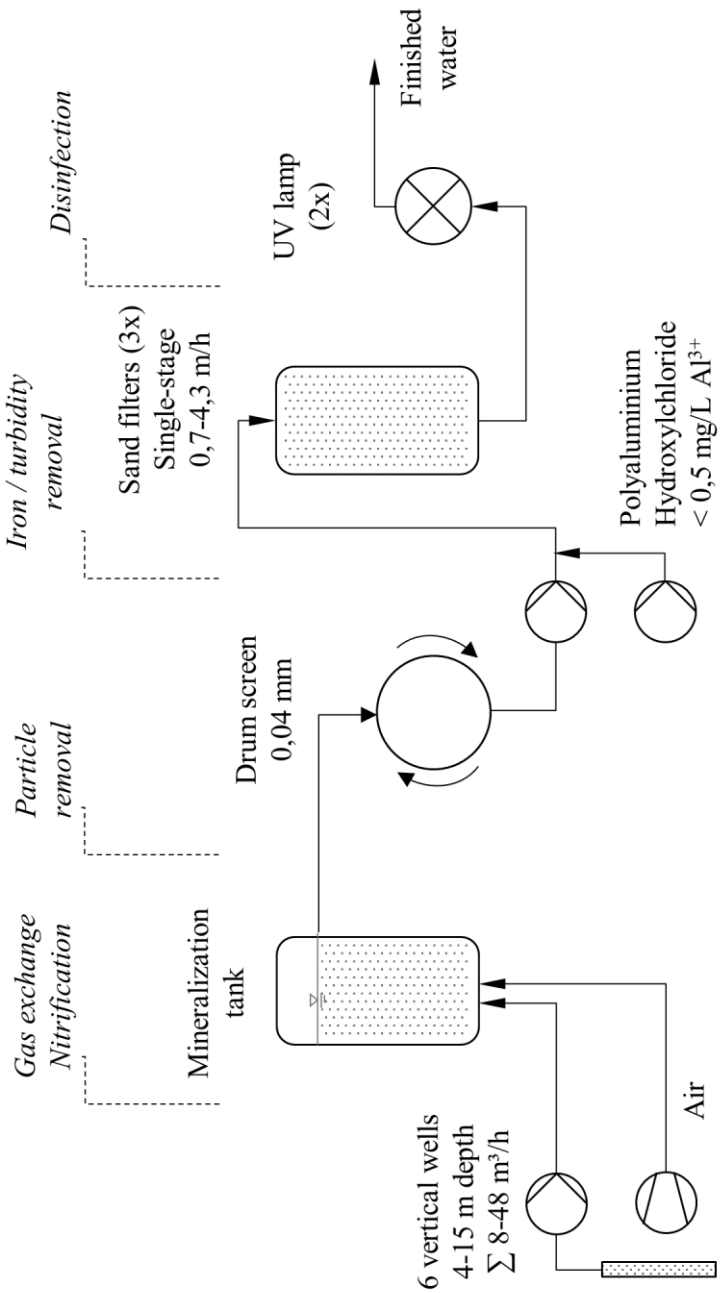

Figure II-1. Treatment scheme of groundwater A

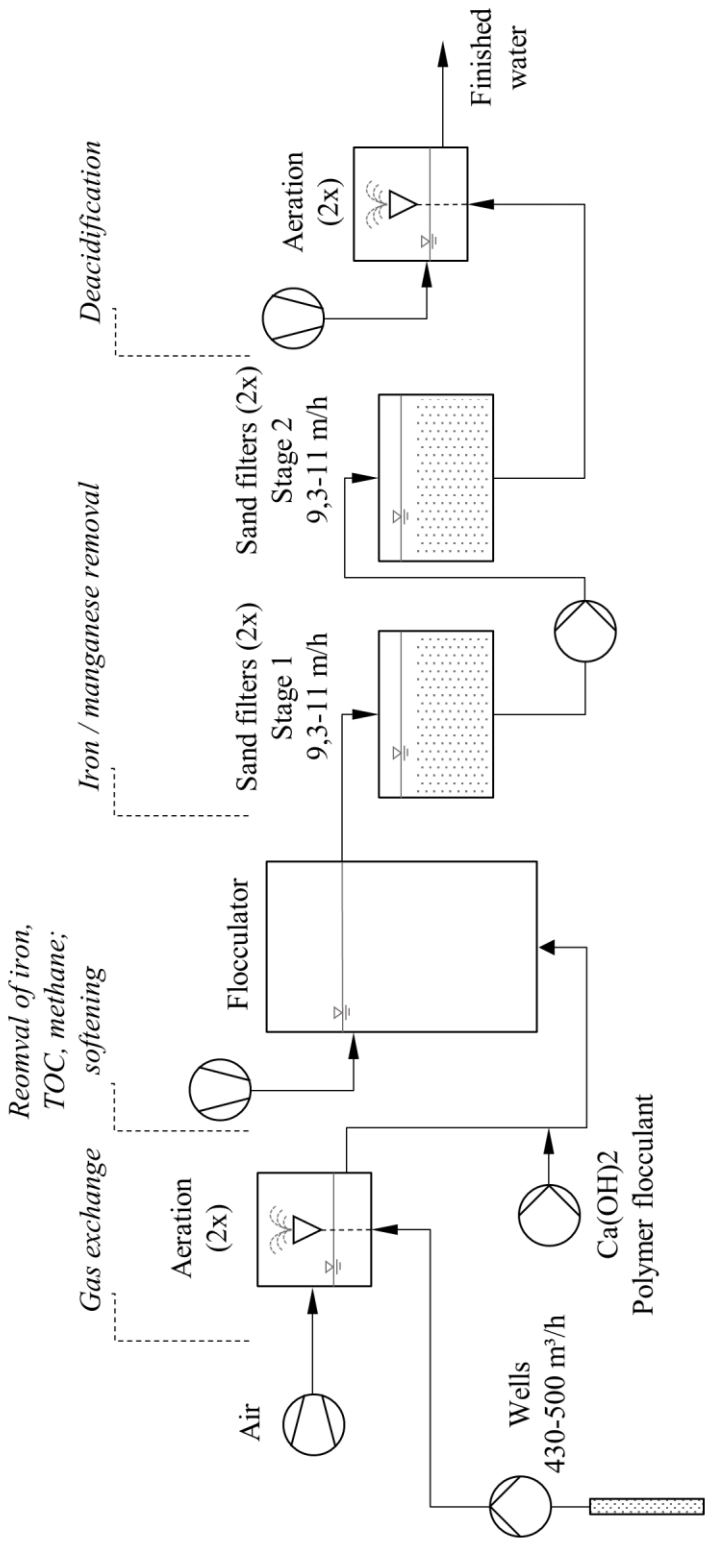

Figure II-2. Treatment scheme of groundwater E

Table II-1. Water A quality specifications for different batches used in experiments. *F = finished or aerated + flocculated + filtered water, A = aerated water, R = raw water. **based on TOC

Groundwater		**$A.1_F$**	**$A.1_R$**	**$A.2_F$**	**$A.2_R$**	**$A.2_A$**	**$A.3_F$**	**$A.4_A$**	**$A.5_F$**	**$A.6_F$**
Date	DD	04	03	22	21	22	05	14	05	22
	MM	11	11	04	04	04	11	05	11	04
	YY	20	20	21	21	22	20	21	20	21
Condition*		F	R	F	R	A	F	A	F	F
pH / -		7.6	7.8	7.7	7.8	7.7	7.6	7.9	8.1	8.4
Alkalinity / $mmol \cdot L^{-1}$		n.a.	n.a.	n.a.	n.a.	n.a.	n.a.	n.a.	2.7	n.a.
TOC / $mg \cdot L^{-1}$		4.5	6.1	4.9	5.2	5.2	4.9	4.0	4.5	4.6
DOC / $mg \cdot L^{-1}$		4.5	6.1	4.9	5.2	5.2	4.9	n.a.	4.5	4.6
UV_{254} / m^{-1}		14.4	23.5	15.1	18.3	18.4	16.4	13.6	14.4	14.4
SAC_{436} / m^{-1}		0.75	1.19	0.60	0.85	0.85	0.80	0.69	0.76	0.76
$SUVA_{254}$ / $L \cdot mg^{-1} \cdot m^{-1}$		3.2	3.9	3.2	3.5	3.5	3.3	3.4**	3.2	3.1
$SSAC_{436}$ / $L \cdot mg^{-1} \cdot m^{-1}$		0.17	0.20	0.12	0.16	0.16	0.16	0.17**	0.17	0.17
UV_{254}/SAC_{436} / -		19	20	26	21	22	20	20	19	19
Bromide / $\mu g \cdot L^{-1}$		290	390	310	300	310	330	160	320	290
Ammonia / $mg\ L^{-1}$		n.a.	0.87	n.a.	0.54	n.a.	n.a.	n.a.	n.a.	n.a.

Table II-2. Water E quality specifications for different batches used in experiments.

Groundwater		**E.1$_F$**	**E.2$_F$**
Date	DD	29	16
	MM	01	07
	YY	20	20
Condition		F	F
pH / -		8.0	7.8
Alkalinity / mmol·L^{-1}		1.6	n.a.
TOC / mg·L^{-1}		5.7	6.3
DOC / mg·L^{-1}		5.6	6.3
UV_{254} / m^{-1}		15.3	16.4
SAC_{436} / m^{-1}		0.48	0.47
$SUVA_{254}$ / L·mg^{-1}·m^{-1}		2.73	2.60
$SSAC_{436}$ / L·mg^{-1}·m^{-1}		0.086	0.075
UV_{254}/SAC_{436} / -		32	35
Bromide / µg·L^{-1}		82	90

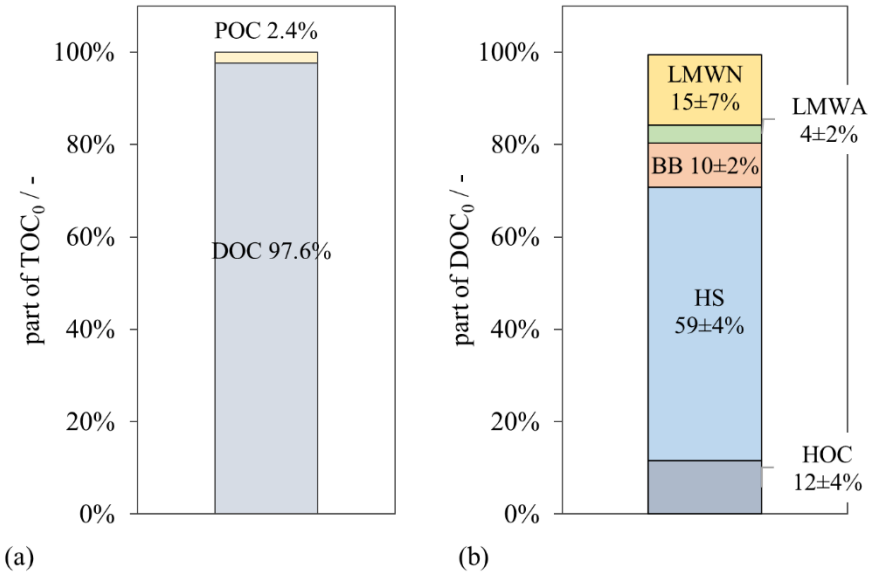

Figure II-3. NOM fractionation of non-ozonated groundwater samples A, B, C, D (Table 3-2) and E.1$_F$ (Table II-2) by **(a)** TOC-V (NPOC) (results given as percentage of TOC measured by TOC-V) and **(b)** LC-OCD measurements. Abbreviations: DOC – dissolved organic carbon, POC, particulate organic carbon, HOC – hydrophobic organic carbon, HS – humic substances, BB – building blocks, LMWA – low molecular-weight acids, LMWN – low molecular-weight neutrals. No humic substances in LMWA fraction assumed.

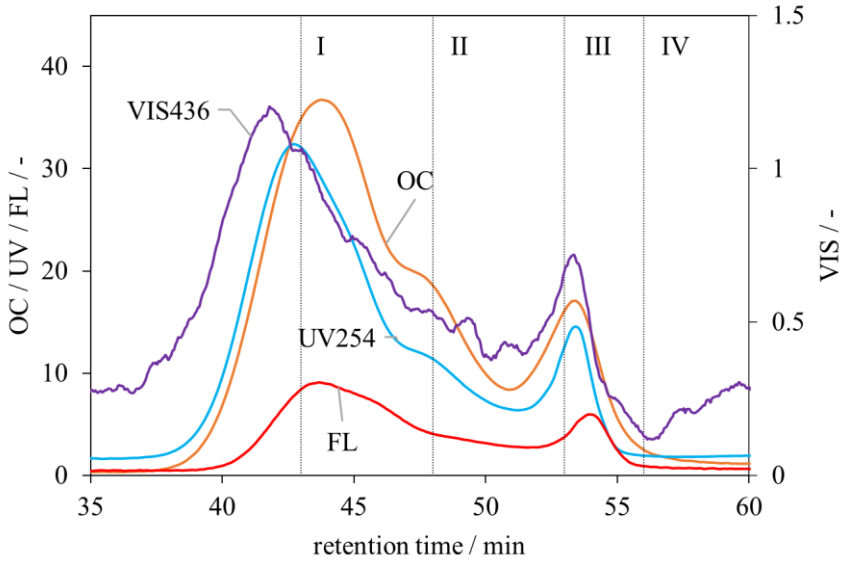

Figure II-4. LC-OCD chromatogram with multiple parameter detection of groundwater E after conventional treatment. Abbreviations: OC – organic carbon detection, VIS436 – visible light absorption at 436 nm, UV254 – UV light absorption at 254 nm, FL – humic fluorescence emission at 380 nm (excitation wavelength 365 nm). NOM fractions according to Huber et al. (2011): I – humic substances, II – building blocks, III – low molecular-weight acids and humic substances, IV low molecular-weight neutrals. Adapted from Kämmler et al. (2022)

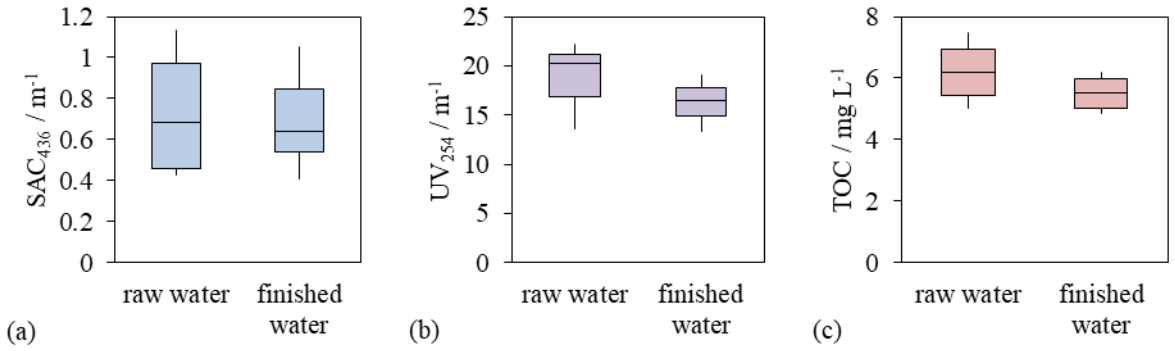

Figure II-5. Impact of groundwater treatment on **(a)** SAC_{436}, **(b)** UV_{254} and **(c)** TOC. Boxplots showing 0 % value (minimum), 25 % value, 50 % value (median), 75 % value and 100 % value (maximum); own data and water supplier information used; SAC_{436} covering groundwaters A, B, C, D and E; UV_{254} covering groundwaters B, D and E; TOC covering groundwaters A, B, D and E.

Table II-3. List of chemicals used for experiments in this work

Chemical	**Grade**	**Manufacturer**	**Experiments**
Ammonium heptamolybdate tetrahydrate	99.98 %	Alfa Aesar	Bromate analysis
Bromate standard 1000 mg L^{-1}		VWR, Radnor, US	Bromate analysis
Indigo trisulfonate (potassium salt)		Thermo Fisher Scientific, Waltham, US	Batch/pilot
H_2O_2, 30 %, ρ = 1.11, stabilized	Analytical	VWR, Radnor, US	Batch/pilot
H_3PO_4 ≥ 85 %	p.a.	Carl Roth, Karlsruhe, DE	Batch
K_2HPO_4	≥ 99.5 %	Carl Roth, Karlsruhe, DE	LC-OCD
KI	≥ 99 %	Carl Roth, Karlsruhe, DE	Bromate analysis
$NaH_2PO_4 \cdot 2\ H_2O$	Ph. Eur.	Merck, Darmstadt, DE	Batch, LC-OCD
$NaNO_2$	≥ 99 %	VWR, Radnor, US	Batch
$(NH_4)_2SO_4$	99.9999 %	Merck, Darmstadt, DE	Pilot
Oxygen	99.95 %	Westfalen, DE	Batch
SYBR Green I		Thermo Fisher Scientific, Waltham, US	TCC analysis

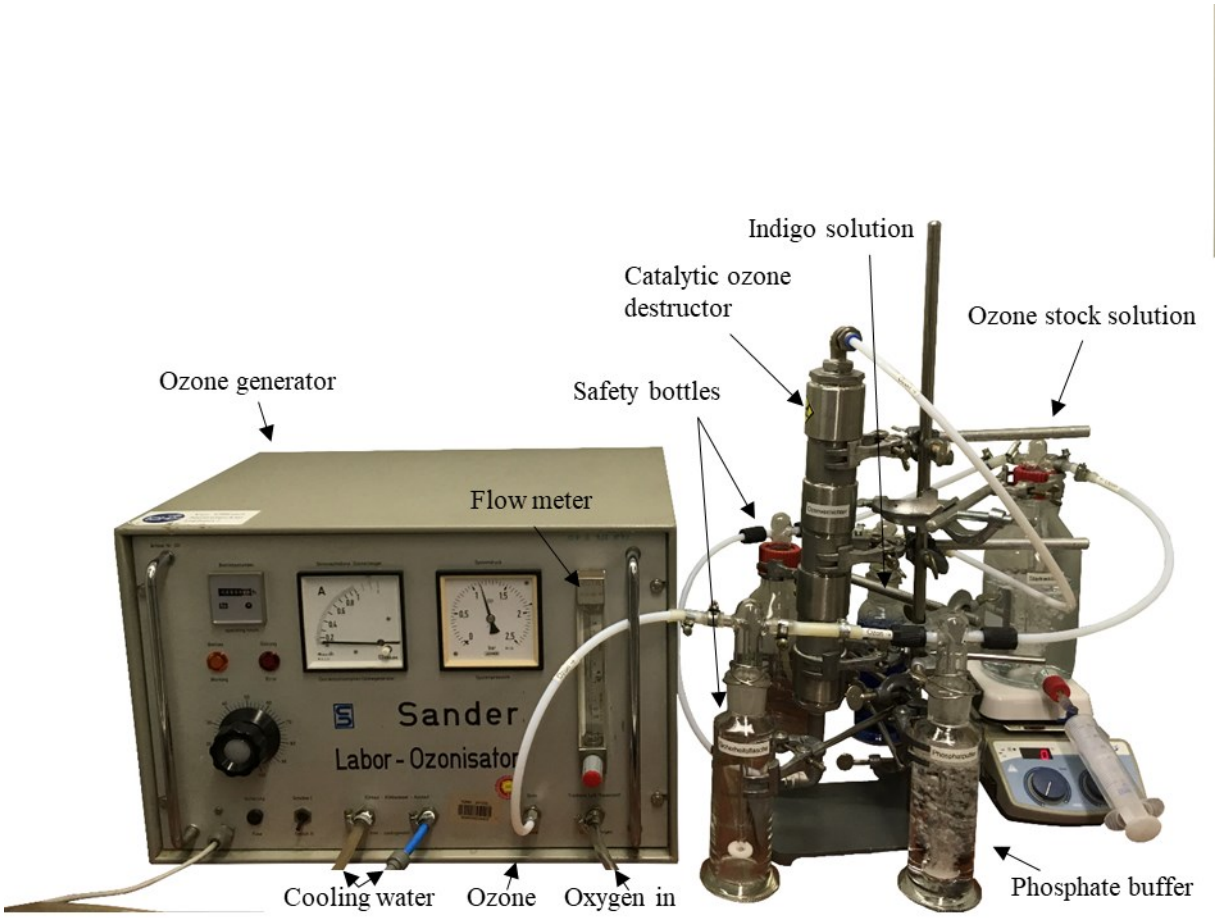

Figure II-6. Production of ozone stock solution for batch experiments. Purpose of components: Safety bottles: Prevention of water intrusion in ozone generator/ozone destructor; phosphate buffer: Removal of potential NO_x contamination; ozone destructor: removal of ozone residuals before release into lab ventilation; indigo solution: visual control of ozone destructor funcionality. Use of phosphate buffer was omitted for some experiments with use of pure oxygen for ozone production. Ozone stock solution was optionally cooled by an ice bath.

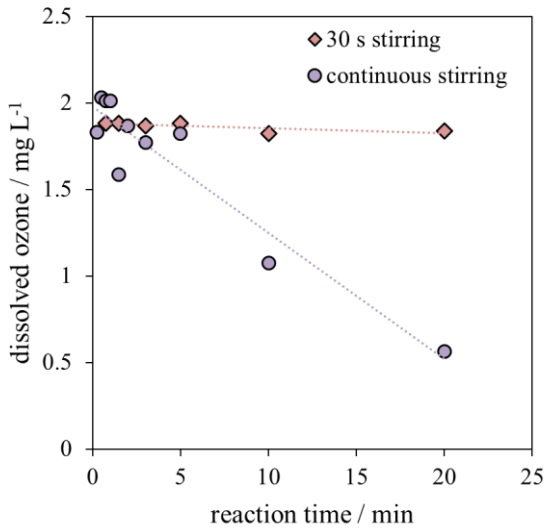

Figure II-7. Ozone stability in the batch kinetic setup (Figure 3-1.b). 20 mM H_3PO_4 in ultrapure water, pH 2, ozone dose 2 mg L^{-1}, n = 1 for each experiment. Continuous stirring for 20 min versus stop of stirring after 30 s.

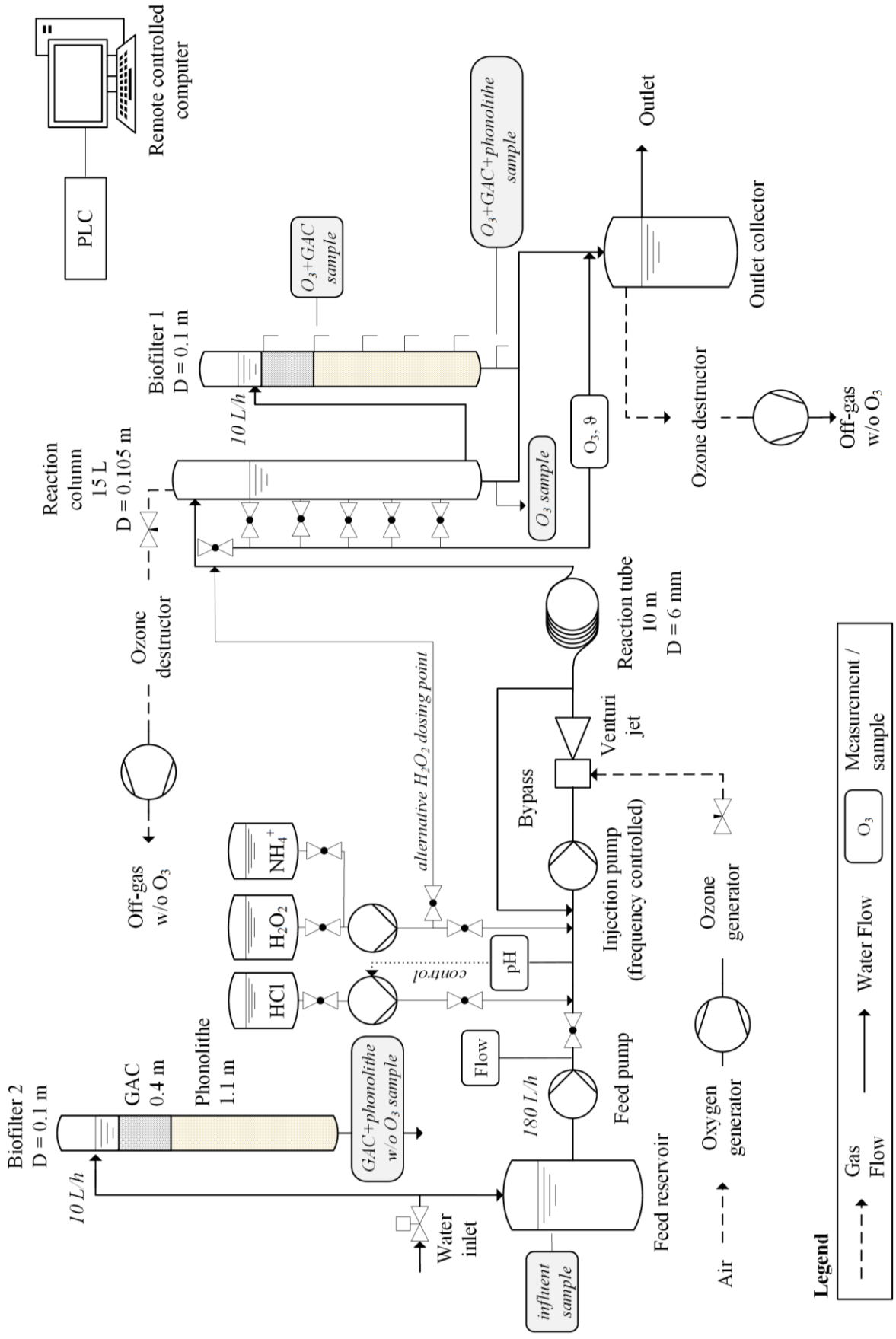

Figure II-8. Small-scale pilot plant schematic drawing. Abbreviations: D – inner diameter, PLC - programmable logic controller

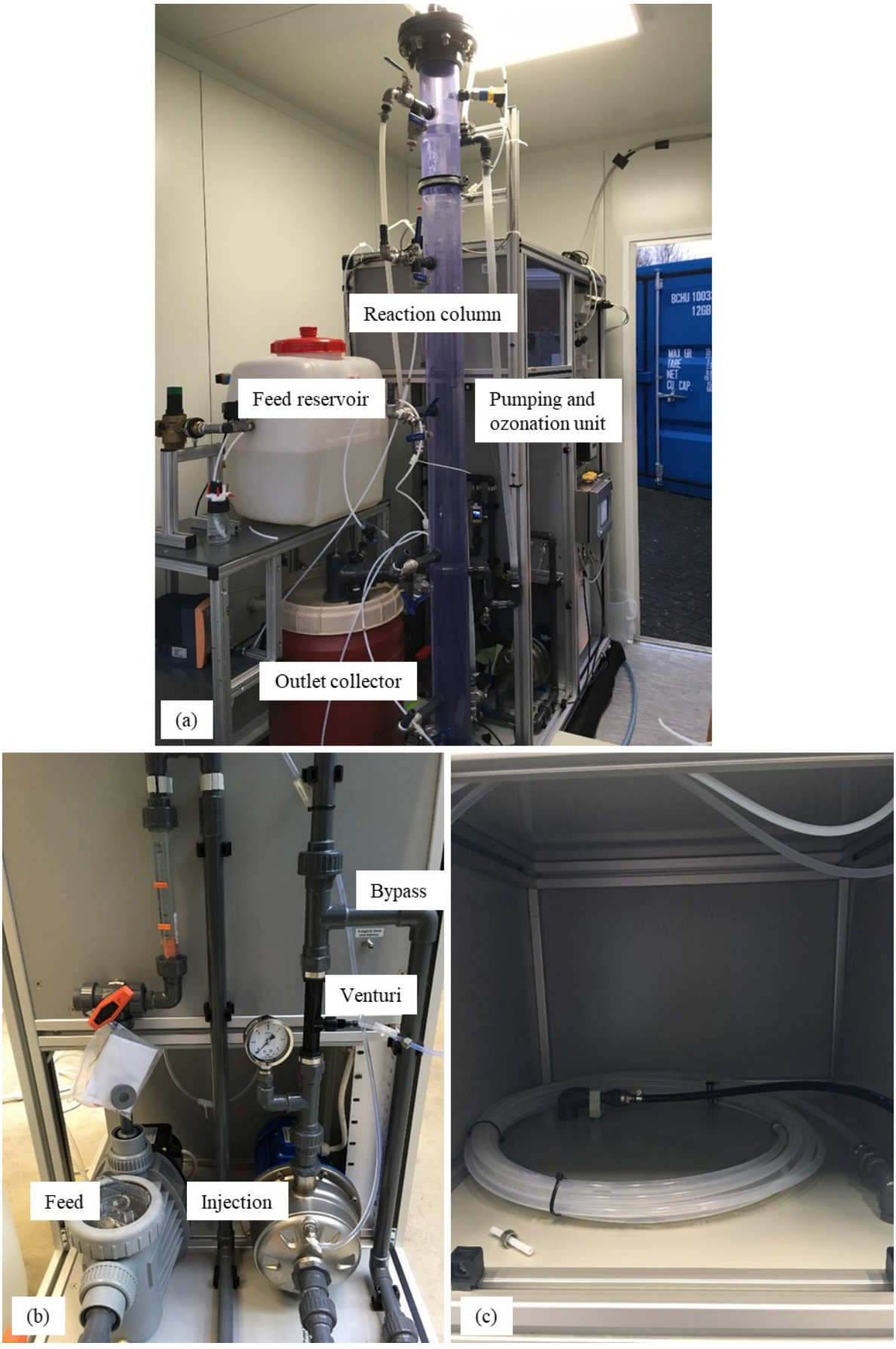

Figure II-9. **(a)** Small-scale ozonation pilot plant (without biofilters), **(b)** detail pumping unit (before equipment with additional measuring devices and dosing points), **(c)** detail reaction tube

Table II-4. Instruments used in the small-scale ozonation pilot plant

Instrument	**Type**	**Manufacturer**
Oxygen generator	SEP 100	Anseros, Tübingen, DE
Oxygen generator	Everflo	Philips Respironics, Murrysville, US
Ozone generator	COM-AD-02	Anseros, Tübingen, US
Ozone feed gas analyzer	GM-OEM	Anseros, Tübingen, US
Ozone off-gas analyzer	Ozomat MP	Anseros, Tübingen, US
Dissolved ozone and temperature measurement	Orbisphere C1100 sensor, membrane 2956A, 410 controller	Hach, Loveland, US
Feed water flow meter	Picomag	Endress+Hauser, Reinach, CH
H_2O_2/NH_4^+ pump	Stepdos 08	KNF Neuberger, Freiburg, DE
HCl pump	gamma/4	ProMinent, Heidelberg, DE
In-line pH electrode	AquaLine 70 pH	SI analytics, Mainz, DE
In-line pH measurement controller	pH 296	WTW, Weilheim, DE
Handheld pH device	pH 320	WTW, Weilheim, DE
Venturi manometer	A10, -0.6–1 bar	WIKA, Klingenberg, DE

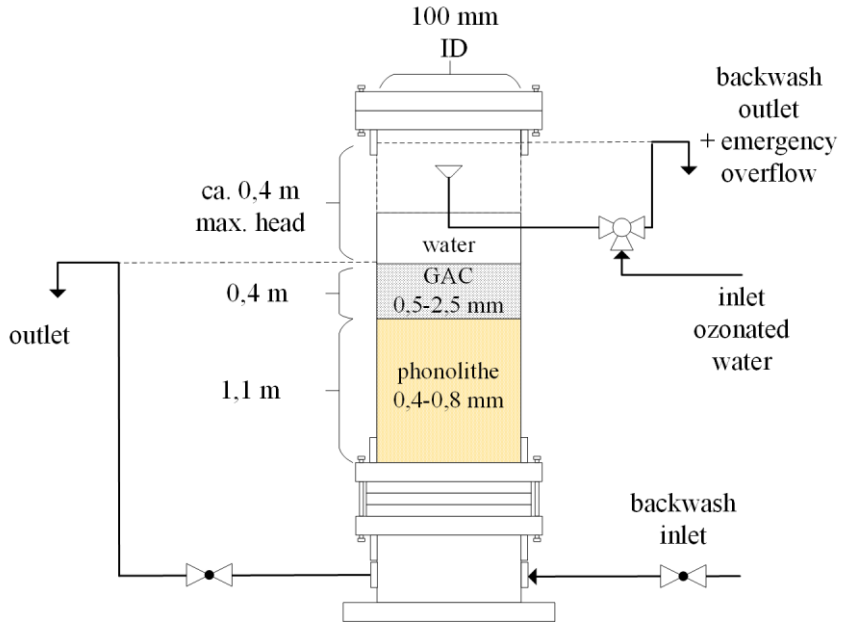

Figure II-10. Scheme and dimensions of biofilters used in small-scale pilot experiments

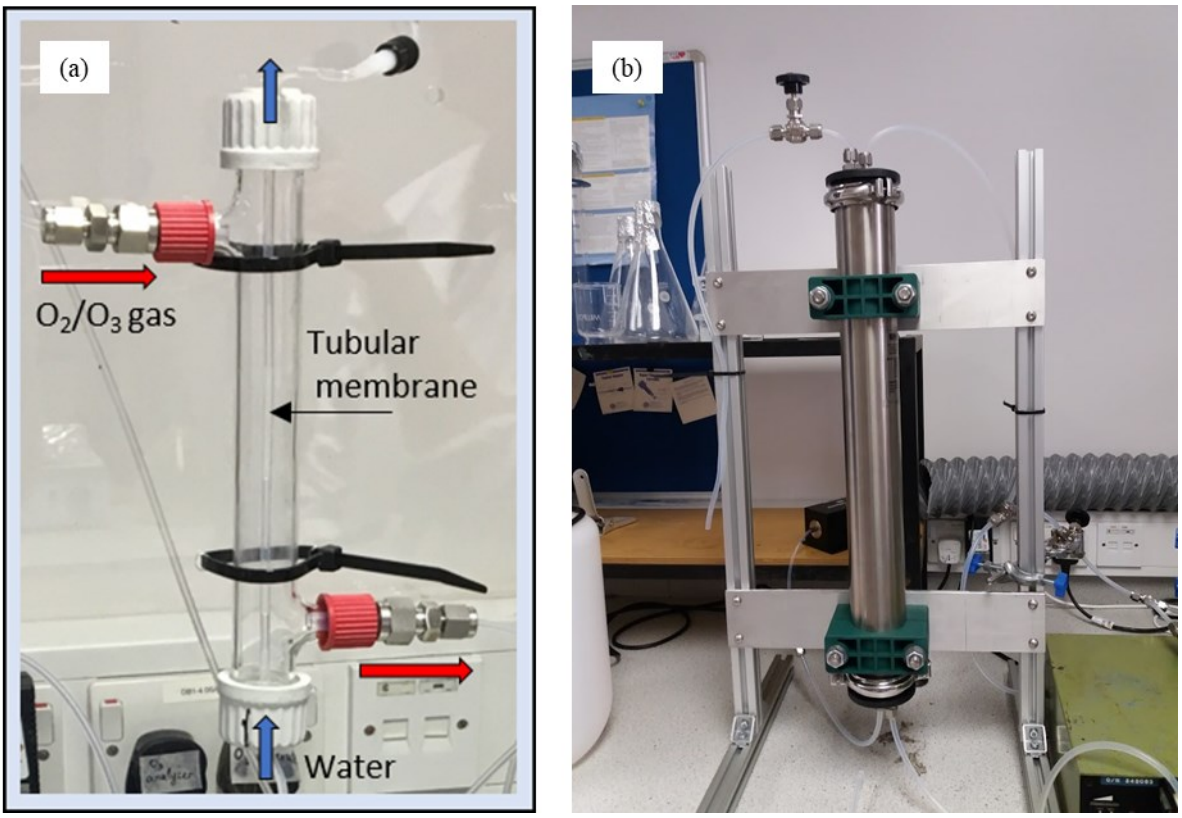

Figure II-11. Membrane ozonation contactors. **(a)** Single-tube PDMS contactor, taken from Zoumpouli et al. (2018). **(b)** multi-tube PTFE contactor, © Garyfalia Zoumpouli

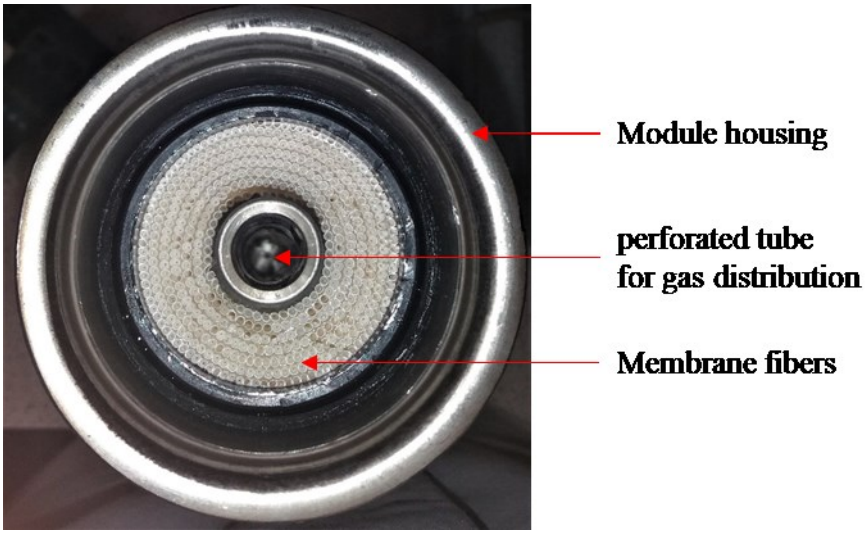

Figure II-12. Top view of the multi-tube membrane ozonation contactor, with the end cap removed. Taken from Kämmler et al. (2022)

Table II-5. **(a)** Membrane contactor specifications. *Based on the inner diameter. **Maximum pore size provided by the manufacturer. **(b)** Experimental flow-dynamic and mass-transfer parameters for membrane ozonation experiments. Adapted from Kämmler et al. (2022). ***Ozone solubility in PDMS from Dingemans et al. (2008). Ozone solubility in PTFE approximated as 1 (Kämmler et al., 2022)

Membrane contactor	**Single-tube**	**Multi-tube**
a. Membrane contactor specifications		
Membrane outer diameter / mm	3.2	1.9
Membrane inner diameter / mm	1.59	1.5
Membrane length / cm	20	46
Number of membrane tubes	1	490
Lumen volume / mL	0.4	400
Shell volume, minus the lumen / mL	50	1000
Membrane surface area* / m^2	0.001	1.1
Membrane specific surface area* / m^2 m^{-3}	2500	2670
Membrane material	non-porous PDMS	porous PTFE
Membrane maximum pore size** / µm	-	0.82
Ozone solubility in membrane material	0.881***	1***

b. Experimental flow-dynamic and mass-transfer parameters							
Liquid-side flow rate / mL min^{-1}	1.2	2.6	5.0	9.7	400	680	920
Water flow velocity / 10^{-2} m s^{-1}	1	2.2	4.2	8.1	0.8	1.3	1.8
Hydraulic retention time / s	20	9.2	4.8	2.5	60	35	26
Reynolds number	18	39	75	145	13	22	30
Liquid-side Sherwood number	7.0	9.1	11	14	4.7	5.6	6.2
Liquid-side ozone mass transfer coefficient k_L / 10^{-6} m s^{-1}	6.9	8.9	11	14	4.9	5.8	6.4
Membrane ozone mass transfer coefficient k_m / 10^{-6} m s^{-1}	3.0				4300		
Theoretical overall ozone mass transfer coefficient K_L (at water flow velocity 10^{-2} m s^{-1}) / 10^{-6} m s^{-1}	1.1				1.5		
Experimental overall ozone mass transfer coefficient K_L (at water flow velocity 10^{-2} m s^{-1}) / 10^{-6} m s^{-1}	1.2±0.1				0.86±0.08		

Calculation of ozone exposure (ct)

The time-dependent ozone concentration profile $c_{O_3}(t)$ was approximated by time-discrete experimental data points in this work. To calculate the total ozone exposure from these data, it was calculated from the stepwise addition of the ozone exposure between neighbouring data points (Equation II-1).

$$ct_{n,n+1} = \int_0^{t_{n+1}-t_n} c_{O_3,t_n} e^{-k_{sec_{n,n+1}} t}\, dt \qquad \text{Equation II-1}$$

$ct_{n,n+1}$	Ozone exposure between t_n and t_{n+1}	mg L^{-1} min

First-order decay of ozone between each pair of time steps t_n and t_{n+1} assumed, the first-order rate constant for ozone decay between these time steps, $k_{sec_{n,n+1}}$, was calculated according to Equation II-2 and Equation II-3 from measured ozone concentrations at t_n and t_{n+1}.

$$c_{O_3,t_{n+1}} = c_{O_3,t_n} e^{-k_{n,n+1}(t_{n+1}-t_n)} \qquad \text{Equation II-2}$$

$k_{sec_{n,n+1}}$	First-order decay rate constant of ozone between t_n and t_{n+1}	s^{-1}

$$-k_{sec_{n,n+1}} = \frac{\ln(\frac{c_{O_3,t_{n+1}}}{c_{O_3,t_n}})}{t_{n+1}-t_n} \qquad \text{Equation II-3}$$

Integration of eq. Equation II-1 and substitution of $k_{sec_{n,n+1}}$ with the expression in Equation II-3 yields eq. Equation II-4, from which the total ozone exposure was obtained from the sum of ozone exposure times between all data points of the experiment.

$$ct_{n,n+1} = c_{O_3,t_n} \frac{t_{n+1}-t_n}{\ln\left(\frac{c_{O_3,t_{n+1}}}{c_{O_3,t_n}}\right)} \left(\frac{c_{O_3,t_{n+1}}}{c_{O_3,t_n}} - 1\right) \qquad \text{Equation II-4}$$

For experiments with dissolved ozone concentration exceeding zero in the last sample taken at final time t_f, ozone exposure from t_f to infinity, $ct_{f,\infty}$, was extrapolated from the indefinite integral of Equation 2-2, resulting in the expression shown in Equation II-5. c_f is the dissolved ozone concentration at the final time step t_f and $\overline{k_{1,f}}$ is the arithmetic mean of k_{sec} values

calculated between first and and final sample taken. The initial ozone concentration was excluded from calculation of $\overline{k_{1,f}}$ as k_{sec} from the initial phase of ozonation may overestimate k_{sec} at a later stage.

$$ct_{f,\infty} = \frac{c_f}{\overline{k_{1,f}}} \qquad \text{Equation II-5}$$

Appendix III. Supplemental Results

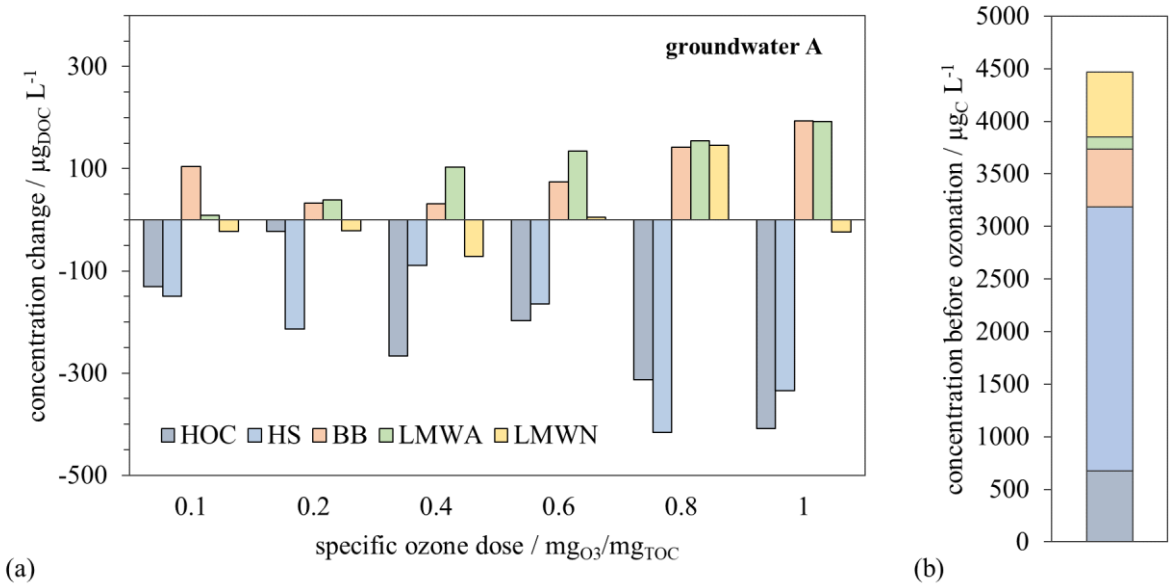

Figure III-1. **(a)** Concentration changes (difference to non-ozonated sample) in NOM fractions of groundwater A due to batch ozonation. ϑ = 20 °C, DOC 4.5 mg L^{-1}, pH 7.8. Determination of fractions by LC-OCD (Huber et al., 2011): HOC – hydrophobic organic carbon, HS – humic substances, BB – building blocks, LMWA – low molecular-weight acids, LMWN – low molecular-weight neutrals. **(b)** fraction concentrations in non-ozonated sample. No humic substances in LMWA fraction assumed. LMWA content, corrected by HS eluting with LMWA: n.q. (not quantified)

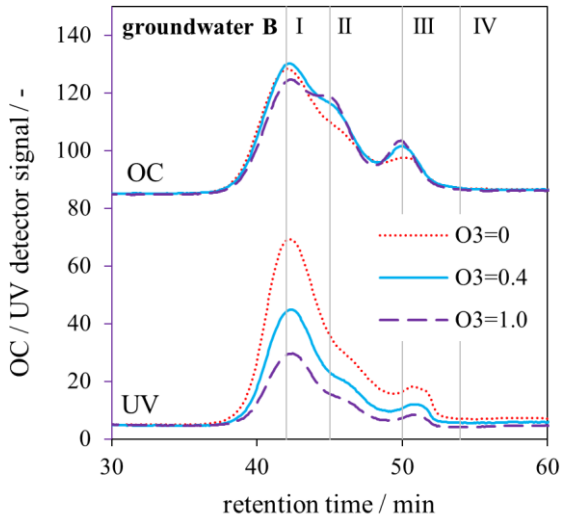

Figure III-2. LC-OCD-UVD diagram of groundwater B (batch ozonation). ϑ = 20 °C, DOC 5.1 mg L^{-1}, pH 7.6. Specific ozone doses 0 (blind sample), 0.4 and 1.0 mg$_{O3}$/mg$_{TOC}$. NOM fractions according to Huber et al. (2011): I – humic substances, II – building blocks, III – low molecular-weight acids and humic substances, IV low molecular-weight neutrals

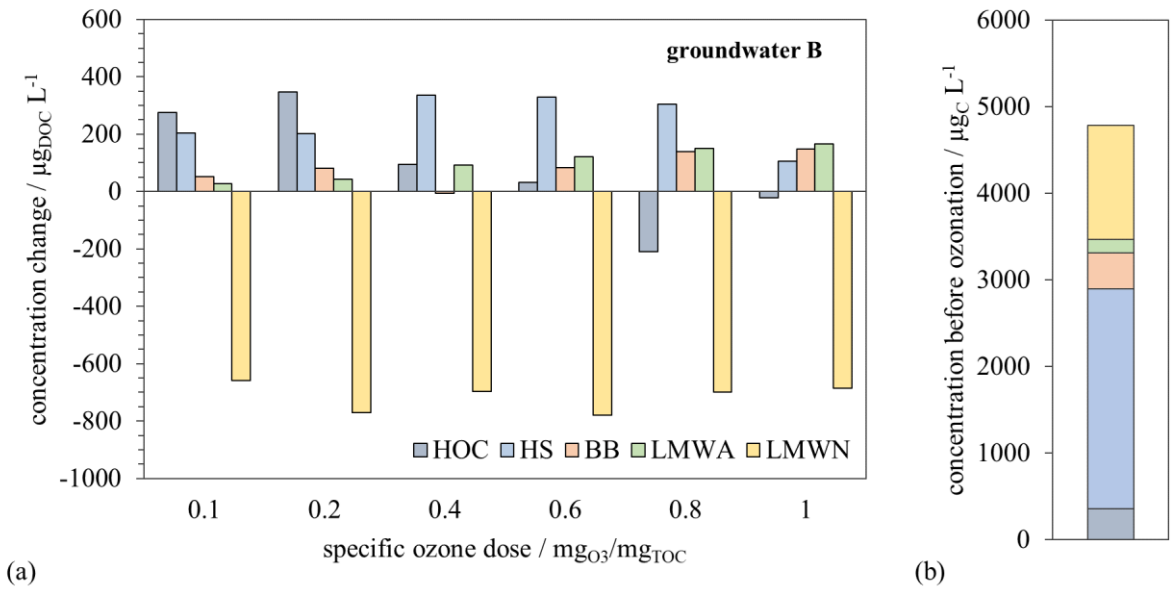

Figure III-3. **(a)** Concentration changes (difference to non-ozonated sample) in NOM fractions of groundwater B due to batch ozonation. ϑ = 20 °C, DOC 5.1 mg L^{-1}, pH 7.6. Determination of fractions by LC-OCD (Huber et al., 2011): HOC – hydrophobic organic carbon, HS – humic substances, BB – building blocks, LMWA – low molecular-weight acids, LMWN – low molecular-weight neutrals. **(b)** fraction concentrations in non-ozonated sample. LMWA content, corrected by HS eluting with LMWA: 38 µg L^{-1}

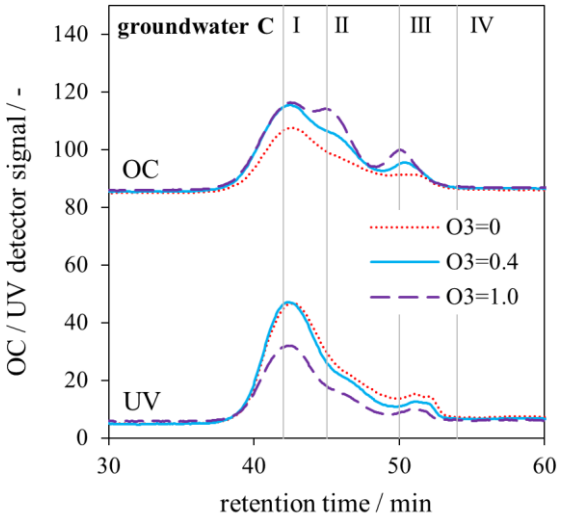

Figure III-4. LC-OCD-UVD diagram of groundwater C (batch ozonation). Specific ozone doses 0 (blind sample), 0.4 and 1.0 mg$_{O3}$/mg$_{TOC}$. ϑ = 10 °C, DOC 3.5 mg L^{-1}, pH 8.0. NOM fractions according to Huber et al. (2011): I – humic substances, II – building blocks, III – low molecular-weight acids and humic substances, IV low molecular-weight neutrals. Results adapted from Preda (2019).

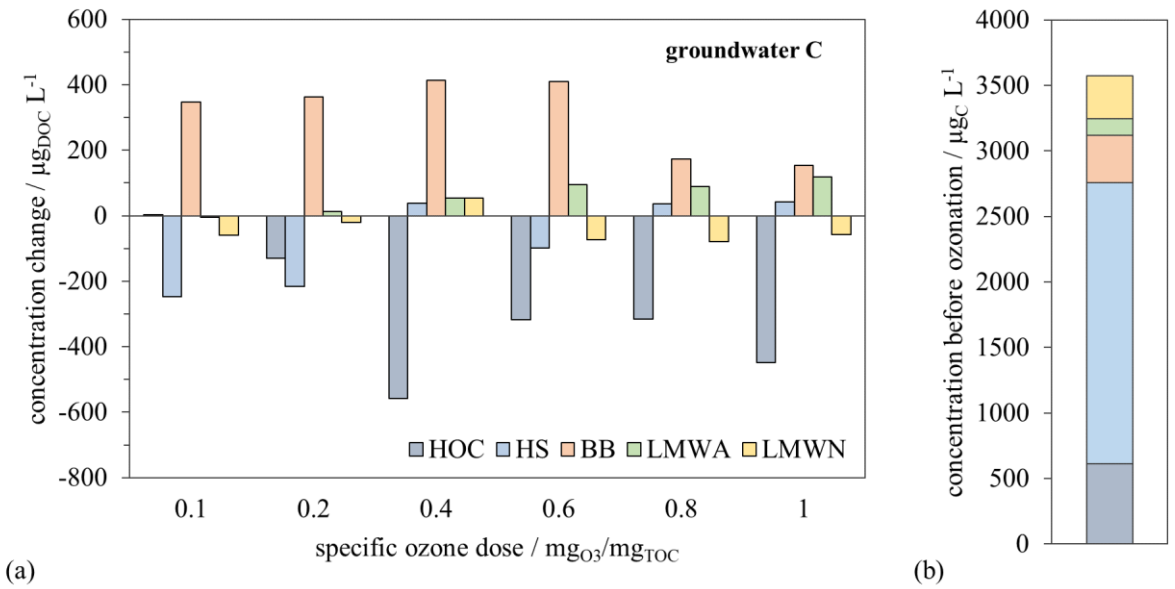

Figure III-5. **(a)** Concentration changes (difference to non-ozonated sample) in NOM fractions of groundwater C due to batch ozonation. ϑ = 10 °C, DOC 3.5 mg L^{-1}, pH 8.0. Determination of fractions by LC-OCD (Huber et al., 2011): HOC – hydrophobic organic carbon, HS – humic substances, BB – building blocks, LMWA – low molecular-weight acids, LMWN – low molecular-weight neutrals. **(b)** fraction concentrations in non-ozonated sample. No humic substances in LMWA fraction assumed. LMWA content, corrected by HS eluting with LMWA: 17 µg L^{-1}. Results adapted from Preda (2019).

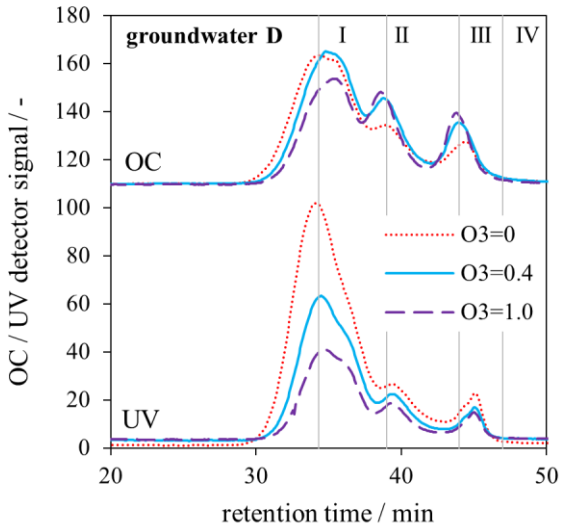

Figure III-6. LC-OCD-UVD diagram of groundwater D (batch ozonation). Specific ozone doses 0 (blind sample), 0.4 and 1.0 mg$_{O3}$/mg$_{TOC}$. ϑ = 20 °C, DOC 6.1 mg L^{-1}, pH 7.7. NOM fractions according to Huber et al. (2011): I – humic substances, II – building blocks, III – low molecular-weight acids and humic substances, IV low molecular-weight neutrals. Results adapted from Specker (2019).

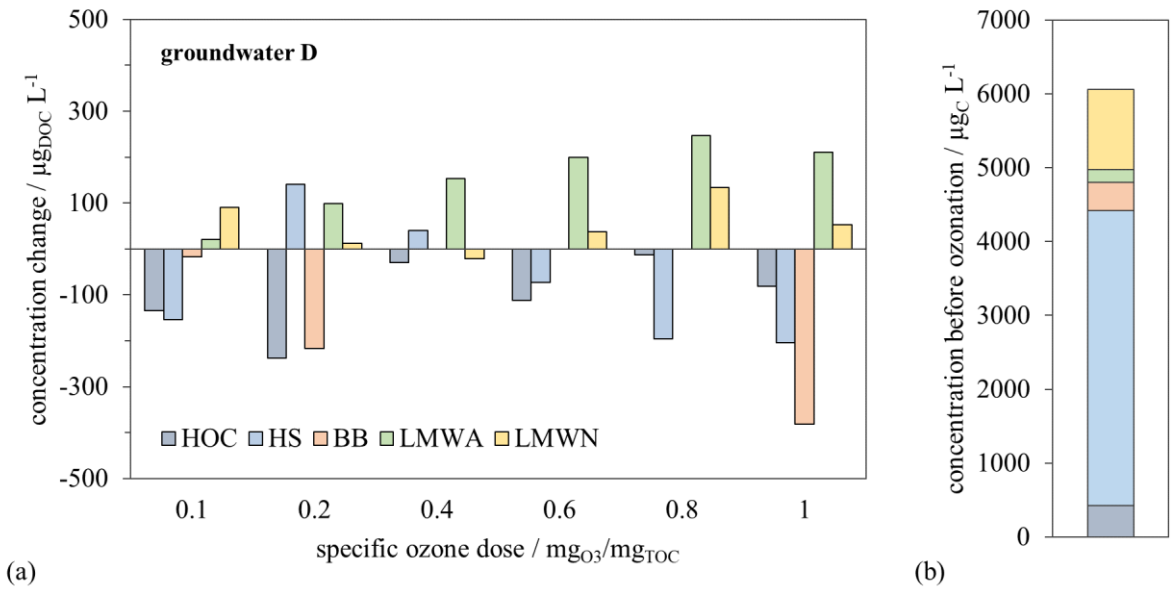

Figure III-7. **(a)** Concentration changes (difference to non-ozonated sample) in NOM fractions of groundwater D due to batch ozonation. ϑ = 20 °C, DOC 6.1 mg L^{-1}, pH 7.7. Determination of fractions by LC-OCD (Huber et al., 2011): HOC – hydrophobic organic carbon, HS – humic substances, BB – building blocks, LMWA – low molecular-weight acids, LMWN – low molecular-weight neutrals. **(b)** fraction concentrations in non-ozonated sample. No humic substances in LMWA fraction assumed. LMWA content, corrected by HS eluting with LMWA: 84 µg L^{-1}. Results adapted from Specker (2019).

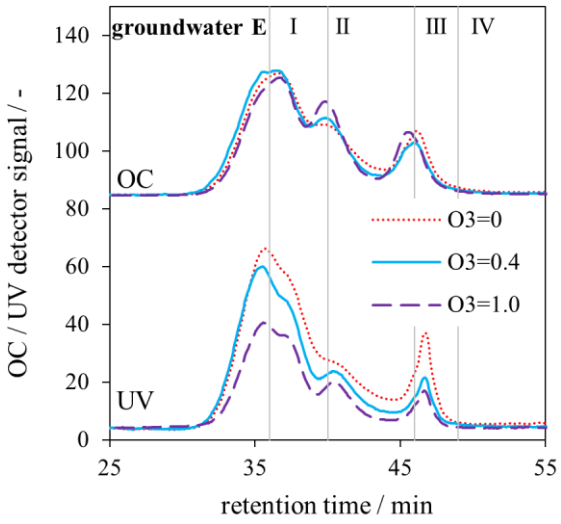

Figure III-8. LC-OCD-UVD diagram of groundwater E.1$_F$ (batch ozonation). Specific ozone doses 0 (blind sample), 0.4 and 1.0 mg$_{O3}$/mg$_{TOC}$. ϑ = 16 °C, DOC 5.6 mg L^{-1}, pH 8.0. NOM fractions according to Huber et al. (2011): I – humic substances, II – building blocks, III – low molecular-weight acids and humic substances, IV low molecular-weight neutrals

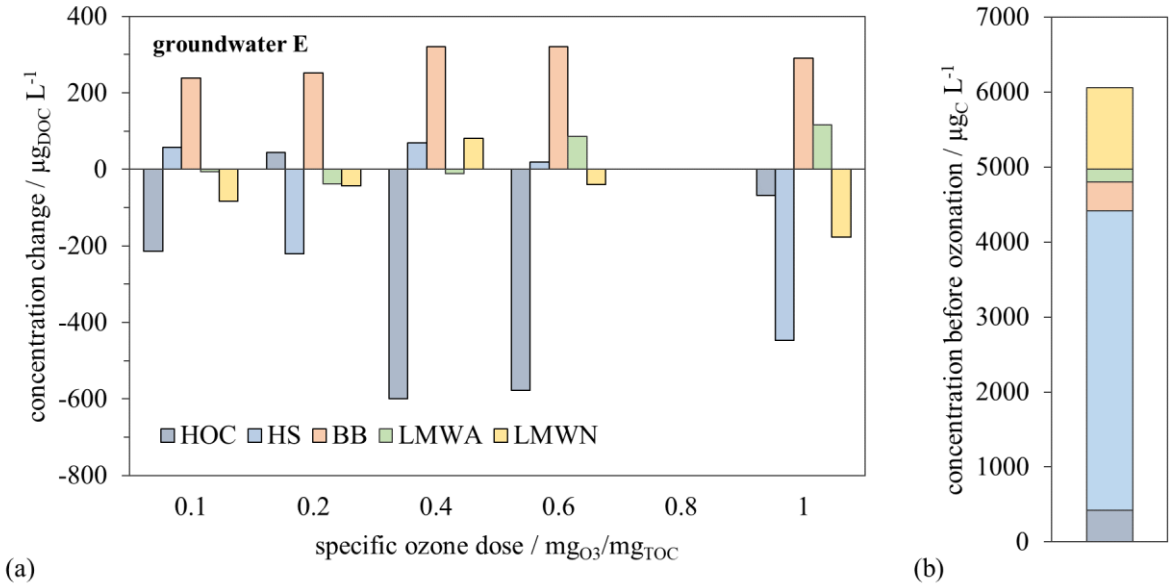

Figure III-9. **(a)** Concentration changes (difference to non-ozonated sample) in NOM fractions of groundwater E.1$_F$ due to batch ozonation. ϑ = 16 °C, DOC 5.6 mg L^{-1}, pH 8.0. Determination of fractions by LC-OCD (Huber et al., 2011): HOC – hydrophobic organic carbon, HS – humic substances, BB – building blocks, LMWA – low molecular-weight acids, LMWN – low molecular-weight neutrals. **(b)** fraction concentrations in non-ozonated sample. No humic substances in LMWA fraction assumed. LMWA content, corrected by HS eluting with LMWA: n.q.

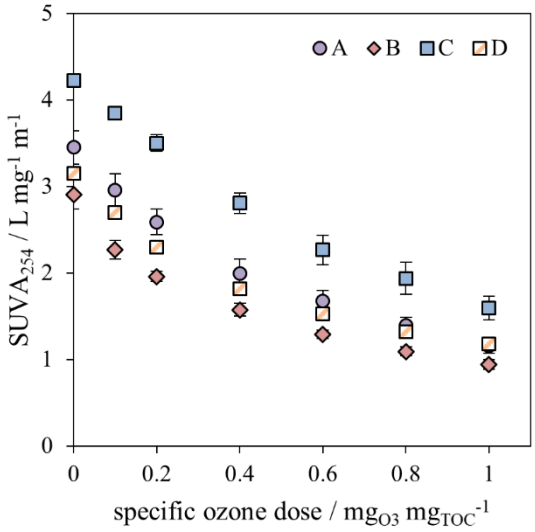

Figure III-10. Specific UV$_{254}$ absorbance (UV$_{254}$:DOC) as a function of specific ozone dose in batch experiments with different groundwaters. Experimental conditions: ϑ = 20 °C, TOC$_0$ 3.5–6.2 mg L^{-1}, pH 7.6–8.0 (Table 3-2). Results partly from Preda (2019) (groundwater C) and Specker (2019) (groundwater D).

Table III-1. Overview of batch ozonation results of five different groundwaters. Mean values, n = 3. Results were obtained from multiplication of measured values with dilution factors caused by addition of ozone stock solution. *Preda (2019), **Specker (2019), ***Sellmann (2020)

Groundwater A				
Specific ozone dose	SAC_{436}	UV_{254}	TOC	Bromate
mg_{O3}/mg_{TOC}	m^{-1}	m^{-1}	mg L^{-1}	µg L^{-1}
0	0.90	16.5	4.8	0.0
0.1	0.69	13.6	4.5	1.8
0.2	0.54	11.9	4.5	4.4
0.4	0.31	9.1	4.5	15
0.6	0.22	7.5	4.4	32
0.8	0.16	6.1	4.4	67
1	0.10	5.0	4.4	119
Groundwater B				
Specific ozone dose	SAC_{436}	UV_{254}	TOC	Bromate
mg_{O3}/mg_{TOC}	m^{-1}	m^{-1}	mg L^{-1}	µg L^{-1}
0	0.43	13.8	4.8	0.0
0.1	0.28	10.7	4.6	0.4
0.2	0.20	9.3	4.6	0.9
0.4	0.11	7.2	4.6	4.0
0.6	0.06	5.9	4.6	11
0.8	0.04	5.0	4.5	28
1	0.03	4.2	4.5	58
Groundwater C*				
Specific ozone dose	SAC_{436}	UV_{254}	TOC	Bromate
mg_{O3}/mg_{TOC}	m^{-1}	m^{-1}	mg L^{-1}	µg L^{-1}
0	1.15	15.1	3.6	0.0
0.1	1.00	13.7	3.6	1.0
0.2	0.86	12.5	3.6	1.8
0.4	0.54	10.1	3.6	4.6
0.6	0.31	8.3	3.6	11
0.8	0.20	6.6	3.5	22
1	0.11	5.6	3.4	44
Groundwater D**				
Specific ozone dose	SAC_{436}	UV_{254}	TOC	Bromate
mg_{O3}/mg_{TOC}	m^{-1}	m^{-1}	mg L^{-1}	µg L^{-1}
0	0.59	19.1	6.1	0.0
0.1	0.50	16.3	6.0	0.3
0.2	0.38	13.8	6.0	0.7
0.4	0.25	10.8	5.9	2.5
0.6	0.19	9.0	5.8	7.4
0.8	0.15	7.6	5.8	14
1	0.14	6.7	5.7	25
Groundwater E***				
Specific ozone dose	SAC_{436}	UV_{254}	TOC	Bromate
mg_{O3}/mg_{TOC}	m^{-1}	m^{-1}	mg L^{-1}	µg L^{-1}
0	0.48	16.3	5.9	0.0
0.1	0.53	14.8	no data	0.3
0.2	0.58	13.9		0.7
0.4	0.41	11.2		1.7
0.6	0.26	8.9		3.3
0.8	0.20	7.4		10
1	0.18	6.6		18

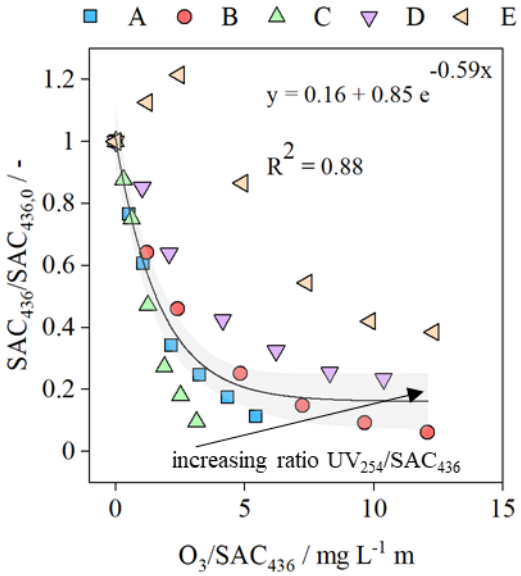

Figure III-11. Relative residual SAC_{436} absorbance versus SAC_{436}-specific ozone dose in batch ozonation with exponential fitting and 95 % confidence interval (Groundwater E not included in fitting). Results partly from Preda (2019) (groundwater C), Specker (2019) (groundwater D) and Sellmann (2020) (groundwater E)

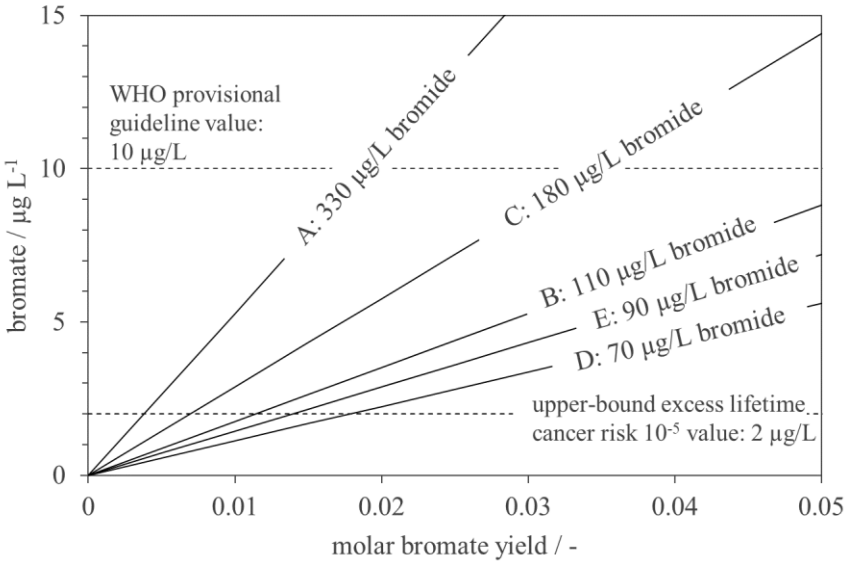

Figure III-12. Bromate concentration depending on raw-water bromide concentration and molar bromate yield. Dashed lines highlight the WHO provisional guideline value of 10 µg L^{-1} and the upper-bound excess lifetime cancer risk of 10^{-5} value of 2 µg L^{-1} (WHO, 2017)

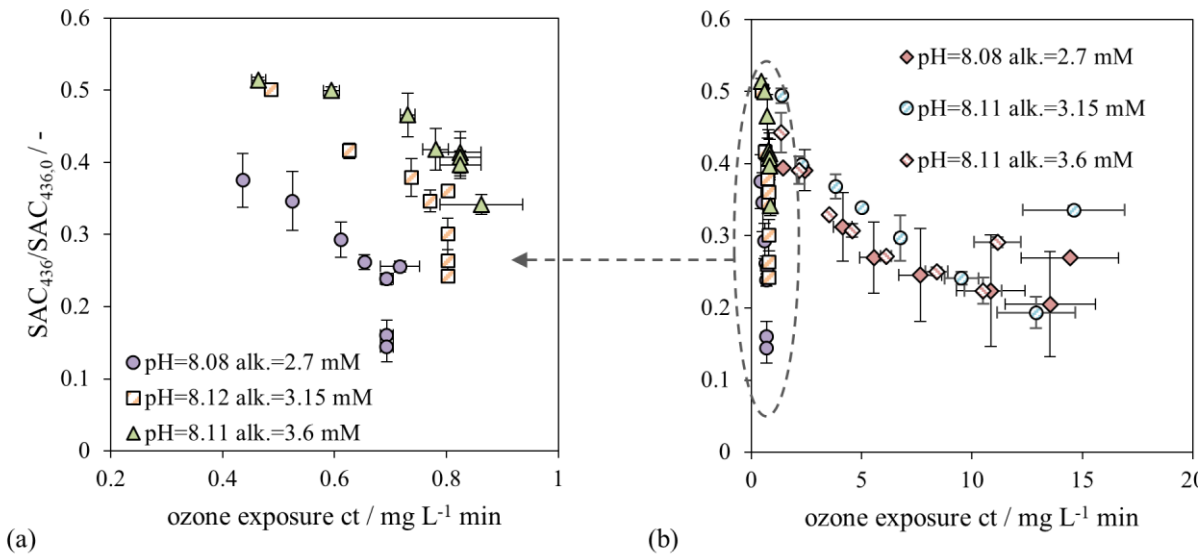

Figure III-13. Effect of alkalinity on color (SAC_{436}) at ozone doses of **(a)** 0.5 and **(b)** 0.5 (encircled) and 1.0 mg_{O3}/mg_{DOC}. Finished groundwater $A.5_F$ (Table II-1), pH 8.1, DOC 4.5 mg L^{-1}, $\vartheta \approx 19$ °C, batch ozonation. Note different axis scaling for (a) and (b). Results adapted from Bharadwaj (2022).

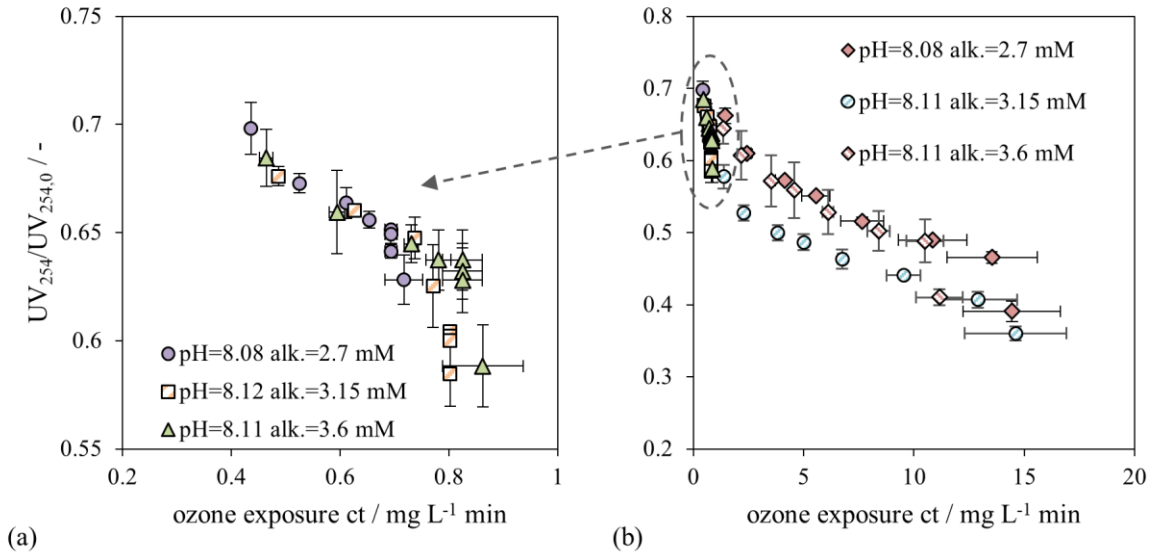

Figure III-14. Effect alkalinity on UV_{254} at ozone doses of **(a)** 0.5 and **(b)** 0.5 (encircled) and 1.0 mg_{O3}/mg_{DOC} Finished groundwater $A.5_F$ (Table II-1), pH 8.1, DOC 4.5 mg L^{-1}, $\vartheta \approx 19$ °C, batch ozonation. Note different axis scaling of (a) and (b). Results adapted from Bharadwaj (2022).

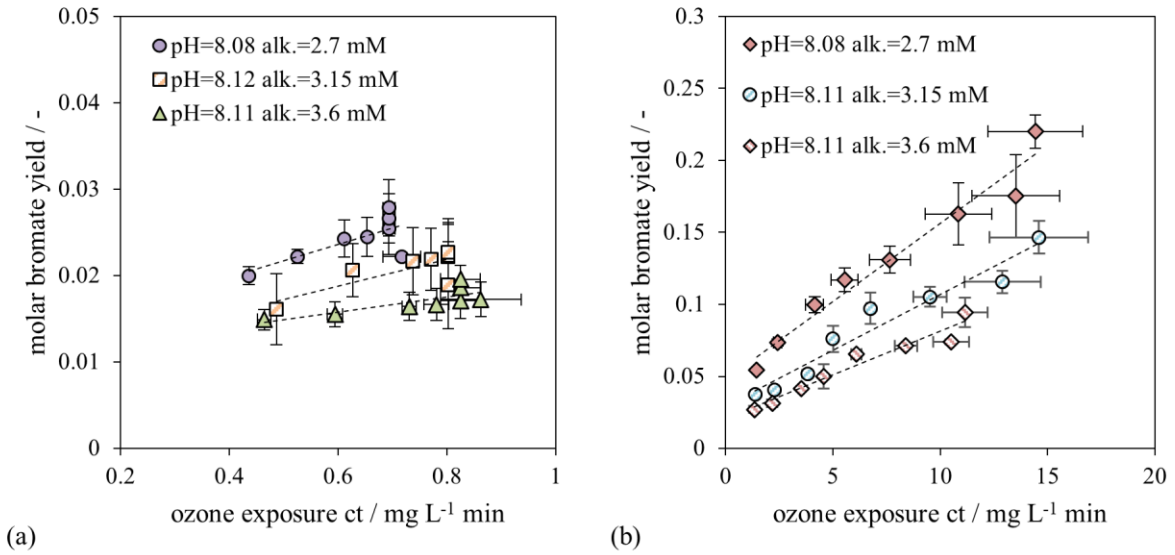

Figure III-15. Effect of alkalinity on molar bromate yield at ozone doses of **(a)** 0.5 mg_{O3}/mg_{DOC} and **(b)** 1.0 mg_{O3}/mg_{DOC}. Finished groundwater $A.5_F$ (Table II-1), pH 8.1, DOC 4.5 mg L^{-1}, $\vartheta \approx 19$ °C, batch ozonation. Linear trendlines added in Microsoft Excel as a guide for the eye. Note different axis scaling for (a) and (b).Results adapted from Bharadwaj (2022).

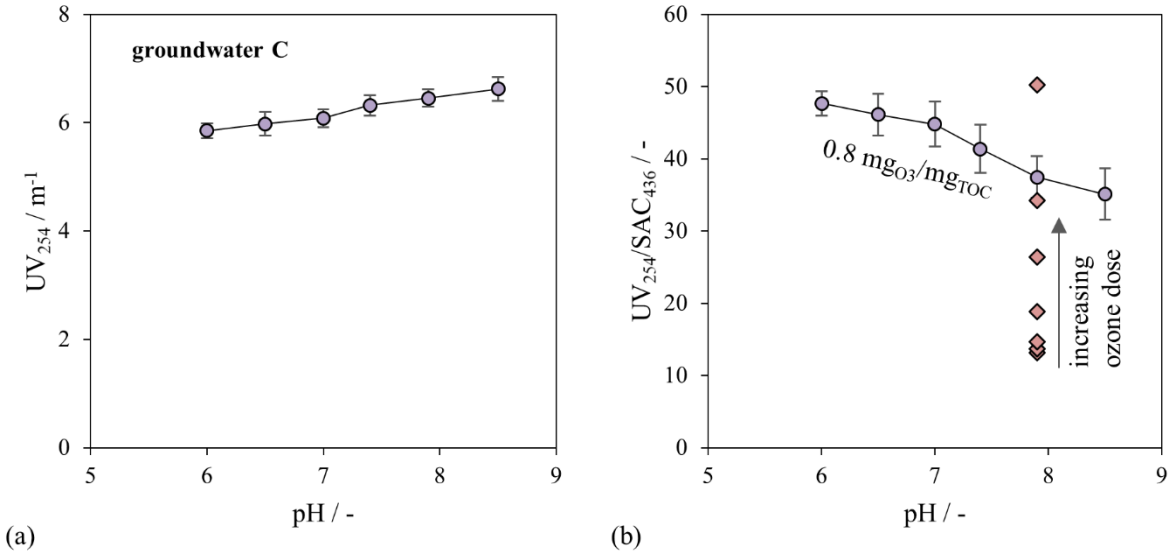

Figure III-16. Effect of pH during batch ozonation of groundwater C on **(a)** UV_{254} at 0.8 mg_{O3}/mg_{TOC} and **(b)** ratio UV_{254}/SAC_{436} at 0.8 mg_{O3}/mg_{TOC}, compared to effect of increasing specific ozone dose (0–1 mg_{O3}/mg_{TOC}). Results adapted from Preda (2019).

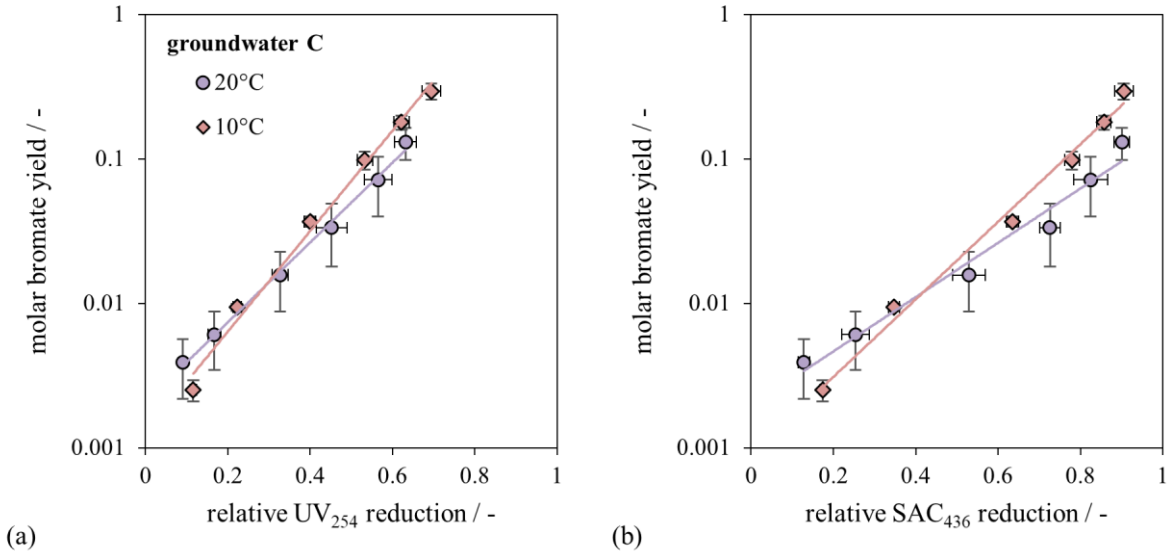

Figure III-17. Effect of sample temperature on molar bromate yield as a function of **(a)** relative UV_{254} reduction ($1\text{-}UV_{254}/UV_{254,0}$) and **(b)** relative SAC_{436} reduction ($1\text{-}SAC_{436}/SAC_{436,0}$). Groundwater C, 3.5 mg_{DOC} L^{-1}, pH 8.0, batch ozonation. Experimental data and exponential fits ($y = a \cdot \exp(b \cdot x)$). Fitting parameters for x = Relative UV_{254} reduction: a = 0.0013, b = 8.0, R^2 = 0.99 (10 °C), a = 0.0021, b = 6.4, R^2 = 1.0 (20 °C); Fitting parameters for x = Relative SAC_{436} reduction: a = 0.0009, b = 6.2, R^2 = 0.99 (10 °C), a = 0.002, b = 4.3, R^2 = 0.97 (20 °C). Results adapted from Preda (2019).

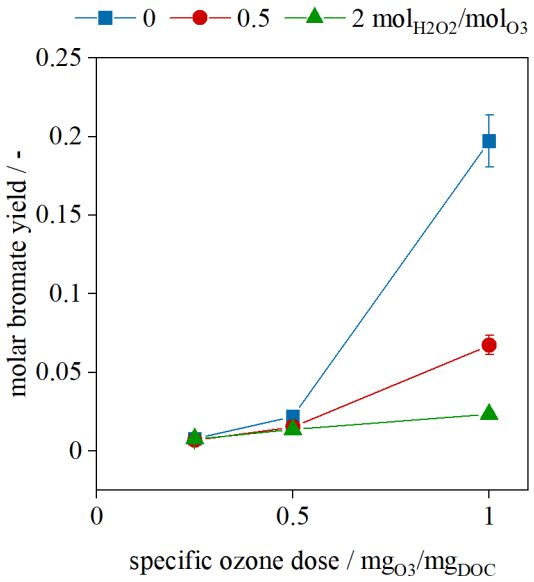

Figure III-18. Molar bromate yield as a function of specific ozone dose for the batch ozonation in combination with H_2O_2 dosage of groundwater $A.6_F$. Results adapted from Eberhard (2021).

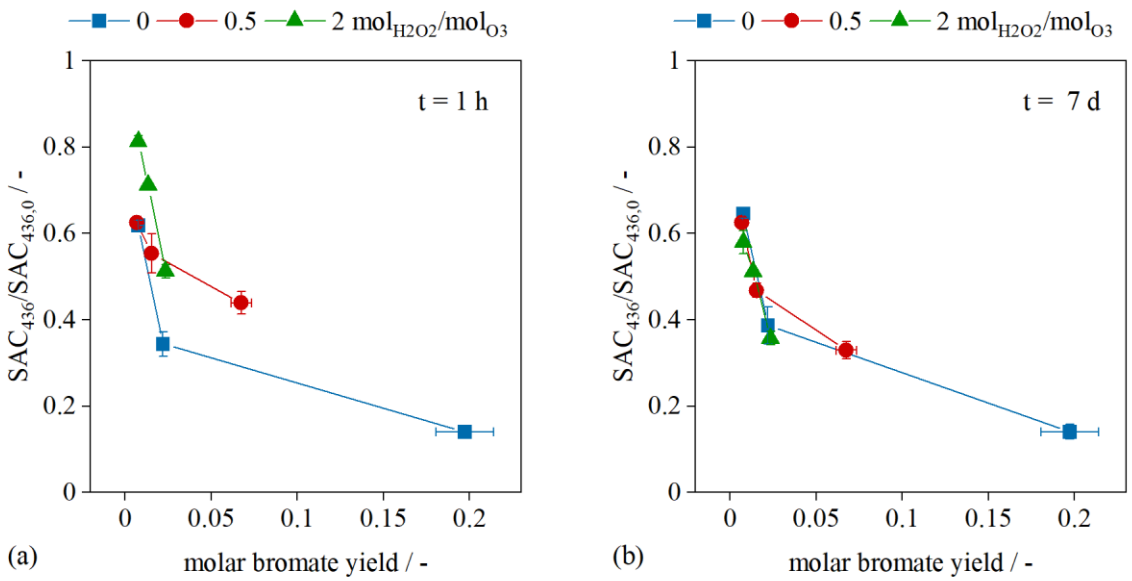

Figure III-19. Relative residual color SAC_{436}/ $SAC_{436,0}$ versus molar bromate yield in batch experiments with groundwater A.6$_F$ (Table II-1) at varying ozone and H_2O_2 doses. **(a)** SAC_{436} 1 h after ozone dosage; **(b)** SAC_{436} 7 d after ozone dosage; bromate was measured only once but showed no significant changes after depletion of ozone. Results adapted from Eberhard (2021). Experimental conditions: pH 8.4, DOC 4.6 mg L^{-1}, $\vartheta \approx 20$ °C

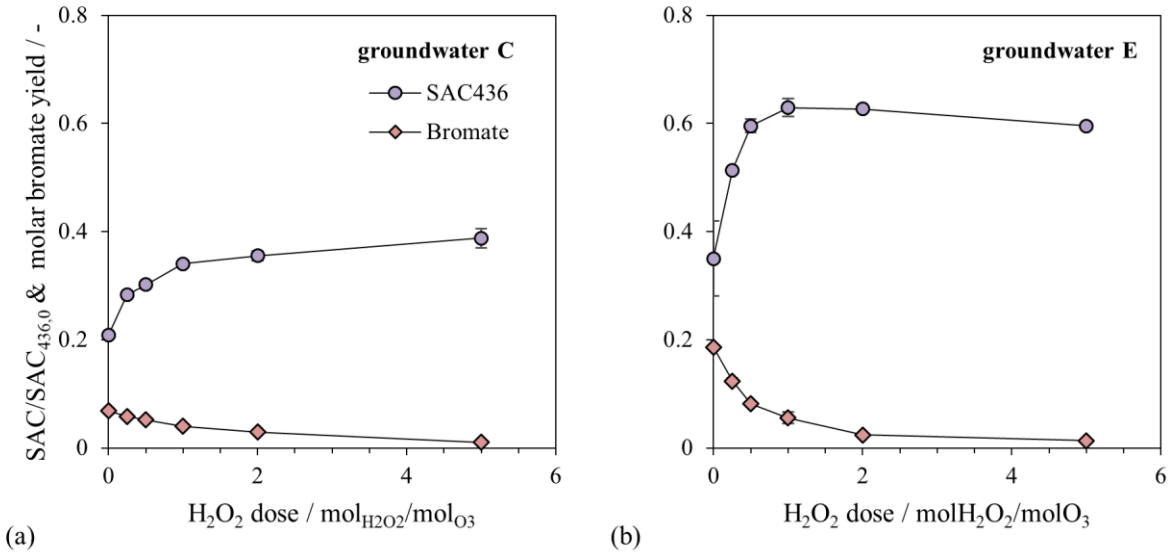

Figure III-20. Relative reduction of SAC_{436} and molar bromate yield in batch ozonation in presence of H_2O_2 as a function of H_2O_2 dose. **(a)** groundwater C, 0.8 mg_{O3}/mg_{TOC}, $\vartheta = 10$ °C, DOC 3.5 mg L^{-1}, pH 8.0, SAC_{436} measured 5 d after ozone dosage (Preda, 2019); **(b)** groundwater E.1$_F$, 1.14±0.03 mg_{O3}/mg_{TOC}, $\vartheta = 20$ °C, DOC 5.6 mg L^{-1}, pH 8.0, SAC_{436} measured 4 h after ozone dosage.

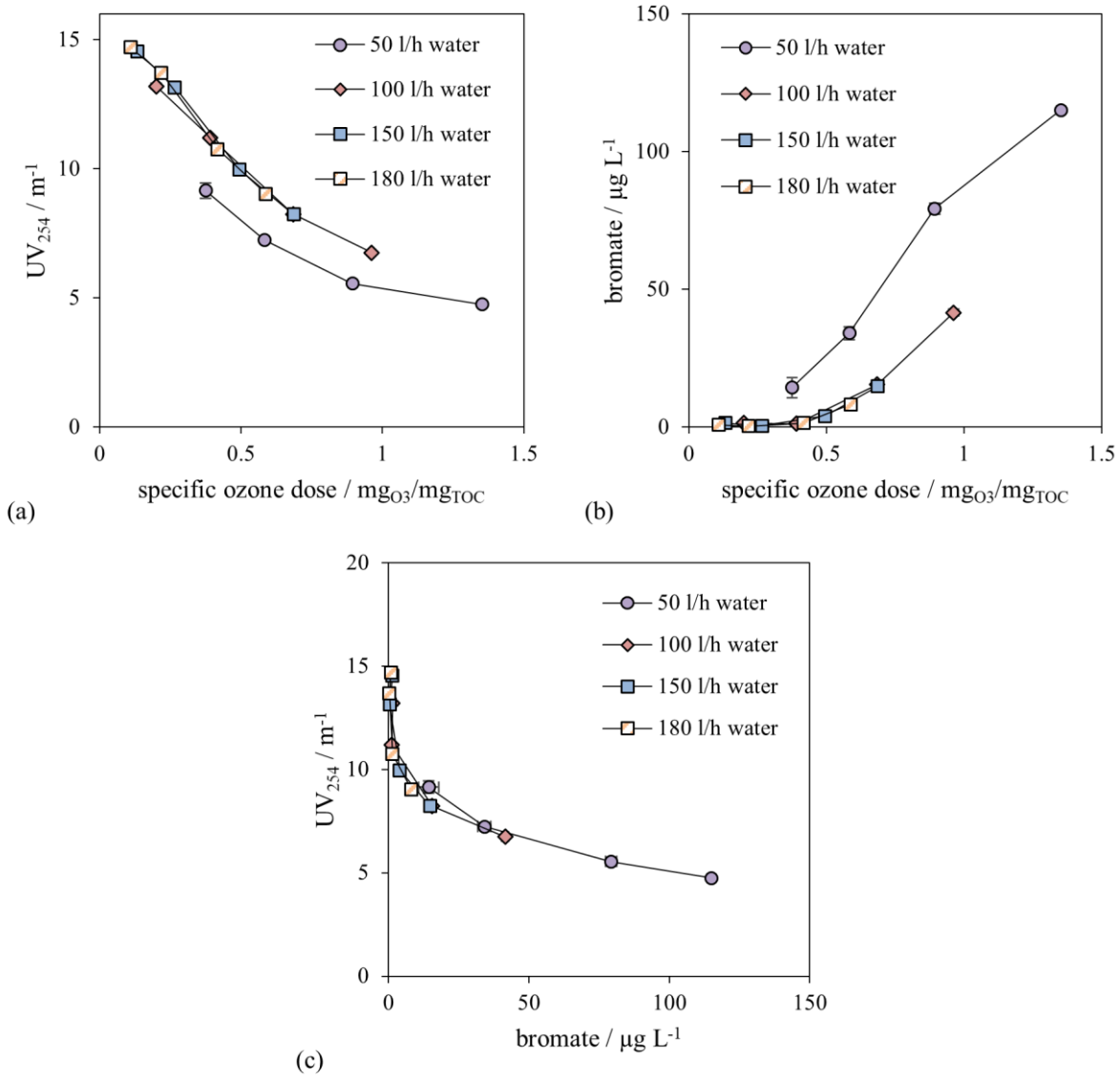

Figure III-21. Small-scale pilot ozonation of groundwater E.2$_F$ at various combinations water flow rate (50, 100, 150, 180 L h^{-1}) and feed gas ozone concentration (5, 10, 20, 30 g m^{-3}). Feed gas flow rate 25 L h^{-1}, ϑ = 15–19 °C, TOC 6.3 mg L^{-1}, pH 7.8. **(a)** UV_{254} versus specific ozone dose. **(b)** bromate versus specific ozone dose. **(c)** UV_{254} versus bromate (data obtained from (a) and (b)).

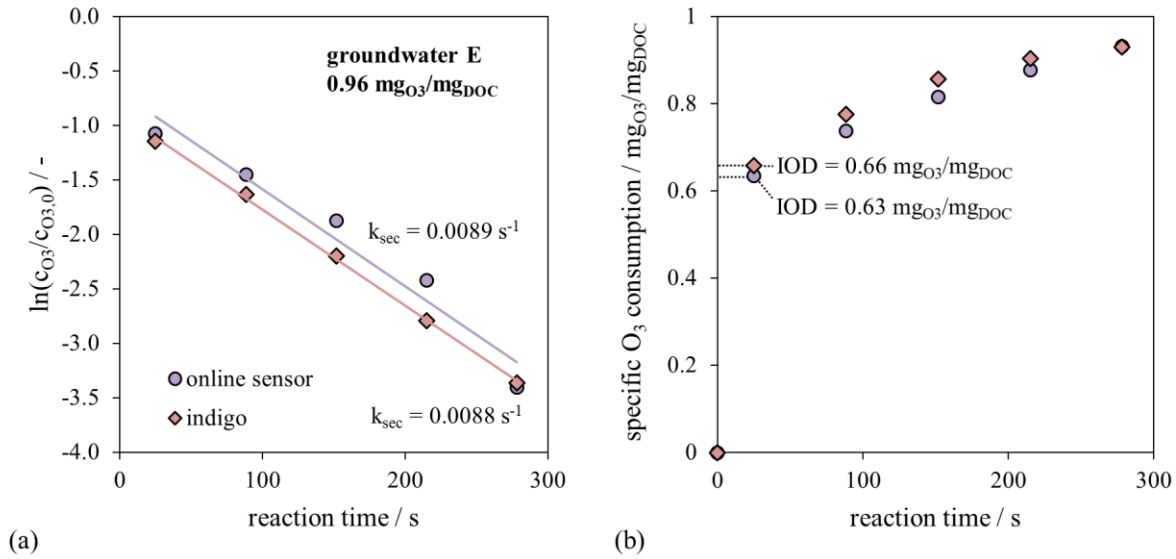

Figure III-22. Reaction kinetics of ozone in finished groundwater E.2$_F$ (small-scale pilot) measured with the online sensor and the indigo method. ϑ = 13 °C, DOC 6.7 mg L^{-1}, specific ozone dose 0.96 mg$_{O3}$/mg$_{DOC}$, pH 7.8. **(a)** logarithmic relative ozone decay kinetics plotted as ln($c_{O3}/c_{O3,0}$), R^2 = 0.96 (online) and 1.00 (indigo). **(b)** Specific ozone consumption (normalized to influent sample DOC concentration) with immediate ozone demand (IOD) after 25 s.

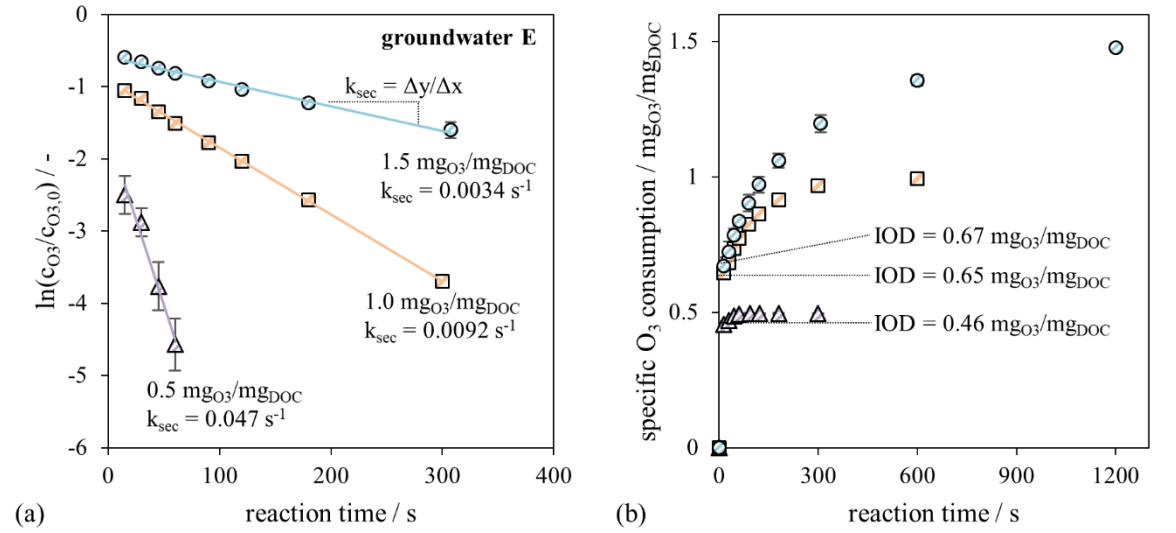

Figure III-23. Reaction kinetics of ozone in groundwater E.1$_F$ (batch). ϑ = 16 °C, pH 8.1, DOC 5.6 mg L^{-1}. **(a)** logarithmic relative ozone decay kinetics plotted as ln($c_{O3}/c_{O3,0}$), R^2 = 0.99, 1.0 and 0.98 for 1.5, 1.0 and 0.5 mg$_{O3}$/mg$_{DOC}$. **(b)** Specific ozone consumption (normalized to initial sample DOC concentration) with immediate ozone demand (IOD) after 15 s for specific ozone doses of 0.5, 1.0 and 1.5 mg$_{O3}$/mg$_{DOC}$. Adapted from Kämmler et al. (2022)

Table III-2. Overview of ozone decay kinetics in groundwater: Immediate ozone demand (IOD) and first-order rate constant for secondary decay k_{sec}. *data adapted from Kämmler et al. (2022). **Batch: IOD time 30 s, pilot: IOD time 25 s. Pilot concentration measured with online sensor

Water	DOC mg L^{-1}	pH	ϑ °C	Batch / Pilot	Specific ozone dose	IOD** mg_{O3}/mg_{DOC}	k_{sec} s^{-1}
$E.1_F$*	5.6	8.1	16	Batch	0.5	0.47	0.047
$E.1_F$*	5.6	8.1	16	Batch	1.0	0.68	0.0092
$E.1_F$*	5.6	8.1	16	Batch	1.5	0.72	0.0034
$E.2_F$	6.3	7.8	13	Pilot	0.96	0.63	0.0089
$A.1_F$	4.5	7.7	14	Pilot	0.54	0.42	0.017
$A.1_F$	4.5	7.7	14	Pilot	1.08	0.56	0.004
$A.1_F$	4.5	7.7	14	Pilot	1.58	0.62	0.0017
$A.2_R$ (raw)	5.2	7.8	14	Pilot	0.59	0.56	0.05
$A.2_R$ (raw)	5.2	7.8	14	Pilot	0.71	0.63	0.019
$A.2_R$ (raw)	5.2	7.8	14	Pilot	0.96	0.74	0.0061
$A.2_R$ (raw)	5.2	7.8	14	Pilot	1.19	0.82	0.0044
$A.2_A$	5.2	7.7	14	Pilot	0.47	0.45	0.051
$A.2_F$	4.9	7.7	14	Pilot	0.38	0.36	0.063
$A.2_F$	4.9	7.7	14	Pilot	0.5	0.44	0.017

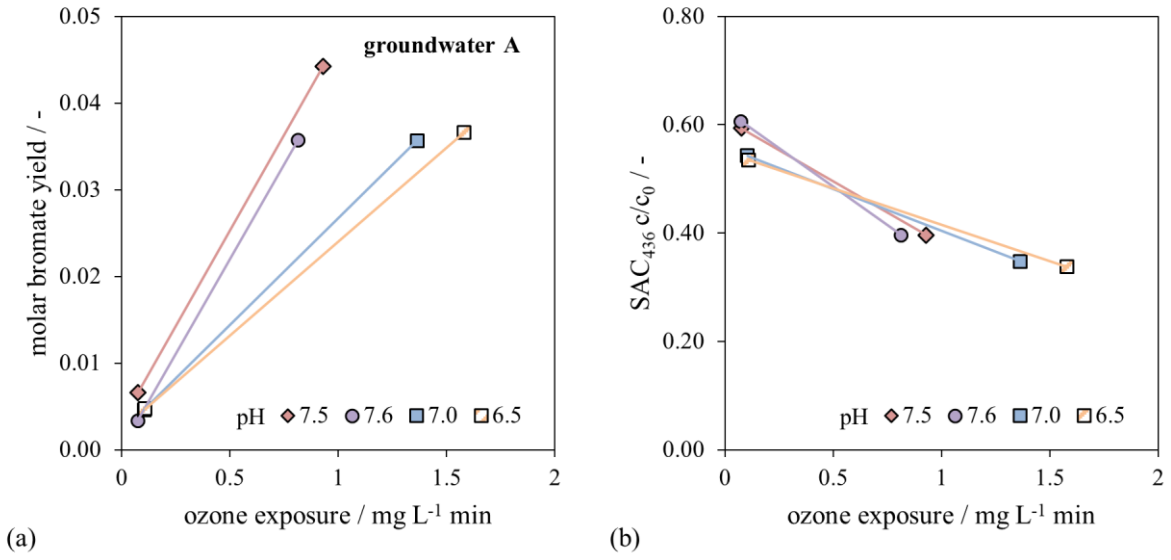

Figure III-24. Effect of ozone exposure on **(a)** molar bromate yield and **(b)** relative residual SAC_{436} for varying pH in the ozonation of groundwater $A.3_F$. pH adjustment by dosage of hydochloric acid. ϑ = 14–15 °C, DOC 4.9 mg L^{-1}, specific ozone doses 0.25 and 0.5 mg_{O3}/mg_{DOC}, small-scale pilot ozonation.

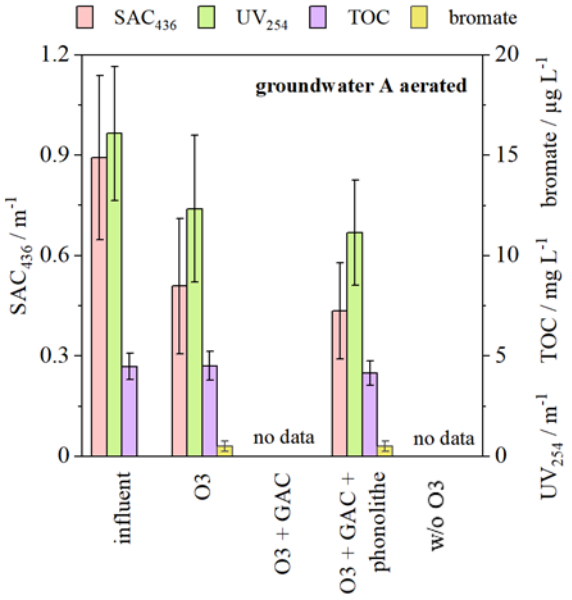

Figure III-25. Small-scale pilot ozonation-biofiltration results for groundwater A after aeration, specific ozone dose = 0.26±0.03 mg_{O3}/mg_{TOC}, pH 7.7–7.9, 15–17 °C, n = 5 samples (four samples for bromate), bromate below limit of quantification (LOQ) of 1.5 µg L^{-1} in two samples (approximation: 0.5 · LOQ) and below limit of detection (LOD) of 0.5 µg L^{-1} in two samples (approximation: 0.5 · LOD). Sample abbreviations: O3 = ozonation effluent; O3 + GAC + phonolithe: ozonation effluent filtered by GAC and phonolithe

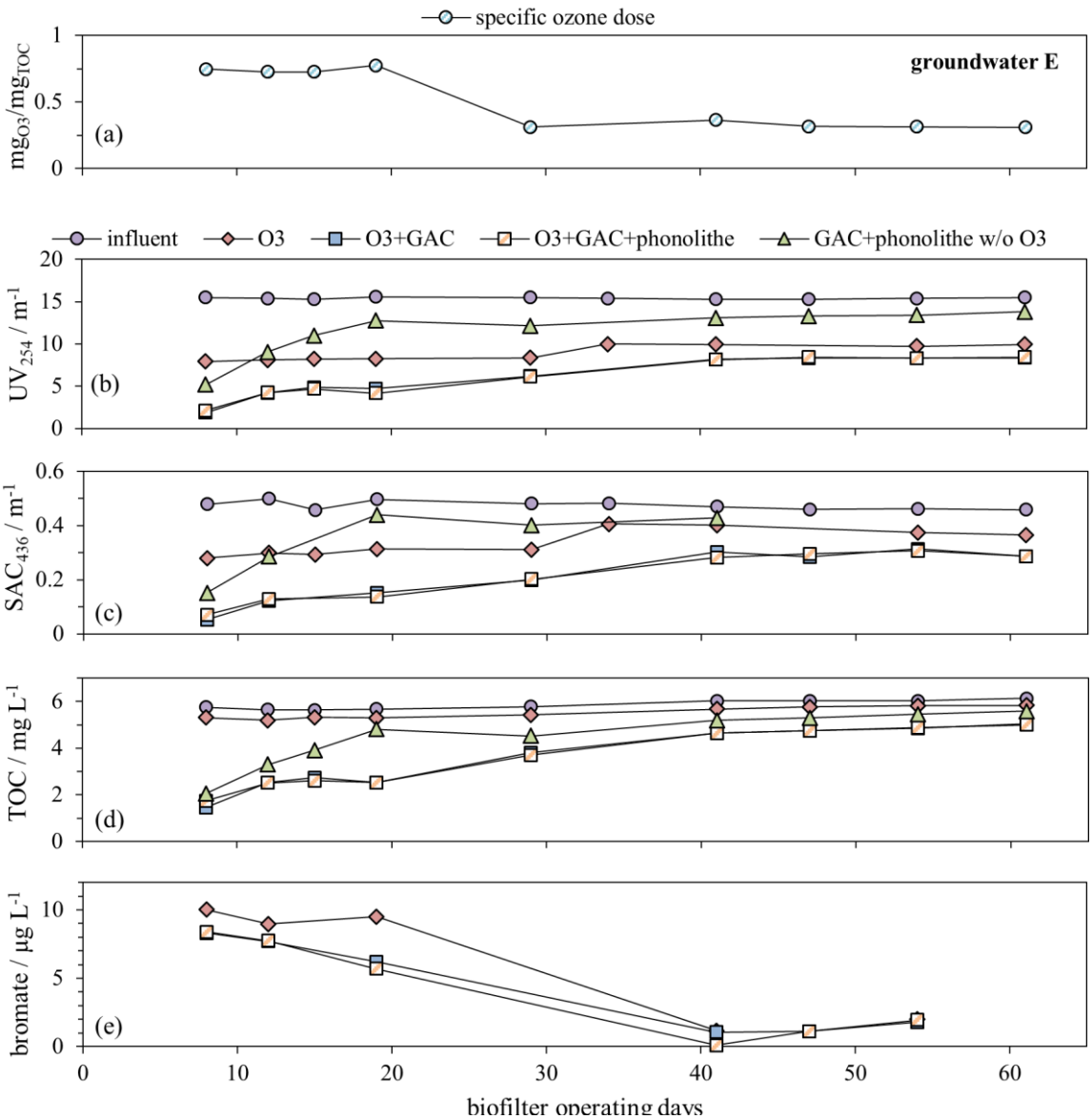

Figure III-26. Conditioning of virgin biofilter (GAC + phonolithe) with groundwater E (small-scale pilot). ϑ 13–17 °C, pH 8.0, bromide n.a., EBCT 35 min. Samples: influent, O3 (ozonation effluent), O3+GAC (GAC effluent), O3+GAC+phonolithe (biofilter effluent), GAC+phonolithe w/o O3 (second identical filter with non-ozonated influent). **(a)** specific ozone dose, **(b)** UV_{254}, **(c)** SAC_{436}, **(d)** TOC, **(e)** bromate.

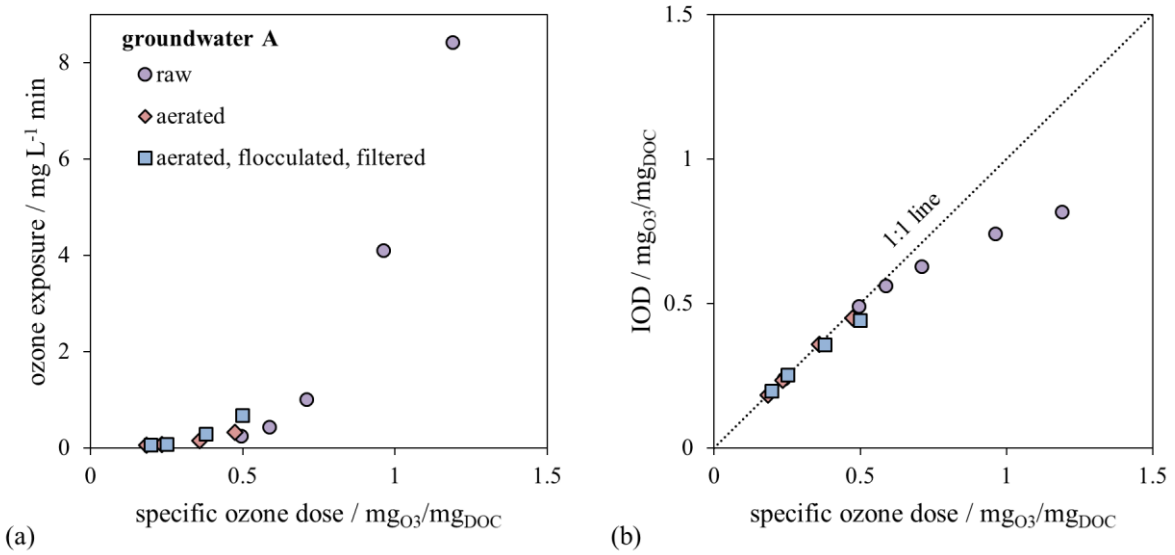

Figure III-27. **(a)** Ozone exposure, **(b)** IOD for small-scale pilot ozonation of raw groundwater (A.2$_R$, 14 °C, 5.2 mg_{DOC} L^{-1}, pH 7.8), aerated groundwater (A.2$_A$, 14 °C, 5.2 mg_{DOC} L^{-1}, pH 7.7) and aerated, flocculated (0.2 mg L^{-1} Al) and sand-filtered groundwater (A.2$_F$, 14 °C, 4.9 mg_{DOC} L^{-1}, pH 7.7).

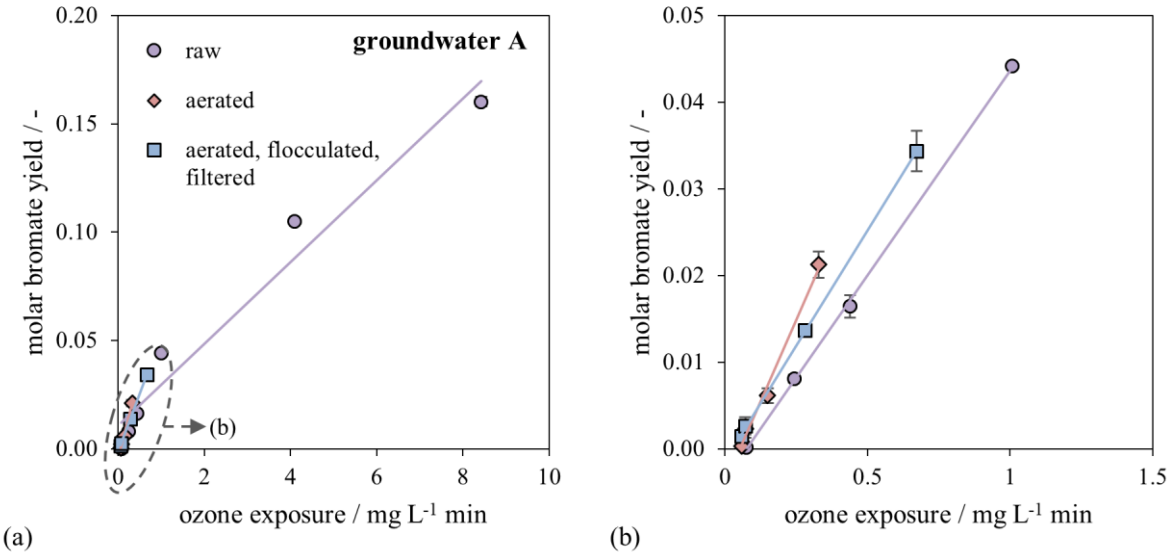

Figure III-28. **(a)** Molar bromate yield versus ozone exposure for raw groundwater (A.2$_R$, 14 °C, 5.2 mg_{DOC} L^{-1}, pH 7.8), aerated groundwater (A.2$_A$, 14 °C, 5.2 mg_{DOC} L^{-1}, pH 7.7) and aerated, flocculated (0.2 mg L^{-1} Al) and sand-filtered groundwater (A.2$_F$, 14 °C, 4.9 mg_{DOC} L^{-1}, pH 7.7). **(b)** Detailed view of data points with ozone exposure ≤ 1.5 mg L^{-1} min. Small-scale pilot ozonation.

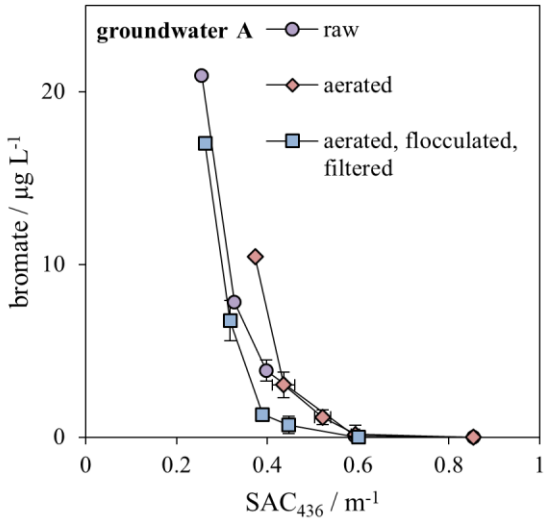

Figure III-29. bromate versus SAC_{436} for raw groundwater (A.2$_R$, 14 °C, 5.2 mg_{DOC} L^{-1}, pH 7.8), aerated groundwater (A.2$_A$, 14 °C, 5.2 mg_{DOC} L^{-1}, pH 7.7) and aerated, flocculated (0.2 mg L^{-1} Al) and sand-filtered groundwater (A.2$_F$, 14 °C, 4.9 mg_{DOC} L^{-1}, pH 7.7). Data points stem from variation of ozone dose in small-scale pilot ozonation.

Table III-3. Overview of results obtained by small-scale pilot ozonation of different feed water qualities of groundwater A. Mean values, n = 2.

Raw groundwater A.2$_R$				
Specific ozone dose	SAC_{436}	UV_{254}	DOC	Bromate
mg_{O3}/mg_{DOC}	m^{-1}	m^{-1}	mg L^{-1}	µg L^{-1}
0.00	0.85	18.3	5.2	0.0
0.24	0.59	15.2	no data	0.1
0.50	0.40	12.3		3.8
0.59	0.33	11.2		7.8
0.71	0.26	9.9		21
0.96	0.19	8.3		50
1.19	0.16	7.4		76
Aerated groundwater A.2$_A$				
Specific ozone dose	SAC_{436}	UV_{254}	DOC	Bromate
mg_{O3}/mg_{DOC}	m^{-1}	m^{-1}	mg L^{-1}	µg L^{-1}
0.00	0.85	18.4	5.2	0.0
0.18	0.59	15.1	no data	0.2
0.24	0.52	14.2		1.2
0.36	0.44	12.9		3.0
0.47	0.37	11.6		10
Aerated, flocculated, filtered groundwater A.2$_F$				
Specific ozone dose	SAC_{436}	UV_{254}	DOC	Bromate
mg_{O3}/mg_{DOC}	m^{-1}	m^{-1}	mg L^{-1}	µg L^{-1}
0.00	0.60	15.4	4.9	0.0
0.20	0.45	12.8	no data	0.7
0.25	0.39	11.9		1.3
0.38	0.32	10.6		6.7
0.50	0.26	9.5		17